SAPIENZA
UNIVERSITÀ DI ROMA

Design and implementation of different receiver architectures for FM-, WiFi-, DVB-SH-based Passive Bistatic Radars

Facoltà di Ingegneria dell’Informazione, Informatica e Statistica

Dottorato di Ricerca in Telerilevamento

XXV Ciclo

Candidato

Antonio Macera

797107

Tutor

Prof. Pierfrancesco Lombardo

INDEX

1. INTRODUCTION

Recently, Passive Bistatic Radar (PBR) has received renewed interest for surveillance purposes, since it allows to perform target detection and localization with many advantages such as low cost, covert operation, low vulnerability to electronic countermeasures, reduced Electro-Magnetic pollution, etc. [1]. PBR is based on the exploitation of an existing transmitter as an illuminator of opportunity. A receiving system is appropriately designed to receive the echoes reflected from air targets and sited to provide coverage of a specific area.

Among all the emitters available in the environment, broadcast transmitters represent some of the most attractive choices for surveillance purposes, owing to their excellent coverage [2]-[7]. The selection of the waveform of opportunity directly affects the design of the receiving system since it sets the expected characteristics of the exploited signal (power levels, RF carriers, frequency bandwidths, etc.). Specifically, the many broadcast signals available in the frequency spectrum, going from the FM and VHF-UHF bands (DAB/DVB-SH/DVB-T) to the S-band (WiFi/WiMax/LTE).

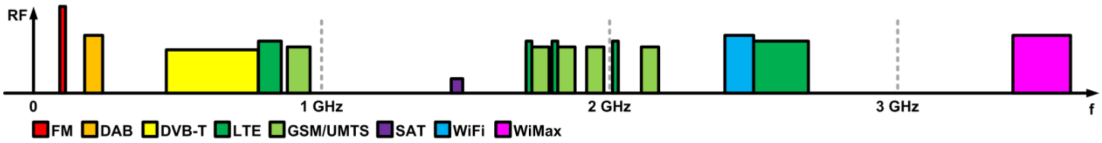

Figure 1 – Broadcast signals available in the frequency spectrum

Different waveform of opportunity allow to realize different PBR. The specific bandwidths, the single communication channel bands, the transmission types, range and velocity resolutions and surveillance applications are summarized in Table 1, for different waveform of opportunity that allows to exploit the passive radar concept in different kinds of application.

For example, a PBR using FM radio broadcast is able to achieve detection ranges up to 150 km (due to the high power of the analogue transmissions) and can be used in Air traffic control applications. Instead, the detection ranges for digital opportunity waveforms results limited by lower power digital signals (such as DAB, DVB-T, WiFi) and results in the order of tens kilometers.

Waveform	Bandwidth [MHz]	Channel Bandwidth [MHz]	Transmission type	Range Resolution	Velocity (Doppler) resolution	Surveillance application	Targets
FM	88÷108	0.2	Continuous	Poor	Very Good	Long Medium	Aircrafts
DAB	174÷240	1,537	Continuous	Good	Good	Medium	Aircrafts Boats
DVB-T	460÷790	8	Continuous	Very Good	Good	Medium Short	Aircrafts Boats
DVB-SH	2175÷2200	5	Continuous	Good	Good	Very Short	Aircrafts Boats
LTE	790÷862 1710÷1785 1805÷1880 2010÷2025 2500÷2690	5 10 15 20	Burst	Good	Good	Short	Aircrafts Boats
WiFi	2400÷2500 5150÷5350 5450÷5725	20	Burst	Good	Good	Short	Humans Cars
WiMAX	3400÷3600	1,25 5 10 20	Burst	Good	Good	Medium Short	Boats Cars Humans

Table 1 – Broadcast signals of opportunity

The passive radar operations imply that the transmitted waveform is not known at the receiver, which needs an additional receiving channel (reference channel) to collect the directly transmitted signal.

Moreover, the detection and localization performance are largely depend on the transmitted waveform of opportunity that is not under the control of the radar designer, who cannot select it appropriately to guarantee desired properties (e.g. narrow peak in both range and Doppler and low side-lobes). Also, target echoes can be masked by different factors: small fraction of the direct signal received by the side/backlobe of the receiver antenna (which might be larger than the clutter echo), strong clutter/multipath echoes, and even other targets with higher returns.

Another aspect of the passive radar regard the accuracy that is strong function of the geometry and the number of receiver and transmitted used. Only one receiver and one transmitter allows to obtain a poor accuracy, with respect a conventional radar system. Typically, in order to increase the performance of the passive systems, more couples transmitter-receiver can be used in a multi-static configuration realizing an effective passive radar network. The necessity of realize a passive radar network requires that the single passive transmitter must be cheap.

In the framework of research activity on passive radar systems for target detection and localization, in this thesis are presented different designs and implementations of receiver architectures. The use of several waveform of opportunity allows to realize passive radar systems for different applications (e.g. Air Traffic Control Surveillance, detection and tracking of human targets).

The design choices presented in the following sections will be motivated on the basis of specific application requirements, costs, coherence of the receiving chains and the dynamic range of the system, possibility to realize multi-channel receivers.

In Section 2, the working principles of passive bistatic radar systems are introduced and described, together with a very short focus on some geometrical considerations related to the bistatic geometry. In addition to the signal processing techniques, an overview of the opportunity waveforms of interest for this thesis is given.

Sections 4, 5 and 6 are dedicated to different waveforms of opportunity of interest in this work: FM radio broadcast, WiFi transmissions and DVB-SH. For each signal, the research activity has regarded the design and the implementation of a receiver able to collect data for the passive radar processing.

In particular Sections 4 is dedicated to the FM based PBR. In this Section, after the study of the general requirements of the system, two architectures for a dedicated passive receiver are presented and described in detail. Test, controlled experiments and experimental results are reported. Specifically, after the laboratory tests, the two systems have been used in different acquisition campaigns, in a real environment, to perform detection and tracking of commercial air traffic. Also a specific acquisition campaign has been carried out in order to verify the performance of the proposed passive radar systems with a dedicated flying of small target. The implemented system allows to perform the target detection in a Cartesian domain by using multiple receiving channel for the angular estimation by signal difference of arrival estimation. This work was carried out under partial support from the Project ARGUS 3D (AiR GUidance and Surveillance 3D), funded by the European Union, 7th framework program, Theme #10 Security, Grant agreement no. 218041.

In Section 5, the concept of PBR is applied to a short range surveillance: detection and tracking human targets (and cars) in indoor and outdoor environments. Also in this Section, a description of two possible architectures for the low cost system realization is reported. A four channel receiver has been realized with COTS components in order to test the processing techniques and realize an effective WiFi based PBR. Different detection results are presented (with one and two targets). This work was carried out under partial support from the Project ATOM (Airport detection and Tracking Of dangerous Materials by passive and active sensors arrays), funded by the European Union, 7th framework program, Theme #7 Transport (including Aeronautics), Grant agreement no. 234014.

In Section 6, is reported the study of a receiver for DVB-SH signals. The Digital Video Broadcast SH is the standard introduced for television transmissions from satellite platforms to mobile devices. The potentialities of a passive radar based on geostationary satellite signals of opportunity is correlated to the wide coverage of the system and its availability. In contrast, the main disadvantage is the low power level of the communication signal. The design of the receiving system is reported, in this Section, with specific reference to the DVB-SH test transmission provided by Eutelsat 10A platform.

Finally, in Section 7, a flexible receiver architecture is described for a Multi-Standard PBR that can exploit any of the many broadcast signals available in the frequency spectrum. Specific front-end receiver sections are foreseen for each selected waveform of opportunity, while a common part of the system performs the I&Q demodulation and the Analog-to-Digital (A/D) conversion. The scheme can be used both for a direct I&Q conversion and for a double conversion (up-conversion stage from Radio Frequency –RF– to a high Intermediate Frequency –IF– and down-conversion from IF to Base Band –BB–) of the received signals for PBR applications. This allows to remove the image frequency even in the wide range of frequencies occupied by the digital TV signals. A prototype of the proposed concept has been developed and fielded, with proper laboratory tests and real data acquisition campaigns. The results obtained with the receiver, in three possible configurations, are reported and discussed: FM-based PBR (for medium/long-range air targets surveillance), DAB/DVB-T (for medium range air and sea surveillance) and WiFi-based PBR (for short-range human target localization).

2. PASSIVE BISTATIC RADAR WORKING PRINCIPLE

2.1. INTRODUCTION

The typical PBR operation is sketched in Figure 2. The low power signal reflected from the target is collected by the main PBR receiver (typically addressed as the surveillance channel), using a directive antenna steered toward the surveillance area. Since the transmitted signal is not known at the receiver, an auxiliary PBR receiver (typically addressed as the reference channel) is usually connected to an additional directive antenna steered towards the transmitter.

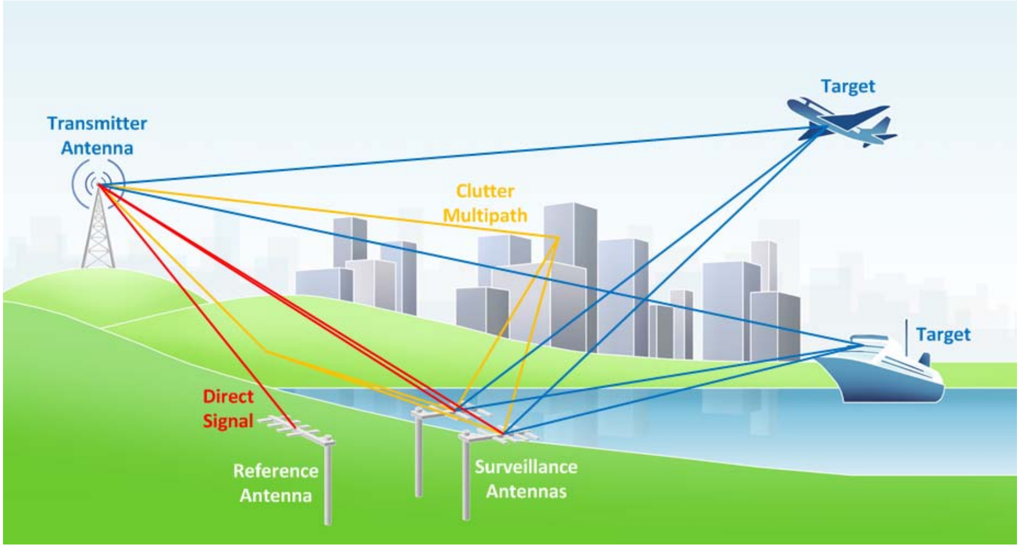

Figure 2 – Basic PBR Processing scheme.

The signal collected at the reference channel is first used to remove undesired contributions, received together with the moving target echo, on the surveillance channel. Specifically these disturbance contributions are due both to the fraction of the direct signal coming from the transmitter and received by the side/backlobes of the surveillance antenna, and by strong clutter/multipath echoes. Different approaches can be exploited to cope with this problem, which can have a major relevance especially when the direct signal contribution is strong and affected by multiple reflections on the surface or on discrete scatterers. After the cancellation stage, the detection process is based on the evaluation of the Bistatic Range-Velocity Cross-Correlation Function (2D-CCF) between the surveillance and the reference signal. A Constant False Alarm Rate (CFAR) threshold can be then applied on the obtained map to automatically detect the potential targets according to a specific CFAR detection scheme.

While the basic detection scheme is fully defined by the described cancellation and integration techniques, the effectiveness of the passive radar operation can be largely enhanced by considering an advanced PBR system equipped with multiple receiving/processing channels. In fact these might be exploited to collect and process simultaneously multiple signals received at different frequencies or at different antennas.

2.2. BISTATIC RADAR EQUATION

With reference to the geometry sketched in Figure 3, received power can be expressed as:

$$P_R = \frac{P_T G_T}{4\pi R_T^2} \frac{\sigma_b}{4\pi R_R^2} \frac{G_R \lambda^2}{4\pi} \qquad (1)$$

where:

- P_R is the received power
- P_T is the transmitted power
- G_T is the transmitter antenna gain
- G_T is the receiver antenna gain
- λ is the signal wavelength [m]
- σ_b is the Bistatic Radar Cross-Section (BRCS) [m2]
- R_T is the transmitter-target distance
- R_R is the receiver-target distance

The first factor in the right-hand side of equation (1) represents the power density per surface unit emitted by the transmitter, the second factor is the portion of power scattered from the target in the receiver direction, the third factor represents the antenna effective area, expressed as a function of the receiver gain.

In order to evaluate the BRCS, we can use some relations with the monostatic RCS that can yield to good approximations. Specifically, we can consider three different regions as a function of the bistatic angle β Z quasi-monostatic, bistatic and forward-scatter region. Inside the first region (quasimonostatic), the BRCS value can be approximated with the monostatic RCS multiplied by $\cos(\beta/2)$ and this relation stands for low bistatic angles $(\beta < 5°)$ and for low frequencies. For bistatic angles higher than $5°$ (bistatic region), BRCS is quite different from the monostatic one, and the following relation is valid:

$$-20dB < \frac{\sigma_{bistatic}}{\sigma_{monostatic}} < -12dB \qquad (2)$$

Finally, if the target is on the baseline $(\beta = 180°)$, we are in the forward-scatter region.

Received power P_R in (1) can be replaced with the smallest received power that can be detected by the radar, $S_{\min}$, expressed by

$$P_R = S_{\min} = KT_0 B_n F_n \left(\frac{S}{N}\right)_{\min} \qquad (3)$$

and also the loss factors L_{PT} and L_{PR} (both lower or equal than one), which represent the losses from transmitter to target and from receiver to target, respectively, can be included, thus obtaining the following relation:

$$\left(\frac{S}{N}\right) = \frac{P_R}{P_N} = \frac{P_T G_T G_R \lambda^2 L_{PT} L_{PR} \sigma_b}{(4\pi)^3 R_T^2 R_R^2 K T_0 B_n F_n} \qquad (4)$$

In the bistatic triangle of Figure 3, formed by target, transmitter and receiver, if the product between R_T and R_R is constant, the locus of points defined by target positions is known as Oval of Cassini. These ovals are composed by points characterized by constant power levels (SNR) at the receiver; in order to obtain the Cassini Ovals we need to consider all the parameter of the bistatic radar equation as constant except for R_T and R_R, so that (4) can be written as

$$\left(\frac{S}{N}\right)=\frac{k}{R_T^2 R_R^2} \tag{5}$$

With

$$k=\frac{P_T G_T G_R \lambda^2 L_{PT} L_{PR} \sigma_b}{(4\pi)^3 K T_0 B_n F_n} \tag{6}$$

This simplified version of bistatic radar equation highlights that, for each point of the space, SNR measured at the receiver depends on the target position with respect to both the transmitter and the receiver.

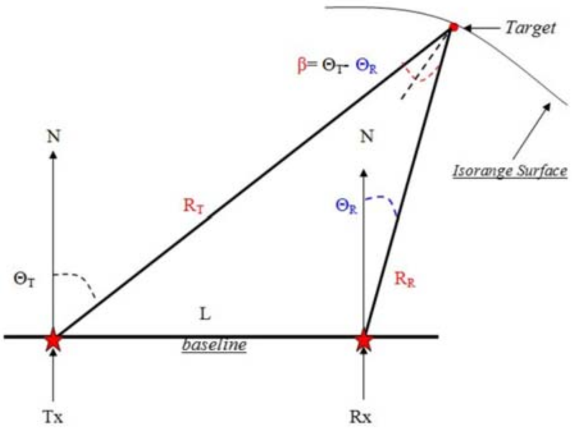

Figure 3 – Basic PBR Processing scheme for a system equipped with 2 receiving channels (REF+SURV).

2.3. SIGNAL PROCESSING TECHNIQUES

The basic PBR processing scheme is depicted in Figure 4. This scheme is intended for a PBR system equipped with two simultaneous receiving channels to be connected to the reference and surveillance antennas, respectively.

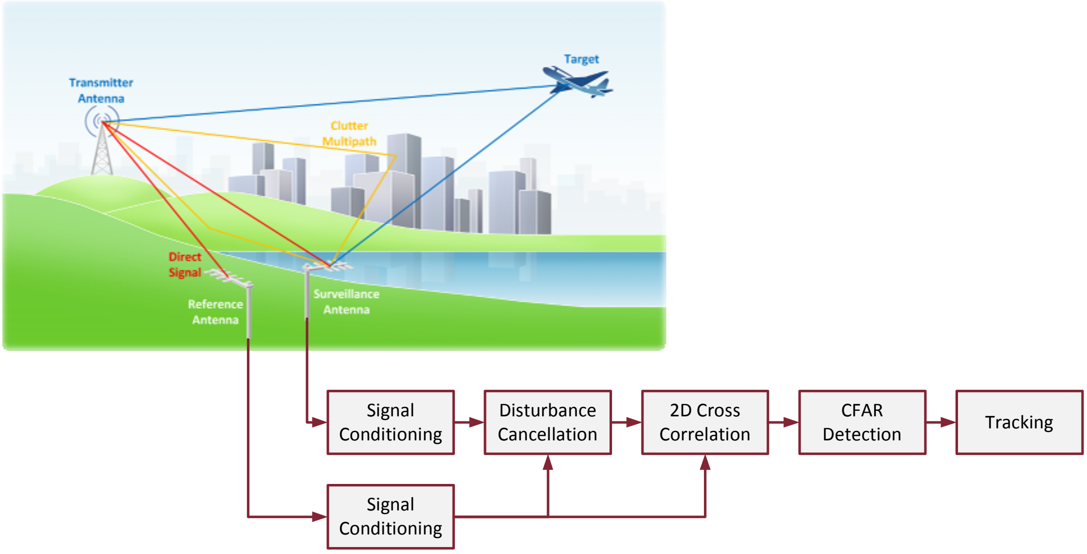

Figure 4 – Basic PBR Processing scheme for a system equipped with 2 receiving channels (REF+SURV).

First of all, depending on the exploited waveform of opportunity, it might be necessary to perform some transmitter-specific conditioning of the received signals:

- high quality analogue band-pass (BP) filtering,
- channel equalization,
- removal of unwanted structures in digital signals.

Then the signal collected at the reference channel is used to remove undesired contributions, received together with the target echo, on the surveillance channel. Specifically these disturbance contributions are due both to the fraction of the direct signal coming from the transmitter and received by the side/backlobes of the surveillance antenna, and by strong clutter/multipath echoes. These undesired contributions can mask the low signals reflected from targets and/or introduce false alarms. Different approaches have been proposed to cope with this problem, which can have a major relevance especially when the direct signal contribution is strong and affected by multiple reflections on the surface or on discrete scatterers, [3]-[7]. The disturbance cancellation technique is of particular importance when it is difficult to avoid a significant signal power arriving directly from the transmitter of opportunity into the sidelobes of the surveillance antenna. For a long range target, the power ratio of direct signal received through the sidelobes and desired signal can get close to 100 dB so that the cancellation technique has a significant challenge. This is especially the case of passive radar operating at relatively low frequency, where it is very difficult to reduce the receiving antenna sidelobes to a very low level.

Also, for digital waveforms of opportunity, the Ambiguity Function shows high sidelobes structures which may strongly affect the target detection capabilities. In order to reduce such effects, the range sidelobes reduction techniques proposed in [8] are preliminarily applied to the signal collected at the reference channel.

After the application of the sidelobes reduction techniques and the cancellation stage, the detection process is based on the evaluation of the Bistatic Range-Velocity Cross-Correlation Function (2D-CCF) between the surveillance and the reference signal. While the evaluation of the 2D-CCF is not especially challenging from a signal processing point of view, it can be challenging in terms of the computational load that it requires for real-time application. The long integration times (order of magnitude of seconds) required to extract the low level target signal from the disturbance implies a large number of complex multiplications to be performed. Moreover, long coherent integration times of this type provide a high Doppler frequency resolution, thus a high number of Doppler filters is required. Finally, the computational load is obviously also proportional to the bandwidth of the specific waveform of opportunity used in the system, which sets the minimum required sampling frequency. By observing that the expected target echo belongs to a limited area of the bistatic Range-Doppler plane, the computational load can be lowered by appropriately selecting the filter implementation approach that best matches the region of the bistatic Range-Doppler plane of interest and by considering approximate filtering schemes.

Targets are then detected on the 2D-CCF map by applying an adaptive threshold according to standard constant false alarm rate (CFAR) algorithms. Finally, plot association and target tracking can be performed in the Range-Doppler space using a simple Kalman filter.

2.3.1. DISTURBANCE CANCELLATION TECHNIQUES

The passive, non-cooperative operation implies that the characteristics of the transmitted waveform are not under the control of the radar designer and typically they are not tailored for radar application. Moreover, being used for transmission of information, they have an intrinsic random appearance as seen by a receiver. This implies that very often their ambiguity function have time-varying sidelobe structures both along bistatic range and Doppler. Moreover, these sidelobes exist at a level not greatly lower than the peak, [7]. This can lead to:

- strong clutter echoes masking targets with high Doppler frequencies,
- a small fraction of the direct signal being received via the side/backlobe of the surveillance antenna (which is still significantly larger than the clutter echo) which masks target echo signals, and
- strong target echoes masking other echoes from other targets of a lower level, even in the presence of large range-Doppler separations.

In addition to using carefully designed waveforms, in active radar systems these problems are typically addressed in two ways: (a) applying tapering to the received signal to lower the sidelobes, and (b) using MTI (Moving Target Indication) canceller filters to remove the strong stationary clutter echoes. Unfortunately none of the two techniques can be directly applied to passive radar.

The standard taper functions are typically effective in controlling sidelobes due to the signal characteristics at the leading and trailing edges of the radar pulses, that have a well known shape and can be modified by appropriate filtering. In contrast, the typical sidelobes of the waveforms of opportunity are due to fast amplitude and phase modulations of the waveform spectrum related to the transmitted information content, that is obviously unknown and time-varying. This does not allow to design filters able to control the sidelobes to very low levels as for nicely designed and fully known waveforms.

Also, the masking effect due to the low peak-sidelobe level of the ambiguity function cannot be removed by conventional MTI techniques. In fact, a standard canceller is based on the idea of subtracting two or more consecutive echoes (with appropriate weights) with the idea that the echo from stationary targets in two consecutive echoes would be exactly the same and the difference will cancel the undesired contributions from the stationary background. In passive radar, two successive batches of the received signals are different even if they have been reflected by the same stationary background, since the transmitted waveform changes continuously.

Hence, proper adaptive cancellation filters have had to be designed for this purpose, [3]-[7], [10]. Generally speaking, the goal of the cancellation stage is to remove as much as possible the undesired interference so to extract the desired target signal from the surveillance signal observation. In fact, the complex envelope of the signal received at the surveillance channel can be written as:

$$s_{surv}(t)=A_{surv}d(t)+\sum_{m=1}^{N_T}a_m d(t-\tau_m)e^{j2\pi f_{dm}t}+\sum_{i=1}^{N_C}c_i d(t-\tau_{ci})+n_{surv}(t) \quad 0\le t<T_0 \tag{7}$$

where T_0 is the observation time and:

- $d(t)$ is the complex envelope of the direct signal (a delayed replica of the transmitted signal);
- A_{surv} is the complex amplitude of the direct signal received via the side/backlobe of the surveillance antenna;
- a_m, τ_m, and f_{dm} are the complex amplitude, the delay (with respect to the direct signal) and the Doppler frequency of the *m*-th target (m=1,..,N_T);
- c_i and τ_{ci} are the complex amplitude and the delay (with respect to the direct signal) of the *i*-th stationary ground scatterer (i=1,..,N_C); multipath and clutter are modelled as a set of small discrete scatterers; a continuous clutter backscattering environment can be emulated by utilising a large number of such ground scatterers;
- $n_{surv}(t)$ is the thermal noise contribution at the surveillance channel.

The principle of operation of the adaptive cancellation filter is the following: by summing up a number of appropriately delayed and weighted replicas of the transmitted waveform, an estimate of the undesired interference signal is obtained. This estimate in then subtracted from the received signal so as to remove the interference component.

To operate following this approach, the knowledge of the transmitted waveform is required. The reference signal is exploited to this purpose by assuming it to be a good replica of the transmitted signal. Specifically, since the direct signal is received by the main lobe of the reference antenna, it is assumed that target and clutter echoes (received from the sidelobes) are negligible. Moreover, for the sake of simplicity, it is assumed that the reference signal is free of multipath. Under these assumptions, by appropriately filtering the reference signal (a FIR filter with a number of taps emulates the multiple reflections from stationary objects) an adaptively estimate the undesired contributions in the surveillance signal is obtained. This estimates is then be subtracted from the original signal leaving only an estimate of the desired target echoes. A widely applied solution for the adaptive cancellation filter is presented in [10] where the joint process estimator algorithm is used. The filter, consists of two parts:

- an adaptive M-stage lattice predictor,
- an adaptive tapped delay line.

As it is apparent, the reference signal samples are first transformed into a corresponding sequence of uncorrelated samples which are then used as the input of the tapped delay line to obtain an estimate of the undesired contributions to be subtracted from the surveillance signal. Specifically the gradient adaptive lattice (GAL), is used to adjust the coefficients in the lattice predictor structure while the Normalised Least Mean Square algorithm (NLMS) is exploited to update the coefficients of the tapped delay line. Both these algorithms are described in details in [11].

In the following we will refer to the block LS approach which has been largely exploited and properly modified by the authors to cope with the interference scenarios encountered in different PBR applications, [7], [12].

2.3.1.1. EXTENSIVE CANCELLATION ALGORITHM (ECA)

To derive the basic block LS algorithm, that we address as ECA, the *N* samples of the surveillance signal collected during a Coherent Processing Interval (CPI) are arranged in a *N*×1 vector:

$$\mathbf{s}_{surv}=\left[s_{surv}[0],s_{surv}[1],s_{surv}[2],\cdots,s_{surv}[N-1]\right]^T \tag{8}$$

Similarly, we collect *N*+*R*-1 samples of the reference signal in the following vector:

$$\mathbf{s}_{ref} = \left[s_{ref}[-R+1], \cdots, s_{ref}[0], \cdots, s_{ref}[N-1]\right]^T \tag{9}$$

where R-1 is the number of additional reference signal samples to be considered in order to obtain the desired integration (namely N integrated samples) over an extent of R time bins.

Assuming that the multipath and clutter echoes are potentially backscattered from the first K range bins, the signal model is exploited by searching for a minimum residual signal power after cancellation of the disturbance (direct signal and ground echoes), thus:

$$\min_{\boldsymbol{\alpha}} \left\{ \left\| \mathbf{s}_{surv} - \mathbf{X}\boldsymbol{\alpha} \right\|^2 \right\} \tag{10}$$

where $\mathbf{X} = \mathbf{B}\,\mathbf{S}_{ref}$, **B** is an incidence matrix that selects only the last N rows of the following matrix, and

$$\mathbf{S}_{ref} = \left[\mathbf{s}_{ref} \quad \mathbf{D}\,\mathbf{s}_{ref} \quad \mathbf{D}^2\mathbf{s}_{ref} \quad \cdots \quad \mathbf{D}^{K-1}\mathbf{s}_{ref}\right] \tag{11}$$

whose columns are the zero-Doppler, delayed versions of the reference signal, and **D** is a 0/1 permutation matrix that applies a delay of a single sample. The columns of matrix **X** define a basis for a K-dimensional disturbance subspace. Solving equation (10) yields:

$$\boldsymbol{\alpha} = \left(\mathbf{X}^H\mathbf{X}\right)^{-1}\mathbf{X}^H\mathbf{s}_{surv} \tag{12}$$

Therefore, the surveillance signal after cancellation becomes

$$\mathbf{s}_{ECA} = \mathbf{s}_{surv} - \mathbf{X}\,\boldsymbol{\alpha} = \left[\mathbf{I}_N - \mathbf{X}\left(\mathbf{X}^H\mathbf{X}\right)^{-1}\mathbf{X}^H\right]\,\mathbf{s}_{surv} = \mathbf{P}\,\mathbf{s}_{surv} \tag{13}$$

where the projection matrix **P** projects the received vector $\mathbf{s}_{surv}$ in the subspace orthogonal to the disturbance subspace.

The performance of this algorithm has been characterized in [5]-[7] and [12] against both simulated and real data.

Specifically, in [7] we show that a better disturbance cancellation can be achieved with the ECA by extending the disturbance subspace dimension represented by the columns of matrix **X** by including Doppler shifted replicas of the reference signal (namely matrix **X** with M>K columns describing a cancellation mask over the range-Doppler plane) thus widening the filter notch in the Doppler dimension. However this approach is computationally intensive, since it corresponds to increasing the dimension of the weight vector α whose evaluation requires the computation and the inversion of the matrix $\mathbf{X}^H\mathbf{X}$ with dimensions M×M which corresponds to O[NM^2+M^2log$M$] complex products.

2.3.1.2. ECA BATCHES

In order to achieve similar or better cancellation performance with a limited computational load, a batch version of the ECA (ECA-B) has been introduced in [7]. Specifically, in this approach, the ECA is applied to a set of b consecutive batches of reduced length T_B= T_{int}/b. If the whole temporal extension T_{int} used for coherent integration (2D-CCF) gives rise to N=$T_{int}\cdot f_s$ samples, the ECA algorithm is applied over b consecutive batches of N_B=N/b samples each.

Three considerations are in order for the ECA batches algorithm:

- At the i-th batch, operating with the same number M of degrees of freedom, the modification of the original ECA will still require the evaluation and inversion of the matrix $\mathbf{X}_i^H\mathbf{X}_i$ with dimension M×M, which in this case corresponds to O[N_BM^2+M^2log$M$] complex products. Clearly this computation needs to be repeated on each batch thus yielding only a limited increase in the computational burden (about the same order of magnitude in terms of complex products), namely O[NM^2 +bM^2log$M$] in place of O[NM^2 + M^2log$M$]. However, at each batch the dimension of the data can be reduced by a factor *b* thus reducing the dynamic storage requirement of the system. Moreover the cancellation processing can run in parallel with the data acquisition since it can be started after the first batch has been received. This typically makes the implementation easier and faster.

- The size N_B of the batch sets the time extent over which the adaptive filter parameters are estimated. Reducing N_B within certain limits increases the adaptivity loss when operating in a stationary environment. However, it allows a certain degree of adaptation to the slowly varying characteristics of typical transmissions, thus making the system more robust.
- By operating with a reduced temporal extent T_B, the Doppler resolution capability of the cancellation filter is degraded with respect to the ECA approach operating over the whole T_{int} period. This results in a wider notch in the Doppler dimension that in turn removes the potential request for additional degrees of freedom to cope with the spectral dispersion of the interfering signals, which would require a higher computational load.

In principle, this algorithm can be expanded into a processing scheme composed of consecutive stages that progressively detect the strongest delay and frequency shifted replicas of the direct signal and hence reduce their effect on the resulting “processed” surveillance signal. The process is repeated iteratively after removing the detected contributions until all the potential targets have been detected. This leads to the ECA Batches & Stages (ECA-B&S) algorithm ([7]) that is very robust since it allows both a more effective clutter/multipath cancellation and the capability to extract some of the weak targets echoes that are likely to be lost by conventional, single stage techniques.

2.3.2. 2D-CCF EVALUATION

The evaluation of the bistatic Range-Velocity Cross-Correlation Function (2D-CCF) is the key step in the PBR processing chain. It corresponds to the implementation of a bank of matched filters, each one tuned to a specific target bistatic velocity. Typically the values of velocity are chosen with a separation approximately equal to the bistatic velocity resolution. Therefore the set of filters covers all the possible target velocities. Moreover, the filter where the target is detected provides the estimates of the bistatic Doppler shift of each target echo. Similarly, the estimate of the bistatic range is given by the sample along range where it is detected. Assuming that the signal $s_{ref}(t)$ collected at the reference antenna is a perfect copy (or at least “good enough” as discussed in the previous section) of the transmitted signal, the 2D-CCF for a PBR is evaluated as:

$$\chi(\tau, f_D) = \int_{-\infty}^{\infty} s_{surv}(t) s_{ref}^{*}(t-\tau) e^{-j2\pi f_D t}\, dt \tag{14}$$

where

- $s_{surv}(t)$ is the complex envelope of the signal collected at the surveillance antenna;
- $\tau = R_B / c$ is the bistatic time difference of arrival (TDOA) of interest, being R_B the relative bistatic range (namely the difference between the 2-way path length and the TX-RX baseline);
- $f_D = v_B / \lambda$ is the Doppler shift of interest, being v_B the bistatic velocity;
- the integral is limited in practice to the Coherent Processing Interval (T_{int}).

Assuming that the signals are sampled at frequency f_s, equation (14) can be easily expressed in discrete time notation as:

$$\chi[l,m] = \sum_{n=0}^{N-1} s_{surv}[n] \cdot s_{ref}^{*}[n-l] \cdot e^{-j2\pi \frac{mn}{N}} \tag{15}$$

where

- $N = \lfloor T_{int} f_s \rfloor$ is the number of integrated samples;
- *l* represents the time bin corresponding to time delay $\tau = l/f_s$;
- *m* represents the Doppler bin corresponding to Doppler shift $f_D = m f_s / N$.

The evaluation of the 2D-CCF for a PBR represents one of the most costly operation in terms of computational burden, [9], [13]-[14]. In fact, the exploited waveform of opportunity has typically a low power level for radar purposes so that a very long integration time is usually required to obtain an acceptable signal-to-noise ratio (SNR). Moreover large 2D maps might be required depending on the desired surveillance region extent in both range (0- $R_{B\max}$) and Doppler dimensions (- $|v_{bis}|_{\max}$, $|v_{bis}|_{\max}$), where $R_{B\max}$ and $|v_{bis}|_{\max}$ are the maximum relative bistatic range and the maximum bistatic velocity of interest. This implies that a huge amount of data has to be managed and a large number of complex operations has to be performed which might require very fast hardware for real time processing. As a reference, the direct evaluation of (15) over N_τ time bins and N_f Doppler bins requires $N(N_\tau+1)N_f$ complex multiplications and $(N-1)N_\tau N_f$ complex additions, where assuming that the 2D-CCF is not oversampled, we have:

$$N_\tau = \left\lceil \frac{R_{B\max}}{c} f_s \right\rceil \quad \text{and} \quad N_f = \left\lceil \frac{2|v_{bis}|_{\max}}{\lambda} \frac{N}{f_s} \right\rceil \tag{16}$$

In the following sub-sections, two different efficient implementations of equation (15) are considered. The different algorithms are compared in terms of achievable performance and computational load along the line presented in [14]. Also, the best selection of the parameters characterizing each algorithm is discussed, aimed at achieving the best trade-off between performance and computational load.

2.3.2.1. EFFICIENT IMPLEMENTATIONS OF THE 2D-CCF BASED ON THE FAST FOURIER TRANSFORM (FFT)

Two alternative efficient implementations can be obtained by rearranging the factors in equation (15) according to different criteria and exploiting the well known FFT algorithm to evaluate of the Discrete Fourier Transform (DFT).

2.3.2.1.1. CORRELATION-FFT

This algorithm is based on the observation that, at the *m*-th Doppler bin, the samples along time of the 2D-CCF correspond to the samples of the cross-correlation between the reference signal and a Doppler shifted version of the surveillance signal $s_m[n] = s_{surv}[n]\exp(-j2\pi mn/N)$:

$$\chi[l,m] = \sum_{n=0}^{N-1} s_m[n] \cdot s_{ref}^*[n-l] = C_m[l] \tag{17}$$

A saving in computation is obtained by evaluating such cross-correlation in the frequency domain as:

$$C_m[l] = IDFT\left\{ DFT\{s_m[n]\} \left(DFT\{s_{ref}[n]\} \right)^* \right\} = IDFT\{S_m[k] S_{ref}^*[k]\} \tag{18}$$

For each one of the N_f Doppler filters, an IDFT (inverse DFT) is evaluated and $N-N_\tau$ output samples are discarded. Moreover, notice that, for a given *m*, the DFT $S_m[k]$ of $s_m[n]$ can be simply obtained as a circular shift of the samples of $S_{surv}[k] = DFT\{s_{surv}[n]\}$. As a consequence, the DFTs of the reference and surveillance signals can be evaluated just once and, at each subsequent iteration, only the *N* complex multiplications and a single IFFT must be performed.

2.3.2.1.2. DIRECT-FFT

This algorithm is based on the observation that, at the *l*-th time bin, the samples along Doppler frequency of the 2D-CCF correspond to the samples of the DFT of the sequence $x_l[n] = s_{surv}[n]s^*_{ref}[n-l]$ obtained as the product of the surveillance signal and the delayed conjugated reference signal, [9]:

$$\chi[l,m] = X_l[m] = DFT\{x_l[n]\} \tag{19}$$

Similar to the previous case, for each one of the N_τ bistatic delays, the DFT is evaluated and N-N_f output samples are discarded. Since its iterations involve the range dimension, this algorithm can be parallelized over the range bins and can be limited to the N_τ range bins of interest. Therefore, at each iteration only *N* complex multiplications and a single FFT must be performed (in contrast to the Direct-FFT algorithm it does not require the preliminary evaluation of the signals DFT).

2.3.2.2. SUB-OPTIMUM IMPLEMENTATIONS OF THE 2D-CCF

Further reduction of the computations required by the 2D-CCF can be obtained by resorting to sub-optimum algorithms, if small degradations can be accepted in terms of SNR. Notice that the required cost for both the Correlation-FFT and the Direct-FFT optimum algorithms is strongly affected by the processing load required by the FFT of the long input sequences. Moreover, only a very small portion of the output FFTs (namely N_τ out of *N*, with $N_\tau \ll N$, or N_f out of *N*, with $N_f \ll N$) is required in the final 2D map while most of the obtained samples are discarded. Therefore, there is still a computational load reduction to be obtained both by avoiding useless computations and by approximating the phase compensations to be performed by appropriately decimating or subdividing in channels the signals according to the following algorithms.

2.3.2.2.1. BATCHES ALGORITHM

This sub-optimum algorithm is obtained by subdividing the CPI into n_B batches (sub-CPIs) of N_B samples each. The Doppler frequency compensation inside each short sub-CPI is neglected, while maintaining only the phase compensation from batch to batch, thus reducing the overall computation complexity with limited loss in signal processing gain. Specifically equation (15) is rewritten as follows:

$$\chi[l,m] = \sum_{r=0}^{n_B-1} e^{-j2\pi\frac{m r N_B}{N}} \sum_{p=0}^{N_B-1} s_{surv}[rN_B+p]\cdot s^*_{ref}[rN_B+p-l]\cdot e^{-j2\pi\frac{mp}{N}} \tag{20}$$

and neglecting the complex exponential term within the inner summation we obtain:

$$\chi[l,m] \cong \sum_{r=0}^{n_B-1} e^{-j2\pi\frac{mr}{n_B}} \sum_{p=0}^{N_B-1} s_{surv}[rN_B+p]\cdot s^*_{ref}[rN_B+p-l] = \sum_{r=0}^{n_B-1} e^{-j2\pi\frac{mr}{n_B}} y_l[r] \tag{21}$$

which represents the DFT of the decimated sequence $y_l[r]$ (r=0,..,n_B-1), obtained by summing the product sequence $x_l[n] = s_{surv}[n]\cdot s^*_{ref}[n-l]$ for each batch.

In general, the number of batches should be selected so that $n_B \geq N_f$; and in particular, no sample is discarded at the FFT output if equality holds. Within this limit, a smaller n_B provides a lower computational load; however it also yields a higher integration loss for fast moving targets whose Doppler shift is not properly compensated. In fact, for a constant modulus signal the SNR loss for a target at range bin *l* and Doppler bin *m* can be written as:

$$L[l,m] = 20\log_{10}\left\{\frac{n_B}{N}\frac{\sin(\pi m/n_B)}{\sin(\pi m/N)}\right\} \tag{22}$$

As it is apparent, it only depends on the considered Doppler bin and reaches its maximum at the highest Doppler value considered in the 2D-CCF, while no loss is experienced at zero Doppler.

As previously mentioned, the desired cost reduction has been obtained by summing the product sequence $x_l[n]$ over each batch of length N_B. This is equivalent to apply a Low-Pass (LP) filter with rectangular impulse response to the signal $x_l[n]$. The shape of the 2D-CCF with frequency at the *l*-th range bin and the SNR loss are a direct consequence of typical sin(xN_B)/sin(x) shape of the transfer function of this specific filter. Following these considerations, different LP filters can be used to have different shape for the SNR loss vs. frequency bin while still providing the possibility to apply decimation to the sequence $x_l[n]$. The advantage of the rectangular filter is that it does not require complex multiplications, while the generic filter might require a certain number of complex multiplications, thus trading the lower SNR loss with computations. Obviously many possible solutions can be used, in particular using a cascaded integrator-comb (CIC) filter to perform the LP operation does not imply any increase in required computations, while providing lower losses. To improve the shape of the CIC filter, it is customary to use in cascade with it a FIR filter with a small number of taps (thus providing a limited increase in required computations), which is able to control the shape of the CIC transfer function (and therefore reduce the loss with target Doppler frequency). As an example, a possible approach is presented in [9] where a CIC filter operating with a decimation factor *D*=128 (N_D=*N*/*D*) is considered together with a 5th order low-pass (symmetric) FIR filter (LPF).

2.3.2.2.2. CHANNELIZATION TECHNIQUE

This sub-optimum algorithm operates by splitting the signals in the frequency domain into n_C frequency bands (channels) which are separately processed. The results can be coherently recombined to build the final map with only a limited gain loss. It can be easily obtained as a further approximation of the Batches Algorithm described above. To show its derivation, we first rewrite equation (15) and then we replace the cross correlation between the *r*-th portions of length n_C of the surveillance and the reference signals, with its approximation evaluated in the frequency domain:

$$\begin{aligned}\chi[l,m] &\cong \sum_{r=0}^{N_C-1} e^{-j2\pi\frac{mr}{N_C}} \sum_{p=0}^{n_C-1} s_{surv}[rn_C+p]\cdot s_{ref}^{*}[rn_C+p-l] \cong \\ &\cong \sum_{r=0}^{N_C-1} e^{-j2\pi\frac{mr}{N_C}} \frac{1}{n_C}\sum_{k=0}^{n_C-1} S_{surv}^{(r)}[k] S_{ref}^{(r)^*}[k] e^{+j2\pi\frac{kl}{n_C}} = \\ &= \frac{1}{n_C}\sum_{k=0}^{n_C-1} e^{+j2\pi\frac{kl}{n_C}} \sum_{r=0}^{N_C-1} Y[k,r] e^{-j2\pi\frac{mr}{N_C}}\end{aligned} \tag{23}$$

Notice that by neglecting the border effects (additional approximation with respect to the Batches Algorithm), the *r*-th sub-sequences are cyclically extended so that their cross-correlation can be evaluated in the frequency domain, as the IDFT of their individual DFTs ($S_{surv}^{(r)}[k]$ and $S_{ref}^{(r)^*}[k]$ in the second line). By rearranging the terms of the summations, the third line of equation (23) is easily obtained.

The resulting algorithm can be subdivided into four steps:

1) evaluate the DFTs of surveillance and reference signals over the N_C batches of n_C samples each;
2) compute the product of the DFTs outputs for each batch and arrange the results in the 2D sequence $Y[k,r]$ (*k*=0,..,n_C-1; *r*=0,..,N_C-1);
3) evaluate the IDFT $X[k,m]$ of $Y[k,r]$ over the index *r* for each *k* (n_C IDFTs); this step represents the parallel processing of the n_C different frequency channels in which the signals have been split;

4) evaluate the DFT of $X[k,m]$ over the index *k* for each *m* (N_C DFTs) to obtain the range samples of the 2D-CCF at the *m*-th Doppler bin.

Notice that evaluating the DFT of short sub-sequences (step 1) separates each sequence into a number of frequency channels (Channelization), that are then independently processed (steps 2-3) and then recombined to provide the final result (step 4).

Notice that the number of channels should be carefully selected since it yields a trade-off between the two adopted approximations of equation (23) which determine the final SNR loss. Specifically, increasing n_C yields a higher integration loss for fast moving targets whose Doppler shift is not properly compensated (as for the Batches Algorithm). However, in this case, reducing n_C enhances the border effects in the evaluation of the batches cross-correlations yielding additional loss for targets at higher bistatic ranges. Assuming a constant modulus signal, the SNR loss for a target at range bin *l* and Doppler bin *m* can be written as:

$$L[l,m] = 20\log_{10}\left\{\frac{1}{n_C}\frac{\sin[\pi m(n_C - l)/N]}{\sin(\pi m/N)}\right\} \tag{24}$$

As it is apparent, for *l*=0 the same Loss of the Batches Algorithm given in equation (22) is obtained at the *m*-th Doppler bin. However, in this case, the SNR Loss for a given n_C increases at higher range bins. Thus the integration loss is maximum at the highest Doppler and Range values considered in the 2D-CCF.

2.3.3. TARGET DETECTION AND TRACKING

As already mentioned, the detection process is mainly based on the evaluation of the bistatic Range-Velocity 2D-CCF between the surveillance and the reference signal. Then, an adaptive threshold can be applied on the obtained map to automatically detect the potential targets according to a specific constant false alarm rate (CFAR) detection scheme.

As well known, in order to maintain a constant probability of false alarm, the detection threshold changes according to an estimate of the noise variance.

To this purpose, the conventional cell-averaging constant false alarm rate with guarded cells algorithm (CA-CFAR) is usually exploited, [15]. Specifically, the 2D version of the CA-CFAR algorithm can be applied which operates on the full Range-Doppler surface.

Alternative CFAR algorithms can be also considered which have been devised to be effective against non-homogeneous background (e.g. Greatest Of-CFAR, GO-CFAR, and Smallest Of-CFAR, SO-CFAR) [16]-[18].

All the above CFAR schemes have well known behaviors for the standard radar systems against homogeneous and non-homogeneous background. In fact, as well known, the CA scheme shows the best performance against homogeneous disturbance background, the GO is the most effective to control the false alarm rate in the presence of disturbance showing step changes (edges) in its power level; whereas the SO avoids strong detection losses in presence of multiple targets. These three schemes have been considered for application to the PBR scheme, both in the single-frequency and in the multi-frequency approaches, aiming at a full performance comparison, as shown in the following sections.

By applying the selected CFAR scheme, a detection is declared at the Range-Doppler locations yielding values above the adaptive threshold. The detected plots are then output to the tracking stage.

Although many conventional air surveillance radars output raw detection data for tracking by an external system, it is better for a passive radar to internally track aircraft detections from each bistatic couple (Tx-Rx). In its basic version, this tracking is performed in the bistatic Range–Doppler domain.

By using an internal tracker, the system is then able to forward the associated plot data for (i) association of returns from different transmitters of the same target (in a multistatic system); (ii) target state estimation.

To this purpose the basic Kalman filter can be exploited, [19]. The measurement vector comprises measurements of range and Doppler from the 2D-CCF surface, and the state vector comprises range, Doppler (which is proportional to the range-rate), Doppler-rate. The fact that the Doppler is proportional to rate of change of range means that it is particularly easy for even the basic Kalman filter to track targets in the range-Doppler space.

Notice that, for a simple dual receiving channel PBR system, the described basic processing scheme only allows target detection and tracking over the Range-Doppler plane. Target localization in Cartesian coordinates can be then obtained by exploiting bearing information which requires the availability of multiple receiving channels for target DoA estimation.

2.4. WAVEFORMS OF OPPORTUNITY

2.4.1. FM

FM broadcasting is a broadcast technology that uses frequency modulation (FM) to provide high-fidelity sound over broadcast radio. For the FM radio broadcast in the 88-108 MHz frequency range, a nominal frequency bandwidth of 200 kHz is assigned by the standard to each FM radio channel. A typical FM radio transmission occupies generally only a frequency bandwidth of about 100 kHz inside it, with a significant power level, thus yielding a radar range resolution of about 1.5 km. Specifically, the power spectral density of the FM signal has the same shape of the probability density function (PDF) of the modulating signal's amplitude. Therefore, the actual range resolution is the first highly varying parameter, which changes with the instantaneous transmitted waveform and thus with the considered FM radio channel. In theory, the PDF is not strictly dependent on the program content and both music and voice can reach optimum conditions (namely wide bandwidths and therefore high range resolutions), which only depend on the amplitude level of the modulating signal. However, usually the average level of the music is higher than for the voice, leading to a slightly better range resolution. In contrast, the presence of long periods of silence or speech pauses in the program content can dramatically degrade the achievable range resolution.

2.4.2. WIFI

Wireless networking applications are proliferating at a very rapid rate for both commercial and private use. One of the most popular systems consists of the IEEE 802.11 Standards based (WiFi) technology, [1].

The first Standard, released in 1997, defined two data rates (1 and 2 Mbps) obtained through a DSSS modulation exploiting a 11-Barker code as spreading sequence. The chipping rate was 11 Mcps thus an actual bandwidth of 11 MHz was specified by the Standard. The adopted carrier frequencies were defined in the 2.4 GHz ISM (industrial, scientific and medical) band.

With the second release, higher data rate were defined (up to 11 Mbps) without changing the modulation and the actual signal bandwidth.

In 2003, the 802.11g Standards was released by IEEE. Data rate up to 54 Mbps were defined by exploiting an OFDM modulation. The actual bandwidth was increased up to 17 MHz while the carrier frequencies, in Europe, remained defined in 2.4 GHz ISM band.

The bandwidth of 11-17 MHz allows an equivalent radar range resolution which spans between 20 and 30 mt for a passive radar exploiting WiFi signals as waveform of opportunity. Such value is well in line with the requirements of the ATOM passive radar. Moreover, the carrier frequency of 2.4 GHz allow a velocity resolution of fraction of 1 meter per second with an integration time of 1 s.

As of 2010 an IEEE 802.11 device is installed in many personal computers, video game consoles, smart phones, printers, and other peripherals, and virtually all laptop or palm-sized computers, thus ensuring a wide coverage practically everywhere, also in the public indoor area of airport, where one or more WiFi hot-spots are almost always present.

Moreover, by exploiting the WiFi access point as transmitter of opportunity, this can be considered partially cooperative, since a copy of the transmitted signal can be obtained by inserting a directional coupler between the AP and the transmitting antenna, thus allowing an excellent capability to access a clean copy of the reference signal.

2.4.2.1. WAVEFORM CHARACTERISTICS (WIFI STANDARDS)

As already mentioned, a number of 802.11 standards have been developed and further versions are being investigated. The three most commonly being deployed are 802.11a, 802.11b and 802.11g. 802.11a is only adopted in the Regulation Domain of the United States while 802.11g represents the third generation of this wireless networking standards after 802.11 and 802.11b and maintains a full compatibility with the older standards. These standards allow different data rates and operate according to different frequency channels plans. The different data rates are achieved by exploiting different modulations and coding schemes according to the physical layer (PHY) specifications adopted by each standard. Table 2 summarizes the main possible combinations of modulations and coding schemes used by the different standards to achieve a given data rate.

Standard / PHY	Data Rate (Mbps)	Modulation	Coding scheme
802.11 / DSSS PHY + **802.11b** / HR-DSSS PHY + **802.11g** / ER-PHY (ERP)	1	DSSS	DBPSK + 11-chip Barker sequence
	2	DSSS	DQPSK + 11-chip Barker sequence
802.11b / HR-DSSS PHY + **802.11g** / ER-PHY (ERP)	5.5	DSSS	CCK (8 complex chips code) + 4 bit/symbol
	(5.5)	DSSS	PBCC (64-state binary conv. code, rate 1/2) + BPSK
	11	DSSS	CCK (8 complex chips code) + 8 bit/symbol
	(11)	DSSS	PBCC (64-state binary conv. code, rate 1/2) + QPSK
802.11g / ER-PHY (ERP)	(22)	DSSS	PBCC (256-state binary conv. code, rate 2/3) + 8-PSK
	(33)	DSSS	PBCC (256-state code, rate 2/3)+ 8-PSK + clock 16.5 MHz
802.11a / OFDM PHY + **802.11g** / ER-PHY (ERP)	6	OFDM (48 sc)	BPSK + coding rate 1/2
	9	OFDM (48 sc)	BPSK + coding rate 3/4
	12	OFDM (48 sc)	QPSK + coding rate 1/2
	18	OFDM (48 sc)	QPSK + coding rate 3/4
	24	OFDM (48 sc)	16-QAM + coding rate 1/2
	36	OFDM (48 sc)	16-QAM + coding rate 3/4
	48	OFDM (48 sc)	64-QAM + coding rate 2/3
	54	OFDM (48 sc)	64-QAM + coding rate 3/4

Table 2 – 802.11 Standards: modulations and coding schemes.

The main modulations are either Direct Sequence Spread Spectrum (DSSS) or OFDM and data rates between 1 and 54 Mbps are currently specified. It can be seen that DSSS is the most common modulation with OFDM dominating only at higher data rates.

Baseband modulation can be Differential Phase Shift Keying (DPSK), Differential Quadrature Phase Shift Keying (DQPSK), Complementary Code Keying (CCK) and 64 phase Quadrature Amplitude Modulation (64-QAM). Specifically CCK and QAM tend to be used at higher data rates. Additional Barker coding is also used at some data rates and error coding is also implemented.

There are a number of formats specified for the data unit based upon the IEE standard Physical Layer Convergence Protocol (PLCP). As an example, the long PLCP Protocol Data Unit (PPDU) for the 80211.b and 802.11g standards consists of a preamble followed by a header then the data transmission within the PLCP Service Data Unit (PSDU). The detailed structure of the PSDU is shown in Figure 8 for the case of 802.11g operating with a OFDM modulation. It is apparent that both the PPDU and the PSDU involve different combinations of modulations and coding schemes.

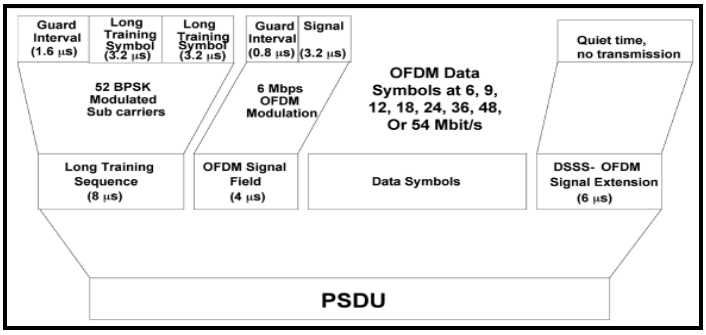

Figure 5 – Detailed format of PSDU (from [24])

Although a detailed analysis of the 802.11 wireless networking standards is not appropriate in this document, a few observations can be made as follows:

- It is clear that the overall 802.11 signal modulation and coding scheme is complex. Moreover it is strongly time-varying since the data rates used are dependent primarily on user range/signal strength.
- In practical situations the 802.11 transmitter may be broadcasting a mix of signals. In addition to a variety of data signals, an 802.11 access point transmits a regular beacon signal broadcasting its presence and channel information. The beacon signal uses a combination of DSSS/DBPSK and DSSS/DQPSK.
- Signal modulation and coding scheme change also within the single transmitted PPDU according to different formats.
- The transmission is of a pulsed type with varying and unpredictable pulse durations depending on the PPDU format and on the PSDU length.

The above characteristics obviously affect the passive radar performance since it is exploiting a time-varying waveform whose characteristics depend on those of each signal type in the mix.

2.4.3. DVB-SH

DVB-SH is the name of a mobile broadcast standard designed to deliver video, audio and data services to small handheld devices such as mobile telephones, and to vehicle-mounted devices. The key feature of DVB-SH is the fact that it is a hybrid satellite/terrestrial system that will allow the use of a satellite to achieve coverage of large regions or even a whole country. In areas where direct reception of the satellite signal is impaired, and for indoor reception, terrestrial repeaters are used to improve service availability.

It is planned to use frequencies below 3 GHz, typically S-Band frequencies around 2.2 GHz adjacent to the 3G terrestrial frequencies.

DVB-SH seeks to exploit the less congested, higher frequency, S-band where there are opportunities for Mobile Satellite Services (MSS) systems, operating in conjunction with Complementary Ground Components (CGC). In particular, on 14 February 2007, the European Commission adopted a decision making 30 MHz of S-Band spectrum harmonized and available throughout Europe for hybrid satellite/terrestrial systems. DVB-SH also leverages on the experience gained by mobile telephone operators while delivering video streams over 3G networks in cellular terrestrial networks operating in the 1.9 to 2.17 GHz UMTS band, which is adjacent to the S-band. This experience is particularly useful when planning the deployment of repeaters for good indoor coverage. And significant savings in deployment cost are expected wherever the re-use of cellular sites, including 3G antennas, will be made possible.

DVB-SH services are aimed at providing IP-based multimedia services to mobile users. These services are targeted at a single user (owner of a personal terminal) or a restricted set of users sharing the same terminal. The user can access the services while on the move, e.g. walking or while travelling in a car or on a train. The main interest is in broadcast services. Typical applications may include:

- broadcasting of classic Radio and TV content;
- broadcasting of audio or video content customized for Mobile TV (e.g. virtual TV channels, podcasts,);
- data delivery (“push”), e.g. for ring tones, logos;
- video-on-demand services;
- informative services (e.g. news) including location-based services;
- interactive services, via an external communications channel (e.g. UMTS).

Thanks to the long experience accumulated within the DVB project – in developing market-driven open standards for the provision of new services, and relying on the rich family of existing DVB standards

(DVB-H, DVB-S2, DVB-IPDC, etc.) – the DVB-SH set of specifications allows the development of products and services for user terminals that can be easily operated in dual mode with other DVB-based similar services. In particular, making reference to the DVB-H case, DVB-SH allows the present UHF-based service offer to be extended to S-Band with a common cross-border allocation, a reduced total network infrastructure cost and an expansion of the offer in terms of number of channels/services.

The DVB-SH standard provides a universal coverage by combining a Satellite Component (SC) and a Complementary Ground Component (CGC): in a cooperative mode, the SC ensures geographical global coverage while the CGC provides cellular-type coverage. All types of environment (outdoor, indoor) can then be served, either using the SC from its first day of service, and/or the CCG that is to be progressively deployed, building on the success of DVB-H. A typical DVB-SH system is based on a hybrid architecture combining a Satellite Component and, where necessary, a CGC consisting of terrestrial repeaters fed by a broadcast distribution network. The repeaters may be of three kinds:

- “Terrestrial Transmitters” are broadcast infrastructure transmitters, which complement reception in areas where satellite reception is difficult, especially in urban areas; they may be co-located with mobile cell sites or standalone. Local content insertion at that level is possible, relying on adequate radio-frequency planning and/or waveform optimizations.
- “Personal Gap-fillers” have limited coverage, providing local on-frequency re-transmission and/or frequency conversion; a typical application is indoor enhancement of satellite coverage; no local content insertion is possible.
- “Mobile transmitters” are mobile broadcast infrastructure transmitters creating a “moving complementary infrastructure”. Typical use is for trains, commercial ships or other environments where continuity of satellite and terrestrial reception is not guaranteed by the fixed infrastructure.

2.4.3.1. DVB-SH ARCHITECTURES

OFDM (Orthogonal Frequency Division Multiplexing) is the natural choice for terrestrial modulation and is the basis of both the DVB-H and DVB-T systems. DVB-SH introduces a second scheme, a Time Division Multiplex (TDM), leading to two reference architectures termed SH-A and SH-B:

- SH-A uses OFDM both on the satellite and the terrestrial link;
- SH-B uses TDM on the satellite link and OFDM for the terrestrial link.

For the OFDM, the possible choices are QPSK, 16-QAM and non-uniform 16-QAM with support for hierarchical modulation. A 1K mode is proposed: in addition to the usual 2K, 4K and 8K modes which does not exist in either DVB-T or DVB-H. The 1K mode targets mainly L-Band where the planned channel bandwidth is 1.75 MHz. For the TDM part, the choices are QPSK, 8-PSK, 16-APSK for power and spectral-efficient modulation formats, with a variety of roll-off factors (0.15, 0.25, 0.35).

When assessing whether SH-A or SH-B should be selected, two main classes of satellite payloads may be considered:

- Single DVB-SH physical layer multiplex per high-power amplifier (HPA);
- Multiple DVB-SH physical layer multiplex per high-power amplifier. This is the case with a multi-beam satellite with reconfigurable antenna architecture, based on large-size reflectors fed by arrays.

In the case of a single-carrier per HPA payload configuration, exploitation of the SH-B (TDM) configuration reduces the signal envelope peak-to-average factor, thus allowing HPA optimum operation close to its saturated power. SH-A is instead penalized by its intrinsic multi-carrier (OFDM) signal nature that requires a higher optimum HPA back-off. However, in the case of a multi-carrier onboard HPA operation, there is little or no difference between the performances obtainable with the SH-A or SH-B configurations. In summary, SH-A requires satellite transponders operated in a quasi-linear mode, whereas SH-B targets satellite transponders operated at full saturation.

2.4.3.2. DVB-SH NETWORK CONFIGURATION

Considering spectrum allocation, SH-B needs a dedicated sub-band for satellite transmission, completed with a part of the sub-band available for the terrestrial local component to re-enforce reception of the satellite programs. Conversely, SH-A allows on-channel terrestrial repetition of the satellite content in the same sub-band as the satellite transmission, leaving all the remaining sub-bands available for terrestrial-only transmission.

On the other hand, for the SH-A case, not only the modulation type (OFDM vs. TDM) is re-used between satellite and terrestrial links, but also the sub-carrier's modulation and coding are strictly identical to allow a repetition at the same carrier frequency in an SFN mode. For the SH-B variant, the carrier's parameters are independent; only the content of the satellite carrier should be repeated on the terrestrial one.

Taking the example of a 15 MHz MSS band, split into three sub-bands of 5 MHz, there would be three satellite spots allocated to three countries, with each country able to reuse two sub-bands of 5 MHz for terrestrial-only transmission.

In SH-A systems, the terrestrial repeaters strictly generate the same carrier symbols as the satellite, in the same 5 MHz sub-band. Each transmitter is synchronized with its neighbors and with the satellite. This synchronization is based on the transmission of a "SHIP" packet, very similar to DVBT's MIP, which allows SH-frames to be synchronized together at the output of transmitters, the terrestrial ones being slaves of the satellite signal. The feeding network includes compensation for the earth-space delays and the signal regeneration at the terrestrial level, thus producing an overall earth-space SFN broadcast network. Two full sub-bands of 5 MHz remain available for terrestrial only

transmission.

In SH-B systems, a different 5 MHz sub-band is used to transmit the satellite content via a terrestrial network in areas where it needs to be re-enforced. Since the receiver can make use, at the physical layer level, of both the symbols received from the satellite and the terrestrial transmitters, the same synchronization technique is applied as for SH-A. Hence information symbols from a given program are close enough in time to be combined at the decoder input to improve the overall link performance. Furthermore, terrestrial transmission (because of its higher signal-to-noise ratio) allows higher spectrum efficiency than the broad satellite transmission. Therefore, the terrestrial carrier can convey additional local content in the same 5 MHz terrestrial sub-band which repeats the satellite content. As a result, out of the 15 MHz MSS band, there is one full 5 MHz sub-band plus a portion of a second 5 MHz sub-band available for terrestrial-only transmission.

3. ARCHITECTURES FOR PBR RECEIVERS

3.1. DIRECT-CONVERSION (HOMODYNE) RECEIVER

In this approach, all the in-band potential channels are frequency translated from the RF directly to baseband (BB) using a single mixer stage. Energy from undesired channels is easily removed with a filtering stage at baseband. In this receiver, there is no need for IF filtering stage to perform image-rejection. Different problems are associated with this architecture: the LO is at the same frequency of the RF carrier. As a consequence the unintentional leakage of LO signal in the RF signal path is reflected off by other components and can be "re-received" by the mixer. The self-mixing with LO results in a time-varying Direct Current (DC) offset at the mixer output that reduces the dynamic range of the receiver. In this receiver, the selection of the desired channel is performed by the baseband filter or in a digital domain.

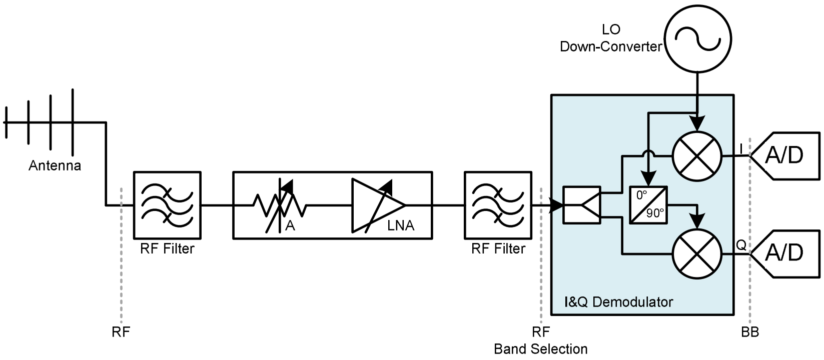

Figure 6 - Architecture Direct-Conversion receiver

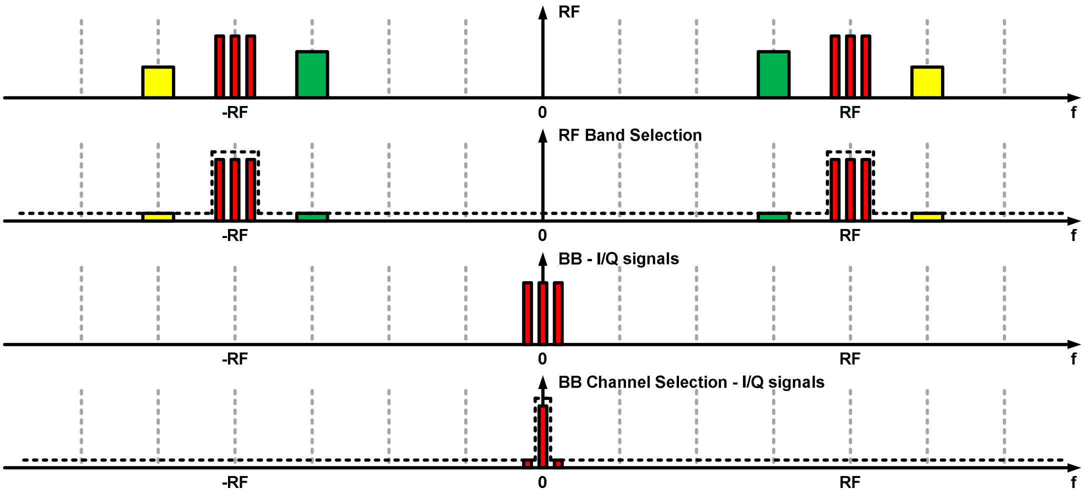

Figure 7 - Direct-Conversion receiver working principle

3.2. SINGLE-CONVERSION (SUPER HETERODYNE) RECEIVER

Most RF commercial communication transceivers today utilize a super heterodyne approach. In this system, the Radio Frequency (RF) Front-End (FE) filter is used to remove out of-band energy and perform rejection of image-band signals. The noise or image-rejection filter, which follows the Low Noise Amplifier (LNA), further attenuates the undesired signals present at the image frequencies. An RF channel-select Local Oscillator (LO) tunes the desired band to a fixed Intermediate Frequency (IF). The IF filters, typically in combination with a variable gain amplifier, reduce the distortion and dynamic range requirements of the subsequent receiver blocks. Also, the IF filters perform the desired telecommunication channel selection for a PBR system. After the IF section, the signals can then be sampled using a sub-sampling approach; with this approach the IF filters act as the A/D converter's anti alias filters. The superheterodyne receiver is currently used in the FM and DVB-T common receivers (whit different IF values). The principal drawback of this architecture is the strong characteristic of the RF filter, which is required to reject the image frequency (in particular for TV signals is necessary a variable RF tracking filter with a notch in correspondence of the image frequency).

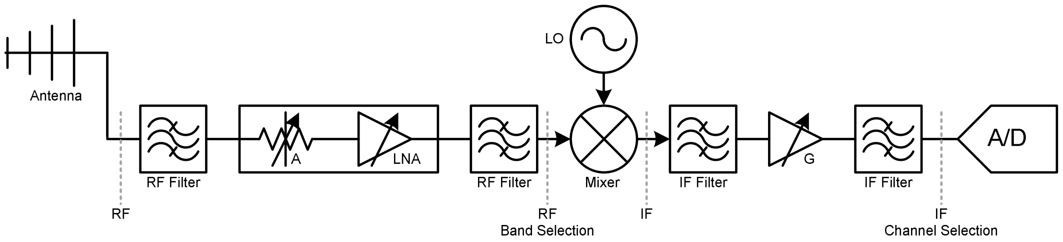

Figure 8 – Architecture Single-Conversion receiver

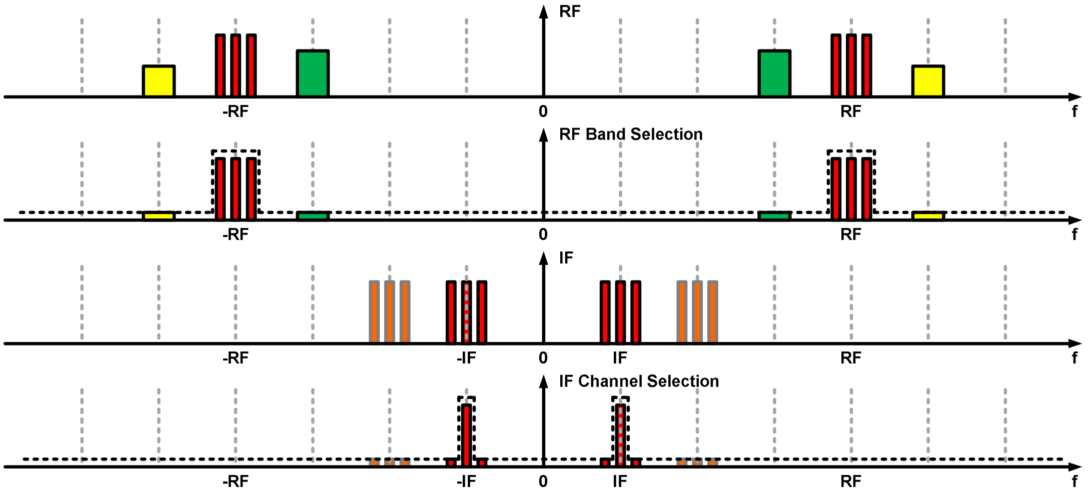

Figure 9 –Single-Conversion receiver working principle

3.3. DOUBLE-CONVERSION (UP & DOWN) RECEIVER

This receiver system, reported in Figure 10, frequency translates the desired channel from RF to an IF greater than the maximum carrier frequency for the selected channel band (up-conversion), using a mixer with a variable frequency LO. A band-pass filter stage is used at IF to remove any undesired up-converted frequency components (including the image-band signal), allowing only desired channel (or a small group of adjacent desired channels) to pass to the second mixer stage. The selected channel at IF is then frequency translated directly to baseband, or to a very low IF, using a fixed frequency synthesizer.

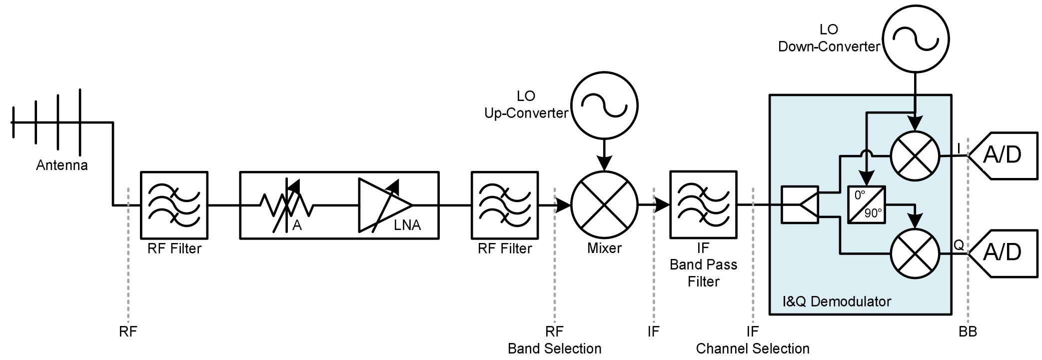

Figure 10 - Architecture Double-Conversion receiver

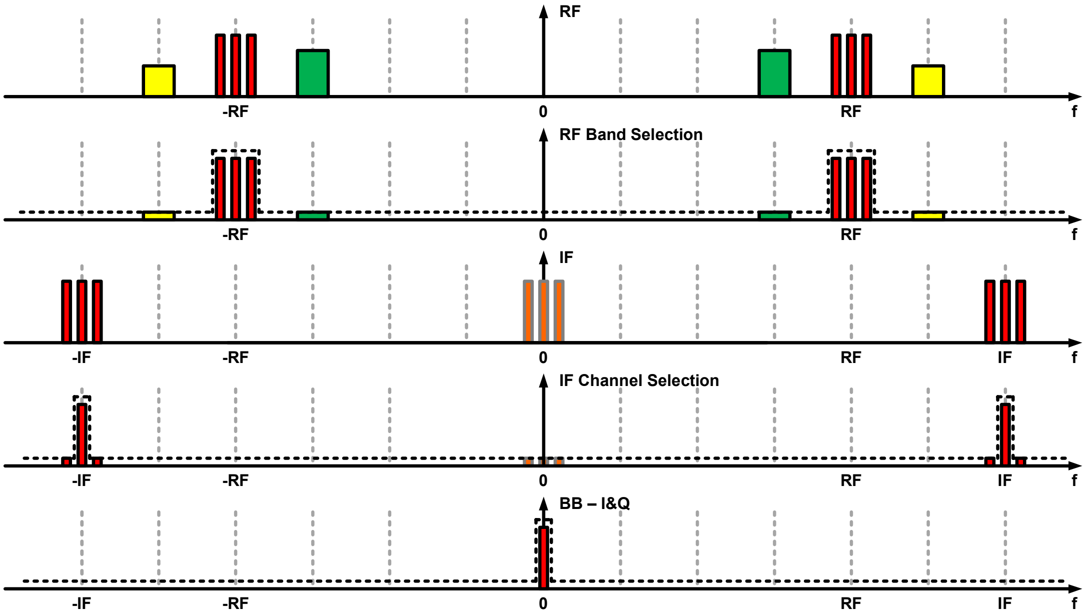

Figure 11 - Double-Conversion receiver working principle

3.4. DIRECT RF SAMPLING RECEIVER

Direct RF Sampling is considered the ultimate goal of the digitals receivers with all the tuning and filtering performed by digital signal processing. In a digital receiver, a single A/D converter is used to digitize the received signal, and digital processing is used to perform the down-conversion to I and Q baseband signals. Continuing advantages in sampling speeds are leading to sampling at increasing frequencies, with the possibility approaching of sampling at very high IF or directly at RF. The benefits of this architecture, with respect to the conventional analog I and Q demodulation, are:

- Virtual elimination of I and Q imbalance,
- Virtual elimination of DC offset errors,
- Improved linearity,
- Flexibility of bandwidth and sample rate,
- Tight filter tolerance, phase linearity, and improved anti-aliasing filtering,
- Reduced component cost, size and weight.

The advantage being the almost complete elimination of analog hardware. However, not only does the A/D converter have to sample the RF directly, but unless it is preceded by tunable RF pre-selector filter, the A/D converter input must have the dynamic range to handle all off the signal present in the band of interest simultaneously. Generally, the interference power entering the A/D converter is proportional to the bandwidth of components in front of the A/D converter.

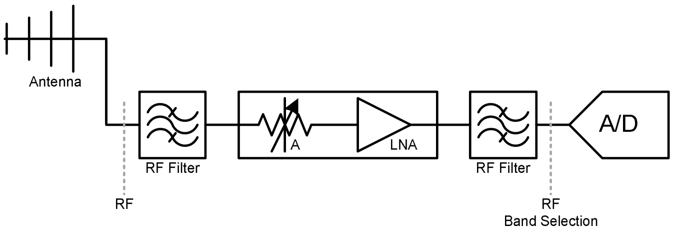

Figure 12 - Architecture Direct RF sampling receiver

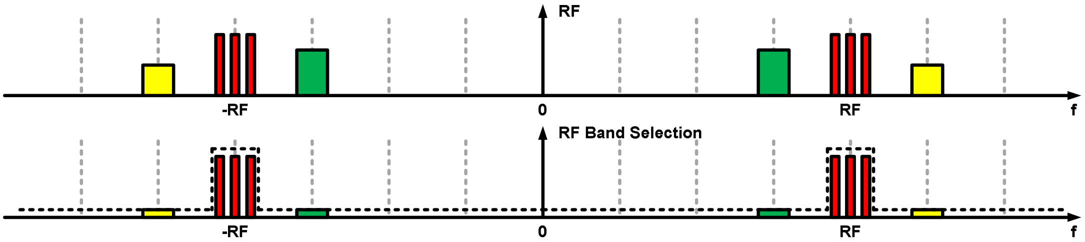

Figure 13 - Direct RF sampling receiver working principle

4. FM-BASED PBR

4.1. INTRODUCTION

An overview of the ARGUS 3D project is provided in the following Section. The FM-based PBR general requirements are reported in Section 4.3. A prototype description of two passive receiver developed is reported in Section 4.4. In Sections 4.5 and 4.6 tests, controlled experiments and the acquisition campaigns are described. Finally, in Section 4.7 summarize the results obtained with the passive sensor in air traffic control application (with commercial and cooperative targets).

4.2. ARGUS 3D EU PROJECT

This section introduces the ARGUS 3D (AiR GUidance and Surveillance 3D) project funded by the European Union (FP7). This project intends to improve the current ATC systems for civil applications, extending their coverage and making them able to detect, recognize and track NCTs, by means of innovative sensors, such as a new enhanced Primary Surveillance Radar (PSR), passive and bistatic radar network.

The recent terroristic acts, e.g. the failed attempt in December 2009 on the flight Amsterdam-Detroit, the attempt in Moscow airport in January 2011 and the current international situation, increased the awareness about the possibility of large-scale, terrorist offensive actions delivered against civil society by means of A/C, that can be used either for carrying out “kinetic attacks” (i.e. crashing planes into buildings) or for delivering chemical and/or biological pollutants. As a consequence, the security theme in the air transportation field, with specific reference to people protection, became central.

Conventional ATC systems for civil applications cover large airspace and are able to locate cooperative and non-cooperative A/C, and to identify only cooperative A/C (i.e. those responding to the interrogations from the Secondary Surveillance Radar - SSR), but are characterized by the following main drawbacks, [15]:

- they do not assure the full coverage, particularly at low altitudes, due to the presence of the so called radar blind zones (i.e. regions where the radar coverage of the PSR and of the SSR are almost ineffective);
- they are not able to fully localize NCTs, because the PSR only returns range and azimuth angle and without response by airborne transponder no information is available concerning the A/C altitude;
- they are not able to identify NCTs, that could be either hostile A/C approaching a forbidden area and/or somehow threatening the homeland security (and therefore deserving a counteraction by the responsible for homeland security) or friend A/C having a breakdown (and therefore requiring some kind of help);
- they are unable to detect A/C characterized by a low value of RCS, because they are tailored for efficiently monitoring large A/C.

The above mentioned limitations are addressed by the ARGUS 3D project, funded by the European Union, 7th framework program, Theme #10 Security, Grant agreement no. 218041, [20]. ARGUS 3D is a 3 year project which started in December 2009. Its consortium is composed of 12 partners from 5 EU Member States (Italy, UK, Germany, Poland, Spain), including industry, research organizations and final users.

In order to achieve this general objective, the ARGUS 3D project intends to carry out research and development activities with the aim of improving the current ATC systems for civil applications, extending their coverage and making them able to detect, recognise and track NCTs.

The scientific and technical objective of ARGUS 3D project is related to conceiving, designing and implementing an innovative, low-cost, multi-sensor, radar-based system for 3D air guidance and surveillance that integrates conventional surveillance systems currently used for civil applications and three classes of non-conventional radar systems:

- innovative PSR sensors;
- networks of multi-operational, high-performing passive radar sensors, [21]-[22];
- bistatic radar sensors, [23].

ARGUS 3D system is composed by two main blocks. The first one is composed by the traditional systems: PSR, SSR, Automatic Dependent Surveillance - Broadcast (ADS-B), etc.; the second one is related to the innovative surveillance systems. These new systems, are composed by:

- innovative PSR sensor, i.e. an enhanced PSR with monopulse estimation capability in the vertical plane, able to provide the altitude information for any detected target, by exploiting the two antenna beams already available inside standard 2D ATC radar;
- network of (low cost) passive radar sensors, which are able to detect and track objects by processing reflections from non-cooperative sources of illumination already available in the environment (e.g. FM Radio, DVB-T, DAB, GSM, etc.);
- bistatic radar sensors, which are able to detect and track potential targets by using the emission of cooperative or non-cooperative primary radar.

The improvement of the overall ARGUS 3D system is given by the combination of the information provided by the conventional and innovative systems which can compensate each other. For example, where the radar coverage of the PSR and of the SSR are almost ineffective (i.e. small and/or low-flying aircrafts), the new passive sensors can act as gap-filler, thus reducing the radar blind zone. Where the two systems are both available, a performance improvement can be obtained, due to the following reasons:

- several systems that observe the same scene by different points of view and in different ways can increase confidence (more than one sensor can confirm the same target);
- the joint information from multiple sensors reduces the set of hypotheses about the target and hence the decision ambiguity and/or improves the estimate of useful parameters (e.g passive radars provide a good velocity estimation).

As a consequence, data fusion and data management play a significant role in the final system.

4.3. FM-BASED PBR GENERAL REQUIREMENTS

4.3.1. FM-BASED PBR IDEAL REFERENCE SCENARIOS

To set appropriate requirements for a passive radar based on FM radio broadcast signal, we start by defining a limited number of reference scenarios, that include:

a) transmitters geometry;

b) receiver location;

c) receiver antenna beam characteristics and pointing;

d) location of desired target detection area;

to complete the scenario definition, the distribution of the power levels emitted in the FM-band must also be specified, which requires:

- FM broadcast channel allocation on each transmitter;

- Equivalent Isotropic Radiated Power (EIRP) of each transmitter;

4.3.1.1. FM TRANSMITTERS GEOMETRY

In the following, these items are individually considered to cover the different possibilities for the reference scenario. The considered reference scenarios include transmitters located ideally with regular cellular schemes as reported in Figure 14.

To estimate the power level received by the surveillance antenna in an area covered by a wide set of transmitters disposed at the center of hexagonal cells (see Figure 14), we operate under the following hypotheses:

- all transmitters operate with the same EIRP;
- all transmitters have isotropic antennas in the horizontal plane;
- the distance between transmitters is D (namely the hexagonal cells have radius D/√3).

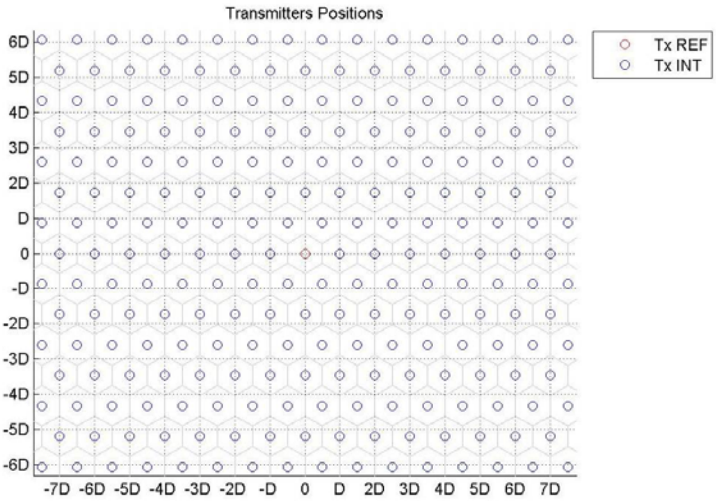

Figure 14 – Wide area covered by hexagonal cell served by broadcast transmitters in the cell center

4.3.1.2. RECEIVER LOCATION AND ANTENNA POINTING

We consider the receiver to be positioned on specific lines, at distance L from the axis origin. Two case studies are considered in the following for the receiver position:

a) along the y axis (see Figure 15);
b) along a line at 30° from the y axis (see Figure 16);

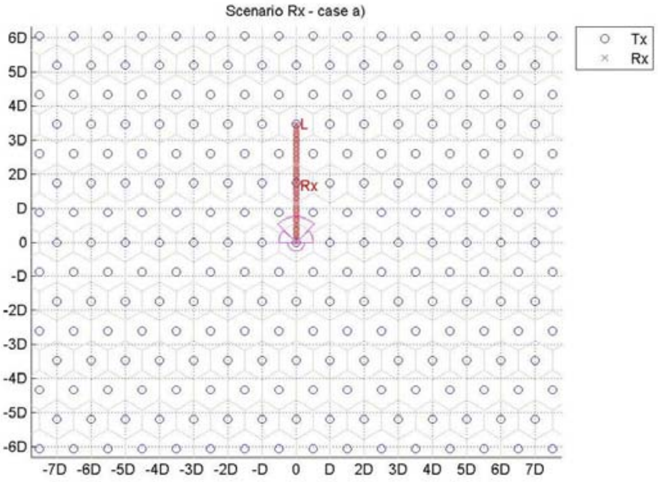

Figure 15 – Receiver position and antenna pointing angle – case a).

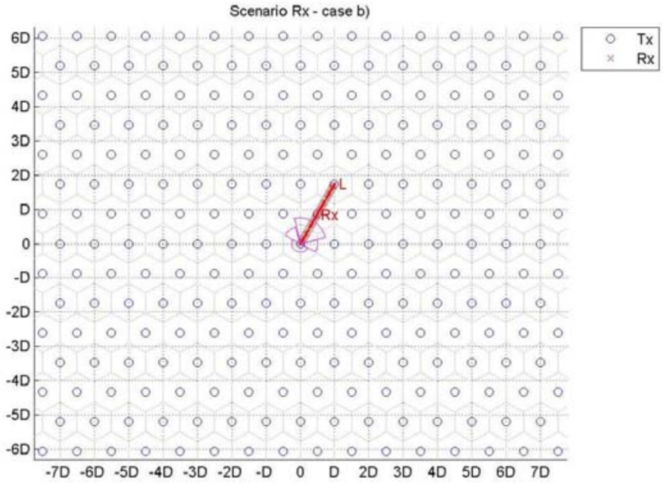

Figure 16 – Receiver position and antenna pointing angle – case b)

4.3.1.3. RECEIVER ANTENNA BEAM CHARACTERISTICS

The antenna is assumed to be steered along the considered line with its back-lobe directed toward the axis origin. The following antenna patterns are considered:

i) step pattern with gain $G(\phi)=\begin{cases} G_0 \; dB, & |\phi|<\pi/4 \\ G_0-10\,dB, & \pi/4 \le |\phi| < \pi/2 \\ G_0-20\,dB, & \pi/2 \le |\phi| < \pi \end{cases}$ where G_0=7 dB

ii) step pattern with gain $G(\phi)=\begin{cases} G_0+1.76 \; dB, & |\phi|<\pi/6 \\ G_0-8.24\,dB, & \pi/4 \le |\phi| < \pi/2 \\ G_0-18.24\,dB, & \pi/2 \le |\phi| < \pi \end{cases}$ where G_0=7 dB

iii) step pattern with gain $G(\phi)=\begin{cases} G_0+3 \; dB, & |\phi|<\pi/8 \\ G_0-7\,dB, & \pi/4 \le |\phi| < \pi/2 \\ G_0-17\,dB, & \pi/2 \le |\phi| < \pi \end{cases}$ where G_0=7 dB

iv) log periodic antenna with 7dBi of directivity in Vertical polarization $\begin{cases} |\phi_{-3dB}| = 66^\circ \\ |\phi_{-10dB}| = 118^\circ \end{cases}$

v) log periodic antenna with 9dBi of directivity in Vertical polarization $\begin{cases} |\phi_{-3dB}| = 50^\circ \\ |\phi_{-10dB}| = 72^\circ \end{cases}$

vi) log periodic antenna with 11dBi of directivity in Vertical polarization $\begin{cases} |\phi_{-3dB}| = 43^\circ \\ |\phi_{-10dB}| = 57^\circ \end{cases}$

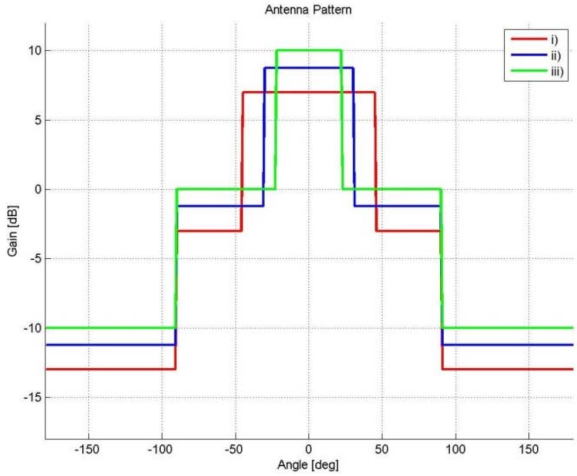

Figure 17 – Antenna pattern (azimuth plane) for case i), ii) and iii).

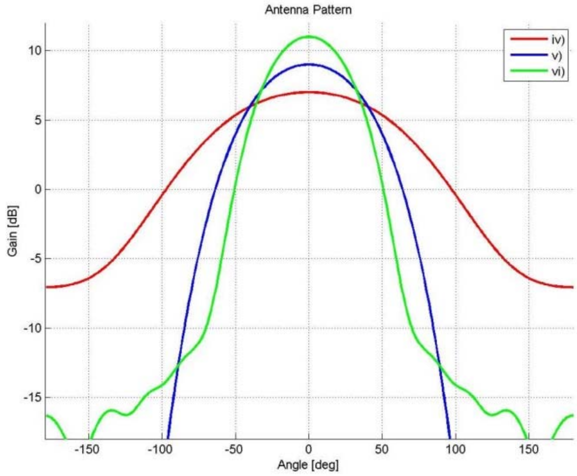

Figure 18 – Antenna pattern (azimuth plane) for case iv), v) and vi).

4.3.1.4. RECEIVER POWER LEVELS UNDER FREE-SPACE PROPAGATION

Assuming free-space propagation, the power received from the $i-th$ transmitter at location (x_i, y_i) can be written as:

$$P_i(L) = \frac{EIRP\,\lambda^2}{(4\pi)^2} \frac{G\left(\tan^{-1}\left[x_i/(y_i-L)\right]\right)}{\left(y_i-L\right)^2+x_i^2} \tag{25}$$

By using the value of the transmitters distance D, the equation above can be rewritten as:

$$P_i(L) = \frac{EIRP\,\lambda^2}{(4\pi)^2} \frac{G\left(\tan^{-1}\left[x_i/(y_i-L)\right]\right)}{\left(y_i-L\right)^2+x_i^2} \tag{26}$$

$$P_i(L) = \frac{EIRP\,\lambda^2}{(4\pi)^2 D^2} \frac{G\left(\tan^{-1}[(x_i/D)/(y_i/D-L/D)]\right)}{\left(\frac{y_i}{D}-\frac{L}{D}\right)^2+\left(\frac{x_i}{D}\right)^2} \tag{27}$$

By introducing the normalized transmitter coordinates $x_{i\,N} = x_i / D, \quad y_{i\,N} = y_i / D$, namely the coordinates expressed in terms of multiples of the transmitters distance D , and denoting with $l = L / D$ the normalized receiver distance from the reference transmitter, we have

$$P_i(l;\, D) = \frac{EIRP\, \lambda^2}{(4\pi)^2 D^2} \; \frac{G\left(\tan^{-1}[x_{i\,N} / (y_{i\,N} - l)] \right)}{\left(y_{i\,N} - l\right)^2 + x_{i\,N}^2} \tag{28}$$

If we denote with $i = 0$ the reference transmitter, at position $(0,0)$, the power from the reference transmitter is

$$P_0(l;\, D) = \frac{EIRP\, \lambda^2}{(4\pi)^2 D^2} \; \frac{G(\pi)}{l^2} \tag{29}$$

Similarly, the interfering power is given by

$$P_{\text{int}}(l;\, D) = \sum_{i=1}^{\infty} P_i(l;\, D) = \frac{EIRP\, \lambda^2}{(4\pi)^2 D^2} \sum_{i=1}^{\infty} \frac{G\left(\tan^{-1}[x_{i\,N} / (y_{i\,N} - l)] \right)}{\left(y_{i\,N} - l\right)^2 + x_{i\,N}^2} \tag{30}$$

And finally, the total power is

$$P_{tot}(l;\, D) = \sum_{i=0}^{\infty} P_i(l;\, D) = \frac{EIRP\, \lambda^2}{(4\pi)^2 D^2} \sum_{i=0}^{\infty} \frac{G\left(\tan^{-1}[x_{i\,N} / (y_{i\,N} - l)] \right)}{\left(y_{i\,N} - l\right)^2 + x_{i\,N}^2} \tag{31}$$

As apparent, the transmitters distance D only acts as a scaling factor on the received power level, while the geometric terms are independent of it and only dependent on l. In particular, we can define the geometric terms:

$$g_0(l) = \frac{G(\pi)}{l^2} \tag{32}$$

$$g_{\text{int}}(l) = \sum_{i=1}^{\infty} \frac{G\left(\tan^{-1}[x_{i\,N} / (y_{i\,N} - l)] \right)}{\left(y_{i\,N} - l\right)^2 + x_{i\,N}^2} \tag{33}$$

$$g_{tot}(l) = \sum_{i=0}^{\infty} \frac{G\left(\tan^{-1}[x_{i\,N} / (y_{i\,N} - l)] \right)}{\left(y_{i\,N} - l\right)^2 + x_{i\,N}^2} \tag{34}$$

So that the different power contributions can be written as:

$$P_0(l;\, D) = \frac{EIRP\, \lambda^2}{(4\pi)^2 D^2} \; g_0(l) \tag{35}$$

$$P_{\text{int}}(l;\, D) = \frac{EIRP\, \lambda^2}{(4\pi)^2 D^2} \; g_{\text{int}}(l) \tag{36}$$

$$P_{tot}(l;\, D) = \frac{EIRP\, \lambda^2}{(4\pi)^2 D^2} \; g_{tot}(l) \tag{37}$$

The three geometric terms g_0 , g_{int} and g_{tot} are shown in the following with reference to different receiver configurations (cases a) and b) of section 4.3.1.2) are shown for in A.1 for different antenna patterns.

As apparent from the different figures, as the receiver moves away from the reference transmitter, the ratio P_{TOT}/P_0 increases, starting from about 0 dB for low values of $l = L/D$ and reaching values up to $40dB$ for $l = L/D$ getting close to one. Higher values are obtained when getting very close to a different transmitter, where the power level received from this transmitter becomes dominant.

4.3.1.5. RECEIVER POWER LEVELS UNDER FLAT-EARTH PROPAGATION

The results in the previous section were obtained with reference to a free-space propagation model, which is a very rough approximation at the FM radio frequencies, considering the height of transmitters and receivers. To check whether these results change with the considered propagation model, we consider a flat-Earth propagation with a single ray (see Figure 19) . The power received from the $i-th$ transmitter at location (x_i, y_i) can be written as:

$$P_i(L) = \frac{EIRP\,\lambda^2}{(4\pi)^2}\;\frac{G\left(\tan^{-1}[x_i/(y_i-L)]\right)}{(y_i-L)^2+x_i^2}\cdot F_i^2 \tag{38}$$

Where

$$F_i = \left|1+\rho\, e^{j\phi}\, e^{-jk_0(R_2-R_1)}\right| \tag{39}$$

and $k_0 = \omega/c$ is the wavenumber, being ω the angular frequency. With reference to **Figure 19**, it can be seen that $R_1 = \left[d^2+(h_2-h_1)^2\right]^{1/2}$ and $R_2 = \left[d^2+(h_1+h_2)^2\right]^{1/2}$.

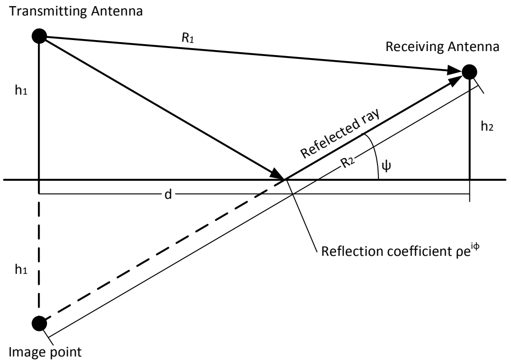

Figure 19 – Flat-Earth propagation geometry.

We assume

$$\rho\, e^{j\phi} = \frac{(\kappa - j\chi)\sin\psi - \sqrt{(\kappa - j\chi)\cos^2\psi}}{(\kappa - j\chi)\sin\psi + \sqrt{(\kappa - j\chi)\cos^2\psi}} \tag{40}$$

where $\chi = \sigma_1/\omega\varepsilon_0$. Typical values for the dielectric constant κ are around 15 , while the conductivity σ_1 might range from 10^{-3} to $3\times10^{-3}S/m$, with $10^{-2}S/m$ being a typical value for flat prairie land.

By using the normalized quantities, (38) becomes:

$$P_i(l;\,D)=\frac{EIRP\,\lambda^2}{(4\pi)^2\,D^2}\;\frac{G\left(\tan^{-1}\left[x_{i\,N}\,/\,(y_{i\,N}-l)\right]\right)}{\left(y_{i\,N}-l\right)^2+x_{i\,N}^2}\;\;F_i^{\,2} \tag{41}$$

The power from the reference transmitter becomes

$$P_0(l;\,D)=\frac{EIRP\,\lambda^2}{(4\pi)^2D^2}\;\frac{G(\pi)}{l^2}\;F_0^{\,2} \tag{42}$$

Similarly, the interfering power is given by

$$P_{\text{int}}(l;\,D)=\sum_{i=1}^{\infty}\,P_i(l;\,D)=\frac{EIRP\,\lambda^2}{(4\pi)^2D^2}\;\sum_{i=1}^{\infty}\;\frac{G\left(\,\tan^{-1}\left[x_{i\,N}\,/\,(y_{i\,N}-l)\right]\,\right)}{\left(y_{i\,N}-l\right)^2+x_{i\,N}^2}F_i^{\,2} \tag{43}$$

And finally, the total power is

$$P_{tot}(l;\,D)=\sum_{i=0}^{\infty}\,P_i(l;\,D)=\frac{EIRP\,\lambda^2}{(4\pi)^2D^2}\;\sum_{i=0}^{\infty}\;\frac{G\left(\,\tan^{-1}\left[x_{i\,N}\,/\,(y_{i\,N}-l)\right]\,\right)}{\left(y_{i\,N}-l\right)^2+x_{i\,N}^2}F_i^{\,2} \tag{44}$$

The transmitters distance D acts as a scaling factor on the received power level, but also influences the multipath factor F. The geometric terms must now be changed into:

$$g_0(l)=\;\frac{G(\pi)}{l^2}F_0^{\,2} \tag{45}$$

$$g_{\text{int}}(l)=\;\sum_{i=1}^{\infty}\;\frac{G\left(\,\tan^{-1}\left[x_{i\,N}\,/\,(y_{i\,N}-l)\right]\,\right)}{\left(y_{i\,N}-l\right)^2+x_{i\,N}^2}\;F_i^{\,2} \tag{46}$$

$$g_{tot}(l)=\;\sum_{i=0}^{\infty}\;\frac{G\left(\,\tan^{-1}\left[x_{i\,N}\,/\,(y_{i\,N}-l)\right]\,\right)}{\left(y_{i\,N}-l\right)^2+x_{i\,N}^2}F_i^{\,2} \tag{47}$$

So that the different power contributions power can be written as:

$$P_0(l;\,D)=\frac{EIRP\,\lambda^2}{(4\pi)^2D^2}\;g_0(l) \tag{48}$$

$$P_{\text{int}}(l;\,D)=\frac{EIRP\,\lambda^2}{(4\pi)^2D^2}\;g_{\text{int}}(l) \tag{49}$$

$$P_{tot}(l;\,D)=\frac{EIRP\,\lambda^2}{(4\pi)^2D^2}\;g_{tot}(l) \tag{50}$$

As a reference evaluation of the expected power levels, the following values are considered in the analysis reported below:

- Tx antenna height (common to all transmitters): $h_{Tx}=200m$
- Rx antenna height: $h_{Rx}=30m$
- Distance between Txs: $D=40km$
- Dielectric constant: $\kappa=15$
- Conductivity: $\sigma_1=10^{-2}S\,/\,m$
- Angular frequency: $\omega=2\pi\times 98\,MHz$ (center frequency of the FM band).

The three geometric terms g_0, g_{int} and g_{tot} for the Flat-Earth propagation model are shown for the receiver configurations of case a) and b) in A.2 for different antenna patterns.

Similarly to the case of free-space propagation, as the receiver moves away from the reference transmitter, the ratio P_{TOT}/P_0 increases, starting from about $0dB$ for low values of L/D reaching values up to $40dB$ and sometimes even $50dB$ for $l=L/D$ getting close to one. Higher values are obtained when getting very close to a different transmitter, where the power level received from this transmitter becomes dominant.

4.3.1.6. TARGET ECHO POWER LEVEL UNDER FREE-SPACE PROPAGATION

The power level of the received echo signal backscattered by the air target can be written as follows:

$$P_{echo}(R_{Tx};R;\varphi)=\frac{EIRP\,\lambda^2\sigma}{(4\pi)^3\,R_{Tx}^2R^2}G(\varphi) \tag{51}$$

where σ is the target radar cross section (RCS), φ is the target angle measured at the receiver while R_{Tx} and R are the distances between the target and the Tx and Rx, respectively.

Assuming that the target position is aligned with the $Tx-Rx$ baseline, the equation above becomes:

$$P_{echo}(L;R)=\frac{EIRP\,\lambda^2\sigma}{(4\pi)^3\,R^2(L+R)^2}G_{FRONT} \tag{52}$$

where G_{FRONT} is the maximum receive antenna gain corresponding to the beam pointing angle. Using the same scale factor introduced in the previous sections, we can rewrite:

$$P_{echo}(L;R)=\frac{EIRP\,\lambda^2}{(4\pi)^2D^2}\;\frac{G_{FRONT}\sigma}{4\pi R^2(L+R)^2}D^2 \tag{53}$$

Therefore we define the following geometric term:

$$g_{echo}(L;D;R)=\frac{G_{FRONT}\sigma}{4\pi R^2(L+R)^2}D^2 \tag{54}$$

By recalling that

$$g_0(l)=\frac{G(\pi)}{l^2}=\frac{G(\pi)}{(L/D)^2}=\frac{G_{BACK}}{(L/D)^2} \tag{55}$$

We can write g_{echo} as a function of g_0, as:

$$g_{echo}(L;D;R)=g_0\frac{G_{FTB}L^2\sigma}{4\pi R^2(L+R)^2} \tag{56}$$

Two target scenarios are considered in the following to evaluate the received power levels:

- for the receiver configuration of case a), the target scenario is represented in **Figure 20**; 5 different target positions are considered along the y axis with varying distances from the receiver.

- for the receiver configuration of case b), the target scenario is represented in **Figure 21**; the same values for target-receiver distances are considered by setting 5 target positions along a line at 30° from the y axis.

Notice that, in both figures, the antenna pattern of type i) has been represented. However, in the following, the analysis is extended to all the considered receive antenna patterns.

Specifically, the geometric terms g_0, g_{int} g_{tot} and g_{echo}, for the free-space propagation model, are compared in the figures reported in A.3. Each figure is composed by 4 sub-figures which have been obtained for different values of the Txs distance D ($10km$, $20km$, $40km$, $80km$). The RCS is assumed equal to $10\,dB$ in all cases.

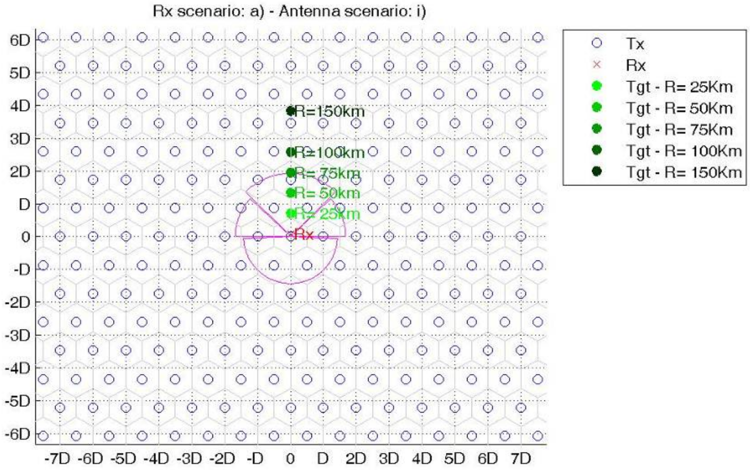

Figure 20 – Scenario Target for case a), antenna i).

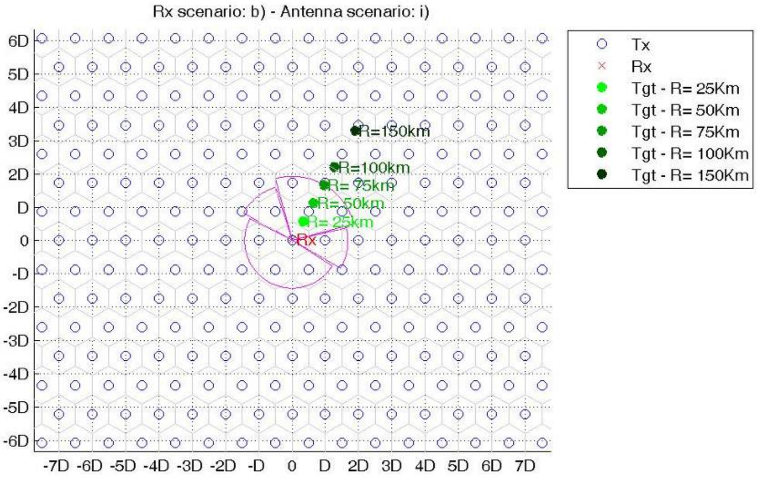

Figure 21 – Scenario Target for case b), antenna i).

A detailed analysis of the figures above allows to set the required global dynamic range, depending on the distance between the target and the receiver; the obtained values are reported in Table 3.

Target distance	From	To
25 Km	90 dB	110 dB
50 Km	100 dB	120 dB
75 Km	105 dB	125 dB
100 Km	110 dB	130 dB
150 Km	120 dB	140 dB
25 Km	90 dB	110 dB

Table 3 –Dynamic range vs the Rx-target distance under free-space propagation.

4.3.1.7. TARGET ECHO POWER LEVEL UNDER FLAT-EARTH PROPAGATION

Similarly to the case of the power levels received directly by the transmitters, the impact of a more realistic propagation model is investigated for the echo backscattered from the target. In this case, the equation (54) for the geometric term for the echo signal is modified by introducing the required multipath factors, as follows:

$$g_{echo}(L;D;R) = \frac{G_{FRONT}\sigma}{4\pi R^2 (L+R)^2} D^2 F^2_{Tx-Tgt} F^2_{Tgt-Rx} \tag{57}$$

where F_{Tx-Tgt} is the multipath factor between the reference transmitter and the target position, and F_{Tgt-Rx} is the multipath factor between target position and receiver. The corresponding equations are reported below:

$$F_{Tx-Tgt} = \left|1 + \rho\, e^{j\phi}\, e^{-jk_0 R_{Tx})}\right| \tag{58}$$

with $R_{Tx} = \left[d^2_{Tx-Tgt} + (h_{Tx} + h_{Tgt})^2\right]^{1/2} - \left[d^2_{Tx-Tgt} + (h_{Tgt} - h_{Tx})^2\right]^{1/2}$, and

$$F_{Tgt-Rx} = \left|1 + \rho\, e^{j\phi}\, e^{-jk_0 R)}\right| \tag{59}$$

with $R = \left[d^2_{Tgti-Rx} + (h_{Tgti} + h_{Rx})^2\right]^{1/2} - \left[d^2_{Tgti-Rx} + (h_{Rx} - h_{Tgti})^2\right]^{1/2}$

As a reference evaluation of the expected power levels, the following values are considered in the analysis reported below:

- Tx antenna height: $h_{Tx} = 200m$
- Rx antenna height: $h_{Rx} = 30m$
- Target height: $h_{Tgt} = 10,\ 5,\ 2.5km$
- Distance between Txs: $D = 40km$
- Dielectric constant: $\kappa = 15$
- Conductivity: $\sigma_1 = 10^{-2} S/m$
- Angular frequency: $\omega = 2\pi \times 98\,MHz$ (center frequency of the FM band).

The two target scenarios described in section 4.3.1.6 (see **Figure 20** and **Figure 21**) are considered in the following figures.

Specifically, the geometric terms g_0, g_{int} g_{tot} and g_{echo}, for the flath-Earth propagation model, are reported in A.4. Each figure is composed by 3 sub-figures which have been obtained for different values of the target height ($10km$, $5km$, $2.5km$). The RCS is assumed equal to $10\,dB$ in all cases.

Based on the analysis above, an approximate synthesis of the results for $D = 40km$ is reported in Table 4 in terms of required dynamic range.

Target distance	From	To
25km	100 dB	110 dB
50km	110 dB	120 dB
75km	117 dB	127 dB
100km	122 dB	132 dB
150km	130 dB	140 dB
25km	100 dB	110 dB

Table 4 –Dynamic range vs the Rx-target distance under flat-Earth propagation.

Apparently, with the flat-Earth model the received power level is different than the prediction obtained with the very simple free-space propagation model and it depends on the target height. The accuracy of the prediction depends on the assumption made for both Earth dielectric constants characterization and on the assumed target RCS.

Moreover, the assumption of a cellular grid of transmitters is very different from the real displacement of the transmitters at least over the Italian territory, due to the topography. Typical non-symmetric structure of the transmitters, many of which in practice have even much lower power levels (for local transmissions), make the above prediction of the required dynamic range rather pessimistic.

4.3.1.8. CONCLUSIONS ON REFERENCE SCENARIOS AND REQUIREMENTS

We denote with $P_{\min}$ the expected power level of the echo from a target with RCS σ, from the maximum range $R_{\max}$. To detect it with the desired performance, we require that the ratio of $P_{\min}$ over the sum of all interference contributions (i.e. thermal noise, interference due to analog RX nonlinearity, ADC spurs, etc…) in the specific considered channel bandwidth, B_{ch}, is greater than an assigned $SDR_{\min}$, after coherent integration over a total integration time of T s.

Obviously, the value of $SDR_{\min}$ depends on the desired performance; in the following we use $SDR_{\min} = 8dB$ as a reference value.

For the FM broadcast case the channel bandwidth $B_{ch} = 200kHz$, and the typical integration time is of $T = 1s$, thus providing an integration gain $G_I = B_{ch}T = 2 \cdot 10^5$, corresponding to $53dB$.

Therefore the detection of targets at the maximum range requires (in dB):

$$P_{\min} + G_I > P_{disturbance}(B_{ch}) + SDR_{\min} \tag{60}$$

As a consequence, we require:

$$P_{\min} - P_{disturbance}(B_{ch}) > SDR_{\min} - G_I \tag{61}$$

This does not include the direct signal contribution P_0, that can be cancelled after ADC conversion.

Using the equations above, the PBR receiver must be designed to receive the total power level P_{TOT}, with a maximum disturbance level over the bandwidth equal to:

$$P_{disturbance}(B_{ch}) < P_{\min} + G_I - SDR_{\min} \tag{62}$$

Therefore, the total dynamic range of the receiver $D_{TOT} = P_{TOT} - P_{disturbance}(B_{ch})$, must verify the inequality:

$$D_{TOT} \geq (P_{TOT} - P_{\min}) - G_I + SDR_{\min} \tag{63}$$

Using the values above $G_I - SDR_{\min} = 53 - 8 = 45\,dB$ and the total receiver dynamic range required to detect the targets within the above reference scenarios are obtained by scaling the values in Table 3 and Table 4 by $40dB$; thus for the free-space propagation model we obtain the values in Table 5.

Target distance	From	To
25 Km	45 dB	60 dB
50 Km	55 dB	70 dB
75 Km	60 dB	75 dB
100 Km	65 dB	80 dB
150 Km	75 dB	90 dB
25 Km	45 dB	60 dB

Table 5 – Dynamic range required to detect the targets under free-space propagation.

The use of the flat-Earth model with the pessimistic parameters of the previous section requires the following total power dynamic ranges for the practical receivers (see Table 6).

Target distance	From	To
25km	55 dB	65 dB
50km	65 dB	75 dB
75km	72 dB	82 dB
100km	77 dB	87 dB
150km	85 dB	95 dB
25km	55 dB	65 dB

Table 6 – Dynamic range required to detect the targets under flat-Earth propagation.

As it is apparent, given a minimum receiver noise figure $F_{\min}$, the level of thermal noise yields a lower bound on the total disturbance level and, in consequence, an upper bound on the maximum dynamic range D_{MAX} potentially achievable as a function of the total input power P_{TOT} in the FM band:

$$D_{MAX}\left(P_{TOT}\right) = P_{TOT} - F_{\min} - KT - B_{ch} \tag{64}$$

The table below reports such values for $F_{\min} = 3dB$ in the FM band.

$\mathrm{P}_{\mathrm{TOT}}^{(\min)}$ (dBm)	-25	-20	-15	-10	-5	0	5	10
KTB (dBm)	-121	-121	-121	-121	-121	-121	-121	-121
$\mathrm{F}_{\min}$ (dBm)	3	3	3	3	3	3	3	3
$\mathrm{D}_{\mathrm{MAX}}$ (dBm)	93	98	103	108	113	118	123	128

Table 7 – Maximum dynamic range DMAX.

This means that for low values of P_{TOT}, a very high dynamic range cannot be provided, no matter how good the receiver design is, since the level of thermal noise cannot be lowered. Therefore, a practical requirement for a passive radar receiver can be to obtain the best achievable dynamic range for any value of the total input power, up to an upper limit value of dynamic range given by the available sensor hardware and structure. However, the achievable values are typically inside the detection requirements, possibly except for very low total input powers, namely very far from the reference transmitters.

It is also clear that the design of a receiver with a dynamic range of about $80dB$ should allow us to detect reasonably targets inside the $50km$ range from the receiver, whichever the assumptions on the propagation model, and in some cases it should allow us to go up to the $75km$ range.

With dynamic ranges of $90-100dB$ the detection inside the $150km$ should be possible in almost all conditions.

4.3.2. IDEAL DYNAMIC RANGE OF FM-BASED PBR RECEIVER SCHEMES

To approach the problem of designing a passive radar receiver, with a high dynamic range, it is interesting to define the upper bounds on the achievable performance. These will be used as guidelines and benchmarks in the design.

Three main limitations are considered here:

- the limitation due to the presence of thermal noise in the analog portion of the receiver;
- the full scale input power level of the analog-to-digital conversion device (ADC);
- the linear dynamic range of the ADC.

(a) The presence of thermal noise gives an upper bound on the receiver dynamic range, that is trivially given by the ratio of the input power to the noise power level in the RF channel under consideration with bandwidth B_{ch}, namely $KT + B_{ch} + F_{\min}$ (all quantities are expressed in dB), with reference to the minimum value of the achievable noise figure $F_{\min}$. Therefore, by defining P0 the power level received at the single channel, the dynamic range cannot exceed $P_0 - KT - B_{ch} - F_{\min}$.

(b) Assuming that the ADC has a full scale power level P_{FS}, to avoid saturation the signal power level at the input of the ADC cannot be higher than this level. Thus for $P_0 > P_{FS}$ the input signal power requires attenuation to level P_{FS}. This modifies the upper bound due to thermal noise as

$$\begin{cases} P_0 - KT - B_{ch} - F_{\min}, & P_0 \le P_{FS} \\ P_{FS} - KT - B_{ch} - F_{\min}, & P_0 \ge P_{FS} \end{cases} \tag{65}$$

(c) Assuming that the ADC has a linear dynamic range $\mathrm{DR}_{\mathrm{ADC,\,FS}}$, the best dynamic range of the whole receiver can get close to $\mathrm{DR}_{\mathrm{ADC,\,FS}}$ if the analog portion of the receiver preceding the ADC is designed to scale the input signal power at the specific channel of interest P_0, as close as possible to P_{FS}.

The upper bound on the dynamic range is therefore given by the parallel of the two bounds related to thermal noise and ADC dynamic range, i.e. by:

$$DR_0^{upper\_bound} = \begin{cases} -10\log_{10}\left[10^{-(P_0 - KT - B_{ch} - F_{\min})/10} + 10^{-DR_{ADC,FS}/10} \right], & P_0 \le P_{FS} \\ -10\log_{10}\left[10^{-(P_{FS} - KT - B_{ch} - F_{\min})/10} + 10^{-DR_{ADC,FS}/10} \right], & P_0 \ge P_{FS} \end{cases} \tag{66}$$

For illustration purposes, we report in Figure 22 the upper bound on the achievable dynamic range as a function of the single channel input power P_0, that is received in the FM band for three values of $\mathrm{DR}_{\mathrm{ADC,\,FS}} = 90dBFS,\ 100dBFS,\ 110dBFS$ and a value of $F_{\min} = 1dB$ (namely $KT + B_{ch} + F_{\min} = -174\,dBm + 53\,dB + 1\,dB = -120\ dBm$) for a typical value of $P_{FS} = 5dBm$. The range of interest for the single channel input power value goes from $-50dBm$ for a receiver very far from all the broadcast transmitters, up to $10dBm$ for a receiver close to a high broadcast transmitter and an antenna beam steered toward it.

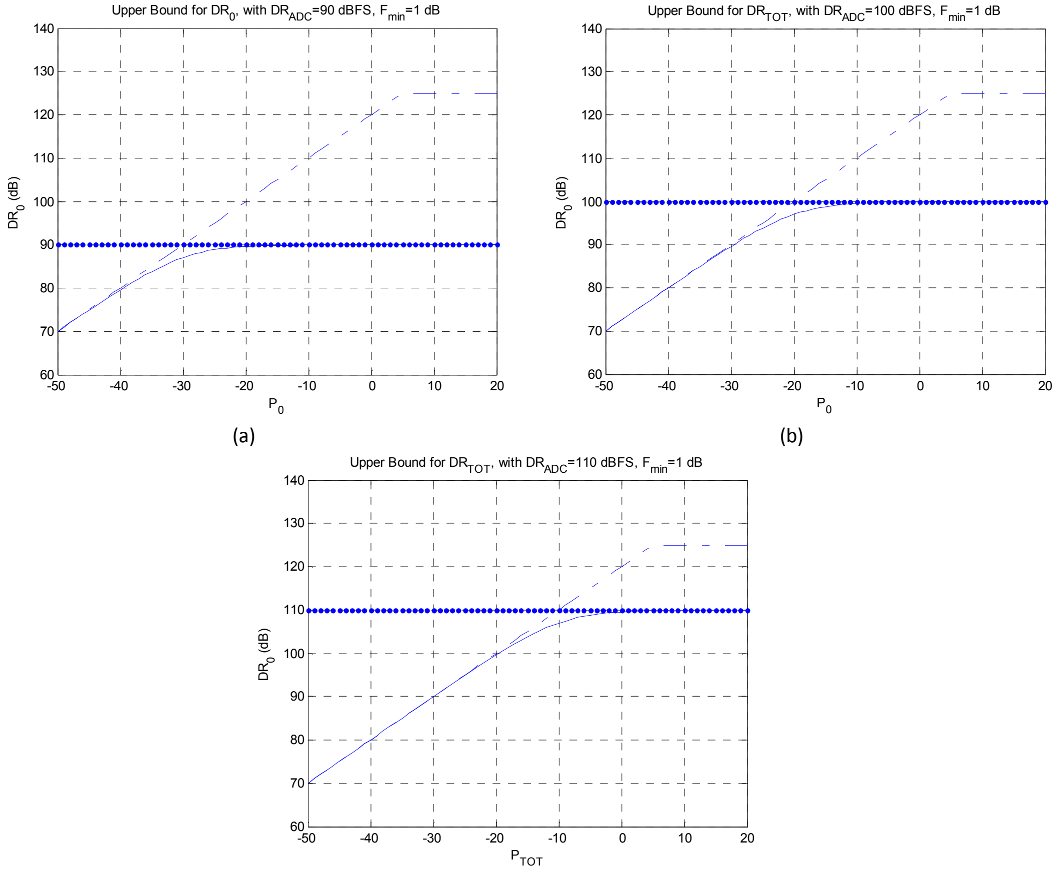

(a) (b)

(c)

Figure 22 – Upper bound for the single channel dynamic range DR₀ as a function of the single channel power level P₀

As apparent the upper bound in Figure 22 can be reached only if the single channel is isolated, whereas typically in the FM band $88-108MHz$ there can be a significant number of high level channels, so that the total input power received in the FM bandwidth, P_{TOT}, can be much higher than the single channel power P_0. For convenience, we consider the power ratio (in dB) $\eta_{BW} = P_{TOT} - P_0$, that can range between almost 0 dB when the specific channel is broadcast by a dedicated transmitter (that only broadcasts the specific channel) and receiver is very close to it, to about $40dB$, when the transmitter is not dedicated and the receiver is far from the transmitter.

For convenience, we could refer to a total dynamic range, defined as the ratio of the total power in the FM band to the total disturbance level. To achieve the total dynamic range, we only need to scale the results in terms of dynamic range referred to the single channel by η_{BW} :

$$
\begin{aligned}
DR_{TOT}^{upper\_bound} &= DR_0^{upper\_bound} + \eta_{BW} = \\
&= \begin{cases} -10\log_{10}\left[10^{-(P_{TOT}-KT-B_{ch}-F_{\min})/10} + 10^{-(DR_{ADC,FS}+\eta_{BW})/10}\right], & P_{TOT} \le P_{FS}+\eta_{BW} \\ -10\log_{10}\left[10^{-(P_{FS}+\eta_{BW}-KT-B_{ch}-F_{\min})/10} + 10^{-(DR_{ADC,FS}+\eta_{BW})/10}\right], & P_{TOT} \ge P_{FS}+\eta_{BW} \end{cases}
\end{aligned} \quad (67)
$$

The upper bound for the total dynamic range is shown in Figure 23 as a function of the total input power P_{TOT} and clearly depends on the value of the parameter η_{BW}, so that it is reported for the four values of $\eta_{BW} = 0dB, 10dB, 20dB, 40dB$ (respectively blue, red, green and magenta curves). The range of interest for the total input value goes from $-30dBm$ for a receiver very far from all the broadcast transmitters , up to $20dBm$ for a receiver close a high broadcast transmitter and an antenna beam steered toward it.

Extra considerations, and therefore restrictions of the achievable dynamic range, can be added when referring to different potential receiver schemes. We consider in the following sections the following cases:

- Mixed PBR receiver with wideband front-end and narrowband second stage (WBNB);
- Fully wideband (WB) PBR receiver;

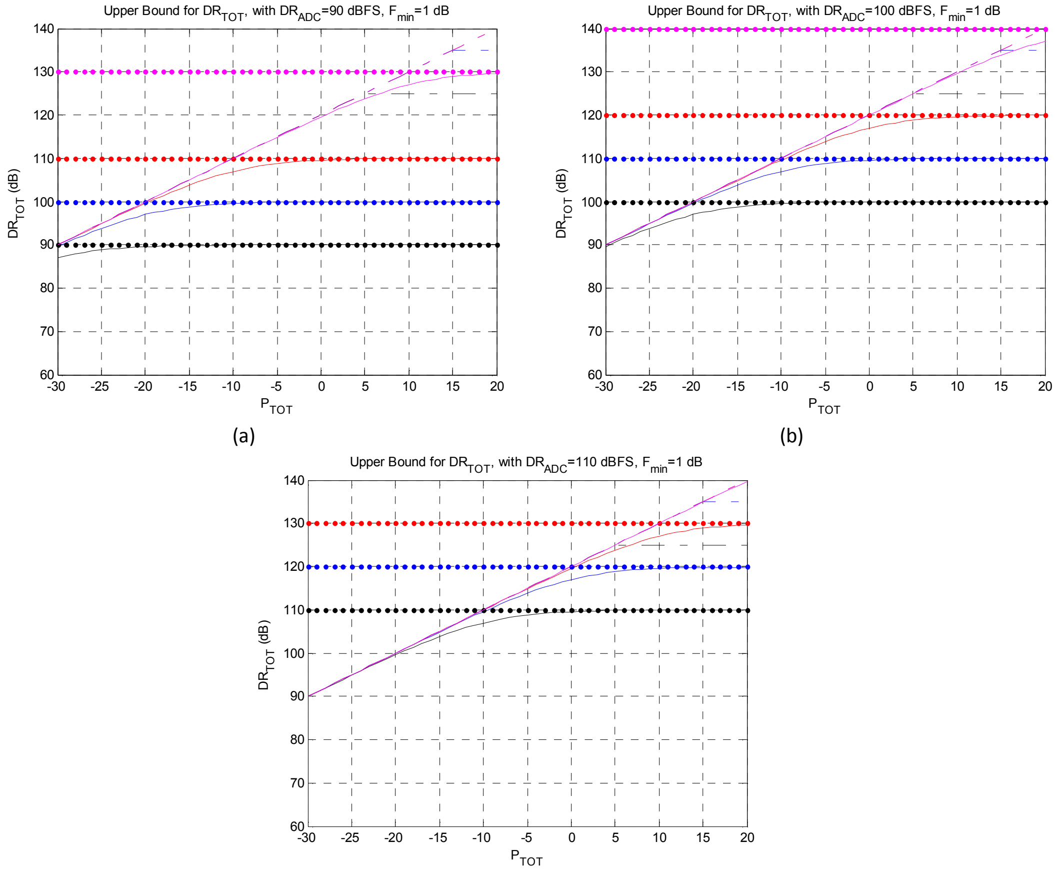

(a) (b)

(c)

Figure 23 – Upper bound for the total dynamic range DR_{TOT} of the ideal receiver as a function of the total input power level P_{TOT}

4.3.2.1. UPPER BOUND FOR WB PBR RECEIVER

A much simpler analog receiver scheme is obtained by avoiding the narrowband filter, which produces a fully WB receiver. The complexity goes into the ADC converter which is required to be able to sample the whole FM band. Thereafter, the individual channels are extracted by digital down-conversion and filtering.

The general scheme of such a receiver is illustrated in Figure 24 below, where an ideal variable attenuation block between the FM band-pass filter and the wideband block is assumed even if not explicitly represented.

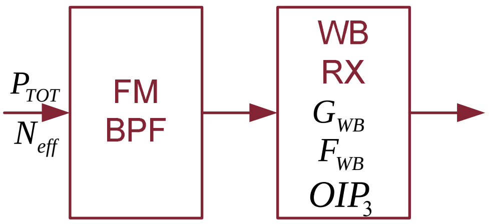

Figure 24 – Simplified scheme of a fully WB PBR receiver.

For a PBR receiver following the above mentioned architecture, we have the following considerations:

- The upper bound limitation to the dynamic range of the WBNB PBR receiver can be evaluated by resorting to the input referred noise figure, which is given by $F_{TOT}^{WB} = \alpha_{FM} + F_{WB}$. Therefore, the upper bound to the dynamic range with respect to the total input power due to thermal noise is given by this value of noise figure by means of $P_{TOT} - KT - B_{ch} - F_{TOT}^{WB}$.
- The signal level at the input of the ADC must be limited for high P_{TOT} values to avoid potential saturation of the ADC. The signal power at the output of the receiver is given by $P_{TOT} - \alpha_{FM} + G_{WB}$. The PBR receiver chain is generally required (better specified in the following section) to have a gain adequate to raise this level to the level P_{FS}, namely the gain is required to be $G_{WB} = P_{FS} - P_{TOT} + \alpha_{FM}$. As P_{TOT} increases, the global gain decreases and when $G_{WB} = 0$, the receiver is globally required to start attenuating the signal level. This applies for $0 = P_{FS} - P_{TOT} + \alpha_{FM}$, namely for $P_{TOT}^{*A} = P_{FS} + \alpha_{FM}$. This value must be increased when the total signal power is given by the sum of the powers of N^{lin} signals with equal levels, i.e. $P_{TOT} - 10\log_{10}(N^{lin}) = P_{TOT} - N$. In this case each component has a maximum amplitude $\sqrt{2/N^{lin}}\ 10^{P_{TOT}/20}$ and when the N^{lin} components are in phase, the total amplitude can reach the value $\sqrt{2N^{lin}}\ 10^{P_{TOT}/20}$, which corresponds to an equivalent power level $20\log_{10}\left[\sqrt{N^{lin}}\,10^{P_{TOT}/20}\right] = P_{TOT} + 10\log_{10}(N^{lin})$. If we refer to an effective number of components, the Full scale value of the ADC must be reduced by $10\log_{10}(N_{eff}^{lin}) = N_{eff}$. This is especially important for the ADC, where the increase of the signal amplitude produces hard saturation, that must be avoided. This changes the limit value to $P_{TOT}^{*A} = P_{FS} + \alpha_{FM} - N_{eff}$.

For the wideband front-end, the limitation to the dynamic range due to the nonlinearities of the receiver must be considered, in terms of the two tones third order inter-modulations. As well known, for an assigned signal power level P_{out} at the wideband receiver output, the disturbance due to the nonlinearity is at a level equal to $P_{out} - 2(OIP_3 - P_{out})$, namely the dynamic range is limited by $2(OIP_3 - P_{out})$. Since the power level at the output of the wideband portion of the receiver is given by $P_{out} = P_{TOT} - \alpha_{FM} + G_{WB}$, the dynamic range of the receiver cannot be larger than $2\,(OIP_3 - P_{TOT} + \alpha_{FM} - G_{WB})$. By defining the Input intercept Point of the third order $IIP_3 = OIP_3 - G_{WB}$, the dynamic range is limited by $2\,(IIP_3 - P_{TOT} + \alpha_{FM})$. As apparent, as P_{TOT} increases the upper bound due to thermal noise increases, while the upper bound due to the nonlinear characteristics of the receiver decreases. The two terms have the same value for

$$2\,(IIP_3 - P_{TOT}^{*B} + \alpha_{FM}) = P_{TOT}^{*B} - KT - B_{ch} - F_{TOT}^{WB} \tag{68}$$

namely, for

$$P_{TOT}^{*B} = \frac{2}{3}\,(IIP_3 + \alpha_{FM}) + \frac{1}{3}(KT + B_{ch} + F_{TOT}^{WB}) \tag{69}$$

where the maximum dynamic range is obtained. For P_{TOT} higher than this level, the bound due to the nonlinearity becomes lower than the bound due to thermal noise and the global dynamic range decreases. Therefore, the wideband receiver is assumed to attenuate the input power level down to the level P_{TOT}^{*B}, before the nonlinearity, to keep the maximum dynamic range DR^{*} available, as a results of the use of a WB device with $IIP_3 = OIP_3 - G_{WB}$.

As apparent, two different requirements lead to an attenuation of the signal level. However, the two limitations have different characteristics:

- WB receiver nonlinearity requires the attenuation to be applied for $P_{TOT} > P_{TOT}^{*B}$ before the WB RX portion;
- ADC saturation requires the attenuation to be applied for $P_{TOT} > P_{TOT}^{*A}$ before the ADC (i.e. possibly also at the end of the analog RX chain, after the NB filter).

Therefore, it is assumed that the wideband gain factor acts somewhat ideally, by attenuating the signal if its power is higher than $P_{FS} - N_{eff}$. It instead amplifies it up to the level $P_{FS} - N_{eff}$, if its power level is lower than this value.

Contribution due to the nonlinearity brings to a dynamic range limitation given by

$$DR_{nonlin}^{ub\_WB} = \begin{cases} 2\,(IIP_3 - P_{TOT} + \alpha_{FM}), & P_{TOT} < P_{TOT}^{*B} \\ \dfrac{2}{3}\,(IIP_3 + \alpha_{FM} - KT - B_{ch} - F_{TOT}^{WB}), & P_{TOT} \geq P_{TOT}^{*B} \end{cases} \tag{70}$$

Contribution due to the thermal noise brings to a dynamic range limitation given by

$$DR_{noise}^{ub\_WB} = \begin{cases} P_{TOT} - KT - B_{ch} - F_{TOT}^{WB}, & P_{TOT} < P_{TOT}^{*} = \min\left\{P_{TOT}^{*A}, P_{TOT}^{*B}\right\} \\ P_{TOT}^{*} - KT - B_{ch} - F_{TOT}^{WB}, & P_{TOT} \geq P_{TOT}^{*} = \min\left\{P_{TOT}^{*A}, P_{TOT}^{*B}\right\} \end{cases} \tag{71}$$

Therefore, by combining the bounds due to thermal noise, nonlinearity of the analog portion, and ADC dynamic level, we have the global upper bound, assuming as for the WNB case that $P_{TOT}^{*A} > P_{TOT}^{*B}$

$$\begin{aligned} & DR_{TOT\_analog}^{ub\_WB} = \\ & = \begin{cases} -10\log_{10}\left[10^{-(P_{TOT}-KT-B_{ch}-F_{TOT}^{WB})/10} + 10^{-2\,(IIP_3-P_{TOT}-\alpha_{FM})/10} + 10^{-(DR_{ADC,FS}-N_{eff})/10}\right], & P_{TOT} \leq P_{TOT}^{*B} \\ -10\log_{10}\left[2\cdot 10^{-\frac{2}{3}(IIP_3+\alpha_{FM}-KT-B_{ch}-F_{TOT}^{WB})/10} + 10^{-(DR_{ADC,FS}-N_{eff})/10}\right], & P_{TOT} \geq P_{TOT}^{*B} \end{cases} \end{aligned} \tag{72}$$

Figure 25 reports the upper bound to the dynamic range as a function of the global input power, for different values of available IIP_3 for the wideband portion, and assuming $N_{eff} = 7dB$.

As apparent, the available dynamic range does not change as the value of the power ratio $\eta_{BW} = P_{TOT} - P_0$ increases, which means that it shows sensibly lower performance for high total input levels, when the useful signal is weak. However, it provides performance better than NB for low values of the total input power.

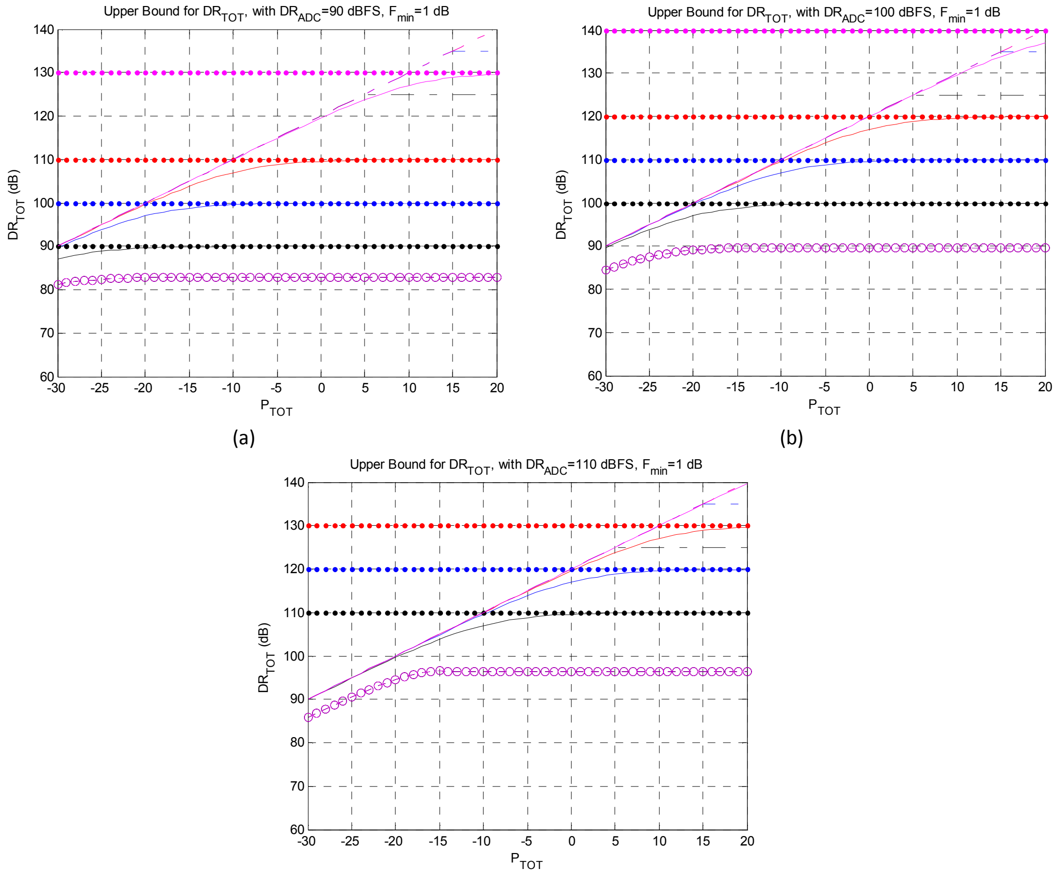

(a) (b)

(c)

Figure 25 – Upper bound for the total dynamic range DR_{TOT} of the WB receiver as a function of the total input power level P_{TOT}

4.3.2.2. UPPER BOUND FOR WB FRONT-END & NB BACK-END PBR RECEIVER

The design of narrow band filters in the FM band is very difficult, moreover either a tunable filter or a bank of filters is required for the fully narrowband receiver. Introducing a wideband front-end in the receiver, that can be used to translate the desired channel at a fixed intermediate frequency, where a single, non-tunable, narrow band filter is more easily designed makes the realization of the PBR receiver much easier.

Moreover, even when the difficulty of the narrowband filtering can be overcome, a wideband front-end could be used to achieve a low noise figure for the receiver, thus avoiding the dynamic range loss of the NB PBR receiver at low P_{TOT} values.

The general scheme of such a receiver is illustrated below.

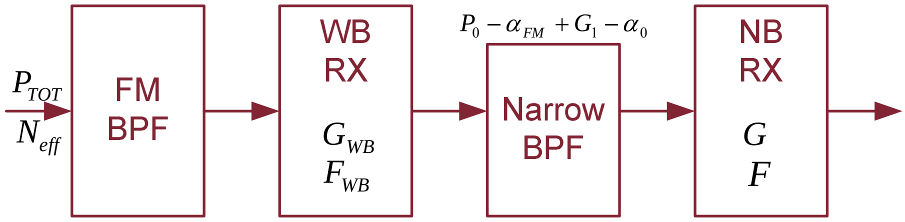

Figure 26 - Simplified scheme of a WBNB PBR receiver.

For a PBR receiver following the above mentioned architecture, we have the following considerations:

- The upper bound limitation to the dynamic range of the WBNB PBR receiver can be evaluated by resorting to the input referred noise figure, which is given by:

  $$(F_{TOT}^{WNB})_{lin} = (\alpha_{FM} + F_{WB})_{lin} + \frac{(\alpha_0 + F_{\min})_{lin} - 1}{(G_{WB} - \alpha_{FM})_{lin}} = (\alpha_{FM})_{lin}\left[(F_{WB})_{lin} + \frac{(\alpha_0 + F_{\min})_{lin} - 1}{(G_{WB})_{lin}}\right] \tag{73}$$

  Therefore, the upper bound to the dynamic range with respect to the total input power due to thermal noise is given by this value of noise figure by means of $P_{TOT} - KT - B_{ch} - F_{TOT}^{WNB}$.

- As for the NB PBR receiver, the signal level at the input of the ADC must be limited for high P_{TOT} values to avoid potential saturation of the ADC. The signal power at the output of the narrow band filter is given by $P_{TOT} - \alpha_{FM} + G_{WB} - \alpha_0 - \eta_{BW} + G$. The complex of WB and NB portion of the PBR receiver chain is generally required (better specified in the following section) to have a gain adequate to raise this level to the level P_{FS}, namely the sum of the gains is required to be $G_{WB} + G = P_{FS} - P_{TOT} + \alpha_{FM} + \alpha_0 + \eta_{BW}$. As P_{TOT} increases, the global gain decreases and when $G_{WB} + G = 0$, the receiver is globally required to start attenuating the signal level. This applies for $G_{WB} + G = P_{FS} - P_{TOT} + \alpha_{FM} + \alpha_0 + \eta_{BW}$, namely for $P_{TOT}^{*A} = P_{FS} + \alpha_{FM} + \alpha_0 + \eta_{BW}$.

- For a wideband front-end, the limitation to the dynamic range due to the nonlinearities of the receiver must be considered, in terms of the two tones third order inter-modulations. As well known, for an assigned signal power level P_{out} at the wideband receiver output, the disturbance due to the nonlinearity is at a level equal to $P_{out} - 2(OIP_3 - P_{out})$, namely the dynamic range is limited by $2(OIP_3 - P_{out})$. Since the power level at the output of the wideband portion of the receiver is given by $P_{out} = P_{TOT} - \alpha_{FM} + G_{WB}$, the dynamic range of the receiver cannot be larger than $2\,(OIP_3 - P_{TOT} + \alpha_{FM} - G_{WB})$. By defining the Input intercept Point of the third order $IIP_3 = OIP_3 - G_{WB}$, the dynamic range is limited by $2\,(IIP_3 - P_{TOT} + \alpha_{FM})$. As apparent, as P_{TOT} increases the upper bound due to thermal noise increases, while the upper bound due to the nonlinear characteristics of the receiver decreases. The two terms have the same value for

  $$2\,(IIP_3 - P_{TOT}^{*B} + \alpha_{FM}) = P_{TOT}^{*B} - KT - B_{ch} - F_{TOT}^{WNB} \tag{74}$$

  namely, for

  $$P_{TOT}^{*B} = \frac{2}{3}\,(IIP_3 + \alpha_{FM}) + \frac{1}{3}(KT + B_{ch} + F_{TOT}^{WNB}) \tag{75}$$

  where the maximum dynamic range is obtained:

$$\begin{aligned} DR^{*} &= P_{TOT}^{*B} - KT - B_{ch} - F_{TOT}^{WNB} = \frac{2}{3}\,(IIP_3 + \alpha_{FM}) + \\ &+ \frac{1}{3}(KT + B_{ch} + F_{TOT}^{WNB}) - KT - B_{ch} - F_{TOT}^{WNB} = \\ &= \frac{2}{3}\,(IIP_3 + \alpha_{FM} - KT - B_{ch} - F_{TOT}^{WNB}) \end{aligned} \tag{76}$$

For P_{TOT} higher than this level, the bound due to the nonlinearity becomes lower than the bound due to thermal noise and the global dynamic range decreases. Therefore, the wideband receiver is assumed to attenuate the input power level down to the level P_{TOT}^{*B}, before the nonlinearity, to keep the maximum dynamic range DR^{*} available, as a results of the use of a WB device with $IIP_3 = OIP_3 - G_{WB}$.

As apparent, two different requirements lead to an attenuation of the signal level. However, the two limitations have different characteristics:

- ADC saturation requires that the attenuation is applied for $P_{TOT} > P_{TOT}^{*A}$ before the ADC (i.e. possibly also at the end of the analog RX chain, after the NB filter);
- WB receiver nonlinearity requires that the attenuation is applied for $P_{TOT} > P_{TOT}^{*B}$ before the WB RX portion.

Contribution due to the nonlinearity brings to a dynamic range limitation given by

$$DR_{nonlin}^{ub\_WNB} = \begin{cases} 2\,(IIP_3 - P_{TOT} + \alpha_{FM}), & P_{TOT} < P_{TOT}^{*B} \\ \dfrac{2}{3}\,(IIP_3 + \alpha_{FM} - KT - B_{ch} - F_{TOT}^{WNB}), & P_{TOT} \geq P_{TOT}^{*B} \end{cases} \tag{77}$$

Contribution due to the thermal noise brings to a dynamic range limitation given by

$$DR_{noise}^{ub\_WNB} = \begin{cases} P_{TOT} - KT - B_{ch} - F_{TOT}^{WNB}, & P_{TOT} < P_{TOT}^{*} = \min\{P_{TOT}^{*A}, P_{TOT}^{*B}\} \\ P_{TOT}^{*} - KT - B_{ch} - F_{TOT}^{WNB}, & P_{TOT} \geq P_{TOT}^{*} = \min\{P_{TOT}^{*A}, P_{TOT}^{*B}\} \end{cases} \tag{78}$$

Therefore, by combining the bounds due to thermal noise, nonlinearity of the analog portion, and ADC dynamic level, we have the global upper bound:

If $P_{TOT}^{*A} > P_{TOT}^{*B}$:

$$\begin{aligned} &DR_{TOT\_analog}^{ub\_WNB} = \\ &= \begin{cases} -10\log_{10}\left[10^{-(P_{TOT}-KT-B_{ch}-F_{TOT}^{WNB})/10} + 10^{-2\,(IIP_3-P_{TOT}-\alpha_{FM})/10} + 10^{-(DR_{ADC,FS}+\eta_{BW})/10}\right], & P_{TOT} \leq P_{TOT}^{*B} \\ -10\log_{10}\left[2\cdot 10^{-\frac{2}{3}\,(IIP_3+\alpha_{FM}-KT-B_{ch}-F_{TOT}^{WNB})/10} + 10^{-(DR_{ADC,FS}+\eta_{BW})/10}\right], & P_{TOT} \geq P_{TOT}^{*B} \end{cases} \end{aligned} \tag{79}$$

Otherwise, if $P_{TOT}^{*A} < P_{TOT}^{*B}$:

$$\begin{aligned} &DR_{TOT\_analog}^{ub\_WNB} = \\ &= \begin{cases} -10\log_{10}\left[10^{-(P_{TOT}-KT-B_{ch}-F_{TOT}^{WNB})/10} + 10^{-2\,(IIP_3-P_{TOT}-\alpha_{FM})/10} + 10^{-(DR_{ADC,FS}+\eta_{BW})/10}\right], & P_{TOT} \leq P_{TOT}^{*A} \\ -10\log_{10}\left[10^{-(P_{TOT}^{*A}-KT-B_{ch}-F_{TOT}^{WNB})/10} + 10^{-2\,(IIP_3-P_{TOT}^{*A}-\alpha_{FM})/10} + 10^{-(DR_{ADC,FS}+\eta_{BW})/10}\right], & P_{TOT} \geq P_{TOT}^{*A} \end{cases} \end{aligned} \tag{80}$$

We notice that $P_{TOT}^{*A} > P_{TOT}^{*B}$ when

$P_{FS} + \alpha_{FM} + \alpha_0 + \eta_{BW} > \frac{2}{3}(IIP_3 + \alpha_{FM}) + \frac{1}{3}(KT + B_{ch} + F_{TOT}^{WNB})$, namely for

$\frac{3}{2}(P_{FS} + \alpha_0 + \eta_{BW}) > IIP_3 + \frac{1}{2}(KT + B_{ch} + F_{TOT}^{WNB} - \alpha_{FM})$. This requires:

$$IIP_3 < \frac{3}{2}(P_{FS} + \alpha_0 + \eta_{BW}) - \frac{1}{2}(KT + B_{ch} + F_{TOT}^{WNB} - \alpha_{FM}) \tag{81}$$

$$IIP_3 < P_{FS} + \alpha_0 + \eta_{BW} + \frac{1}{2}(P_{FS} + \alpha_0 + \eta_{BW} - KT - B_{ch} - F_{TOT}^{WNB} + \alpha_{FM}) \tag{82}$$

Since $KT + B_{ch} = -121\,dB$, even using a high noise figure so that $F_{TOT}^{WNB} - \alpha_{FM}$ is around 7 dB, the term $-\frac{1}{2}(KT + B_{ch} + F_{TOT}^{WNB} - \alpha_{FM})$ is around $+57dBm$. Except for ADC with extremely low full scale input levels, the inequality is verified. Therefore it is very likely that $P_{TOT}^{*A} > P_{TOT}^{*B}$, at least for standard components available on the market with limited IIP$_3$ and the first expression applies for the upper bound.

Figure 27 reports the upper bound to the dynamic range as a function of the global input power, for available $IIP_3 = 40dB$ and $F_{WB} = 7.5dB$ for the wideband portion, in the ideal case that the noise figure is only limited by the first filter and the WB amplifier (namely $F_{TOT}^{WB} = \alpha_{FM} + F_{WB}$). Similarly, Figure 28 shows the case of $IIP_3 = 36dB$ and $F_{WB} = 4dB$. The former is representative of a very high dynamic range mixer component used to translate the desired FM channel at the fixed frequency of a narrow filter. The latter of a high dynamic amplifier that tries to limit the loss of using the narrowband filter as first stage.

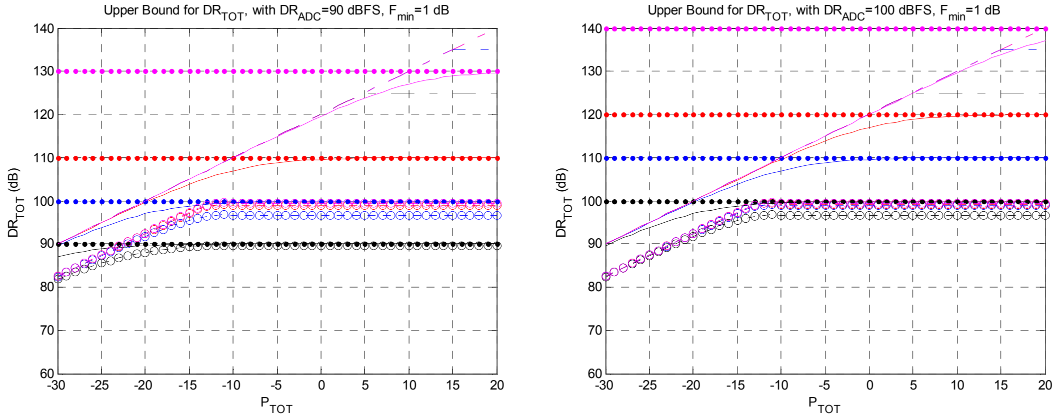

(a) (b)

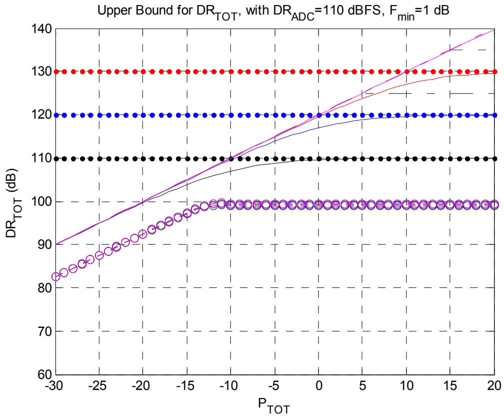

(c)

Figure 27 – Upper bound for the total power dynamic range DR$_{TOT}$ for the WBNB receiver as a function of the total power for IIP$_3$=40 dB, F$_{WB}$=7.5

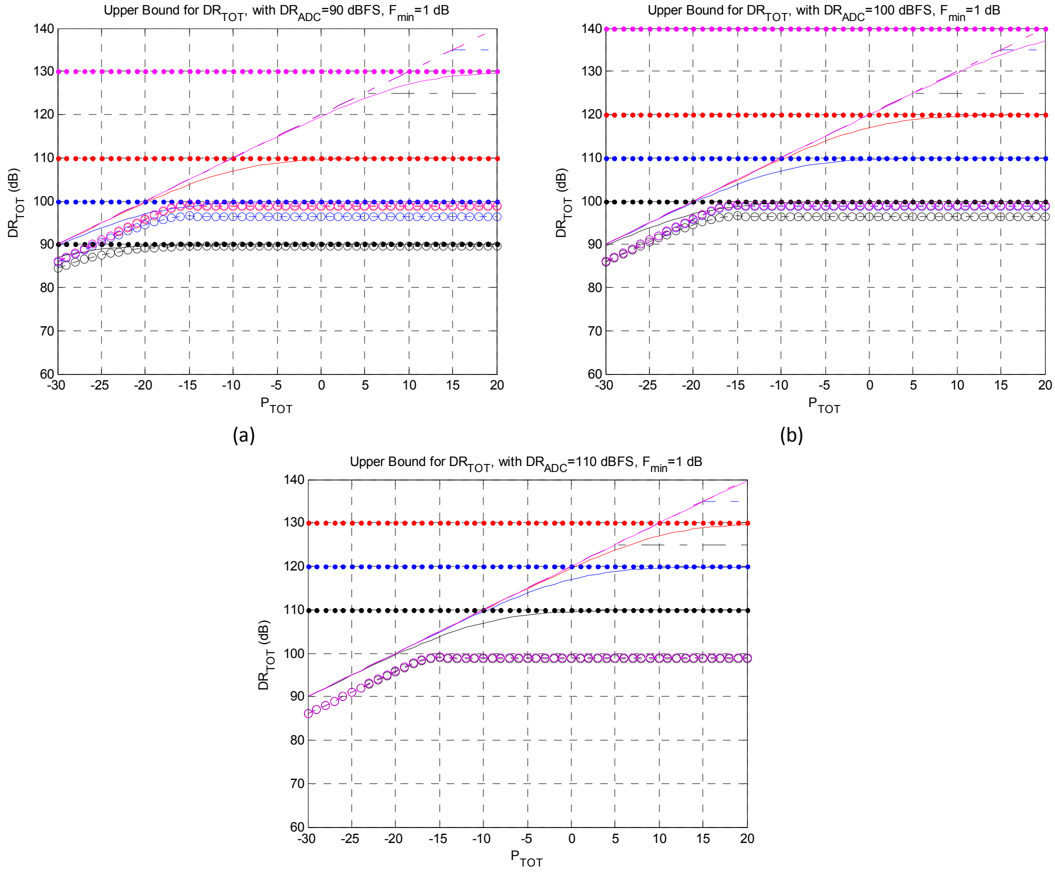

(a)

(b)

(c)

Figure 28 – Upper bound for the total power dynamic range DR$_{TOT}$ for the WBNB receiver as a function of the total power for IIP$_3$=36 dB, F$_{WB}$=4 dB

4.4. PROTOTYPES DESCRIPTION

Two different architectures for the realization of a multi-channel FM-based PBR receiver have been developed and fielded with proper laboratory tests and acquisition campaigns. Specifically, the two considered solutions are:

- Wide-Band (WB): all signals of the FM spectrum (88÷108 MHz) are digitized.
- Wide-Band front-end with Narrow-Band back-end (NB): a single radio channel is digitized.

The WB solution, sketched in Figure 29, is based on a direct RF sampling approach and only the appropriate amplification/attenuation chain needs to be defined; the selection of the desired radio channels is performed in the digital domain, thus allowing the application of the Multi-Frequency (MF) approach. The NB solution, sketched in Figure 41, foresees a conversion stage to a desired Intermediate Frequency (IF), adequate filtering stages to select the single radio channel of interest (or a small group of adjacent radio channels), and the A/D conversion; this solution allows a better exploitation of the receiver dynamic range.

Notice that, at this stage of the prototypes development, the NB solution allows only the detection and tracking of targets (only two receiver chains), while the WB solution allows the use of two or three surveillance antennas and therefore the Direction of Arrival (DoA) estimation.

4.4.1. WIDE BAND (WB) RECEIVER

The WB solution, sketched in Figure 29, is based on a direct Radio-Frequency (RF) sampling approach; the whole FM spectrum (88÷108 MHz) is digitized.

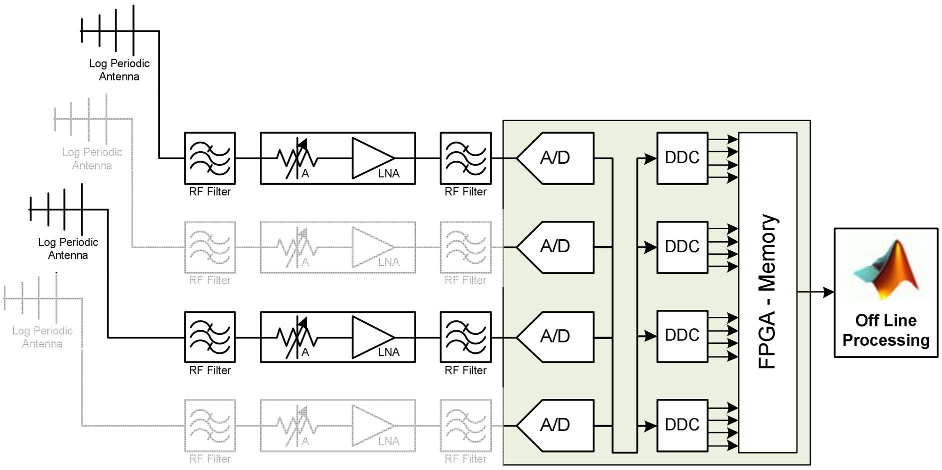

Figure 29 - Architecture of WB receiver

The adjustable RF attenuation provides increased dynamic range with respect to that provided by the A/D converter. The attenuator (ZX76-31R5-PN+ by Mini-Circuits) is followed by an RF amplifier, often referred to as a Low-Noise-Amplifier (LNA, ZHL-2010 or ZHL-1010 by Mini-Circuits). This amplifier provides a low noise figure, to minimize the degradation of the overall radar noise figure due to subsequent components, and a sufficient gain to raise the signal level required for subsequent processing and to set the correct signal level into the A/D converters. If sufficient gain is provided in the antenna prior to the receiver, it may be possible to eliminate this gain stage. The RF Filters (FM-band Murata filters) provide rejection of out-of-band interference and nonlinearity effects.

The A/D conversion is performed by means of the ICS-554 PMC module (produced by GE Fanuc Embedded Systems). This module consists of four 14-bit ADCs sampling synchronously the properly amplified analogue signals from up to four input channels. Simultaneous down conversion of up to 16 arbitrary signal bands (e.g. 16 FM radio channels) is provided by four Graychip GC4016 quad digital down-converters (DDC). A detailed description of this data capture module is reported in sub-section 4.4.3. After A/D conversion, the selection of the desired radio channels is performed in the digital domain, thus allowing the application of the MF approach. The main limitation of this solution is represented by the need of a wide linear dynamic range to acquire the whole FM spectrum.

The analog components required for the RF Front-End realization and for data capture, have been selected through a market analysis based on the following requirements:

- RF filter should have the following requirements:
    - rejection of out-of FM band signals: > 50 dB
- Variable attenuator should have the following requirements:
    - maximum attenuation: ≥ 15 dB
    - attenuation step: ≤ 2 dB
- Amplifier should have the following requirements:
    - Gain: ≥ 10 dB
    - IIP3: ≥ 30 dB
    - Noise Figure: ≤ 5 dB
- A/D conversion device should have the following requirements:
    - input bandwidth: ≥ 108 MHz (-1 dB)
    - sampling frequency: > 54MHz
    - Full-scale input value: 5 dBm
    - linear dynamic range: ≥ 90 dB
    - number of bits: ≥ 11

In most cases COTS components have been chosen. The principal selected devices and relative characteristics are:

- **RF Filter - FM-band Murata filter**: typical ceramic filter for FM receiver Front-End. Three components have been mounted in series in order to improve the selectivity.
  The main features of this product are:
    - Bandwidth: 80 ÷ 120MHz
    - Impedance: 50Ω
    - Insertion loss: ~2dB

- **Variable Attenuator - ZX76-31R5-PN+ by Mini-Circuits**: 50Ω digital step attenuator that offers an attenuation range up to 31.5dB in 0.5dB steps. The control is performed by a 6-bit parallel interface. The model operates on a dual supply voltage.

Figure 30 - ZX76-31R5-PN+ by Mini-Circuits

The main features of this product are:

- Bandwidth: 0 ÷ 2400MHz
- Impedance: 50Ω
- Low insertion loss
- High IP3: +52dBm typical
- Excellent return loss: 20dB typical
- Excellent accuracy: 0.1dB typical
- Dual supply voltage: VDD=+3V, VSS=-3V

For more details, see the component datasheet.

- **LNA - ZHL-2010+ by Mini-Circuits**: High IP3 LNA, see Figure 31

Figure 31 – ZHL-2010+ by Mini-Circuits

The main features of this product are:

- Gain: 20dB Min
- Bandwidth: 50 ÷ 1000MHz
- Impedance: 50Ω
- Low Noise Figure: 3.7dB typical
- High IP3: +46dBm typical
- Very high IP2: 68 ÷ 83dBm typical
- Supply voltage: V=+12V

For more details, see the component datasheet.

- **LNA - ZHL-1010+ by Mini-Circuits**: High IP3 LNA, see Figure 32

Figure 32 – ZHL-1010+ by Mini-Circuits

The main features of this product are:

- Gain: 9.5dB Min
- Bandwidth: 50 ÷ 1000MHz
- Impedance: 50Ω
- Low Noise Figure: 3.7dB typical
- High IP3: +46dBm typical
- Very high IP2: 68 ÷ 83dBm typical
- Supply voltage: V=+12V

For more details, see the component datasheet.

- **Data capture ICS-554B by GE Fanuc Embedded Systems**, widely described in sub-section 4.4.3.

4.4.2. NARROW BAND RECEIVER

In the NB solution, sketched in Figure 33, a single radio channel (or a small group of adjacent radio channels) is digitized.

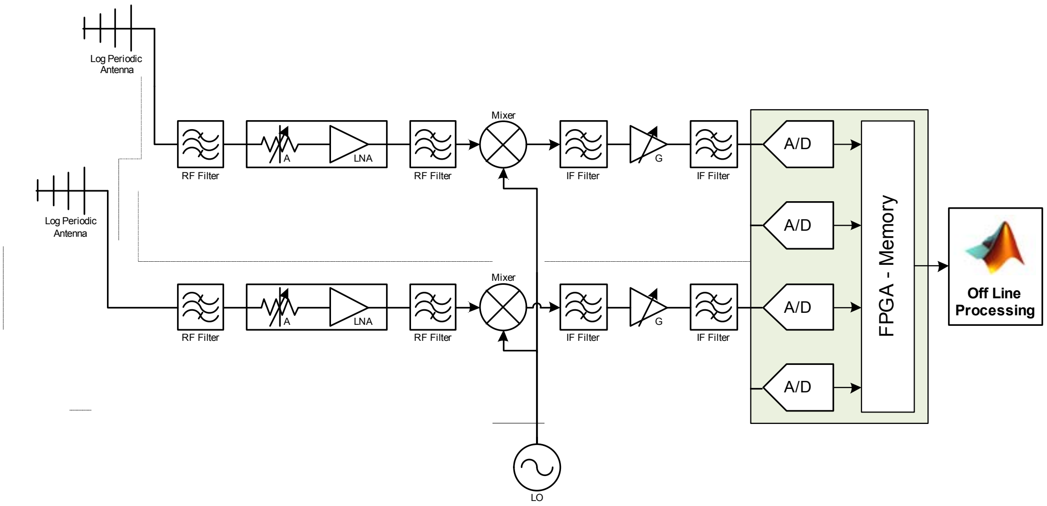

Figure 33 - Architecture of NB receiver

The RF Front-End is the same of the WB architecture. The RF Filters (FM-band Murata filters) provide rejection of out-of-band interference and nonlinearity effects. The attenuator (ZX76-31R5-PN+ by Mini-Circuits) is followed by an RF amplifier (LNA, ZHL-2010 or ZHL-1010 by Mini-Circuits). This amplifier provides a low noise figure, to minimize the degradation of the overall radar noise figure due to subsequent components. After a down-conversion stage from RF to IF (about 70 MHz), two IF band-pass filters provide the rejection of unwanted signals and the selection of the desired radio channel; then, an amplifier (ZHL-2010 by Mini-Circuits) provides proper amplification of the signal. The signal is digitized by A/D conversion for the off-line digital processing.

The A/D conversion is performed by means of the same module used for the WB receiver (ICS-554B, see the following sub-section) and allows to verify the performance of the analog sections of the two proposed receiver architectures.

The NB solution allows a better exploitation of the receiver dynamic range (optimized with respect to the single FM radio channel of interest) and a reduction of the intermodulation effects on the signal.

The analog components required for the RF Front-End realization and for data capture, have been selected through a market analysis based on the requirements defined following:

- Variable attenuator should have the following requirements:
    - maximum attenuation: ≥ 20 dB
    - attenuation step: ≤ 2 dB
- RF filter should have the following requirements:
    - rejection of out-of FM band signals: > 50 dB
- Mixer and amplifier chain should have the following requirements:
    - Gain: ≥ 10 dB
    - IIP3: ≥ 30 dB
    - Noise Figure: ≤ 5 dB
- IF filter must have the following characteristics:
    - -3 dB filter bandwidth: ≤ 200 KHz
    - selectivity at 1 MHz: > 60 dB
- The required A/D conversion device should have the following requirements:
    - input bandwidth: ≥ 73 MHz (-1 dB)
    - sampling frequency: > 4 MHz
    - Full-scale input value: 5 dBm
    - linear dynamic range: ≥ 90 dB
    - number of bits: ≥ 12

In most cases COTS components have been chosen. The principal devices and relative characteristics are:

- **RF Filter - FM-band Murata filter**: see sub-section 4.4.1
- **Variable Attenuator - ZX76-31R5-PN+ by Mini-Circuits**: sub-section 4.4.1.
- **LNA - ZHL-2010+ by Mini-Circuits**: sub-section 4.4.1.
- **LNA - ZHL-1010+ by Mini-Circuits**: sub-section 4.4.1.
- **Analog Mixer ZX05-1MHW+ by Mini-Circuits**: frequency mixer for Down-Conversion of the signal from RF to IF (see Figure 34).

Figure 34 – ZX05-1MHW+ by Mini-Circuits

The main features of this product are:

- Frequency LO (Local Oscillator)/RF: 0.5 ÷ 600MHz
- Frequency IF: DC ÷ 600MHz
- LO power: +13dBm
- Conversion loss: 5.2dB typical
- 1dB Compression Point: +9dBm

For more details, see the component datasheet.

- IF Filter F-72M-K9: Band-pass filter for a single FM channel with center frequency 72MHz and bandwidth of about 200kHz. An example of the Gain shape for the filter used in the prototype is reported in Figure 35.

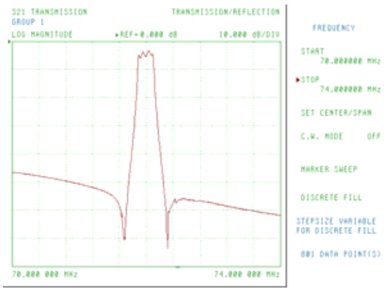

Figure 35 - F-72M-K9 filter Gain

The main features of this product are:

- Center frequency: 72MHz
- Bandwidth: 180kHz
- Impedance: 50Ω
- Insertion loss: ~3.5dB

- **IF Amplifier - ZHL-2010+ by Mini-Circuits**: sub-section 4.4.1.
- **Data capture ICS-554B by GE Fanuc Embedded Systems**, widely described in sub-section 4.4.3.

4.4.3. A/D CONVERTER – ICS-554

As previously mentioned, the A/D conversion is performed by means of the ICS-554 PMC module (produced by GE Fanuc Embedded Systems). ICS-554 (see Figure 36) is a four channel, 14-bit A/D module in a PCI Mezzanine Card (PMC) format. It has a nominal signal input impedance of 50 Ohms, and conforms to the PCI 2.2 (64-bit, 66 MHz) standard, with Master Burst Mode (DMA) capability. Five different versions are available, identified with letters from *A* to *E*; the *B* version, selected for this project, has a 105 MHZ maximum sample rate per channel, and a one million gate Field Programmable Gate Array (FPGA). The internal sample clock oscillator is a 100 MHz fixed frequency crystal.

Figure 36 – ICS-554B

Figure 37 shows a simplified block diagram of the ICS-554B board. The board uses four 14-bit Analog-to-Digital Converters (ADCs), Analog Devices AD6645. The ICS-554 includes a 66 MHz/64-bit PCI bus interface conforming to the PCI 2.2 specification. The PCI interface uses the QuickLogic QL5064 chip to support a master burst transfer (DMA) interface. The ICS-554 can generate PCI bus interrupts at any user-programmed interval (number of samples acquired).

The sampling clock and the trigger can be either internal or external. The internal ADC clock is a crystal oscillator with a fixed frequency of 100 MHz; the external clock signal may be either a TTL level or sinewave signal with a frequency in the range 30 – 100 MHz.

The ADCs can be operated in a number of different modes. In the continuous mode, data is continuously converted on all selected channels and supplied to the PCI Bus interface upon application of a trigger signal, until the acquisition is disabled. In capture mode, a fixed number of samples are acquired upon each application of the trigger. The number of samples acquired at each application of the trigger is programmable with a resolution of four samples per channel or less, up to the maximum capacity of the buffer. The programmable ADC output decimator can reduce the output data rate by a factor of up to thirty-two.

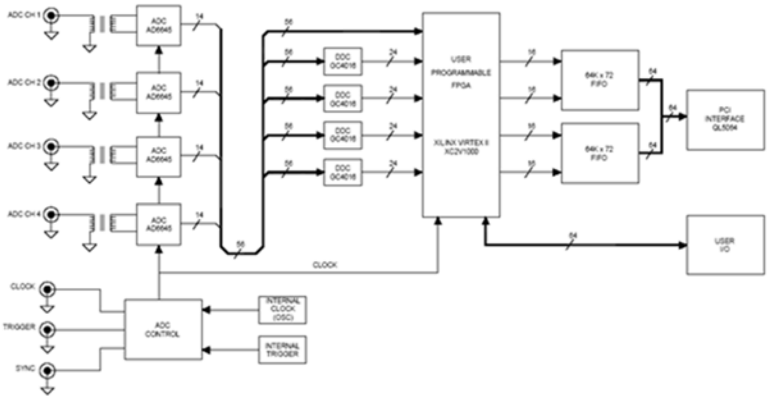

Figure 37 – ICS-554B block diagram

The outputs of the ADCs are applied to a bank of four quad digital down-converter (DDC) modules, which are Graychip GC4016 devices (see **Figure 38**); specifically, each GC4016 module includes four independent DDC channels, thus allowing the simultaneous down conversion of up to 16 arbitrary signal bands (e.g. 16 FM channels). Note that the ADC outputs are also connected to a Xilinx FPGA for direct processing of the ADC data. A crossbar switch is supplied as standard firmware in the FPGA to enable the user to select either the ADC output or the DDC output, under program control. This FPGA is almost entirely available for user applications, providing a powerful signal processing capability. The ICS-554 also offers 1 MByte of onboard memory storage organized as two independent 0.5 MByte FIFOs, thus providing for simultaneous wideband and narrowband operation. The ICS-554 supports coherent sampling on single channels (from trigger interval to trigger interval), across multiple channels on the same board or across multiple boards. The latter capability provides for beam forming and time-of-arrival applications.

ICS-554B technical specifications are summarized in the following:

- four analog input channels (ADCs)
- ADC resolution: 14 bits
- input impedance: 50Ω
- full scale input: 1.2 $V_{pk\text{-}pk}$ (about 5.5 dBm)
- input signal bandwidth: 2 ÷ 200 MHz
- internal or external clock and trigger
- maximum sampling rate: 100 MHz for four channel, simultaneous
- minimum sampling rate: 30 MHz for four channel, simultaneous
- internal sample clock oscillator: 100 MHz fixed frequency crystal
- Spurious Free Dynamic Range (SFDR) > 85 dB
- SNR > 71 dB
- user programmable FPGA (one million gates)
- programmable decimation of the ADC data stream
- SMA coaxial connectors
- maximum DDC output bandwidth:
    - 10 MHz (sampling frequency = 100 MHz, four channel output)
    - 5 MHz (sampling frequency = 100 MHz, eight channel output)
    - 2.5 MHz (sampling frequency = 100 MHz, 16 channel output)
- minimum DDC output bandwidth:
    - 4.9 KHz (sampling frequency = 100 MHz, 16 channel output)

The ICS-554 provides the ability to select the number of channels to be used, under software control. From one to four channels may be selected. When one ADC channel is enabled, the ICS-554 stores the data from ADC channel 1 into FIFO 1. The other three channels are unused. When data is read over PCI Bus, only the data for channel 1 will be read. When two ADC channels are enabled, the ICS-554 stores the data from ADC channel 1 into FIFO 1, and the data from ADC channel 3 into FIFO 2. The other two channels are unused. When data is read over PCI Bus, only the data for channels 1 and 3 will be read. When three ADC channels are enabled, the ICS-554 stores the data from ADC channel 1 into FIFO 1, and the data from ADC channels 3 and 4 into FIFO 2. Channel 2 is unused. When data is read over PCI Bus, only the data for channels 1, 3 and 4 will be read. When four ADC channels are enabled, the ICS-554 stores the data from ADC channels 1 and 2 into FIFO 1, and the data from ADC channels 3 and 4 into FIFO 2. When data is read over PCI Bus, data for all four channels will be read.

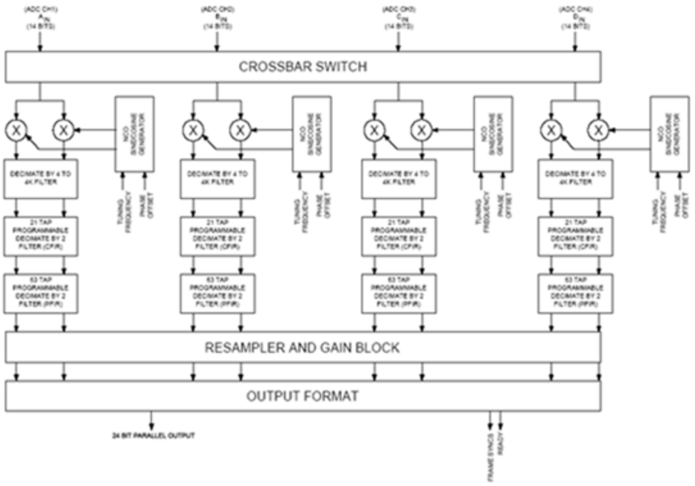

Figure 38 – GC 4016 block diagram

4.4.3.1. GRAYCHIP

As previously mentioned, ICS-554B includes four Graychip GC4016 DDC chips, each containing four identical down-conversion circuits, giving a total of up to 16 individual output channels. A block diagram of a single GC4016 device is shown in **Figure 38**. The crossbar switch allows the user to route any input source to any down-converter channel. The data inputs to each of the GC4016 chips consist of four independent 14-bit data buses from the ADC outputs, so that any of the output channels may use any of the A/D input channels as its data source.

Each GC4016 output channel can be configured to select and down-convert a signal band from the input data stream centered on a specific input frequency (the IF or tuning frequency).

Each of the four identical down-converters on the DDC chip accepts a real sample rate up to 100 MHz, down-converts a selected IF frequency to zero, filters the signal, decimates the signal rate by a programmable factor ranging from 32 to 16384 and then resamples the channel to adjust the sample rate up or down by an arbitrary factor. The channels on a DDC may be combined to produce wider band and/or oversampled outputs or to process complex input data. The chip contains two user-programmable output filters per path which can be used to arbitrarily shape the received data spectrum. These filters can be used as Nyquist receive filters for digital data transmission. The chip also contains a resampling filter to provide additional filtering and to allow the user complete flexibility in the selection of input and output sample rates. Two down-converter paths can be merged to be used as a single complex input down-conversion circuit. Two paths may also be combined to support wider band output rates or oversampled outputs. Four paths may be combined to support both wider band output and oversampling. The down-converters are designed to maintain over 115 dB of spur free dynamic range and over 100 dB of out of band rejection. A five stage CIC and 20 bit internal data paths support this high dynamic range digital signal processing requirement. Each down-convert circuit accepts 14-bit inputs and produces 24-bit outputs. The frequencies and phase offsets of the four sine/cosine sequence generators can be independently specified, as can the decimation and filter parameters of each circuit.

Groups of DDC output channels that feed into the same FIFO memory, i.e. the upper or lower 8 down-converter channels must use the same bandwidth (i.e. same decimation factor). Thus the upper 8 down-converter channels may use a different bandwidth than the lower 8 down-converter channels. Each channel can be programmed independently for filter coefficients and input selection, centre (IF) frequency, phase and gain. Each down-converter channel contains three filters in sequence to low-pass filter and isolate the down-converted signal(s), see Figure 39. Users have the option to download filter coefficient sets provided by ICS with the software device drivers for the ICS-554B, or to use their own custom filter coefficients.

The maximum signal bandwidth that can be processed by a single channel is dependent upon the clock frequency, the decimation ratio and the type of filter, or the filter coefficients. By combining channels, the signal bandwidth can be increased, as described below. The GC4016 provides a number of options for combining channels and converting the standard complex data output format to real data. The DDCs in the Graychips contain multichannel mode functionality. The maximum single channel output bandwidth is approximately 2.5 MHz. This output bandwidth can be doubled by combining two channels using the Split-I/Q mode. Four channels may be combined to provide three to four times the single channel output bandwidth. Two channels can be combined to process complex input data, doubling the input bandwidth. Four channels can be combined to both process complex input data and to double the output bandwidth of the chip. Two or four multichannel modes may also be used in the complex to real mode.

Figure 39 illustrates the structure of a single down-converter channel; there are four such down-converters in each of the four DDC chips. A Numerically Controlled Oscillator (NCO) and mixer are used to quadrature down-convert a signal from the tuning frequency to baseband. A positive tuning frequency is normally used to down-convert the signal; however, a negative tuning frequency can be used to invert the output spectrum.

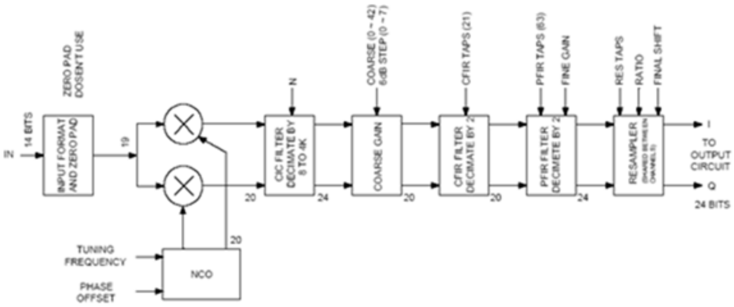

Figure 39 – GC 4016 single channel block diagram

The CIC (Cascade Integrate Comb) filter decimates the inputs from the NCO by a factor N, where N is from 8 to 4096. The inputs have to be scaled before this filter to prevent overflow. This scaling is done in the shift down block indicated in Figure 43: the user must select (via software) the desired values in order to avoid overflow.

Coarse gain is set for each channel in the CFIR register and it can be used to boost the channel's gain by up to 42 dB.

The output of the coarse gain circuit is filtered in the CFIR (Compensating FIR) filter stage. This stage is a 21-tap decimate by 2 filter with programmable 16-bit coefficients. Since this filter decimates by two, a stop-band must be created in that portion of the spectrum that would alias into the signal of interest.

The second stage decimate by two filter (Programmable FIR filter – PFIR) is a 63-tap decimate-by-2 filter with programmable 16-bit coefficients. Fine gain is applied at the output of the PFIR and rounded to 24 bits. Overflows are detected and hard limited. Overflows can be directed to the channel overflow detection block. The PFIR filter pass-band must be flat in the region of the signal of interest, and have the desired out of band rejection in the region that will alias into the signal's bandwidth after decimation. The externally downloaded coefficients can be used to tailor the spectral response to the user's needs. For example, it can be programmed as a Nyquist (typically a root-raised-cosine) filter for matched filtering of digital data. The user downloaded filter coefficients are 16 bit 2's complement numbers.

The resampler will independently filter and change the data rate of each channel. The most common application of the resampler is to increase the sample rate of the data so that it will match a desired symbol or bit rate. It can also be used as an additional filter to optimize the pass-band or stop-band response of the channel.

The ICS-554B module is integrated into a dedicated Workstation with Windows XP Professional operating system and is driven by proper software programs developed in Matlab® and C.

4.4.3.2. CLOCK SOURCE

The clock reference used to generate the sampling frequency for the A/D conversion is the CG – ClockGen module by Innovative integration reported in Figure 40.

The ClockGen is a precision clock generator on a PMC IO module for sample rate generation, system clock synchronization, and clock distribution. The four output clocks, external clock and reference clock inputs are front panel SMA connectors. Each output can drive a 50 ohm load. The ClockGen PMC generates four clock outputs over a frequency range of 100 KHz to 270 MHz (with 0.1 Hz tuning resolution).

The clocks can be locked to a reference clock input or an optional Statum III (0.5 ppb) stable reference. In the clock distribution mode, the ClockGen PMC makes four low-skew copies of the input clock driven to the outputs. Clock rates for the distribution mode are DC to 350 MHz. The ClockGen PMC generates output clocks that have jitter of less than 1 ps RMS over the range 6.25 MHz to 270 MHz. These can be used as sample clocks for high frequency inputs and in under-sampling applications. For lower sample rates in the 100 KHz to 6.25 MHz range, jitter is <50 pS RMS.

The application software for the ClockGen PMC allows complete configuration and control from its virtual instrumentation panel. Integration into system software is fully supported making the ClockGen a flexible solution to system clocking requirements.

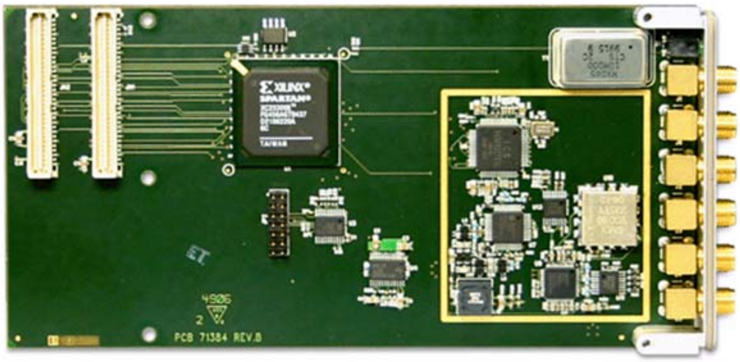

Figure 40 – CG – ClockGen by Innovative Integration

This module has been selected due to its reduced dimensions and to the possibility to integrate it into the same Workstation where the ICS-554B is mounted. This allows to obtain an integrated data capture system of reduced dimensions.

4.5. TESTS AND CONTROLLED EXPERIMENTS

Different setup tests have been performed in controlled situations in order to verify the disturbance cancellation capability achievable with the FM-based PBR prototypes. Specifically, three different kinds of tests were performed for the two proposed system architectures (WB and NB):

- analysis without useful signals, aiming at verifying the system compliance to thermal noise specifications, on both the receiving channels;
- “single antenna acquisitions”: the signal of a single antenna was split with a power divider and sent to two receiving channels. The acquired data sets were processed using the cancellation algorithms described in [6]-[7] and the obtained cancellation was evaluated as the ratio between the power levels measured, over a 200 kHz bandwidth, at the input and at the output of the cancellation filter. In the considered situation, this parameter only depends on the correlation properties between the signals at the two receiving channels. Since the two receiving channels are fed with exactly the same input signal, this test allowed us to characterize the channel decorrelation effects due to the devices non-idealities and thermal noise thus leading to the evaluation of the theoretical maximum cancellation level that can be obtained.
- “double antenna acquisitions”: each receiving channel is fed by the signal of a specific antenna (for example reference and surveillance antennas). This allows to measure disturbance cancellation capability of the system in its operative configuration.

4.5.1. NOISE MEASURES AND LEVELS DIAGRAM

In this section are reported the results obtained without useful signals, aiming at verifying the system compliance to thermal noise specifications, on each receiving channel, for WB and NB receivers.

As general rule, the system noise is due to two factors:

- Thermal noise
- Quantization noise

Thermal noise is specific of each active component and it is expressed by the Noise Figure (F) that characterize each single component. The quantization noise is generated only during the signal digitalization by the A/D converter. Both these noise factors limit the dynamic of the A/D converter. Specifically, each commercial A/D converter is characterized by a single value of SNR that is evaluated by a single noise value (that includes thermal noise and quantization noise).

The thermal noise power is defined as:

$$N_{Th} = K \cdot T_0 \cdot B_n \cdot F \tag{83}$$

$$N_{Th}\big|_{dBm} = -174 + 10\log_{10}(B_n) + F \tag{84}$$

where:

- K is the Boltzmann's constant (joules per Kelvin)
- T_0 is the resistor's absolute temperature (Kelvin)
- B_n is the system analog bandwidth
- F is the system Noise Figure

Equation (84) can be used to calculate the thermal noise generated by each single component of the receiving chain by using the F value provided by the constructor in the respective datasheet.

In order to evaluate the thermal noise of the entire system, it is possible to calculate the overall F of the receiver through the level diagram reported in Table 8:

		C1	**C2**	**…**	**CN**	**A/D**
$N_{ThCn}\,Input\ \ [dBm]$						
$F_{Cn}\,Input\ \ [dB]$						
		C1	**C2**	**…**	**CN**	**A/D**
		C1 name	**C2 name**	**…**	**CN name**	**A/D name**
$F_{Cn}\ \ [dB]$		**F$_{C1}$**	**F$_{C2}$**	**…**	**F$_{CN}$**	**F$_{A/D}$**
$G_{Cn}\ \ [dB]$		**G$_{C1}$**	**G$_{C2}$**	**…**	**G$_{CN}$**	
$\sum G_{Cn}\ \ [dB]$	**xx**					
$B_n\ \ [MHz]$	**xx**					

Table 8 – Level diagram (example)

For each component of the receiving chain (indicated with $C1, C2, \ldots CN$ in the different columns), each row contains the following parameters:

- $N_{ThCn}\ Input \quad [dBm]$: thermal noise in input to n-th component expressed in dBm (estimated over the bandwidth B_n)
    - $$\begin{cases} N_{ThC1}\ Input\big|_{dBm} = -174 + 10\log_{10}(B_n) + F_{C1}\ Input & n = 1 \\ N_{ThCn}\ Input\big|_{dBm} = N_{ThCn-1}\ Input\big|_{dBm} + G_{Cn-1}\big|_{dB} & n > 1 \end{cases}$$
- $F_{Cn}\ Input \quad [dB]$: Noise Figure reported in input to the n-th component
    - $$F_{Cn}\ Input\big|_{\mathrm{dB}} = 10\log_{10}\left[10^{\frac{F_{Cn}}{10}} + \left(\frac{10^{\frac{F_{C(n+1)}}{10}} - 1}{10^{\frac{G_{Cn}}{10}}}\right)\right]$$

    Notice that, $F_{C1}\ Input$ represent the Noise Figure in input to the overall receiving chain; the thermal noise of the system and consequently the dynamic of the receiver depends on this value
- $F_{Cn} \quad [dB]$: Noise Figure of the n-th component (reported in the datasheet)
- $G_{Cn} \quad [dB]$: Gain of the n-th component (reported in the datasheet) expressed in dB

The Noise Figure of the data-capture, which is used in the level diagram, depends on the noise of the A/D converter. As previously mentioned, in addition to the thermal noise, the quantization noise is generated by the A/D converter.

The quantization noise power is characterized as follows:

$$N_Q\big|_{dBm} = 10\log_{10}\left(\frac{\sigma^2}{f_S} \cdot 2 \cdot B_{A/D}\right) + 30 \tag{85}$$

Where:

- $\sigma^2 = \dfrac{q^2}{12}$ is the variance of quantization error
- $q = \dfrac{V_{FS}}{2^b}$ is the quantum (in Volt), V_{FS} represent the A/D converter full-scale
- b is the bit number of the A/D converter
- f_S is the sampling frequency
- $B_{A/D}$ is the A/D converter analog bandwidth

Typically the quantization noise is lower than the thermal noise of the specific component. Therefore, the dynamic range of the A/D converter is limited by the thermal noise and can be indicated in terms of SNR. The SNR value can be evaluated by considering the maximum power level in input to the A/D (equal to the A/D converter full-scale):

$$SNR^{A/D} = \frac{P_{FS}^{A/D}}{N_{Th}^{A/D} + N_Q^{A/D}} \tag{86}$$

Where:

- $P_{FS}^{A/D}$ is the maximum power in input to the A/D converter (that corresponds to the full-scale)
- $N_{Th}^{A/D}$ is the thermal noise of the A/D converter
- $N_{Q}^{A/D}$ is the quantization noise of the A/D converter

The theoretical SNR of the A/D converter, evaluated only considering the quantization noise, is:

$$SNR_Q^{A/D} = \frac{P_{FS}^{A/D}}{N_{Th}^{A/D}} = \frac{(V_{FS}/2)^2/2}{\sigma^2} = \frac{(V_{FS}/2)^2/2}{V_{FS}^2/2^{2n}} \cdot 12 = \frac{3}{2} \cdot 2^{2n} \tag{87}$$

From equation (87), the value of the theoretical SNR of the A/D converter expressed in dB, evaluated only considering the quantization noise, can be obtained:

$$SNR_Q^{A/D}\Big|_{dB} = 10\log_{10}\left(\frac{3}{2}\right) + 10\log_{10}\left(2^{2n}\right) = 1.76 + 6.02 \cdot n \tag{88}$$

The A/D converters are typically characterized, in their technical documentation, by another parameter called $ENOB$ (Effective Number Of Bits):

$$ENOB = \frac{SINAD - 1.76}{6.02} \tag{89}$$

Where $SINAD$ is the Signal to Noise and Distortion ratio that considers not only the thermal noise of the A/D converter, but also the distortion introduced on the signal by the first 5 harmonics:

$$SINAD = 10\log_{10}\frac{P_S}{N^{A/D} + P_D} \tag{90}$$

(where P_S indicates the power of the signal, $N^{A/D} = N_{Th}^{A/D} + N_{Q}^{A/D}$ is the noise power and P_D is the distortion power of the first 5 harmonics).

In particular, for the data capture described in section 4.4.3 (ICS-554B), the noise specifications are reported below.

- The theoretical SNR of the (14-bit) A/D converter is: $SNR_Q^{A/D}\Big|_{dB} = 1.76 + 6.02 \cdot 14 = 86.04dB$
- The A/D converter Full-scale power is $P_{FS}^{A/D} = +5.5dBm$
- The theoretical thermal noise for the ICS-554B A/D converters is $N_{Th}^{A/D} = -80.54dBm$
- The noise measured in laboratory tests (input grounded by a 50Ω impedance load) is: $N^{A/D}(B_n = 200kHz) = -73dBm$; as previously mentioned, this value represents the sum of thermal and quantization noises. Therefore, as expected, the thermal noise is greater than the quantization noise, and it limits the dynamic of the A/D converter.
- From the measured value of noise ($N^{A/D}(B_n = 200kHz)$), the $ENOB$ value can be obtained: $ENOB \cong 11.83$

Also, from the equation (84), the noise figure of the A/D converter can be evaluated: $F = +174 - 10\log 10(B_n) + N^{A/D} = +174 - 10\log 10(200000) + -73 \cong 48dB$. This value will be used for the calculation of the overall noise figure of the receivers.

4.5.1.1. RESULTS FOR WB ARCHITECTURE

In order to measure the noise power in the WB receiver, the input of the receiving chain is connected to ground by a 50Ω load (see the corresponding block diagram in Figure 41).

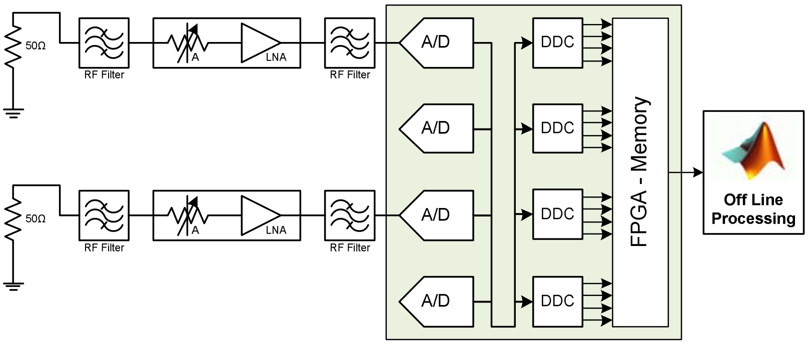

Figure 41 – WB noise measures block diagram

Before performing the noise measurements, the level diagram (reported in Table 9) has been realized in order to calculate the expected noise values for the reference (REF) and surveillance (SURV) channels of the WB receiver. In this level diagram, and in the test measures, the considered bandwidth is $B_n = 200kHz$.

REF			Variable Attenuator	A/D
$N_{ThCn}\,Input\ \ [dBm]$		-61,99	-63,99	-72,99
$F_{Cn}\,Input\ \ [dB]$		59,00	57,00	48,00
			Variable Attenuator	A/D
			ZX76-31R5-PN+	ICS-554B
$F_{Cn}\ \ [dB]$		2,0	9,00	48,00
$G_{Cn}\ \ [dB]$		-2,0	-9,00	0,00
$\sum G_{Cn}\ \ [dB]$	-11,0			
$B_n\ \ [MHz]$	0,2			

SURV			Variable Attenuator	A/D
$N_{ThCn}\,Input\ \ [dBm]$		-59,19	-61,19	-72,99
$F_{Cn}\,Input\ \ [dB]$		61,80	59,80	48,00
			Variable Attenuator	A/D
			ZX76-31R5-PN+	ICS-554B
$F_{Cn}\ \ [dB]$		2,0	11,80	48,00
$G_{Cn}\ \ [dB]$		-2,0	-11,80	0,00
$\sum G_{Cn}\ \ [dB]$	-13,8			
$B_n\ \ [MHz]$	0,2			

Table 9 – Level diagram of WB receiver

The results for the WB receiver noise measures, for different values of frequency, are reported in Figure 42. The measures have been performed for the FM radio channels frequencies of interest.

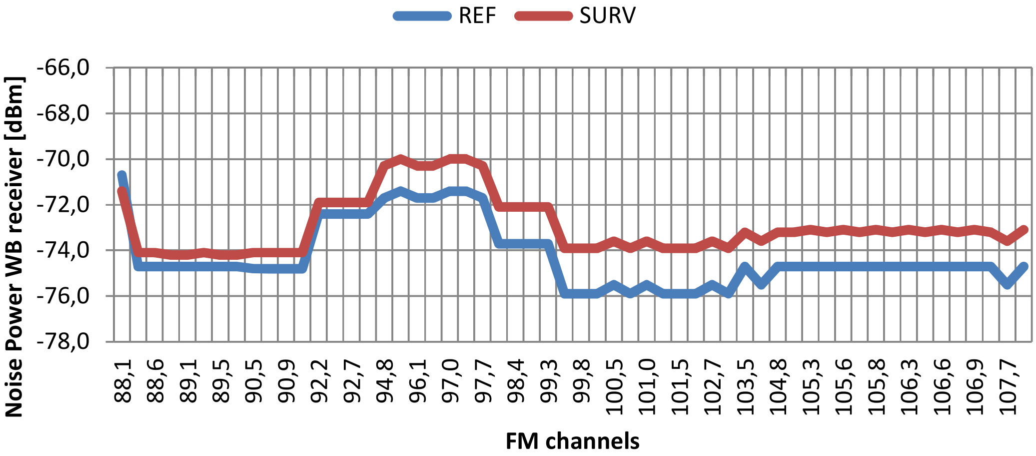

Figure 42 – WB receiver noise measures

As shown in Figure 42, the results obtained are comparable with the noise values expected. However, there are differences due to interfering disturbances with power level higher than to the noise power.

4.5.1.2. RESULTS FOR NB ARCHITECTURE

The same procedure has been repeated to measure the noise power in the NB (see the corresponding block diagram in Figure 43).

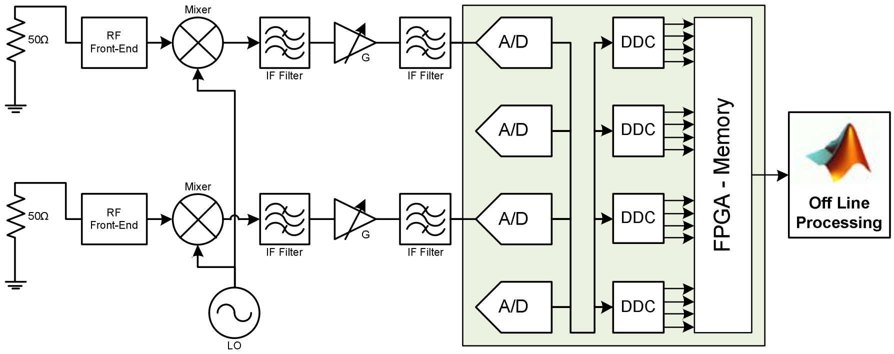

Figure 43 – NB noise measures block diagram

Before performing the noise measurements, the level diagram (reported in Table 10) has been realized in order to calculate the expected noise values for the reference (REF) and surveillance (SURV) channels of the WB receiver. In this level diagram, and in the test measures, the considered bandwidth is $B_n = 200\,kHz$.

REF		RF Filter	Variable Attenuator	Mixer	IF Filter	Amplifier	Amplifier	A/D
$N_{ThCn}\ Input\ [dBm]$		-79,02	-81,02	-102,02	-107,22	-114,22	-92,22	-70,22
$F_{Cn}\ Input\ [dB]$		41,97	39,97	18,97	13,77	6,77	26,02	48,00
		RF Filter	Variable Attenuator	Mixer	IF Filter	Amplifier	Amplifier	A/D
		88÷108 MHz	ZX76-31R5-PN+	ZX05-1MHW		ZHL-2010+	ZHL-2010+	ICS-554B
$F_{Cn}\ [dB]$		2,00	21,00	5,20	7,00	3,50	3,50	48,00
$G_{Cn}\ [dB]$		-2,00	-21,00	-5,20	-7,00	22,00	22,00	0,00
$\sum G_{Cn}\ [dB]$	8,8							
$B_n\ [MHz]$	0,2							

SURV		RF Filter	Variable Attenuator	Mixer	IF Filter	Amplifier	Amplifier	A/D
$N_{ThCn}\ Input\ [dBm]$		-73,22	-75,22	-102,02	-107,22	-114,22	-92,22	-70,22
$F_{Cn}\ Input\ [dB]$		47,77	45,77	18,97	13,77	6,77	26,02	48,00
		RF Filter	Variable Attenuator	Mixer	IF Filter	Amplifier	Amplifier	A/D
		88÷108 MHz	ZX76-31R5-PN+	ZX05-1MHW		ZHL-2010+	ZHL-2010+	ICS-554B
$F_{Cn}\ [dB]$		2,00	26,80	5,20	7,00	3,50	3,50	48,00
$G_{Cn}\ [dB]$		-2,00	-26,80	-5,20	-7,00	22,00	22,00	0,00
$\sum G_{Cn}\ [dB]$	3,0							
$B_n\ [MHz]$	0,2							

Table 10 – Level diagram of NB receiver

The results for the NB receiver noise measures, for different values of frequency, are reported in Figure 44. The measures have been performed for the FM radio channels frequencies of interest.

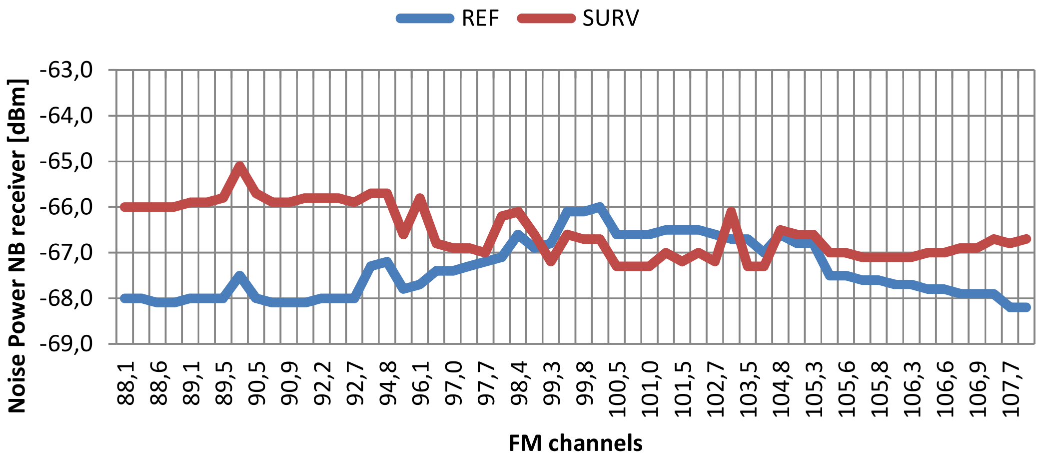

Figure 44 – NB receiver noise measures

As shown in Figure 44, the measured power is greater than the expected level. In this case, we do not have a true measure of noise, but a measure of all disturbance components (system intermodulation) in the single radio channel bandwidth. As a consequence, this is the disturbance level which determinates the dynamic of the system.

4.5.2. DISTURBANCE CANCELLATION PERFORMANCE

Different tests were performed to evaluate the theoretical maximum cancellation level that can be obtained with the two developed architectures. This parameter is directly related to the correlation level between the signals acquired with the different receiver channels. The acquired data sets were processed using the cancellation algorithms described in [6].

The tests have been performed in the laboratory of DIET Department of University of Rome "La Sapienza". This location is indicated as Site 1 in 4.6 where some details are reported for each scenario. All the different tests are referred to both receiver architectures: WB results are reported in sub-section 4.5.2.1, NB results in sub-section 4.5.2.2 and a comparison between both systems is reported in sub-section 4.5.2.3.

4.5.2.1. RESULTS FOR WB ARCHITECTURE

In Figure 45 is reported the block diagram of the WB receiver configuration used to performed tests in controlled scenario: a single antenna is connected to two receiving channels by a power divider. The analogue Front-End is composed by an FM pass-band filter and a Variable attenuator (the FM signal power level in Site 1, where laboratory tests have been performed, is greater than the full-scale of the data-capture). A preliminary analysis has been conducted in order to select a proper attenuation level for each receiving channel, matching the A/D converter dynamic range. The selected attenuation values are:

- 9 dB (6 dB by variable attenuator and 3 dB by power divider) for the signal provided by reference antenna (pointed toward Monte Cavo, bearing angle 120°, measured clockwise with respect to North)
- 11.8 dB (8.8 dB by variable attenuator and 3 dB by power divider) for the signal provided by surveillance antenna (pointed toward Monte Mario, bearing angle 300°)

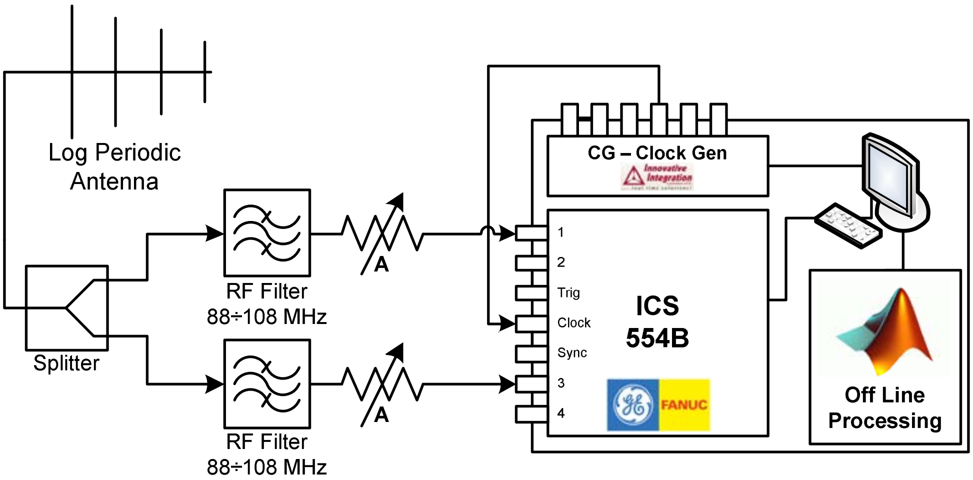

Figure 45 – WB receiver block diagram for "single antenna" disturbance cancellation tests

The cancellation values obtained with WB receiver for some FM radio channels of interest are summarized in Table 11. Specifically, each row contains the Direct-to-Noise Ratio (DNR) measured over the two receiving channels, the theoretical cancellation (function of DNR value), the measured cancellation (obtained as the ratio between the power levels measured, over a 200 kHz bandwidth, at the input and at the output of the cancellation filter), and the difference between theoretical and measured cancellation (CA Loss).

Ch Radio [MHz]	DNR REF [dB]	DNR SURV [dB]	CA TEO [dB]	CA MEAS [dB]	CA LOSS [dB]
90.7	50.1	49.1	46.6	46.4	0.2
91.2	46.4	45.3	42.8	42.4	0.4
92.4	57.3	56.1	53.6	53.4	0.2
92.7	56.1	55.2	52.6	52.4	0.2
103.0	58.5	56.4	54.3	54.3	0.0
105.3	65.8	63.5	61.5	61.1	0.4

Table 11 – Disturbance cancellation values for WB receiver (single antenna acquisitions)

As is apparent, this solution is able to achieve measured cancellation values comparable with the theoretical reference.

In Figure 46 is reported the block diagram of WB receiver configuration used to perform “double antenna acquisitions”: two antennas are connected to two receiving channels. As for the previous test, the analogue Front-End is composed by an FM pass band filter and a Variable attenuator (the FM signal power level in Site 1, where laboratory tests have been performed, is greater than the full-scale of the data-capture). A preliminary analysis has been conducted in order to select a proper attenuation level for each receiving channel, matching the A/D converter dynamic range. The selected attenuation values are:

- 9 dB for the signal provided by reference antenna (pointed toward Monte Cavo, bearing angle 120° N)
- 11.8 dB for the signal provided by surveillance antenna (pointed toward Monte Mario, bearing angle 300° N).

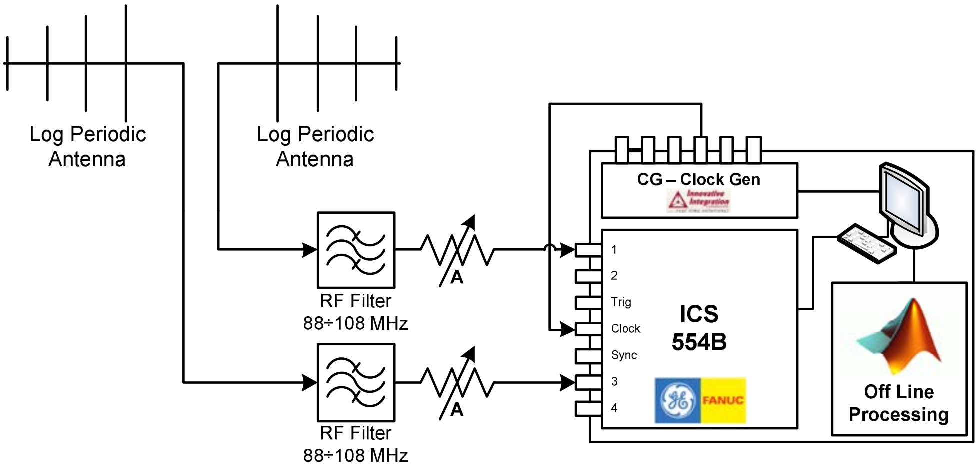

Figure 46 – WB receiver block diagram for “double antenna” disturbance cancellation tests

The cancellation values obtained with WB receiver are summarized in **Table 12**. In this analysis, all the FM channels transmitted by Rocca di Papa, Monte Cavo and Montecompatri transmitters are considered (for more details on geometrical aspects and transmitters of opportunity selection, see sub-section 4.6). Specifically, each row contains the Power (Pow) measured over the two receiving channels, DNR measured over the two receiving channels, the theoretical cancellation (function of DNR value), the measured cancellation (obtained as the ratio between the power levels measured, over a 200 kHz bandwidth, at the input and at the output of the cancellation filter), and the difference between theoretical and measured cancellation (CA Loss).

Ch Radio [MHz]	Pow REF [dBm]	Pow SURV [dBm]	DNR REF [dB]	DNR SURV [dB]	CA TEO [dB]	CA MEAS [dB]	CA LOSS [dB]
88,1	-24,9	-35,7	45,8	35,7	35,3	33,1	2,2
88,3	-26,7	-35,1	48,0	39,0	38,5	32,2	6,3
88,6	-18,0	-27,5	56,7	46,6	46,2	29,8	16,4
88,9	-21,3	-31,7	53,4	42,5	42,1	23,0	19,1
89,1	-24,4	-34,3	50,3	39,9	39,5	20,8	18,7
89,3	-20,8	-30,7	53,9	43,4	43,1	23,9	19,2
89,5	-27,1	-37,2	47,6	37,0	36,6	18,1	18,5
90,3	-20,8	-32,6	53,9	41,6	41,3	35,1	6,2
90,5	-24,3	-34,8	50,5	39,3	39,0	32,0	7,0
90,7	-25,3	-37,3	49,5	36,8	36,5	27,6	8,9
90,9	-17,3	-29,4	57,5	44,7	44,4	35,3	9,2
91,2	-25,7	-40,9	49,1	33,2	33,1	25,7	7,4
92,2	-54,7	-61,5	17,7	10,4	10,0	1,9	8,1
92,4	-18,9	-32,4	53,5	39,5	39,4	33,8	5,6
92,7	-16,8	-28,1	55,6	43,8	43,5	36,6	6,9
94,5	-16,8	-30,5	55,6	41,4	41,3	34,8	6,4
94,8	-26,6	-38,8	45,1	31,5	31,3	22,7	8,6
95,5	-24,5	-36,1	46,9	33,9	33,7	28,9	4,8
96,1	-18,2	-31,1	53,5	39,2	39,1	22,4	16,7
96,8	-23,4	-34,5	48,3	35,8	35,5	20,7	14,8
97,0	-28,9	-41,7	42,5	28,3	28,2	12,8	15,3
97,2	-30,0	-45,3	41,4	24,7	24,6	9,5	15,1
97,7	-21,4	-38,3	50,3	32,0	31,9	20,2	11,7
98,1	-22,6	-36,8	51,1	35,3	35,1	15,8	19,3
98,4	-24,2	-35,9	49,5	36,2	36,0	19,0	17,0
99,0	-21,6	-35,8	52,1	36,3	36,2	18,8	17,3
99,3	-27,5	-38,2	46,2	33,9	33,7	22,0	11,7
99,6	-20,6	-31,1	55,3	42,8	42,6	35,9	6,7
99,8	-23,4	-35,6	52,5	38,3	38,1	31,7	6,4
100,0	-21,5	-34,4	54,4	39,5	39,4	33,8	5,6
100,5	-27,4	-28,6	48,1	45,0	43,3	0,5	42,7
100,7	-20,1	-32,2	55,8	41,7	41,6	34,4	7,1
101,0	-23,7	-44,8	51,8	28,8	28,8	19,3	9,5
101,3	-22,7	-35,1	53,2	38,8	38,6	32,7	5,9
101,5	-19,9	-30,8	56,0	43,1	42,9	37,1	5,8
101,9	-14,8	-25,0	61,1	48,9	48,7	40,7	8,0
102,7	-18,0	-41,8	57,5	31,8	31,8	23,9	7,8
103,0	-15,4	-28,8	60,5	45,1	44,9	40,8	4,1
103,5	-25,1	-38,4	49,6	34,8	34,7	28,6	6,1
104,2	-23,9	-44,7	51,6	28,9	28,9	23,4	5,5
104,8	-20,5	-35,0	54,2	38,2	38,1	12,7	25,3
105,3	-17,5	-30,0	57,2	43,2	43,0	38,2	4,9
105,6	-18,9	-31,4	55,8	41,7	41,5	32,1	9,5
105,8	-19,5	-30,6	55,2	42,5	42,3	38,7	3,5
106,3	-21,6	-34,3	53,1	38,9	38,7	29,1	9,6
106,3	-21,7	-34,4	53,0	38,7	38,6	28,3	10,3
106,6	-19,5	-33,0	55,2	40,1	39,9	30,7	9,2
106,9	-28,6	-43,7	46,1	29,5	29,4	25,2	4,2
106,9	-28,7	-43,7	46,0	29,4	29,3	25,3	4,0
107,1	-28,6	-43,7	46,1	29,5	29,4	25,2	4,2
107,7	-25,8	-40,3	49,7	33,3	33,2	27,3	5,9
107,9	-19,9	-32,9	54,8	40,2	40,1	36,8	3,2

Table 12 – Disturbance cancellation values for WB receiver (double antenna acquisitions)

The measured cancellation values show significant differences among the considered FM radio channels. In fact, this parameter also depends on the instantaneous characteristics of the radio transmission and of e.m. propagation.

In all cases, the theoretical cancellation is directly related to the signal DNR. The measured cancellation is influenced by the decorrelation effects between reference and surveillance signals. The decorrelation level is directly related to the frequency response difference of the different receiver chains.

This preliminary extensive analysis allowed to select, among the considered ones, the best radio channels, namely the channels with high level of measured CA and low CA Loss value, in order to perform the following tests.

4.5.2.2. RESULTS FOR NB ARCHITECTURE

In Figure 47 is reported the block diagram of the NB receiver configuration used to perform tests in a controlled scenario: a single antenna is connected to two receiving channel by a power divider. The analogue Front-End is composed only by an FM pass-band filter and a variable attenuator (the FM signal power level in Site 1, where laboratory tests has been performed, is greater than the dynamic input of the mixer). The IF amplification is provided by two ZHL-2010+ devices mounted in series. The NI_PXI_5670 device has been used as Local Oscillator source for the laboratory tests. A preliminary analysis has been realized in order to select a proper attenuation value for the RF Front-End section of each receiving channel. The selected attenuation values are:

- 21 dB (18 dB by variable attenuator and 3 dB by power divider) for the signal provided by reference antenna (pointed toward Monte Cavo, bearing angle 120° N)
- 26.8 dB (23.8 dB by variable attenuator and 3 dB by power divider) for the signal provided by surveillance antenna (pointed toward Monte Mario, bearing angle 300° N).

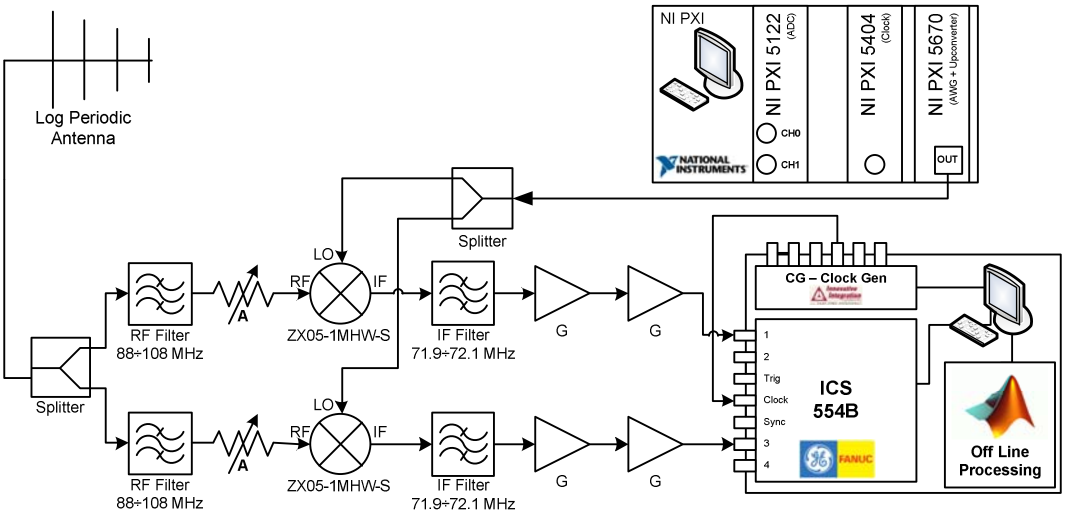

Figure 47 – NB receiver block diagram for “single antenna” disturbance cancellation tests

The cancellation values obtained with NB receiver for some FM radio channels of interest are summarized in **Table 13**. Specifically, each row contains the DNR measured over the two receiving channels, the theoretical cancellation (function of DNR value), the measured cancellation (obtained as the ratio between the power levels measured, over a 200 kHz bandwidth, at the input and at the output of the cancellation filter), and the difference between theoretical and measured cancellation (CA Loss).

Ch Radio [MHz]	DNR REF [dB]	DNR SURV [dB]	CA TEO [dB]	CA MEAS [dB]	CA LOSS [dB]
90.7	61.0	60.2	57.6	54.7	2.8
91.2	56.6	55.7	53.1	51.8	1.3
92.4	65.8	64.8	62.2	55.9	6.3
92.7	71.4	70.4	67.9	61.9	6.0
103.0	60.0	60.4	57.2	55.1	2.0
105.3	58.5	59.3	55.9	52.2	3.7

Table 13 – Disturbance cancellation values for NB receiver (single antenna acquisitions)

As is apparent, this solution is able to achieve measured cancellation values comparable with the theoretical reference but not as good as in the WB system. The slightly higher CA losses in NB solution are probably due to residual decorrelation effects in the two channels of the receiver.

In Figure 48 is reported the block diagram of the NB receiver configuration used to perform “double antenna acquisitions”: two antennas are connected to two receiving channels. The receiver configuration is the same used for the single antenna tests (without the power divider). The analogue Front-End is composed only by an FM pass-band filter and a variable attenuator. The IF amplification is provided by two ZHL-2010+ devices mounted in series. The NI_PXI_5670 device has been used as LO source for the laboratory tests. A preliminary analysis has been realized in order to select a proper attenuation value for the RF Front-End section of each receiving channel. The selected attenuation values are:

- 21 dB for the signal provided by reference antenna (pointed toward Monte Cavo, bearing angle 120° N)
- 26.8 dB for the signal provided by surveillance antenna (pointed toward Monte Mario, bearing angle 300° N).

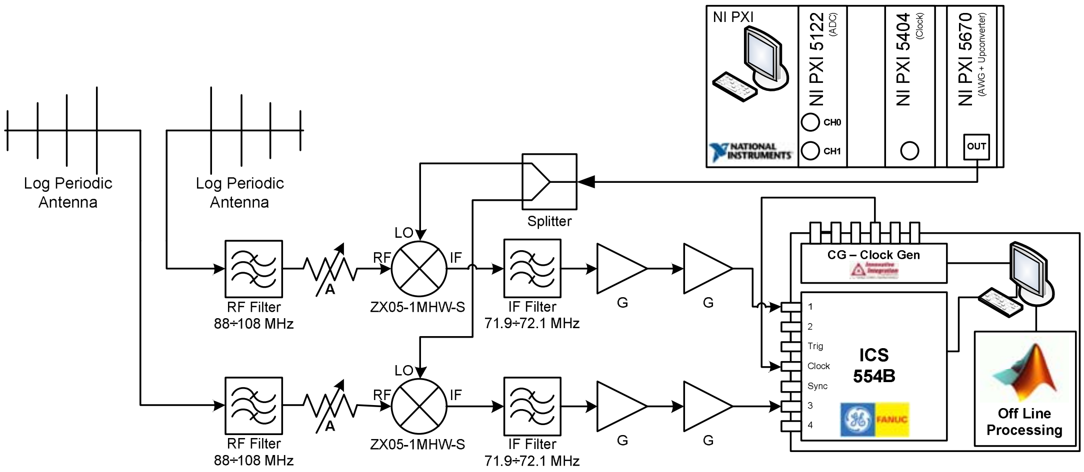

Figure 48 – NB receiver block diagram for “single antenna” disturbance cancellation tests

The cancellation values obtained with NB receiver are summarized in **Table 14**. As for the WB receiver, in this analysis are considered all FM channels transmitted by Rocca di Papa, Monte Cavo and Montecompatri transmitters (for more details on geometrical aspects and transmitters of opportunity selection, see sub-section 4.6). Specifically, each row contains the Power (Pow) measured over the two receiving channels, DNR measured over the two receiving channels, the theoretical cancellation (function of DNR value), the measured cancellation (obtained as the ratio between the power levels measured, over a 200 kHz bandwidth, at the input and at the output of the cancellation filter), and the difference between theoretical and measured cancellation (CA Loss).

Ch Radio [MHz]	Pow REF [dBm]	Pow SURV [dBm]	DNR REF [dB]	DNR SURV [dB]	CA TEO [dB]	CA MEAS [dB]	CA LOSS [dB]
88,1	-3,0	-19,2	51,8	32,7	32,7	30,7	2,0
88,3	-5,4	-19,7	49,4	32,2	32,1	27,8	4,3
88,6	3,9	-10,4	58,7	41,4	41,3	39,1	2,2
88,9	0,1	-16,6	54,9	35,1	35,0	30,2	4,8
89,1	-3,3	-19,4	51,6	32,3	32,3	29,8	2,5
89,3	0,3	-17,2	55,2	34,4	34,4	32,4	2,0
89,5	-6,6	-24,4	48,2	27,1	27,0	24,0	3,0
90,3	1,1	-18,8	55,1	31,6	31,6	29,4	2,2
90,5	-3,8	-21,5	51,1	30,0	30,0	26,7	3,3
90,7	-2,7	-25,1	51,4	27,0	27,0	21,8	5,2
90,9	4,0	-16,5	58,9	34,8	34,8	31,8	3,0
91,2	-3,6	-31,2	51,4	20,1	20,2	17,9	2,3
92,2	-36,8	-43,4	17,8	7,9	8,1	2,2	5,9
92,4	3,4	-16,5	58,1	34,8	34,8	31,6	3,2
92,7	4,8	-12,1	59,4	39,3	39,3	34,5	4,8
94,5	5,1	-12,9	60,1	38,4	38,3	33,4	4,9
94,8	-3,8	-20,1	49,5	31,2	31,2	22,5	8,7
95,5	-2,1	-15,8	51,9	36,8	36,7	31,4	5,3
96,1	3,3	-11,4	57,4	41,6	41,5	23,0	18,5
96,8	-1,7	-15,7	52,0	37,4	37,3	32,9	4,4
97,0	-7,4	-23,6	46,0	29,5	29,4	23,5	5,9
97,2	-7,3	-26,2	46,0	27,1	27,1	17,0	10,1
97,7	0,0	-20,8	53,2	32,5	32,5	26,6	5,9
98,1	-1,4	-20,1	51,6	33,3	33,3	28,2	5,1
98,4	-2,6	-18,4	50,3	35,2	35,1	30,7	4,4
99,0	-1,4	-17,8	51,2	36,0	35,9	31,3	4,6
99,3	-6,2	-18,5	46,3	35,4	35,1	30,1	5,0
99,6	0,6	-11,5	53,0	42,4	42,1	36,2	5,9
99,8	-2,8	-17,2	48,6	35,8	35,6	31,9	3,7
100,0	-3,8	-19,8	47,4	32,1	32,0	29,2	2,8
100,5	-7,2	-10,0	45,0	44,1	41,5	0,1	41,4
100,7	-5,7	-20,9	46,5	33,3	33,1	27,9	5,2
101,0	-5,2	-29,8	46,9	24,1	24,1	17,2	6,9
101,3	-3,0	-19,0	49,2	35,2	35,0	30,0	5,0
101,5	0,1	-14,0	52,3	40,1	39,8	35,5	4,3
101,9	5,3	-8,6	57,5	45,4	45,1	35,9	9,2
102,7	1,1	-29,7	54,4	24,3	24,3	17,8	6,5
103,0	3,9	-11,9	56,3	42,1	41,9	37,8	4,1
103,5	-5,5	-21,5	47,3	32,6	32,4	26,6	5,8
104,2	-4,9	-30,5	47,9	23,6	23,6	18,7	4,9
104,8	-0,4	-17,9	52,0	35,1	35,0	16,9	18,1
105,3	2,8	-12,4	55,5	40,6	40,5	35,2	5,3
105,6	1,0	-13,3	54,7	40,6	40,4	34,4	6,0
105,8	1,1	-12,5	55,0	41,5	41,3	36,9	4,4
106,3	-1,4	-17,3	52,8	36,5	36,4	29,7	6,7
106,6	1,1	-16,6	55,6	36,8	36,8	32,7	4,1
106,9	-5,9	-25,6	48,5	27,8	27,7	23,8	3,9
107,1	-3,3	-19,4	51,2	33,9	33,8	29,8	4,0
107,7	-4,7	-22,7	50,2	30,6	30,6	25,3	5,3
107,9	1,4	-13,9	56,5	39,3	39,2	33,7	5,5

Table 14 – Disturbance cancellation values for NB receiver (double antenna acquisitions)

Also in this case, as for the WB receiver, the measured cancellation values show significant differences among the considered FM radio channels.

Notice that, despite in the NB solution the analog section of the receiver is greater than the WB solution, the decorrelation effect is limited.

As already mentioned for the WB receiver, this preliminary extensive analysis allowed to select, among the considered ones, the best radio channels, namely the channels with high level of measured CA and low CA Loss value, in order to perform the following tests.

4.5.2.3. COMPARISON

In Figure 49 is reported the block diagram of the configuration used to compare the disturbance cancellation performance of WB and NB receivers. In this test, the two receivers analogue section (described in the previous section) are connected to the same data capture (ICS-554B). Reference antenna and surveillance antenna are connected to a dedicated channel of each system by a power divider. Data collected by both systems are recorded simultaneously. As previously mentioned, in Site 1, where laboratory tests have been performed, the analogue Front-End is composed only by an FM pass-band filter and a variable attenuator. A preliminary analysis has been realized in order to select a proper attenuation value for the RF Front-End section of each receiving channel. The selected attenuation values are:

- 21 dB for NB reference receiving channel (18 dB by variable attenuator and 3 dB by power divider)
- 26.8 dB for NB surveillance receiving channel (23.8 dB by variable attenuator and 3 dB by power divider)
- 9 dB for NB reference receiving channel (6 dB by variable attenuator and 3 dB by power divider)
- 11.8 dB for NB surveillance receiving channel (8.8 dB by variable attenuator and 3 dB by power divider)

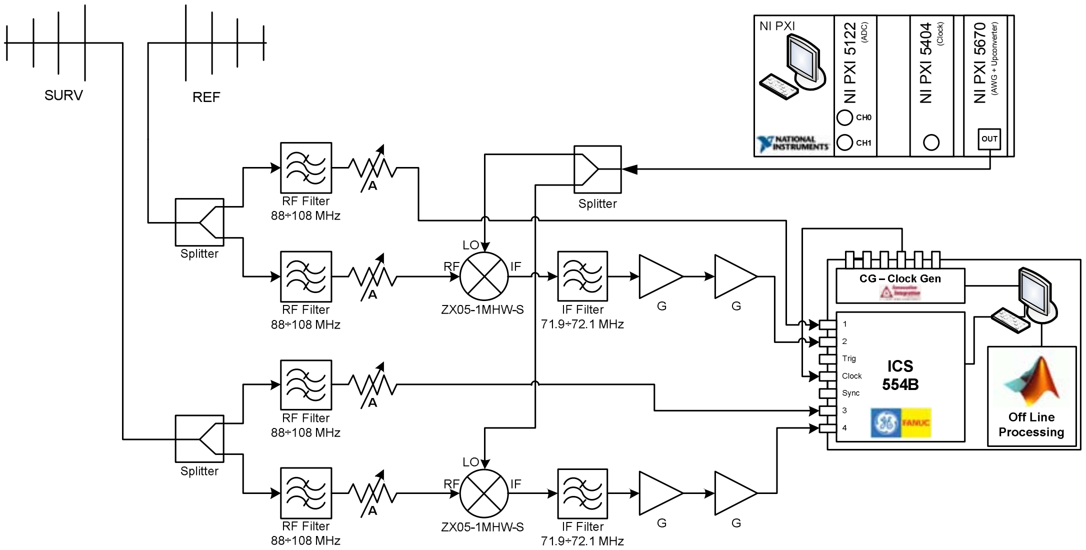

Figure 49 – block diagram of receiver configuration for WB and NB disturbance cancellation comparison

The cancellation values obtained with WB and NB receivers are summarized in **Table 15**. Also in this analysis all FM channels transmitted by Rocca di Papa, Monte Cavo and Montecompatri transmitters are considered (for more details on geometrical aspects and transmitters of opportunity selection, see sub-section 4.6). Specifically, each couple of rows contains (for WB and NB systems respectively) the Power (Pow) measured over the two receiving channels, DNR measured over the two receiving channels, the theoretical cancellation (function of DNR value), the measured cancellation (obtained as the ratio between the power levels measured, over a 200 kHz bandwidth, at the input and at the output of the cancellation filter), and the difference between theoretical and measured cancellation (CA Loss).

Ch Radio [MHz]	System	Pow REF [dBm]	Pow SURV [dBm]	DNR REF [dB]	DNR SURV [dB]	CA TEO [dB]	CA MEAS [dB]	CA LOSS [dB]
88,1	WB	-25,3	-40,3	45,4	31,1	30,9	23,8	7,1
88,1	NB	-4,0	-20,9	50,8	31,0	31,0	29,2	1,8
88,3	WB	-26,8	-39,6	47,7	34,2	34,0	29,6	4,5
88,3	NB	-5,7	-20,2	49,1	31,7	31,6	27,7	4,0
88,6	WB	-17,9	-31,3	56,9	42,7	42,5	29,6	12,9
88,6	NB	3,2	-11,8	58,0	40,0	40,0	37,8	2,1
88,9	WB	-21,5	-36,4	53,4	37,8	37,6	16,3	21,3
88,9	NB	-0,5	-17,5	54,3	34,2	34,2	29,6	4,6
89,1	WB	-24,7	-36,8	50,2	37,4	35,8	17,8	18,0
89,1	NB	-3,8	-20,0	51,1	31,7	31,7	28,3	3,4
89,3	WB	-21,2	-36,3	53,8	37,9	37,8	18,5	19,3
89,3	NB	0,0	-16,7	54,9	34,9	34,8	32,0	2,8
89,5	WB	-28,0	-43,6	47,0	30,7	30,6	12,7	17,9
89,5	NB	-6,9	-24,3	47,9	27,2	27,2	23,2	4,0
90,3	WB	-20,3	-37,6	54,7	36,7	36,7	30,7	6,0
90,3	NB	0,6	-17,9	54,6	32,5	32,4	29,5	2,9
90,5	WB	-24,5	-37,7	50,5	36,6	35,1	28,9	6,1
90,5	NB	-4,0	-21,1	50,9	30,4	30,3	27,0	3,3
90,7	WB	-24,7	-44,1	50,1	29,9	29,8	23,9	6,0
90,7	NB	-3,9	-25,0	50,2	27,1	27,1	22,3	4,8
90,9	WB	-17,8	-36,3	57,0	37,9	37,9	32,0	5,8
90,9	NB	3,1	-16,7	58,0	34,6	34,6	30,9	3,7
91,2	WB	-25,8	-47,8	48,8	26,2	26,2	20,0	6,2
91,2	NB	-4,8	-28,7	50,2	22,6	22,6	19,4	3,2
92,4	WB	-15,1	-33,2	57,6	39,2	39,1	30,5	8,6
92,4	NB	2,7	-16,0	57,4	35,3	35,3	31,0	4,4
92,7	WB	-17,4	-32,3	54,7	39,5	39,4	33,4	6,0
92,7	NB	4,1	-11,8	58,7	39,6	39,5	34,8	4,7
94,5	WB	-17,2	-34,1	54,3	36,3	36,2	33,9	2,3
94,5	NB	4,7	-13,8	59,7	37,5	37,5	32,1	5,4
94,8	WB	-26,7	-42,3	45,0	28,2	28,1	20,3	7,8
94,8	NB	-4,8	-21,7	48,5	29,6	29,6	20,9	8,7
95,5	WB	-25,0	-37,0	46,6	33,2	33,1	27,1	5,9
95,5	NB	-3,0	-16,6	51,0	36,0	35,9	30,3	5,6
96,8	WB	-24,9	-35,8	46,8	34,4	32,2	17,5	14,7
96,8	NB	-2,6	-18,4	51,1	34,7	34,6	30,1	4,5
97,0	WB	-29,2	-41,5	42,2	28,5	26,8	14,7	12,1
97,0	NB	-7,3	-24,5	46,1	28,6	28,5	22,9	5,6
97,7	WB	-23,0	-42,5	48,9	28,0	28,0	17,8	10,1
97,7	NB	-1,0	-22,6	52,3	30,7	30,7	24,7	6,0
98,1	WB	-23,6	-40,4	48,8	30,7	30,6	15,0	15,6
98,1	NB	-1,9	-20,8	51,1	32,6	32,6	27,2	5,4
98,4	WB	-25,3	-38,8	47,7	32,8	32,7	16,9	15,8
98,4	NB	-3,5	-19,0	49,3	34,6	34,4	30,1	4,3
99,3	WB	-28,4	-39,4	46,5	33,8	33,6	20,3	13,3
99,3	NB	-7,0	-19,9	45,5	34,0	33,7	28,4	5,4
99,6	WB	-20,9	-32,2	54,4	41,4	41,2	35,5	5,7
99,6	NB	-0,1	-13,2	52,3	40,7	40,4	34,0	6,4
99,8	WB	-24,2	-37,5	51,4	36,3	36,1	30,9	5,2
99,8	NB	-3,3	-18,6	48,1	34,4	34,3	30,1	4,1
99,9	WB	-23,9	-36,0	50,4	36,8	35,3	15,8	19,5

Ch Radio [MHz]	System	Pow REF [dBm]	Pow SURV [dBm]	DNR REF [dB]	DNR SURV [dB]	CA TEO [dB]	CA MEAS [dB]	CA LOSS [dB]
99,9	NB	-2,7	-19,4	49,9	34,4	34,3	29,2	5,1
100,0	WB	-22,2	-37,0	53,5	36,9	36,8	33,4	3,4
100,0	NB	-1,5	-18,3	49,7	33,6	33,5	30,3	3,2
100,7	WB	-21,4	-35,2	54,7	38,9	38,8	33,9	4,9
100,7	NB	-1,2	-16,9	51,0	37,3	37,1	31,1	6,0
101,0	WB	-25,8	-48,1	50,3	26,0	26,0	18,0	8,0
101,0	NB	-5,5	-29,8	46,6	24,1	24,1	16,9	7,2
101,3	WB	-23,8	-37,8	52,3	36,3	36,2	34,0	2,2
101,3	NB	-3,8	-19,8	48,4	34,4	34,2	28,7	5,5
101,5	WB	-20,5	-32,5	54,7	41,5	41,3	39,0	2,3
101,5	NB	-0,2	-14,2	52,0	39,9	39,6	34,7	5,0
101,9	WB	-15,2	-25,0	60,9	48,9	47,5	40,2	7,3
101,9	NB	4,6	-9,2	56,8	44,8	44,6	35,0	9,5
102,7	WB	-18,7	-47,3	57,0	26,4	26,4	22,0	4,4
102,7	NB	1,0	-29,7	53,3	24,3	24,3	17,3	6,9
103,0	WB	-16,5	-31,6	59,1	42,0	41,9	41,6	0,3
103,0	NB	3,4	-13,9	55,8	40,1	40,0	35,1	4,9
103,5	WB	-25,7	-40,7	49,6	32,6	32,5	28,2	4,3
103,5	NB	-5,7	-23,2	47,1	30,9	30,8	24,4	6,5
104,2	WB	-27,9	-51,4	47,0	21,8	21,8	19,1	2,7
104,2	NB	-8,0	-33,8	44,8	20,3	20,4	14,6	5,8
105,3	WB	-18,2	-31,3	56,4	41,9	41,7	39,8	1,9
105,3	NB	2,1	-13,2	54,8	39,8	39,7	34,0	5,7
105,6	WB	-17,1	-30,7	57,4	42,6	42,4	32,9	9,5
105,6	NB	0,5	-14,4	54,2	39,5	39,3	32,8	6,6
105,8	WB	-20,2	-32,1	54,4	41,2	41,0	40,5	0,5
105,8	NB	0,7	-13,5	54,6	40,5	40,3	34,7	5,6
106,3	WB	-23,2	-36,7	51,6	36,6	36,4	30,4	6,1
106,3	NB	-2,3	-18,3	51,9	35,5	35,4	29,0	6,4
106,6	WB	-20,6	-36,2	53,9	36,9	36,8	30,5	6,3
106,6	NB	0,5	-17,4	55,0	36,0	35,9	31,5	4,4
106,9	WB	-28,0	-43,2	46,8	29,8	28,8	26,2	2,6
106,9	NB	-6,9	-26,8	47,5	26,6	26,5	22,2	4,3
107,1	WB	-22,9	-40,8	51,9	32,2	32,2	32,0	0,2
107,1	NB	-1,7	-21,6	52,8	31,7	31,6	28,3	3,3
107,7	WB	-21,5	-38,4	53,3	34,5	34,4	27,6	6,9
107,7	NB	-5,0	-22,8	49,9	30,5	30,5	24,9	5,6
107,9	WB	-20,6	-34,3	54,2	38,5	38,3	38,0	0,3
107,9	NB	0,9	-14,7	56,0	38,5	38,4	32,7	5,7

Table 15 – Disturbance cancellation: comparison between WB and NB receivers

As previously said, the results obtained with both receivers are reported in Table 15. As is apparent, for a given FM channel, the DNR values obtained with WB and NB solution are comparable (both receivers have the same dynamic range for the reference and surveillance signals). On the contrary, different results have been obtained in terms of measured cancellation: WB system allows to obtain higher cancellation values for the FM radio channels with greater power. Vice versa, for the radio channels with low power, the NB receiver allows to obtain a greater cancellation because the dynamic range of the desired radio channel is properly matched with the full scale of the A/D converter.

As for the previous tests, this extensive acquisition campaigns represents a preliminary analysis aimed at the selection of the best performing radio channels for PBR operation.

4.6. ACQUISITION CAMPAIGNS

In order to perform the experimental activities different urban and rural sites have been identified for the field tests of the two developed PBR receivers.

In each site (see Figure 50), the reference antenna is steered towards a transmitter located on Monte Cavo (about 25km south-east of Rome), while the surveillance antenna (antennas) was pointed so as to include in its main beam many of the standard arrival/departure routes of the Leonardo da Vinci (Fiumicino) and Ciampino international airports.

Figure 50 – Sites for field tests

In the following, some information is summarized about the different identified sites. Specifically, latitude and longitude information is reported for each site, together with reference and surveillance antenna bearing angles (measured clockwise with respect to North). Also, position information about the considered transmitters of opportunity and about Ciampino and Fiumicino airports is reported:

- Site 1
    - Position: 41.892992 N – 12.493319 E (height 120m)
    - Ref antenna bearing: 120°
    - Surv antenna bearing: 300°
- Site 2
    - Position: 42.052642 N – 12.212178 E (height 245m)
    - Ref antenna bearing: 129°
    - Surv antenna bearing: 309°
- Site 3A
    - Position: 41.780980 N – 12.281103 E (height 58m)
    - Ref antenna bearing: 95°
    - Surv antenna bearing: 340°
- Site 3B
    - Position: 41.780980 N – 12.281103 E (height 58m)
    - Ref antenna bearing: 90°
    - Surv antenna bearing: 270°
- Site 4
    - Position: 41.759956 N – 12.450841 E (height 115.5m)
    - Ref antenna bearing: 92.5°

    - Surv antenna bearing: 310°
- Tx: Rocca di Papa / Monte Cavo
    - Position: 41.751061 N – 12.709800 E (height 927m)
- Tx: Montecompatri
    - Position: 41.800000 N – 12.733333 E (height 676m)
- Airport FCO (Leonardo da Vinci – Fiumicino)
    - Position: 41.801798 N – 12.241538 E
- Airport CIA (Ciampino)
    - Position: 41.798948 N – 12.595183 E

In each site, the first operation for the correct set up of the PBR system is the radio channel selection in order to maximize the performance of the receiver. As previously mentioned, in all the considered sites the reference antenna is steered towards a transmitter located on Monte Cavo. In fact, this preliminary analysis was performed in order to identify all radio channels transmitted by the radio broadcasting systems located in the Monte Cavo area. For this purpose Table 16 summarizes all the FM radio channels transmitted by transmitters reported in Figure 50 (Monte Cavo, Rocca di Papa and Montecompatri). For each radio channel, the information relative to the signal polarization, radio name and transmitter, is reported.

Ch Radio [MHz]	Pol.	Program	Transmitter
88,3	v	Ecoradio	Rocca di Papa (rm)
87,6	c	RAI Radio1 (Lazio)	Rocca di Papa/Monte Cavo vetta (RAI) (rm)
87,9	v	Radio Onda Rossa-ROR	Rocca di Papa/Monte Cavo (rm)
88,1	v	Radio Manà Manà Sport	Rocca di Papa/Monte Cavo (rm)
88,6	v	Radio Radicale	Rocca di Papa/Monte Cavo (rm)
88,9	v	Radio Città Aperta	Rocca di Papa/Monte Cavo (rm)
89,1	v	Radio Manà Manà	Rocca di Papa/Monte Cavo (rm)
89,3	v	Qlub Radio	Rocca di Papa/Monte Cavo (rm)
89,5	v	Radio Classica	Rocca di Papa/Monte Cavo (rm)
90,3	v	Radio Deejay	Rocca di Papa/Monte Cavo (rm)
90,5	v	m2o	Rocca di Papa (rm)
90,7	v	Teleradiostereo 2	Rocca di Papa (rm)
90,9	v	Radio Manà Manà Sport	Rocca di Papa/Monte Cavo (rm)
91,2	h	RAI Radio2	Rocca di Papa/Monte Cavo vetta (RAI) (rm)
92,2	v	RTL 102.5	Rocca di Papa/Monte Cavo (rm)
92,4	v	RTL 102.5	Rocca di Papa/Monte Cavo (rm)
92,7	v	Teleradiostereo	Rocca di Papa (rm)
94,5	v	Radio Subasio	Rocca di Papa/Monte Cavo (rm)
94,7		Radio Subasio	Rocca di Papa-Via Ariccia (rm)
94,8	v	Radio Maria	Rocca di Papa/Monte Cavo (rm)
95,1	v	Radio Maria	Montecompatri (rm)
95,5	v	Radio Capital	Montecompatri (rm)
96,1	v	Radio 105 Network	Rocca di Papa/Monte Cavo (rm)
96,8	v	Radio Incontro Italia	Rocca di Papa/Monte Cavo (rm)
97,0	v	m2o	Montecompatri (rm)
97,2	v	Radio Kiss Kiss	Montecompatri (rm)
97,7	v	Radio Città Futura	Rocca di Papa/Monte Cavo (rm)
98,1	v	Radio Sei	Rocca di Papa/Monte Cavo (rm)
98,4	h	RAI Radio3	Rocca di Papa/Monte Cavo vetta (RAI) (rm)
99,0	v	Radio Ti Ricordi	Rocca di Papa (rm)
99,3	v	RAI GR Parlamento	Rocca di Papa/Monte Cavo vetta (RAI) (rm)
99,6	v	Radio Globo	Rocca di Papa/Monte Cavo (rm)
99,8	v	Radio Ies	Rocca di Papa (rm)
100,0	v	R101	Rocca di Papa/Monte Cavo (rm)
100,5	v	Radio Globale	Montecompatri (rm)
100,7	v	Voxson Vintage Radio	Rocca di Papa/Monte Cavo (rm)
101,0	v	Radio Deejay	Montecompatri (rm)

Ch Radio [MHz]	Pol.	Program	Transmitter
101,3	v	Radio Centro Suono	Rocca di Papa/Monte Cavo (rm)
101,5	v	Radio Centro Suono Sport	Rocca di Papa/Monte Cavo (rm)
101,7	v	Radio Evangelo (Roma)	Rocca di Papa/Monte Cavo (rm)
101,9	v	Dimensione Suono Roma	Rocca di Papa/Monte Cavo (rm)
102,7	v	RAM Power	Montecompatri (rm)
103,0	v	RDS - Radio Dimensione Suono	Rocca di Papa/Monte Cavo (rm)
103,5	v	RAI Isoradio	Rocca di Papa (RAI) (rm)
104,0	v	Radio Roma	Montecompatri (rm)
104,2	v	Radio Italia Solo Musica Italiana	Montecompatri (rm)
104,8	v	Radio Voce della Speranza	Rocca di Papa/Monte Cavo (rm)
105,3	v	Dimensione Suono Due	Rocca di Papa/Monte Cavo (rm)
105,6	v	Rete Sport	Rocca di Papa (rm)
105,8	v	Radio Incontro	Rocca di Papa/Monte Cavo (rm)
106,3	v	RMC - Radio Monte Carlo	Rocca di Papa/Monte Cavo (rm)
106,6	v	Radio Rock	Rocca di Papa/Monte Cavo (rm)
106,9	v	Radio Mambo	Rocca di Papa/Monte Cavo (rm)
107,1	v	Antenna Uno	Rocca di Papa/Monte Cavo (rm)
107,7	v	Radio Romantica	Montecompatri (rm)
107,9	v	Radio 24	Rocca di Papa/Monte Cavo (rm)

Table 16 – List of FM radio channels transmitted by Monte Cavo, Rocca di Papa and Montecompatri

In each site, a preliminary analysis of the FM frequency spectrum is performed aiming at selecting the best three/four channels according to proper parameters. This selection can be based on analysis performed in both temporal and spectral domain by scanning all the available carrier frequencies. Specifically, the following main criteria can be adopted for the selection of the best suited channels for FM-based PBR purposes:

- Direct signal-to-Noise Ratio (DNR): the channels characterized by higher values of the DNR might be firstly selected since this parameter allows to identify the high power transmissions and strongly affects the theoretical cancellation and the detection performance of the system.

- Reference to Surveillance Power Ratio: based on the PBR geometry, the ratio of the power levels measured over a single channel on the reference and surveillance antennas should be comparable to the Front-to-Back ratio of the used antennas. This criterion allows to identify the FM radio channels transmitted by transmitters contained into the 3 dB reference antenna pattern, as required by the PBR geometry. Moreover it allows to roughly discard all the FM radio channels which are highly affected by multipath and co-/inter-channel interferences.

- Program content: due to the deep impact of the waveform's characteristics on the PBR performance, it is reasonable to prefer FM radio channels usually broadcasting music and to discard the ones that usually or currently transmit speech radio programs.

4.6.1. SUMMARY OF PERFORMED TESTS & ACQUISITIONS

Different tests and acquisition campaigns have been performed in the identified sites: **Table 17** summarizes the most important acquisition campaigns performed in the last months, together with the indication of the exploited receiver configuration (WB, NB or both) and a short description of the performed acquisitions: Multi-channel, single channel and so on. Notice that, at this stage of its development, the NB receiver allows the acquisition of a single FM channel or of a small group of adjacent FM radio channels.

Different tests and acquisition campaigns have been performed in the identified sites: **Table 17** summarizes the most important acquisition campaigns performed in the last months, together with the indication of the exploited receiver configuration (Wide-Band – WB, Narrow-Band – NB, or both) and a short description of the performed acquisitions: multi-channel, single channel, time, duration and so on. In particular, in this document, we report the most interesting results obtained with the passive sensor and specifically in the Site 3(A-B), for all the acquisition campaigns scheduled in Table 17. Notice that, after the preliminary tests, we have focused the attention on site (3A-B), which has been selected as the most suited to perform the test bed validation in cooperation with Selex-SI and ENAV: this joint test has been performed on 12th December 2012, aimed at detecting and tracking a small target (Piaggio P180 aircraft) in a short range. The results of this acquisition campaign are reported in Section 4.7.1.2. This site represents an interesting choice also for the acquisition of civil air traffic; moreover, two different pointing angles for the surveillance antennas have been considered during the performed acquisition campaigns:

- Site 3A is defined in order to detect and localize targets approaching to Leonardo da Vinci (FCO) Airport in Fiumicino (in Rome). The surveillance antennas bearing is about 340° North clockwise
- Site 3B is defined in order to detect and localize the cooperative target used in the joint validation acquisition campaign (as described in the Section 4.7.1.2). The surveillance antennas bearing is about 270° North clockwise

Date	Site / Sites	RX configuration	General description
02/09/2011	2	WB	Single-channel / Multi-channel
16/09/2011	3A	WB	Single-channel / Multi-channel
16/09/2011	4	WB	Single-channel
01/12/2011	1	WB	Multi-channel
05/12/2011	1	WB	Multi-channel
06/12/2011	1	WB	Multi-channel
17/02/2012	1	WB / NB	Multi-channel (WB) / Single-channel (NB)
23/02/2012	1	WB / NB	Multi-channel (WB) / Single-channel (NB)
31/05/2012	3A / 1	WB / NB	Multi-channel (WB) / Single-channel (NB)
06/06/2012	4 / 1	WB / NB	Multi-channel (WB) / Single-channel (NB)
07/06/2012	3A / 1	WB / NB	Multi-channel (WB) / Single-channel (NB)
11/06/2012	3A / 1	WB / NB	Multi-channel (WB) / Single-channel (NB)
20/11/2012	3A / 3B	WB	Multi-channel (WB)
22/11/2012	3A / 3B	WB	Multi-channel (WB)
12/12/2012	3A / 3B	WB	Multi-channel (WB)

Table 17 – Summary of the main acquisition campaigns performed

For each site, the following information are reported:

- Short description of the site
- Receiver configuration
- List of the analyzed FM radio channels with the corresponding measured power levels and cancellation values
- List of the FM radio channels selected for PBR acquisitions.

A. Site 1

Site 1 is located in the centre of Rome and corresponds to the roof of the DIET Dept. of University of Rome "La Sapienza". This is the site where all the preliminary tests described in the previous sections have been performed. The position (see Figure 50) allows to perform acquisitions observing the glideslope of Ciampino Airport. However, from an electromagnetic point of view, this site is characterized by the presence of significant co-/inter-channel interferences, due to the high number of FM transmitters located in the surroundings.

The FM radio channels analyzed in this site are summarized in Table 15 together with the Power measured over the two receiving channels, DNR measured over the two receiving channels, the theoretical cancellation, the measured cancellation, and the difference between theoretical and measured cancellation (CA Loss).

Based on the performed analysis, the following FM radio channels have been selected for PBR acquisitions: 90.7, 91.2, 92.4, 92.7, 103.0 and 105.3 MHz.

B. Site 2

Site 2 (see Figure 50) is located in a rural area about 30 km North of Rome (near Bracciano lake). This site is located in the proximities of the beginning of the two main glideslopes to Fiumicino Airport. Both Monte Mario and Monte Cavo can be used in this site as transmitters of opportunity, however, for the Monte Cavo transmitter the baseline is significantly longer than in the other considered sites (see Figure 50), thus resulting in a reduced coverage for the PBR system.

The FM radio channels analyzed in this site are summarized in Table 18 together with the Power measured over the two receiving channels and the measured cancellation values evaluated with the WB receiver with the following Front-End configuration:

- REF chain gain: 0dB
- SURV chain gain: 15dB.

Ch Radio [MHz]	Pol.	Transmitter	Pow REF [dBm]	Pow SURV [dBm]	CA MEAS [dB]
87,6	c	Rocca di Papa/Monte Cavo vetta (RAI) (rm)	-24,3	-33,2	20,2
92,4	v	Rocca di Papa/Monte Cavo (rm)	-18,1	-21,7	32,0
94,5	v	Rocca di Papa/Monte Cavo (rm)	-12,3	-18,8	34,3
95,1	v	Montecompatri (rm)	-17,7	-23,7	24,4
96,8	v	Rocca di Papa/Monte Cavo (rm)	-20,0	-24,9	25,6

Table 18 – Power level and cancellation values in site 2

C. Site 3A

Site 3A (see Figure 50) is a rural site located in the proximities of Fiumicino Airport. In this site, preliminary tests for the evaluation of the PBR DoA estimation capability have been performed with two surveillance antennas pointed towards the two main glideslopes to Fiumicino Airport.

The FM radio channels analyzed in this site are summarized in Table 19 together with the power level measured over the three receiving channels and the measured cancellation values evaluated with the WB receiver with the following Front-End configuration:

- REF chain gain: 0dB
- SURV 1 chain gain: 5.7dB
- SURV 1 chain gain: 5.7dB.

Based on the performed analysis, the following FM radio channels have been selected for PBR acquisitions: 90.3, 94.5, 99.6, 103.0, 106.6 and 107.1 MHz.

Ch Radio [MHz]	Pol.	Transmitter	Pow REF [dBm]	Pow SURV 1 [dBm]	Pow SURV 2 [dBm]	CA MEAS 1 [dB]	CA MEAS 2 [dB]
88,9	v	Rocca di Papa/Monte Cavo (rm)	-17,4	-19,3	-19,3	37,3	36,8
89,1	v	Rocca di Papa/Monte Cavo (rm)	-19,9	-21,5	-19,5	39,8	40,0
90,3	v	Rocca di Papa/Monte Cavo (rm)	-16,3	-17,0	-16,3	46,0	45,0
92,4	v	Rocca di Papa/Monte Cavo (rm)	-13,0	-12,5	-13,4	34,8	34,8
94,5	v	Rocca di Papa/Monte Cavo (rm)	-12,7	-13,0	-14,3	48,5	46,0
98,1	v	Rocca di Papa/Monte Cavo (rm)	-12,0	-16,0	-14,0	29,7	30,0
99,6	v	Rocca di Papa/Monte Cavo (rm)	-15,2	-17,1	-18,4	37,3	35,0
101,7	v	Rocca di Papa/Monte Cavo (rm)	-14,4	-17,8	-18,6	40,0	38,2
102,7	v	Montecompatri (rm)	-16,0	-18,6	-16,5	35,0	36,0
103,0	v	Rocca di Papa/Monte Cavo (rm)	-18,0	-22,0	-20,0	41,8	42,7
104,2	v	Montecompatri (rm)	-18,0	-20,0	-20,0	36,8	36,6
106,6	v	Rocca di Papa/Monte Cavo (rm)	-16,6	-18,0	-20,0	39,7	36,6
107,1	v	Rocca di Papa/Monte Cavo (rm)	-14,1	-17,0	-15,0	39,7	40,0

Table 19 – Power levels and cancellation values in site 3A

D. Site 3B

Site 3B (see Figure 50) is a rural site located in the proximities of Fiumicino Airport. In this site, preliminary tests for the evaluation of the PBR DoA estimation capability have been performed with two surveillance antennas pointed towards the identified area for the validation flying performed by ENAV.

The FM radio channels analyzed in this site are summarized in Table 20 together with the power levels measured over the three receiving channels and the measured cancellation values evaluated with the WB receiver with the following Front-End configuration:

- REF chain gain: 8,2dB
- SURV 1 chain gain: 15,7dB
- SURV 1 chain gain: 15,2dB.

Based on the performed analysis, the following FM radio channels have been selected for PBR acquisitions: 92.4, 94.5, 99.6, 103.0, 106.6 and 107.1 MHz.

Ch Radio [MHz]	Pol.	Transmitter	Pow REF [dBm]	Pow SURV 1 [dBm]	Pow SURV 2 [dBm]	CA MEAS 1 [dB]	CA MEAS 2 [dB]
90,3	v	Rocca di Papa/Monte Cavo (rm)	-20,0	-21,8	-21,8	39,9	39,6
92,4	v	Rocca di Papa/Monte Cavo (rm)	-11,5	-14,0	-13,7	40,7	40,8
94,5	v	Rocca di Papa/Monte Cavo (rm)	-12,7	-13,8	-13,8	47,2	47,6
99,6	v	Rocca di Papa/Monte Cavo (rm)	-16,7	-15,8	-16,7	40,0	38,0
103,0	v	Rocca di Papa/Monte Cavo (rm)	-18,7	-18,1	-20,0	44,8	44,5
106,6	v	Rocca di Papa/Monte Cavo (rm)	-16,2	-14,9	-14,5	41,0	42,0
107,1	v	Rocca di Papa/Monte Cavo (rm)	-15,5	-13,0	-14,0	41,0	42,0

Table 20 – Power level and cancellation values in site 3B

E. Site 4

Site 4 (see Figure 50) is a rural site located about 15 km South-West of Rome. In this site, preliminary tests for the evaluation of the PBR DoA estimation capability have been performed with two surveillance antennas pointed towards Fiumicino Airport (see Figure 50).

The FM radio channels analyzed in this site are summarized in **Table 21** together with the Power measured over the three receiving channels and the measured cancellation values evaluated with the WB receiver with the following Front-End configuration:

- REF chain gain: 1.7dB
- SURV 1 chain gain: 7.2dB
- SURV 1 chain gain: 6.7dB.

Based on the performed analysis, the following FM radio channels have been selected for PBR acquisitions: 90.3, 90.5, 92.4, 99.6, 103.0, 105.3 and 105.6 MHz.

Ch. Radio [MHz]	Pol.	Transmitter	Pow REF [dBm]	Pow SURV 1 [dBm]	Pow SURV 2 [dBm]	CA MEAS 1 [dB]	CA MEAS 2 [dB]
88,6	v	Rocca di Papa/Monte Cavo (rm)	-22,0	-15,0	-18,0	33,0	13,0
89,3	v	Rocca di Papa/Monte Cavo (rm)	-20,0	-14,0	-19,0	32,0	31,5
90,3	v	Rocca di Papa/Monte Cavo (rm)	-19,1	-14,9	-16,9	40,5	44,5
90,5	v	Rocca di Papa (rm)	-21,0	-26,5	-19,2	39,5	38,5
91,2	h	Rocca di Papa/Monte Cavo vetta (RAI) (rm)	-22,0	-17,0	-20,3	40,0	40,5
92,4	v	Rocca di Papa/Monte Cavo (rm)	-16,4	-8,6	-13,9	40,0	40,0
94,5	v	Rocca di Papa/Monte Cavo (rm)	-25,0	-11,0	-11,1	33,0	32,0
96,1	v	Rocca di Papa/Monte Cavo (rm)	-21,0	-20,0	-29,0	31,0	27,0
97,0	v	Montecompatri (rm)	-24,0	-36,0	-22,0	5,0	11,0

Ch. Radio [MHz]	Pol.	Transmitter	Pow REF [dBm]	Pow SURV 1 [dBm]	Pow SURV 2 [dBm]	CA MEAS 1 [dB]	CA MEAS 2 [dB]
97,2	v	Montecompatri (rm)	-25,0	-35,0	-25,0	10,0	21,0
98,1	v	Rocca di Papa/Monte Cavo (rm)	-11,0	-24,0	-17,0	20,0	27,0
99,0	v	Rocca di Papa (rm)	-17,0	-25,0	-24,0	29,0	35,0
99,6	v	Rocca di Papa/Monte Cavo (rm)	-14,6	-22,0	-20,0	27,0	32,0
103,0	v	Rocca di Papa/Monte Cavo (rm)	-14,0	-20,5	-21,0	40,0	42,0
103,5	v	Rocca di Papa (RAI) (rm)	-23,0	-30,0	-29,0	21,5	22,5
105,3	v	Rocca di Papa/Monte Cavo (rm)	-12,6	-21,3	-21,0	30,5	30,7
105,6	v	Rocca di Papa (rm)	-11,7	-20,0	-20,9	35,5	34,1
105,8	v	Rocca di Papa/Monte Cavo (rm)	-14,1	-21,0	-21,5	33,9	33,1
106,3	v	Rocca di Papa/Monte Cavo (rm)	-18,3	-26,8	-25,8	27,5	28,0
106,6	v	Rocca di Papa/Monte Cavo (rm)	-15,7	-21,0	-25,0	29,0	26,0

Table 21 – Power level and cancellation values in site 4

4.6.1.1. PLANNING OF ACQUISITION LENGTH AND REQUIRED DATA STORAGE

A key-point of the planning stage is represented by the definition and assessment of acquisition length and of the required data storage. These parameters strongly depend by processing requirements and by technical constraints, as for example the bus transfer rate from A/D to the host PC hard-disk. Specifically, acquisition length is directly related to the integration time required to achieve reasonable SNR values for detection purposes: typical values for this parameter are in the order of one second. Based on the previous considerations, burst acquisitions are performed with the PBR receiver, with the following characteristics:

- Single acquisition duration: 1.15sec
- Separation between consecutive acquisitions: about 1.35sec
- Sampling frequency: 56MHz
- Sampling frequency after DDC (stored data): 200KHz
- Memory occupation (single acquisition, 16FM channels): about 30MB
- Memory occupation (1 hour, 16 FM channels): about 43GB

The time separation between consecutive acquisitions depends on the time needed for data transfer and storage on the hard-disk of the host-PC. Sampling frequency selected is 56MHz according to the considerations reported for RF sampling approach for the WB solution and Nyquist criterion. Finally, memory occupation for a single acquisition is directly related to the number of bits used to represent each sample after DDC, to the sampling frequency after DDC and to the number of acquired FM radio channels.

4.6.1.2. LIVE AIR TRAFFIC CONTROL REGISTRATIONS

Live Air Traffic Control (ATC) registrations have been collected during the described acquisition campaigns. These registrations refer to the area where the acquisition campaigns have been performed, so that a complete comparison is possible between real air traffic and the detection results obtained with the developed receivers. Moreover, ATC data allow an effective evaluation of the PBR detection capabilities achievable with the two developed architectures and a complete and effective comparison of the results obtained with the single FM radio channels and with the multi-frequency approaches.

ATC data are collected by means of a Mode-S/Automatic dependent surveillance-broadcast (ADS-B) receiver that allows the tracking of ADS-B aircrafts and the identification of Mode-S equipped aircrafts. For each cooperative target, it allows a complete real-time identification, 3-D localization and tracking, including information such as ModeS address (i.e. flight ID), Callsign, Country, Altitude, Latitude, Longitude, Vertical Rate, Ground Speed, Track (heading angle with respect to North), and so on.

Figure 51 shows an example of live air traffic visualization allowed by the considered ADS-B receiver. As is apparent, aircrafts are shown in the left portion of the display with different colours to indicate whether they are climbing, descending or flying level. The Aircraft list is also reported on the right and summarizes, for each flight, the above mentioned information.

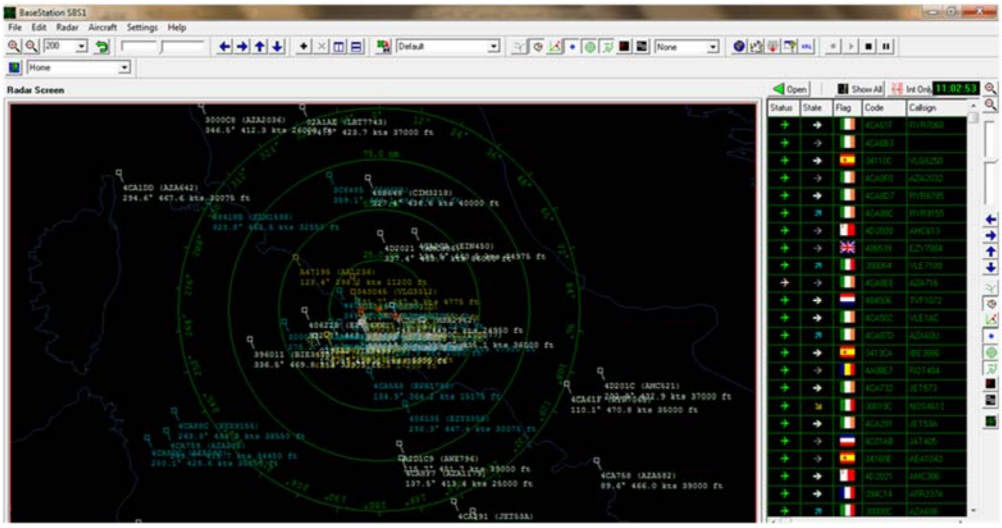

Figure 51 – ADS-B receiver display

All receiver aircraft transponder messages can be also recorded for off-line processing in a proprietary format file (.bst). Information saved in this files during the acquisition campaigns can be then post-processed by Matlab® thus resulting in the complete availability of the ground-truth required for an extensive and complete PBR system performance evaluation. In order to compare PBR data with ADS-B receiver registrations and merge them in an unique display, both data are time stamped with an absolute time.

The first step of the above mentioned Matlab® off-line processing performed over ADS-B registrations is to split the information related to each single aircraft by means of their ModeS code; then the position information (Altitude, Latitude, Longitude) for each time interval of interest are properly converted to be displayed in the same formats used to represent PBR detections: in Range-Doppler domain and in the X-Y plane (with (0,0) point corresponding to the receiver position), as shown in the example reported in Figure 52(a) and (b), respectively.

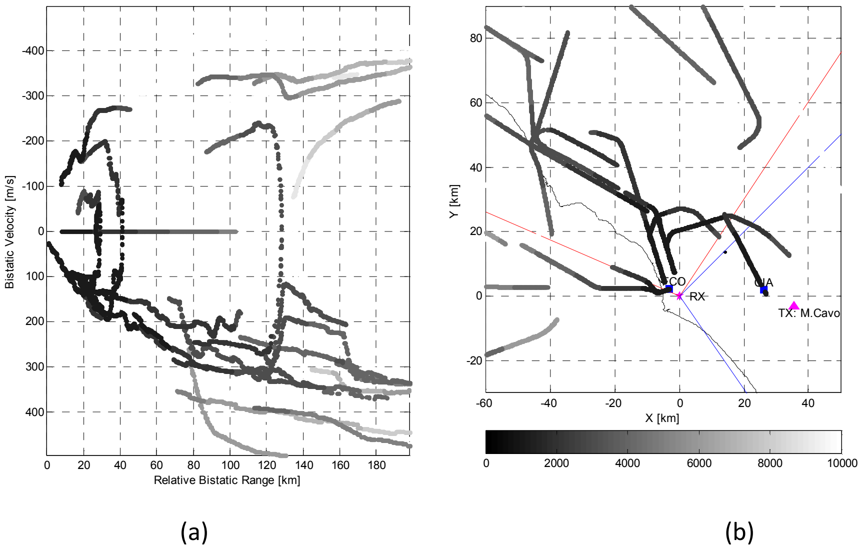

(a) (b)

Figure 52 – Example of ATC data displayed (a) in Range-Doppler domain and (b) in X-Y plane

4.7. EXPERIMENTAL RESULTS

4.7.1. ACQUISITIONS OF TARGETS OF OPPORTUNITY

In this Section are reported the detection results of civil air traffic obtained with the FM-based PBR during the different acquisition campaigns summarized in Table 17. In each acquisition campaign, multiple FM radio channels have been acquired by means of the WB and NB prototypes developed by DIET Department of University of Roma “La Sapienza”, described in 4.4.

Each acquisition campaign is identified with date and time (see **Table 17**), has different duration and it is composed by a different number of files (acquisitions of 1.15 s each). To make the results more readable, for each acquisition campaign they are presented in groups of about 100 files (corresponding to a duration of about 4.5 minutes).

For each group of 100 files, the left figure reports the detection results over the bistatic range-velocity plane (the red plots indicate passive radar detections while the live ATC registrations are reported in grey scale related to the targets quote); the right figure shows the results of target localization over the x-y plane (the grey scale traces refer to the true air traffic while the red colour is used to indicate the results obtained with the passive radar; the triangle marker indicates the Tx of opportunity, the star represents the Rx position, while the blue markers indicate the Leonardo da Vinci - FCO - and Ciampino - CIA - airports).

By using single bistatic couples, target localization is performed by jointly exploiting the bistatic range and DoA measures provided by the single passive sensor. Notice that all (x,y) measures are affected by angle ambiguity due to the interferometric approach. Specifically, the angular measures, and its relative ambiguity, are dependent by the wavelength corresponding to the specific carrier frequency of the exploited FM radio channel (for example, for the FM radio channel 88.0 MHz, the ambiguity interval is about [-58.5°, 58.5°] while for 108.0 MHz the same interval is about [-44°, 44°]). So, each detected target, independently of its real angle with respect to the surveillance antenna pointing, will result in a measure located inside this ambiguity interval.

In the following Sub-Sections, where not expressly stated otherwise, for each acquisition campaign are reported the results obtained with each single FM radio channel acquired, and after the application of the MF integration algorithm with different groups of radio channels.

4.7.1.1. ACQUISITION CAMPAIGN, SITE 3A, 11TH JUNE 2012, 18.56.57

In this Section, the detection and localization results are reported for WB FM-based passive sensor in real environment, after the off-line processing developed and described in detail in Deliverable 2.3. The aim of this analysis is to verify the effectiveness of the passive sensor for target detection and localization. Specifically, we report the results obtained in the Site 3A (see Figure 50) on 11th June 2012 at 18.56.57 for an acquisition duration of 40 minutes (900 files). Each sub-Section refers to a specific single FM radio channels among those acquired in the considered Site or to a specific MF configuration.

In particular, the single FM radio channels are:

- 90.3 MHz (Section 4.7.1.1.1)
- 94.5 MHz (Section 4.7.1.1.2)
- 103.0 MHz (Section 4.7.1.1.3)
- 106.6 MHz (Section 4.7.1.1.4)

The MF elaboration has been performed by integrating the following group of FM radio channels:

- 90.3 – 94.5 – 103.0 MHz (Section 4.7.1.1.5)

Additionally, in this acquisition campaign, a data set has been collected by the NB receiver located in Site 1 (see Figure 50). The files acquired through the NB receiver are 830. Notice that, for the NB system, the angular target localization is not available because the receiver prototype has only two receiving chains used for the reference and surveillance antennas, respectively. The detection results are reported in dedicated sub-Sections where they are compared with the MF integration elaboration results obtained with the WB receiver. The FM radio channels simultaneously acquired with the NB receiver are:

- 92.4 MHz (Section 4.7.1.1.6)
- 92.7 MHz (Section 4.7.1.1.7)

4.7.1.1.1. SINGLE FM RADIO CHANNEL 90.3 MHZ

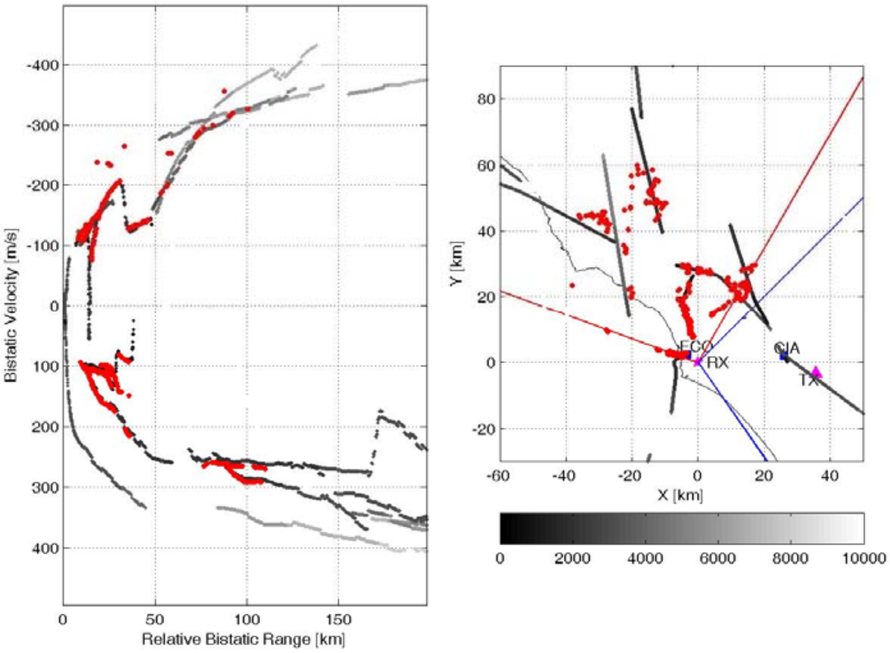

Figure 53 – Detection results, FM radio channel 90.3 MHz, files 1-100

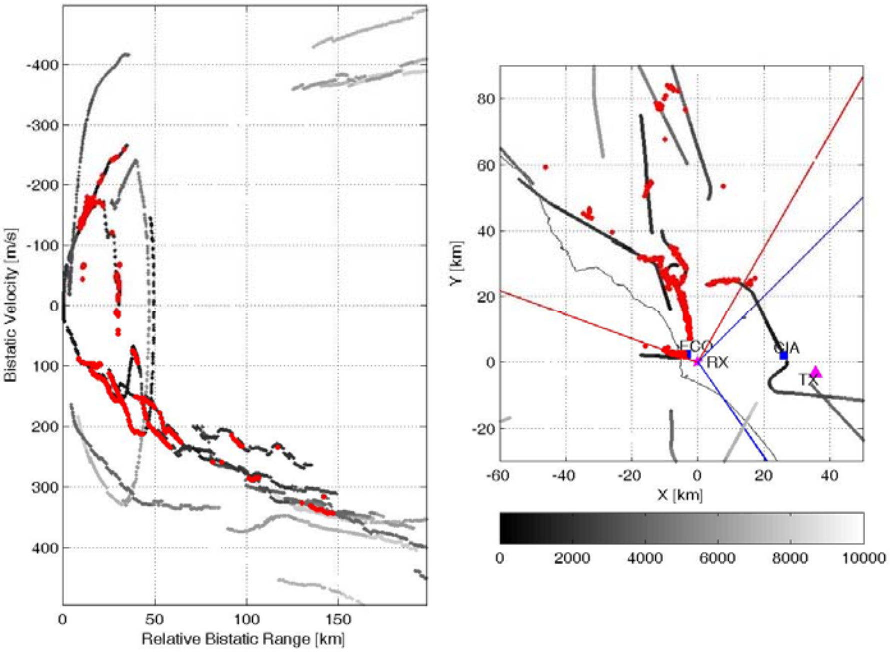

Figure 54 – Detection results, FM radio channel 90.3 MHz, files 101-200

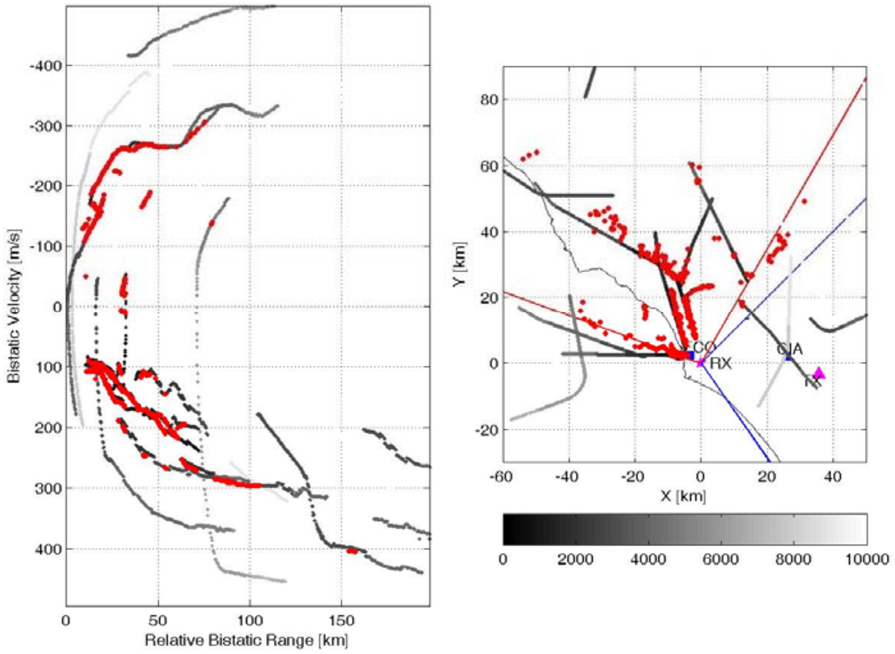

Figure 55 – Detection results, FM radio channel 90.3 MHz, files 201-300

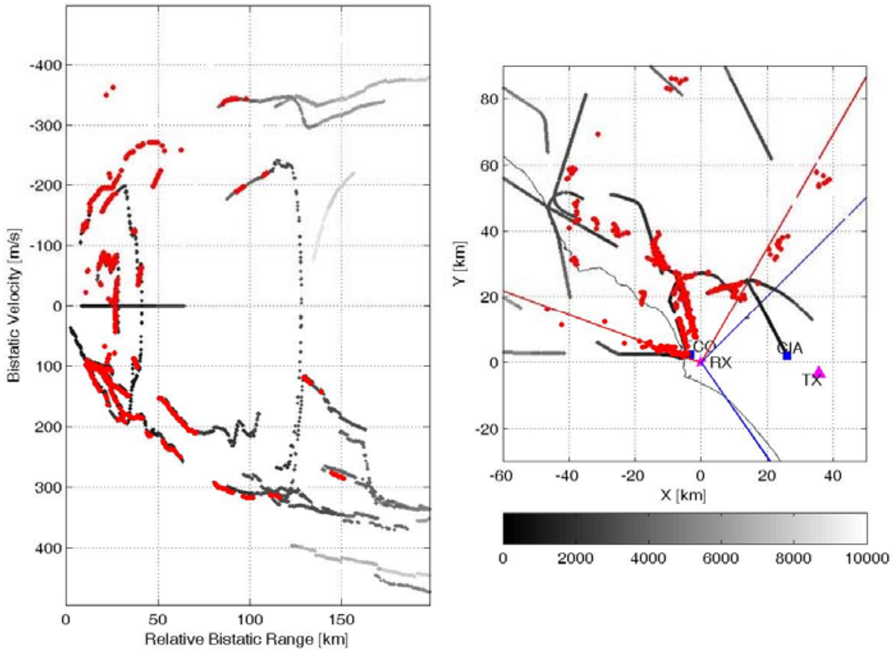

Figure 56 – Detection results, FM radio channel 90.3 MHz, files 301-400

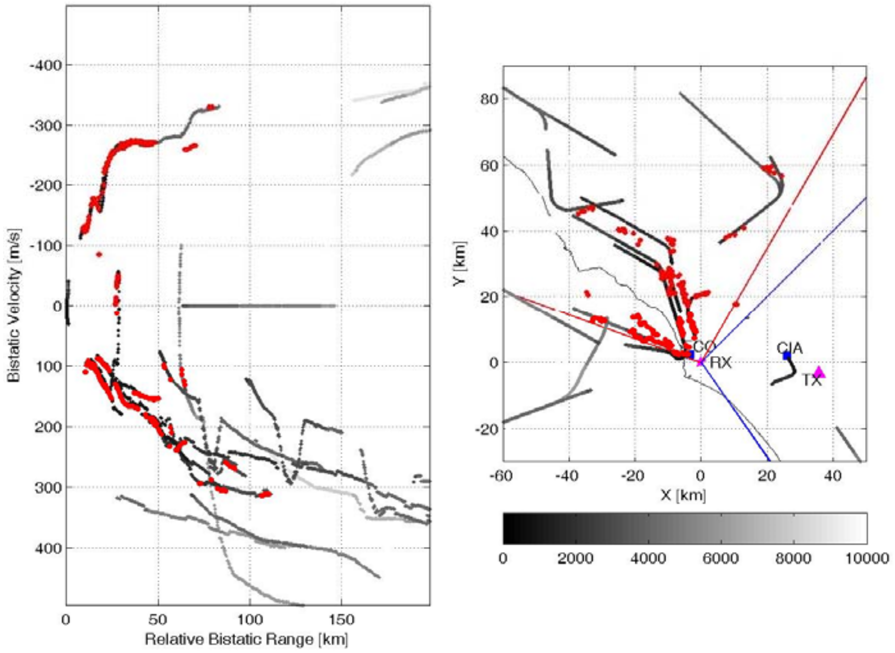

Figure 57 – Detection results, FM radio channel 90.3 MHz, files 401-500

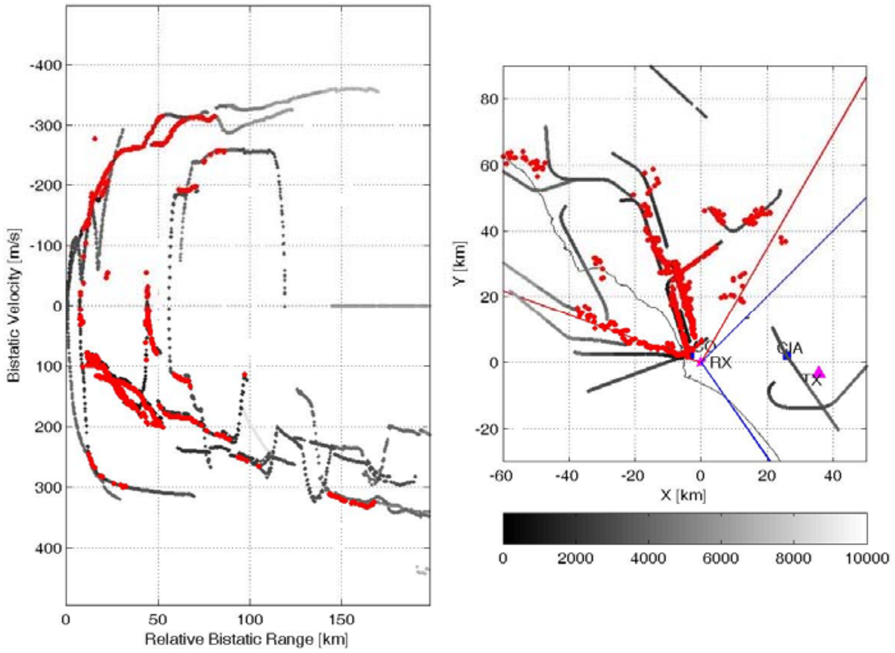

Figure 58 – Detection results, FM radio channel 90.3 MHz, files 501-600

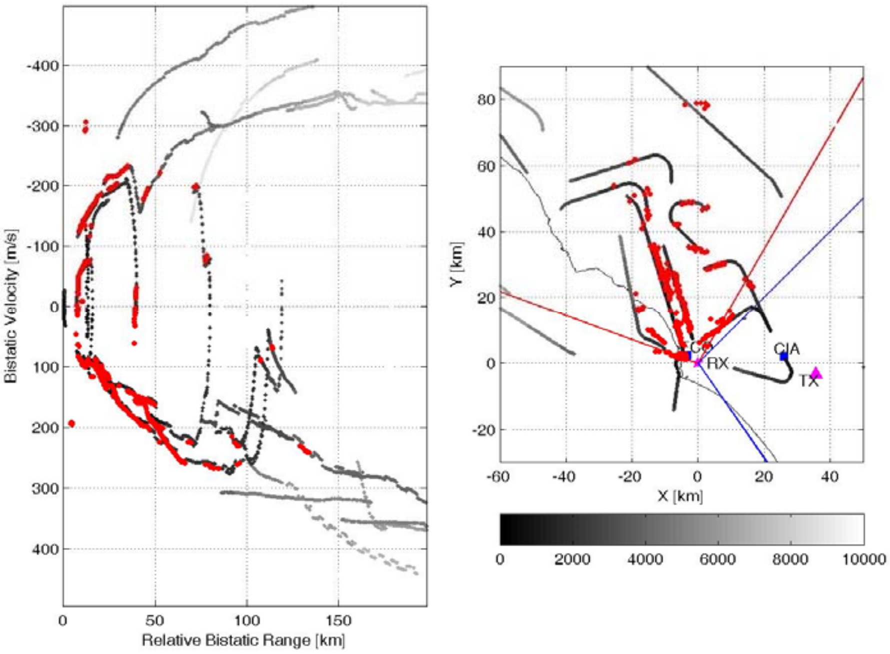

Figure 59 – Detection results, FM radio channel 90.3 MHz, files 601-700

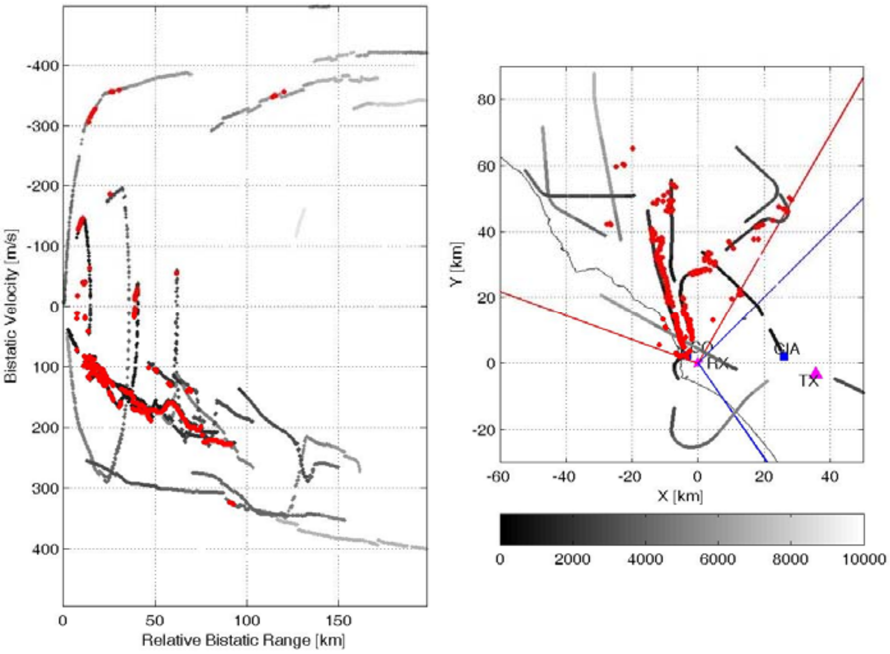

Figure 60 – Detection results, FM radio channel 90.3 MHz, files 701-800

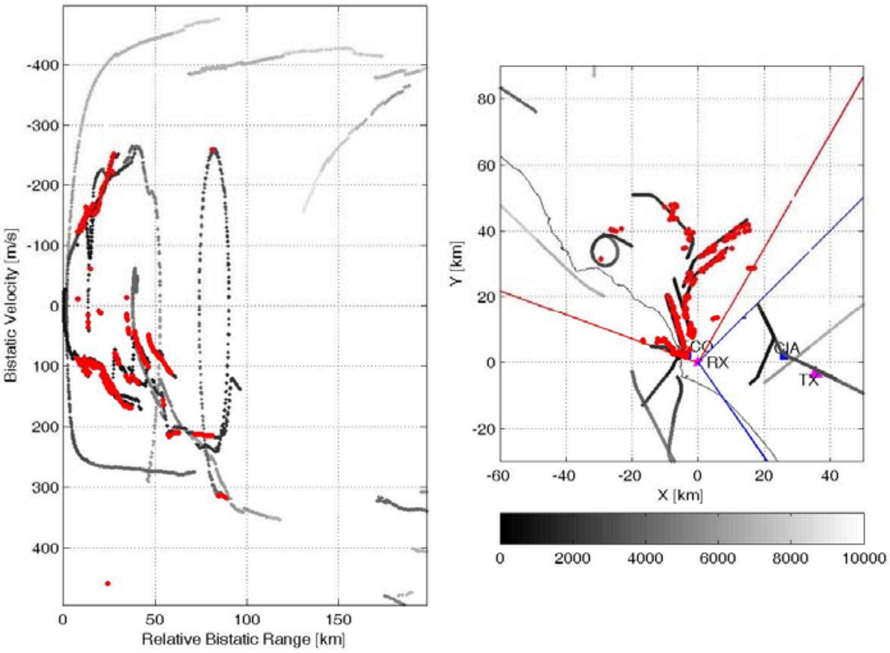

Figure 61 – Detection results, FM radio channel 90.3 MHz, files 801-900

4.7.1.1.2. SINGLE FM RADIO CHANNEL 94.5 MHZ

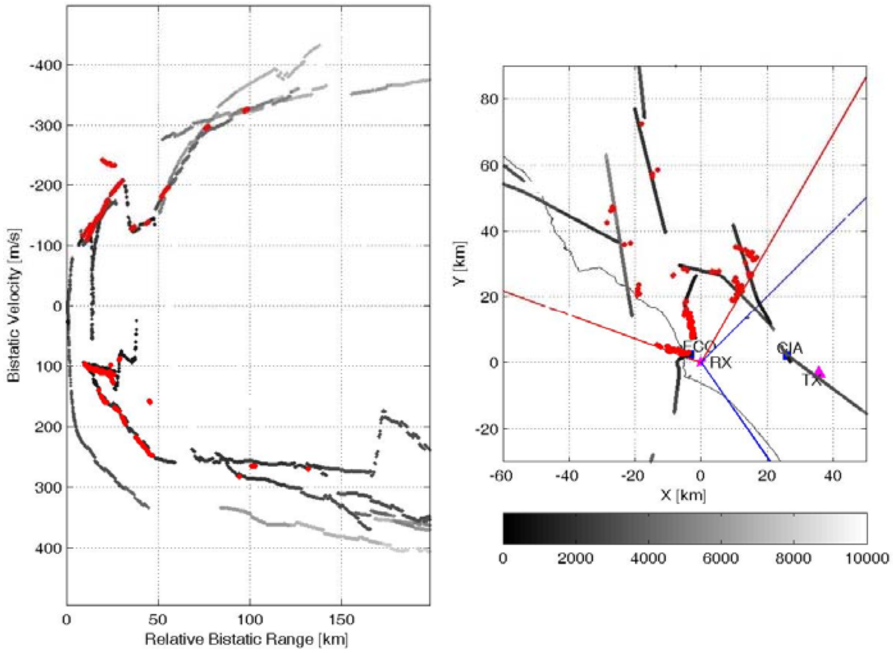

Figure 62 – Detection results, FM radio channel 94.5 MHz, files 1-100

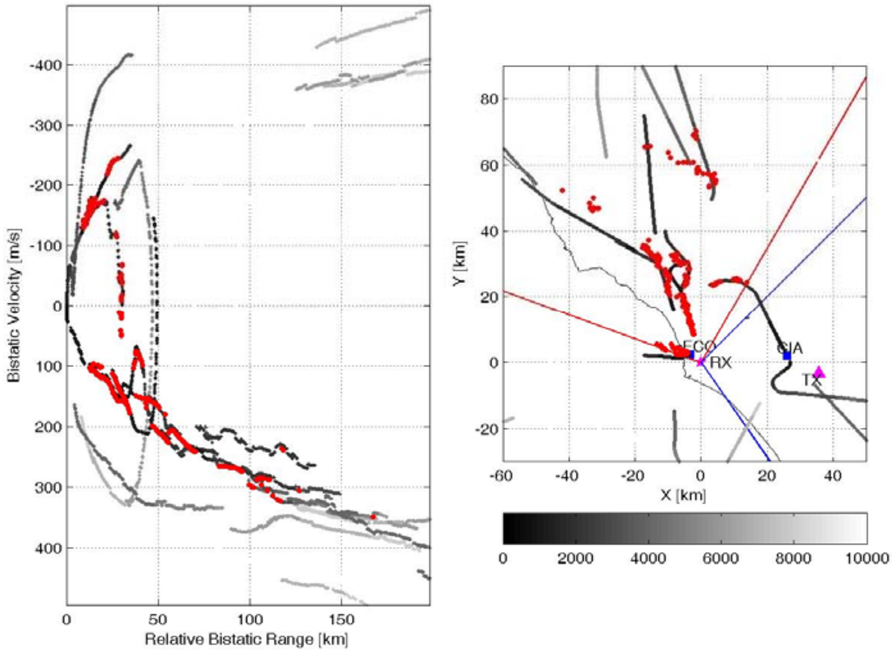

Figure 63 – Detection results, FM radio channel 94.5 MHz, files 101-200

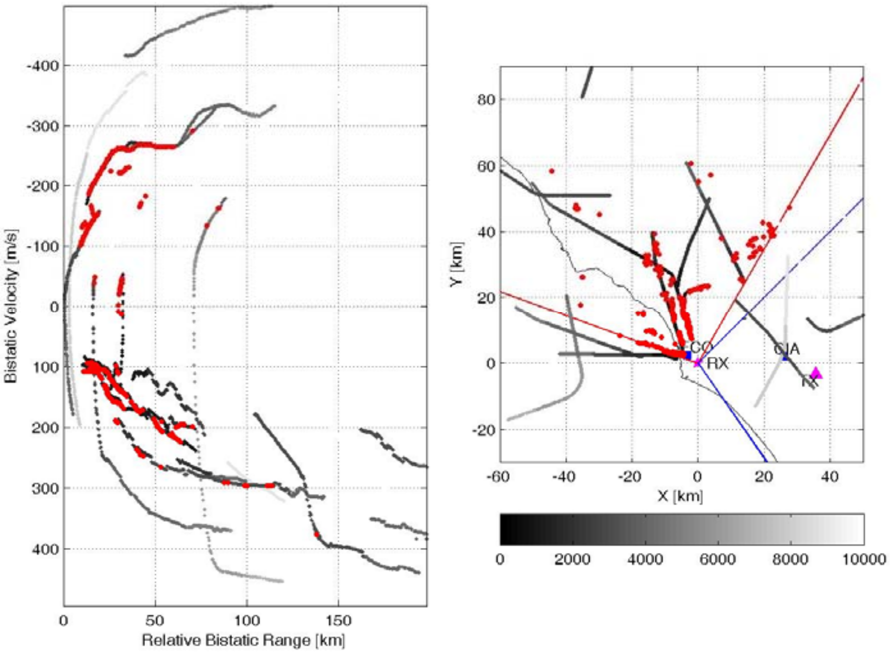

Figure 64 – Detection results, FM radio channel 94.5 MHz, files 201-300

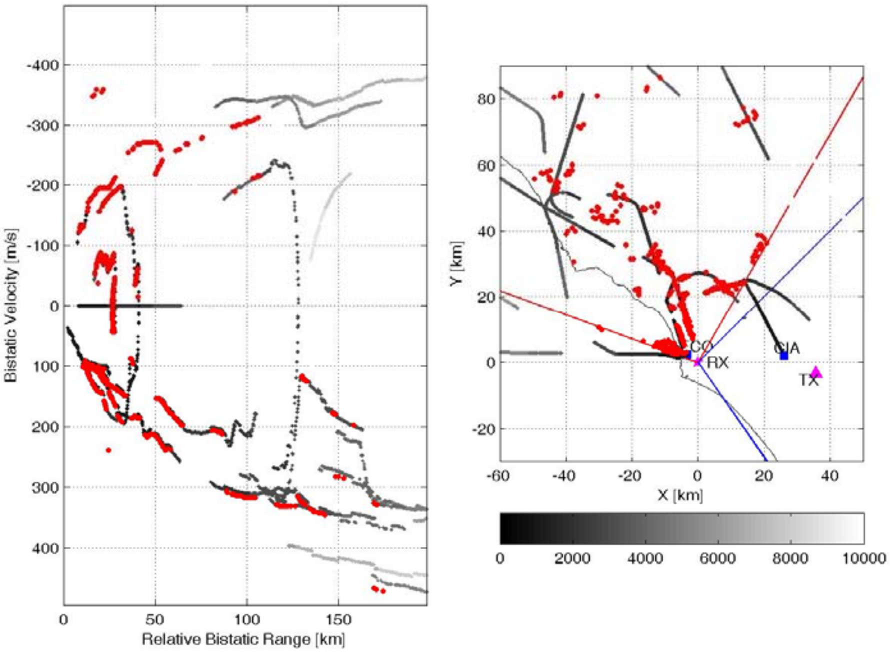

Figure 65 – Detection results, FM radio channel 94.5 MHz, files 301-400

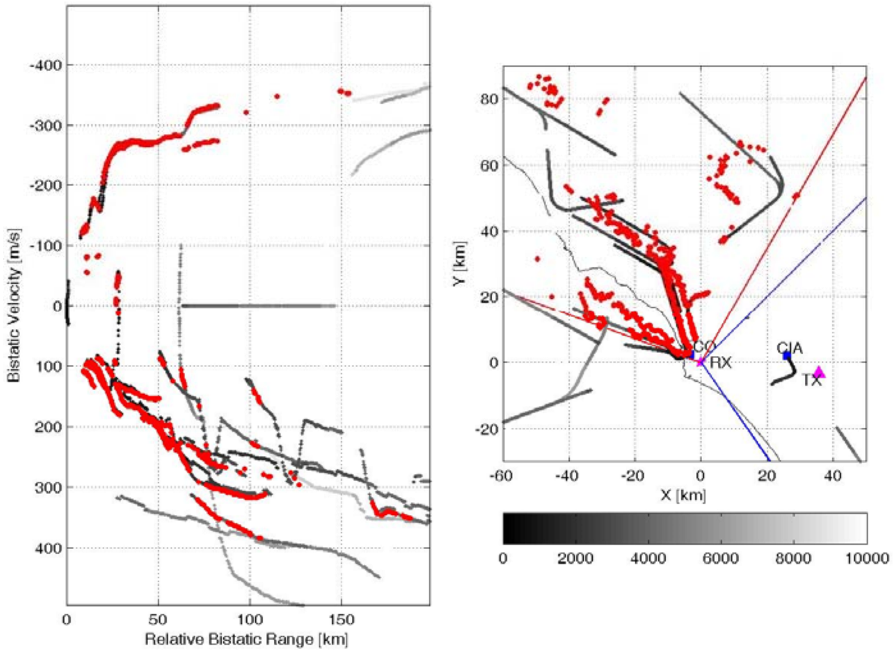

Figure 66 – Detection results, FM radio channel 94.5 MHz, files 401-500

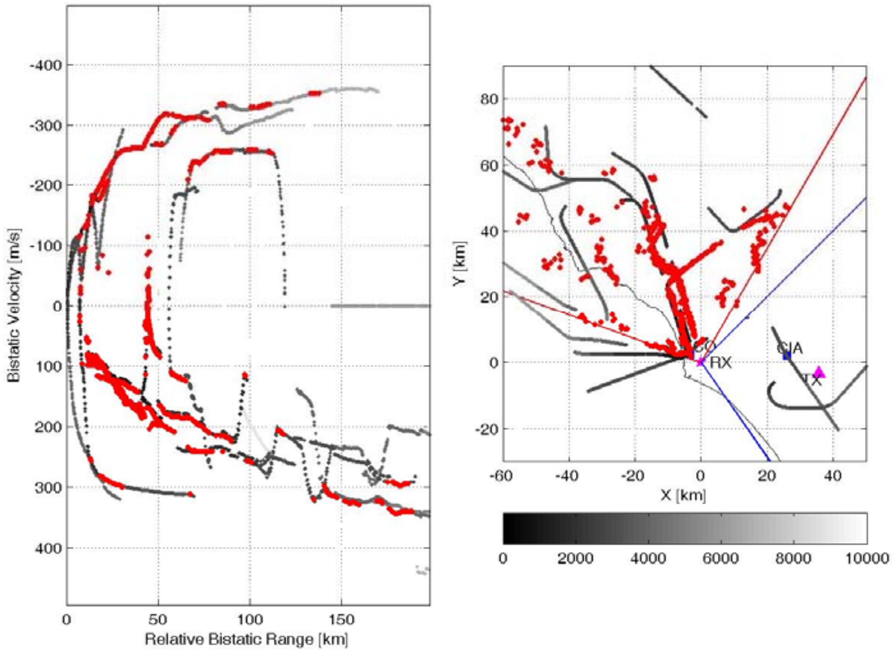

Figure 67 – Detection results, FM radio channel 94.5 MHz, files 501-600

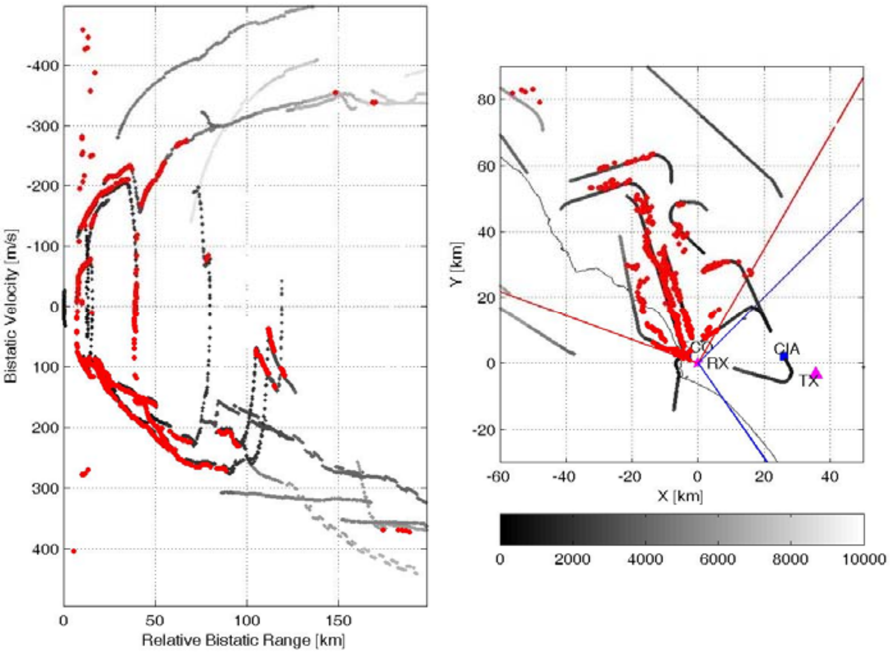

Figure 68 – Detection results, FM radio channel 94.5 MHz, files 601-700

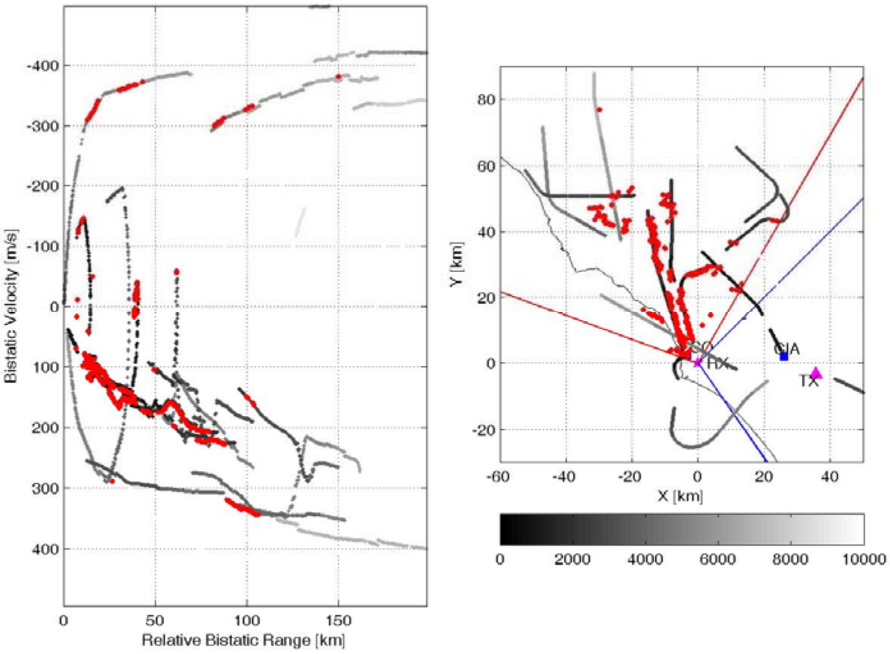

Figure 69 – Detection results, FM radio channel 94.5 MHz, files 701-800

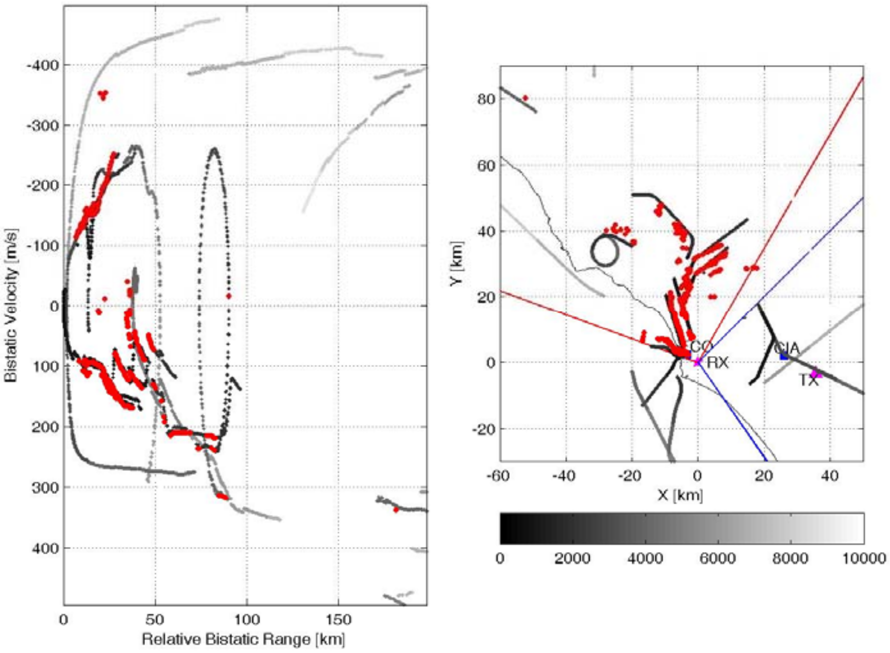

Figure 70 – Detection results, FM radio channel 94.5 MHz, files 801-900

4.7.1.1.3. SINGLE FM RADIO CHANNEL 103.0 MHZ

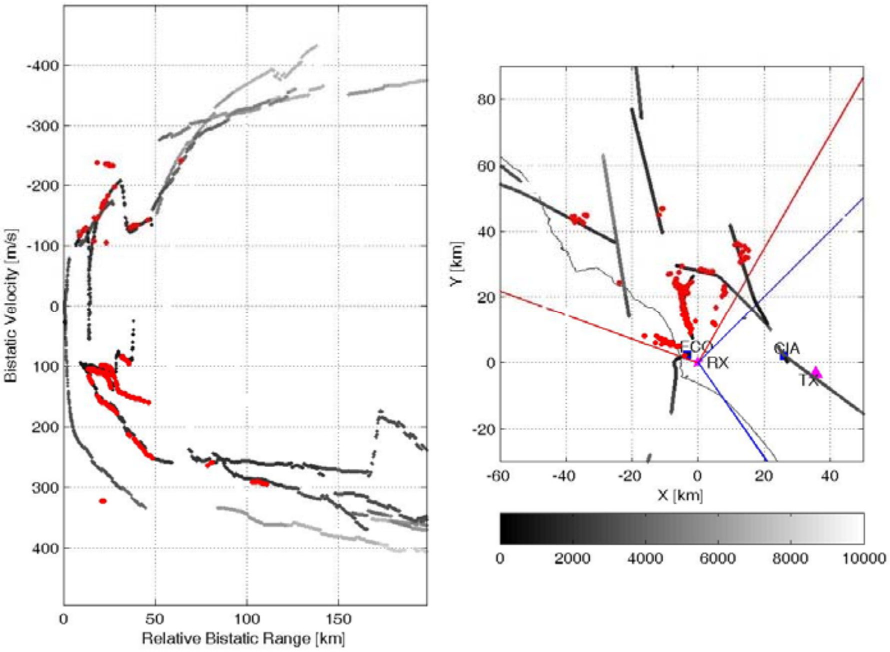

Figure 71 – Detection results, FM radio channel 103.0 MHz, files 1-100

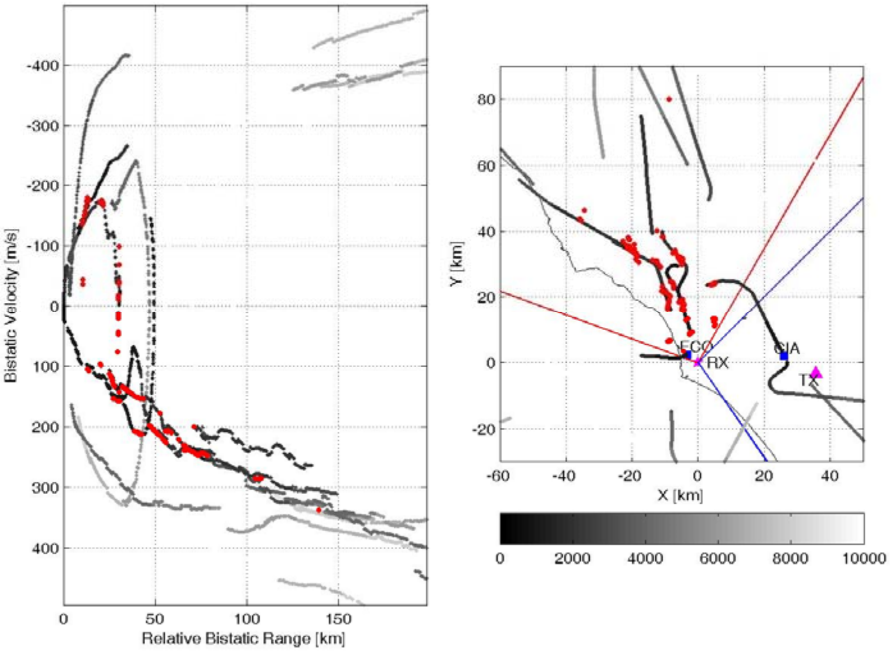

Figure 72 – Detection results, FM radio channel 103.0 MHz, files 101-200

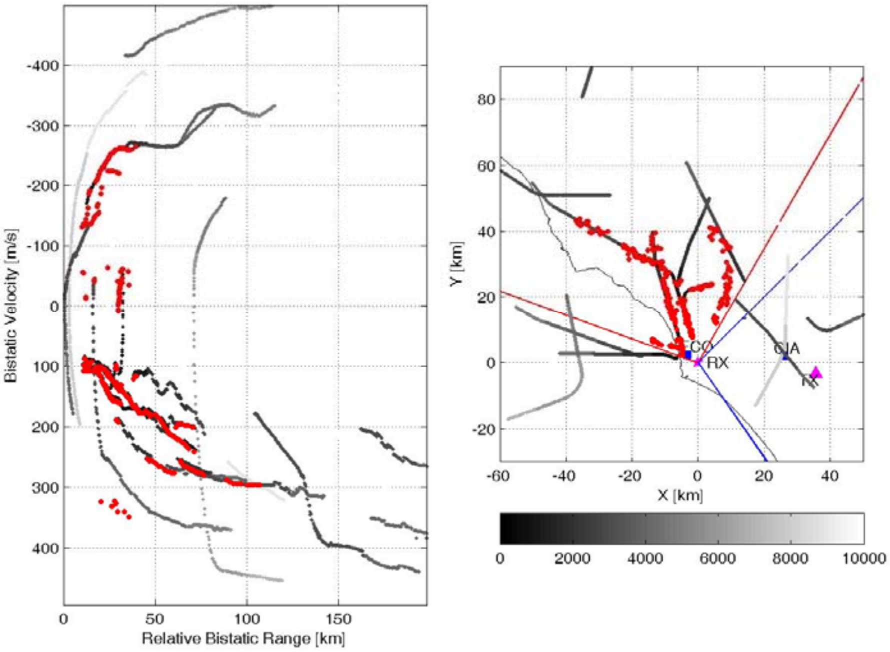

Figure 73 – Detection results, FM radio channel 103.0 MHz, files 201-300

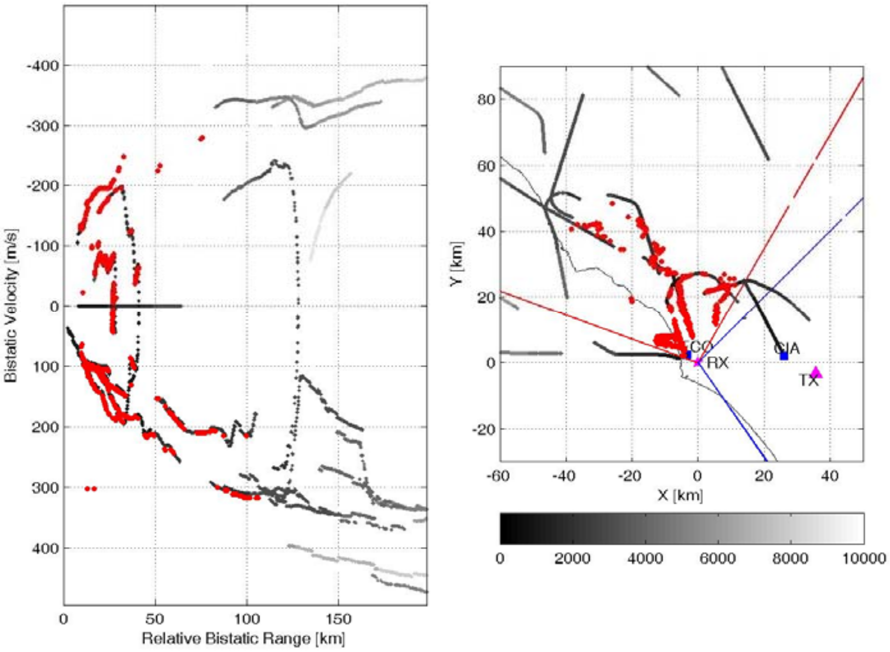

Figure 74 – Detection results, FM radio channel 103.0 MHz, files 301-400

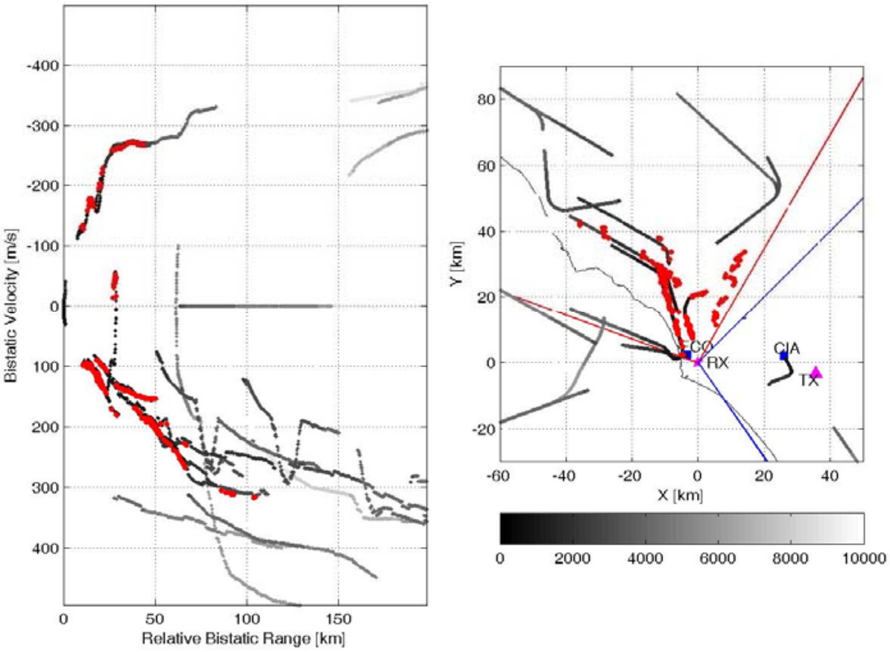

Figure 75 – Detection results, FM radio channel 103.0 MHz, files 401-500

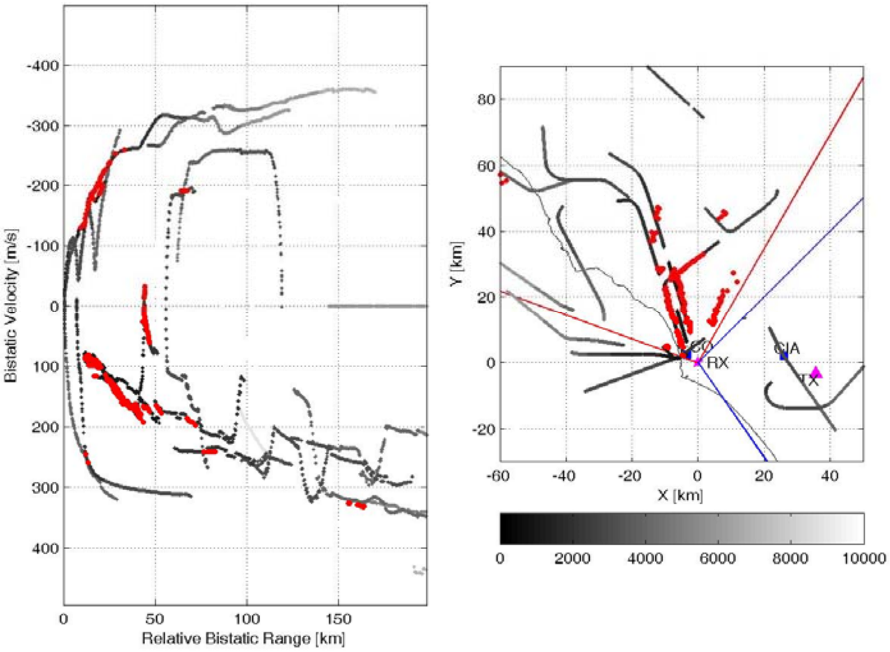

Figure 76 – Detection results, FM radio channel 103.0 MHz, files 501-600

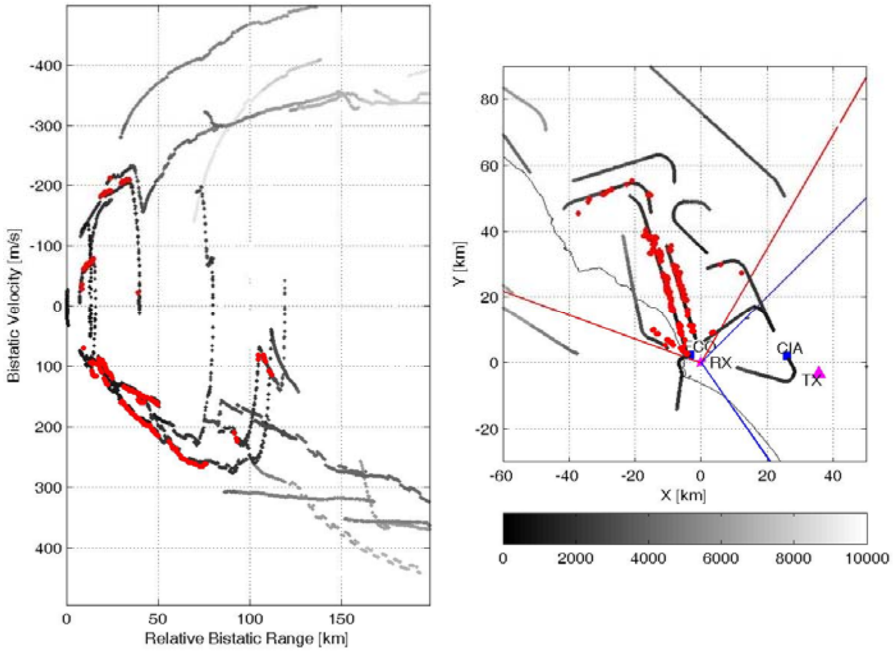

Figure 77 – Detection results, FM radio channel 103.0 MHz, files 601-700

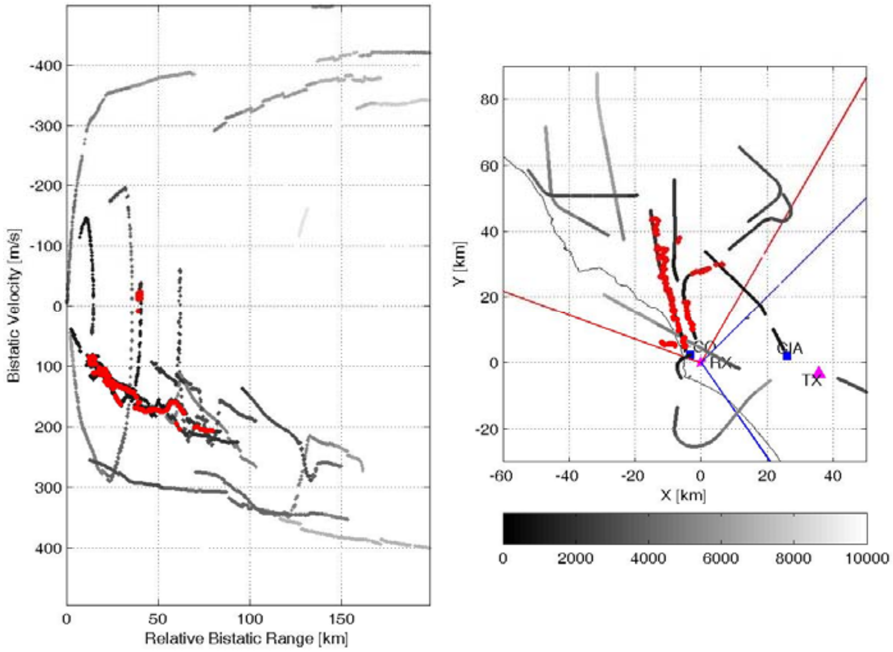

Figure 78 – Detection results, FM radio channel 103.0 MHz, files 701-800

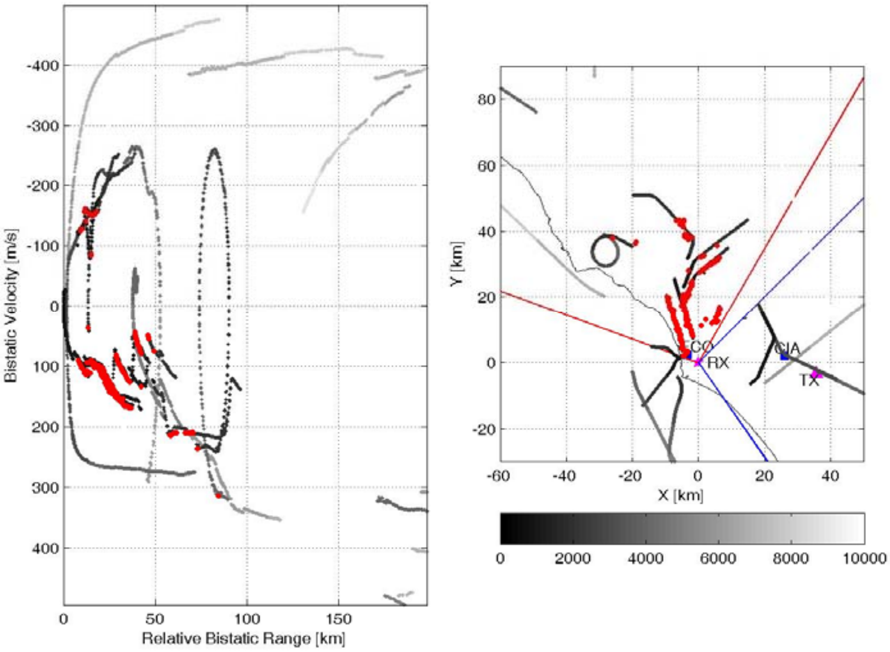

Figure 79 – Detection results, FM radio channel 103.0 MHz, files 801-900

4.7.1.1.4. SINGLE FM RADIO CHANNEL 106.6 MHZ

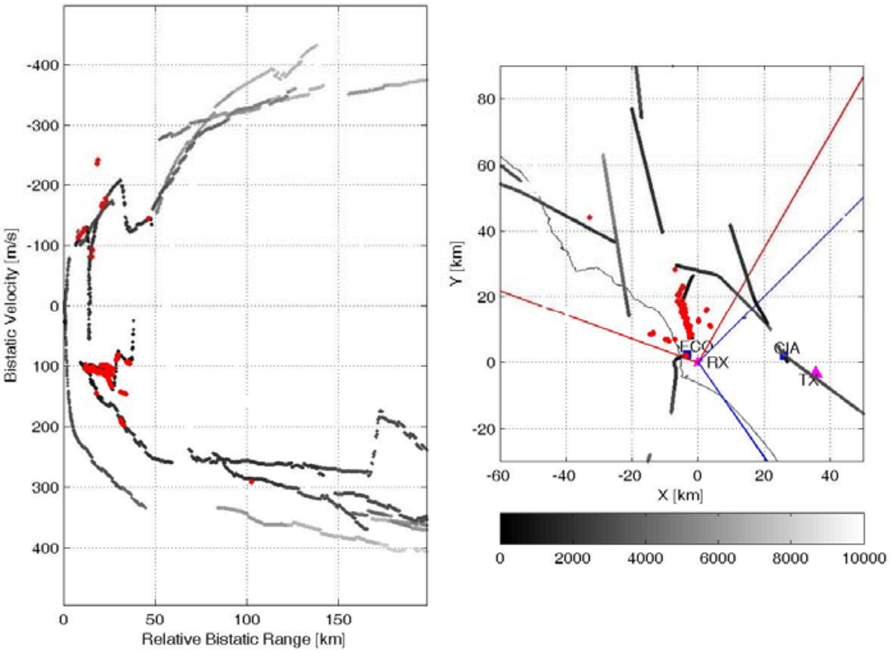

Figure 80 – Detection results, FM radio channel 106.6 MHz, files 1-100

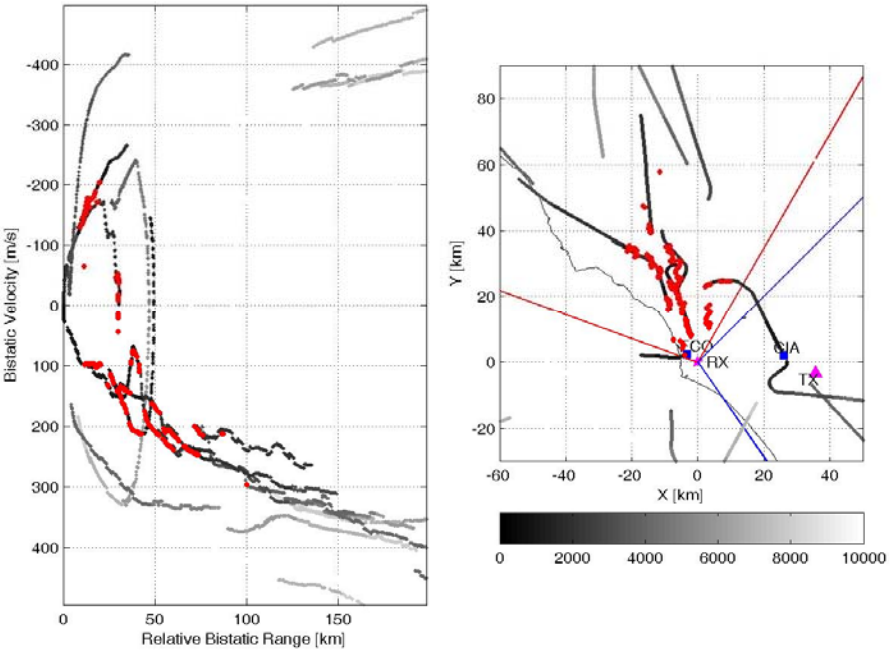

Figure 81 – Detection results, FM radio channel 106.6 MHz, files 101-200

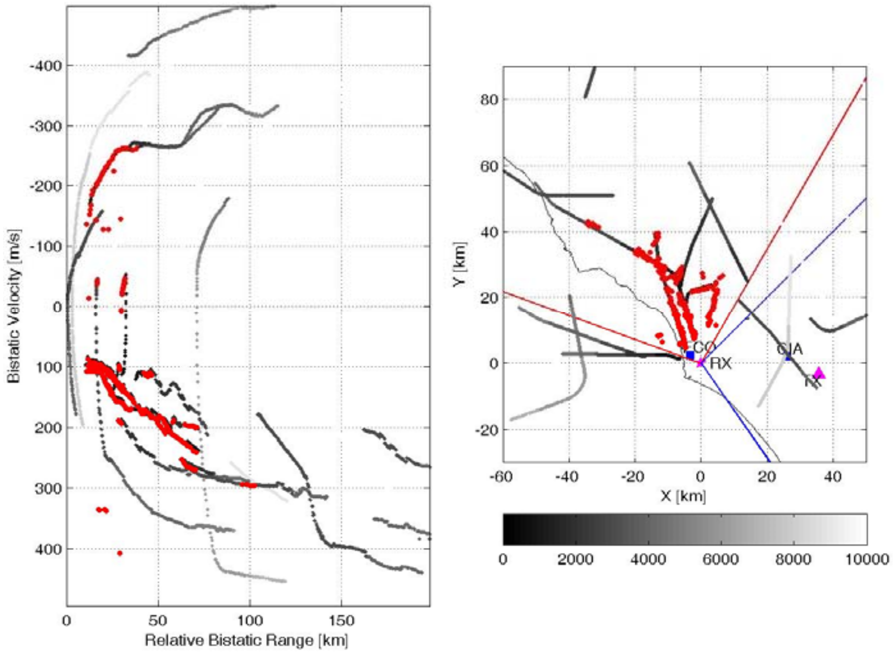

Figure 82 – Detection results, FM radio channel 106.6 MHz, files 201-300

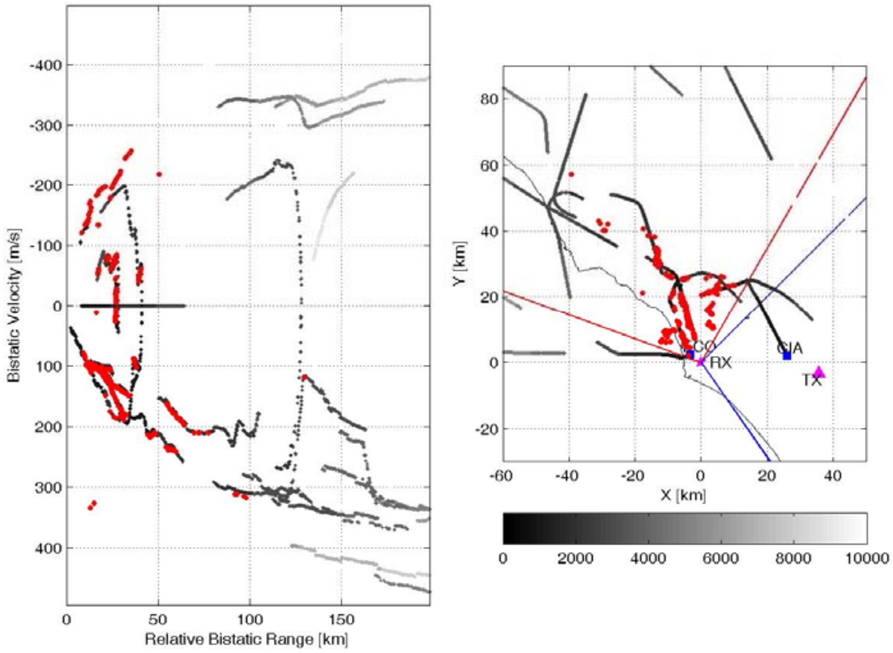

Figure 83 – Detection results, FM radio channel 106.6 MHz, files 301-400

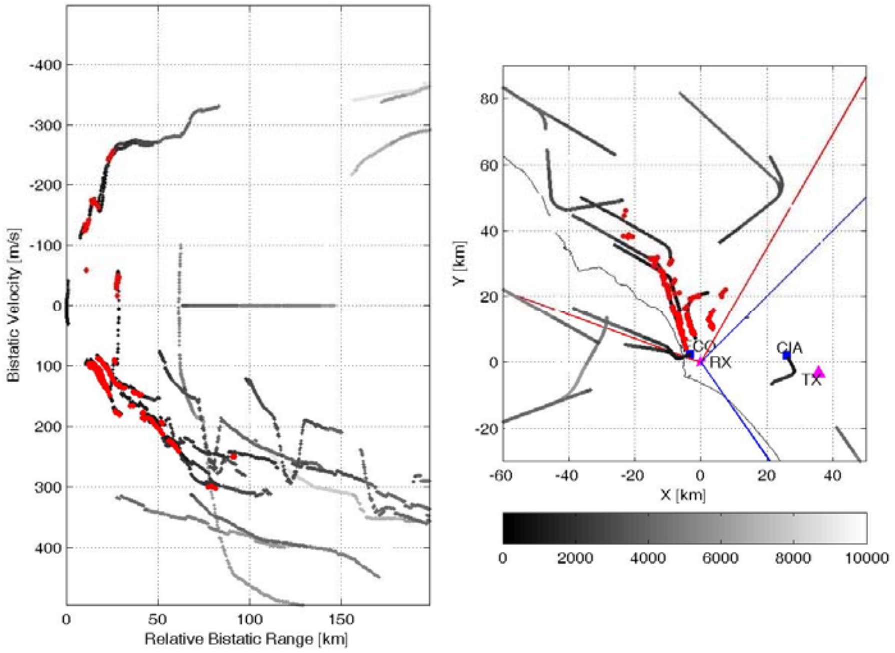

Figure 84 – Detection results, FM radio channel 106.6 MHz, files 401-500

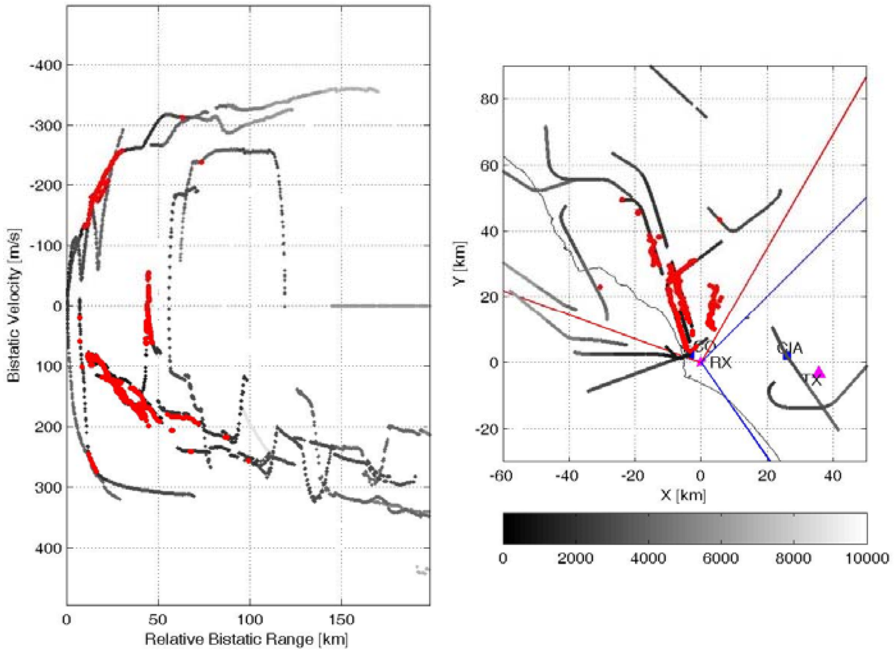

Figure 85 – Detection results, FM radio channel 106.6 MHz, files 501-600

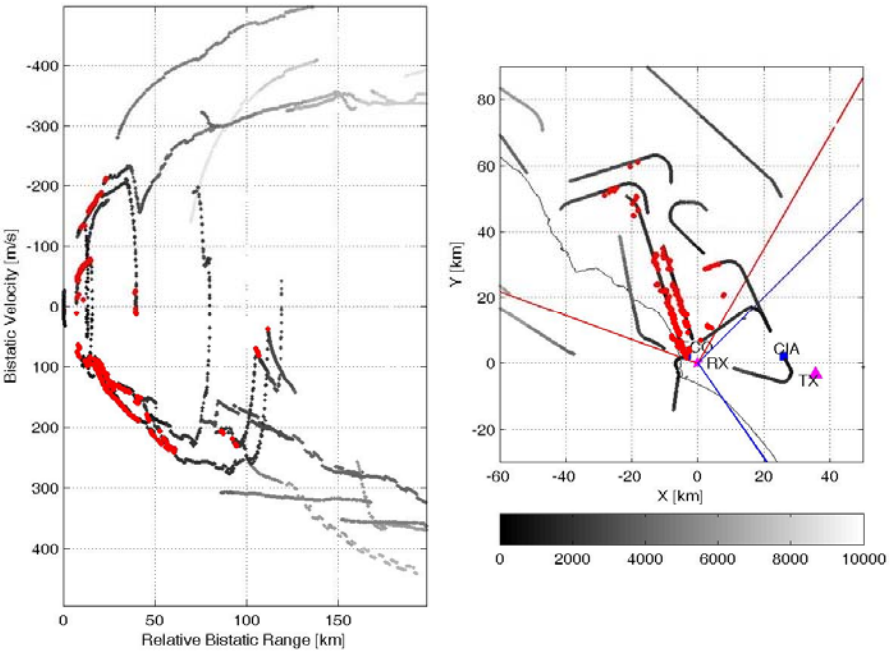

Figure 86 – Detection results, FM radio channel 106.6 MHz, files 601-700

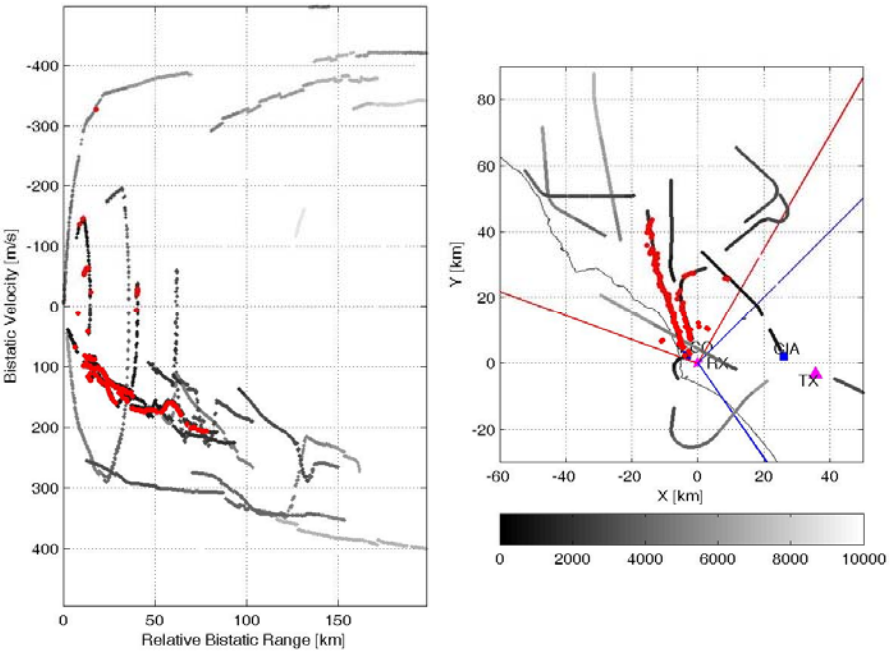

Figure 87 – Detection results, FM radio channel 106.6 MHz, files 701-800

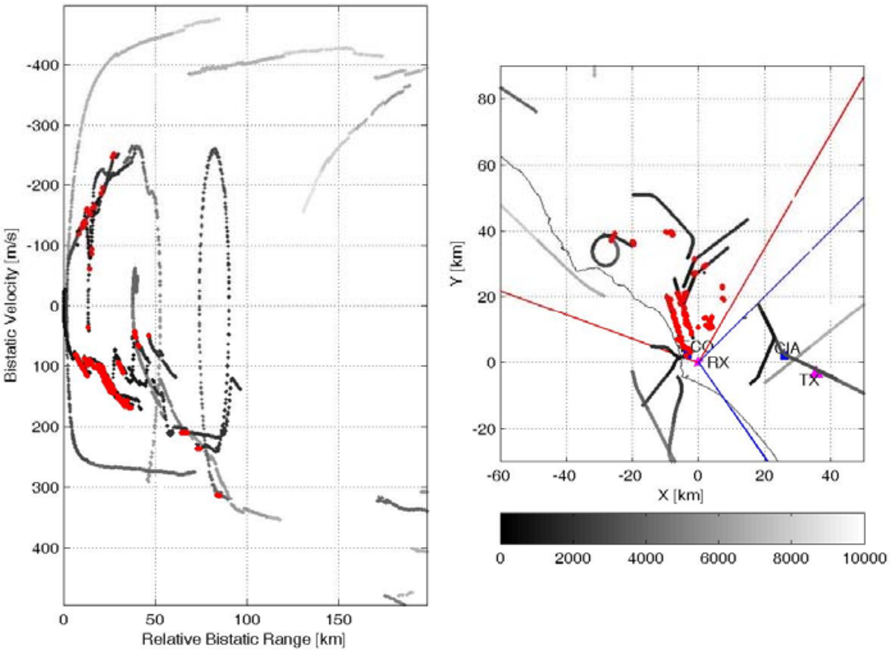

Figure 88 – Detection results, FM radio channel 106.6 MHz, files 801-900

4.7.1.1.5. MULTI-FREQUENCY INTEGRATION FM RADIO CHANNELS 90.3 – 94.5 – 103.0 MHZ

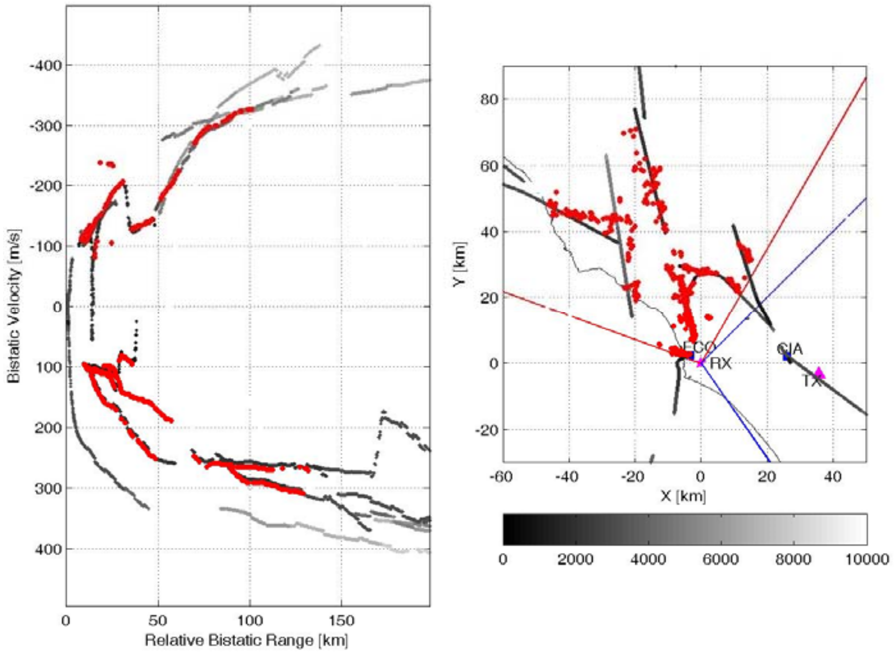

Figure 89 – Detection results, FM radio channels 90.3 – 94.5 – 103.0 MHz, files 1-100

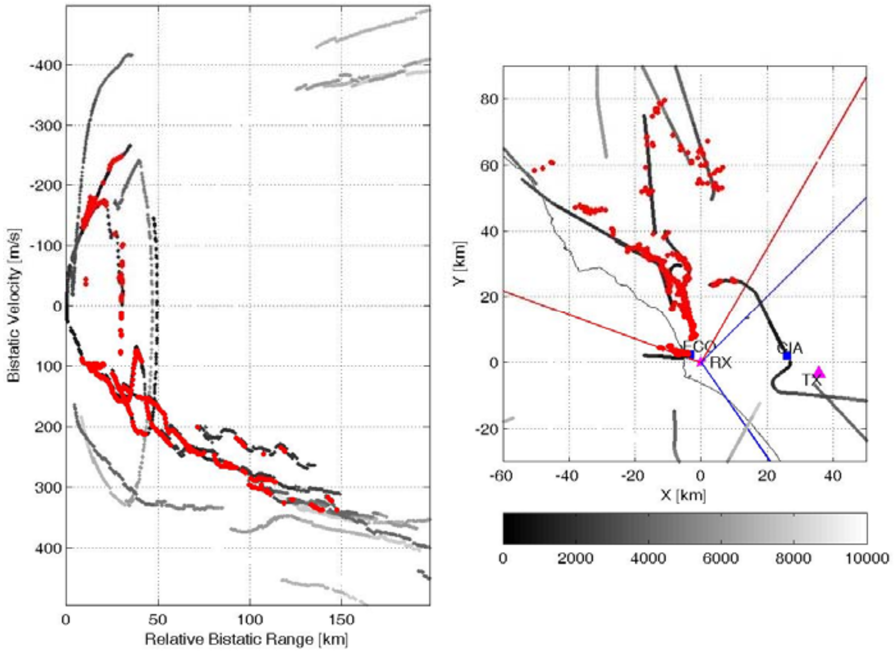

Figure 90 – Detection results, FM radio channels 90.3 – 94.5 – 103.0 MHz, files 101-200

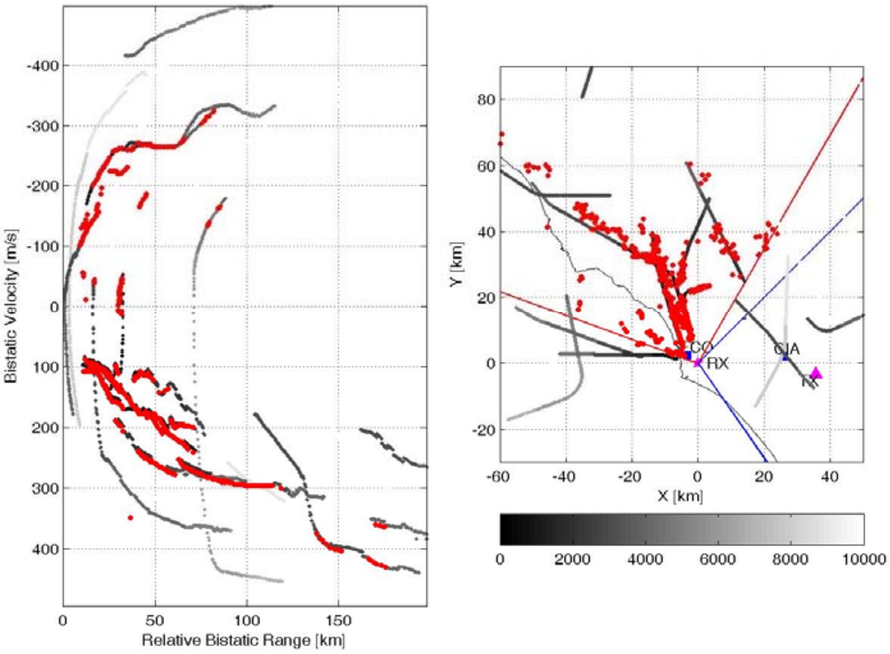

Figure 91 – Detection results, FM radio channels 90.3 – 94.5 – 103.0 MHz, files 201-300

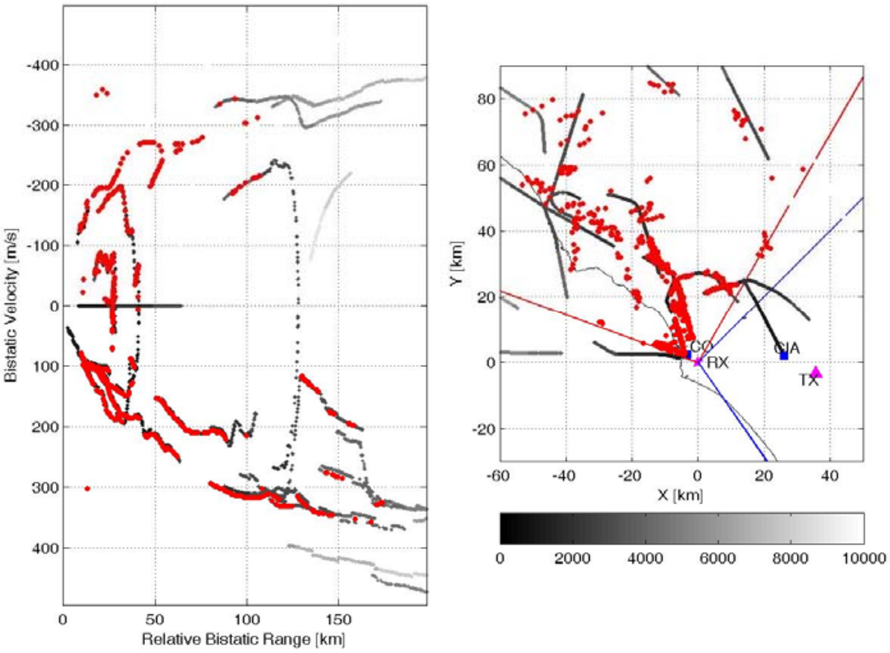

Figure 92 – Detection results, FM radio channels 90.3 – 94.5 – 103.0 MHz, files 301-400

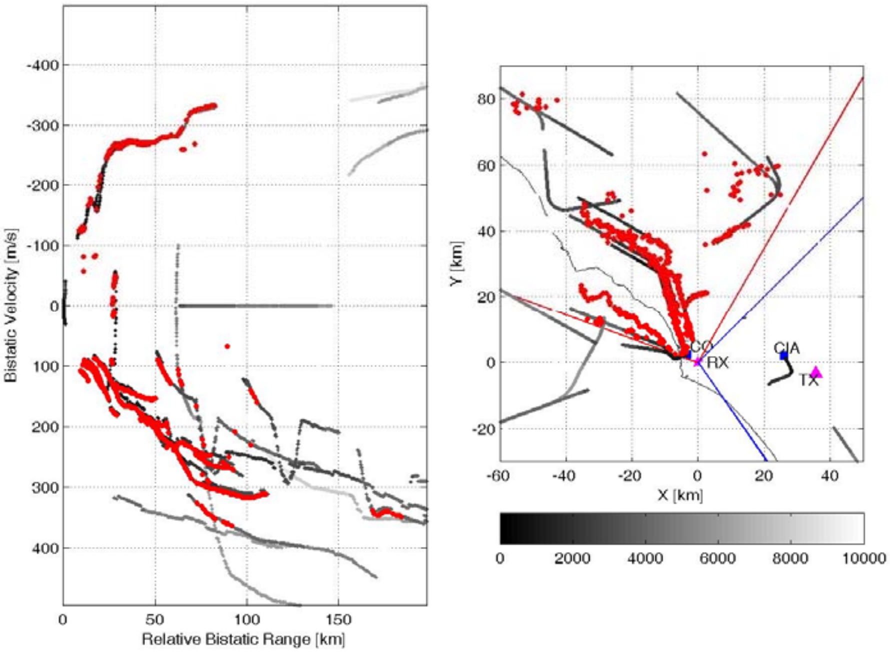

Figure 93 – Detection results, FM radio channels 90.3 – 94.5 – 103.0 MHz, files 401-500

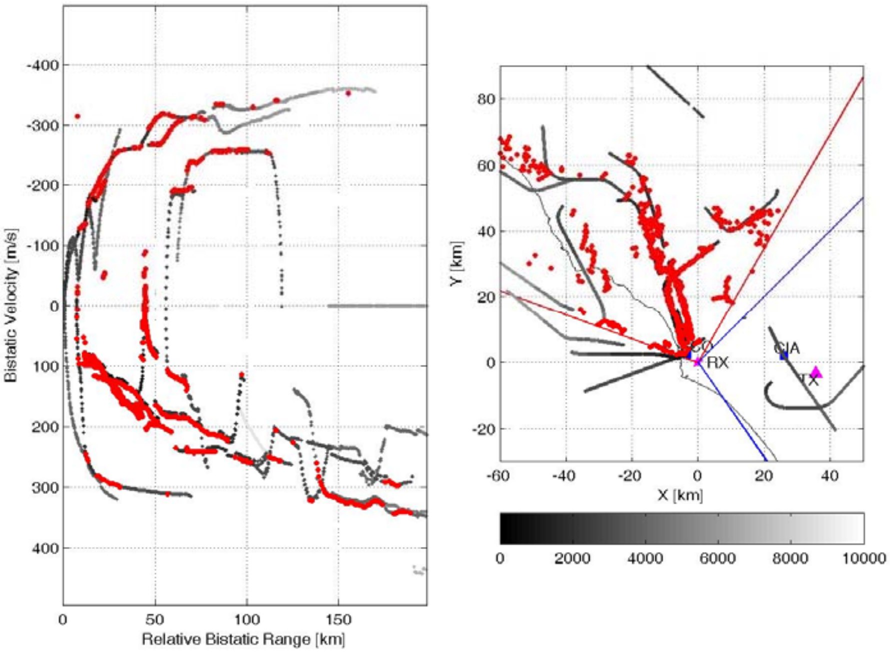

Figure 94 – Detection results, FM radio channels 90.3 – 94.5 – 103.0 MHz, files 501-600

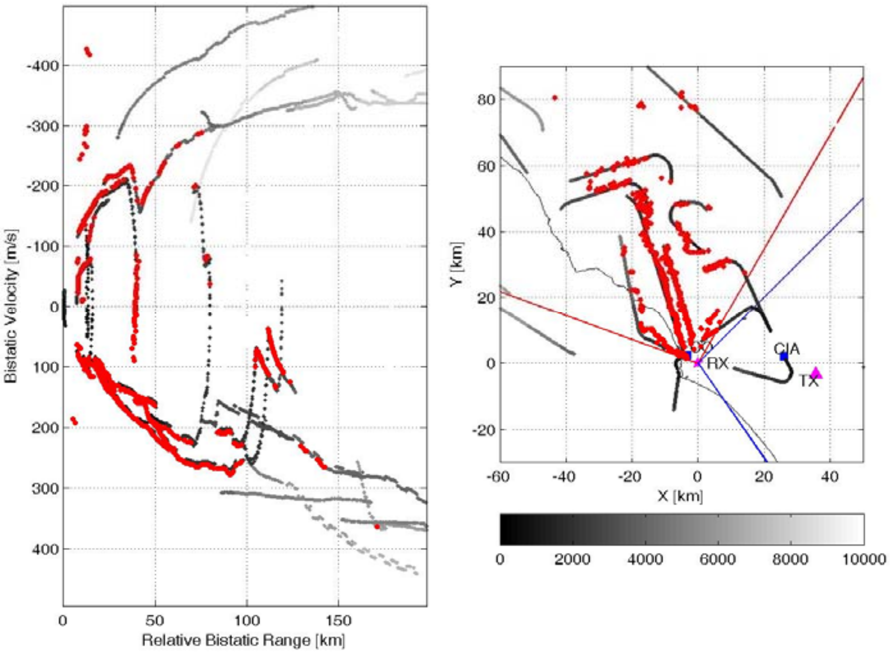

Figure 95 – Detection results, FM radio channels 90.3 – 94.5 – 103.0 MHz, files 601-700

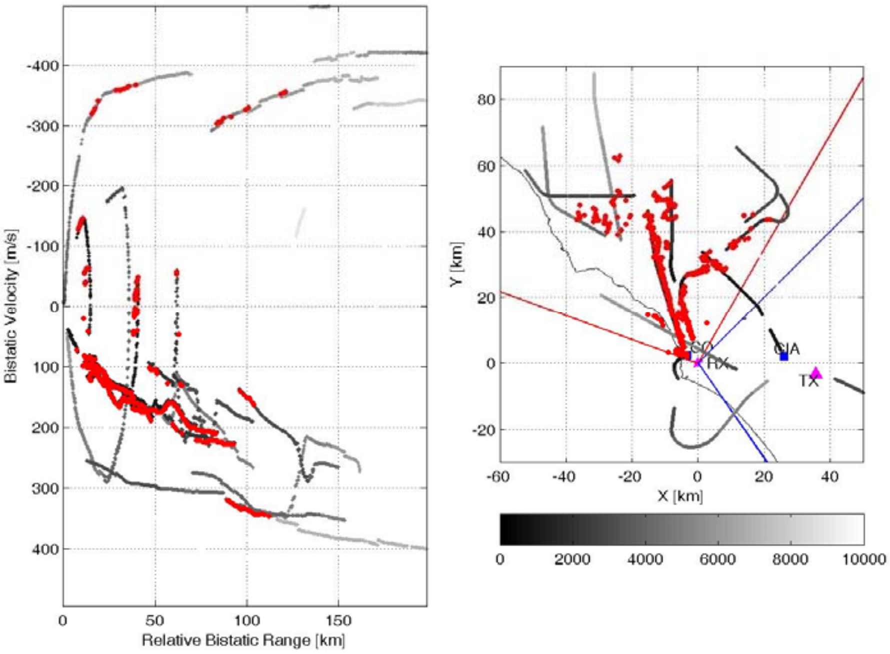

Figure 96 – Detection results, FM radio channels 90.3 – 94.5 – 103.0 MHz, files 701-800

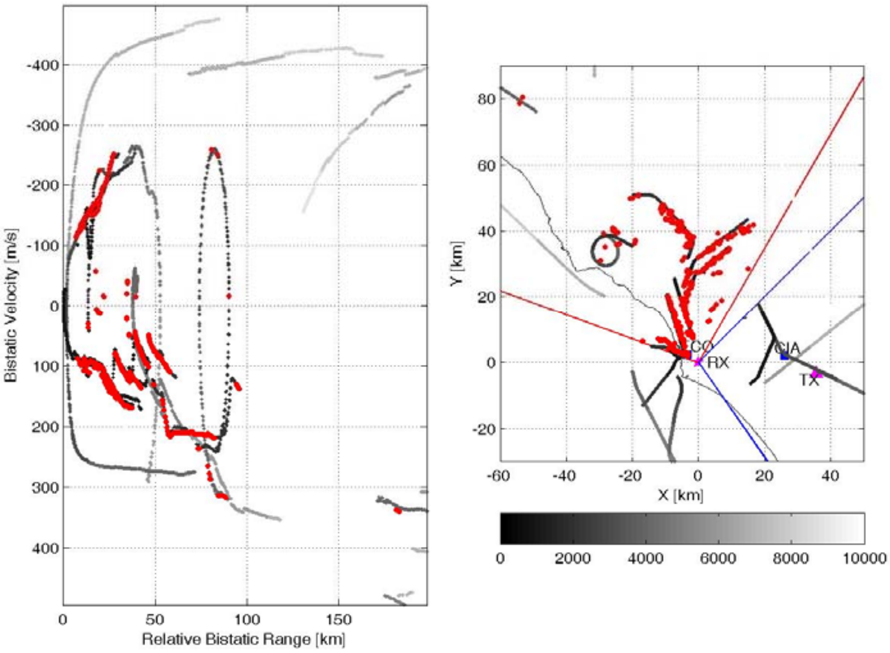

Figure 97 – Detection results, FM radio channels 90.3 – 94.5 – 103.0 MHz, files 801-900

4.7.1.1.6. WB MF INTEGRATION VS NB SINGLE CHANNEL (92.4 MHZ) RESULTS

In this section are reported the detection results obtained with the WB receiver and NB receiver proposed and tested in the WP9 (see Sections 4.4 and 4.5).

For each group of files, corresponding to a time interval of about 3.5 minutes, the left Figures report the detection results over the bistatic range-velocity plane. The green plots and the red plots indicate passive radar detection results obtained by WB and NB receivers respectively, while the live ATC registrations are reported in grey.

The right figure shows the results of target localization over the x-y plane. The grey traces refer to the true air traffic, the green colour is used to indicate the results obtained with the WB receiver passive radar, while the red plots indicate the live ATC registration corresponding to the detection obtained by the NB sensor; the triangle marker indicates the Tx of opportunity, the star represents the Rx position, while the blue markers indicate the Leonardo da Vinci FCO and Ciampino CIA airports).

Notice that the WB receiver is located in Site 3A (as mentioned in Section 4.6) and exploits a configuration with 2 surveillance antennas for angular localization (DoA estimation). For the NB receiver, a single surveillance antenna has been used: as a consequence, it is not possible to estimate the angular localization of the targets, then, the results reported in the x-y domain related to the NB system are purely indicative and correspond to the portions of live ATC registration associated to target detections (highlighted in red in the right figure).

Also, in the following Figures, the WB results refer to the MF integration with 90.3, 94.5 and 103.0 MHz FM radio channels, while the NB results refer to the single FM radio channel 92.4 MHz.

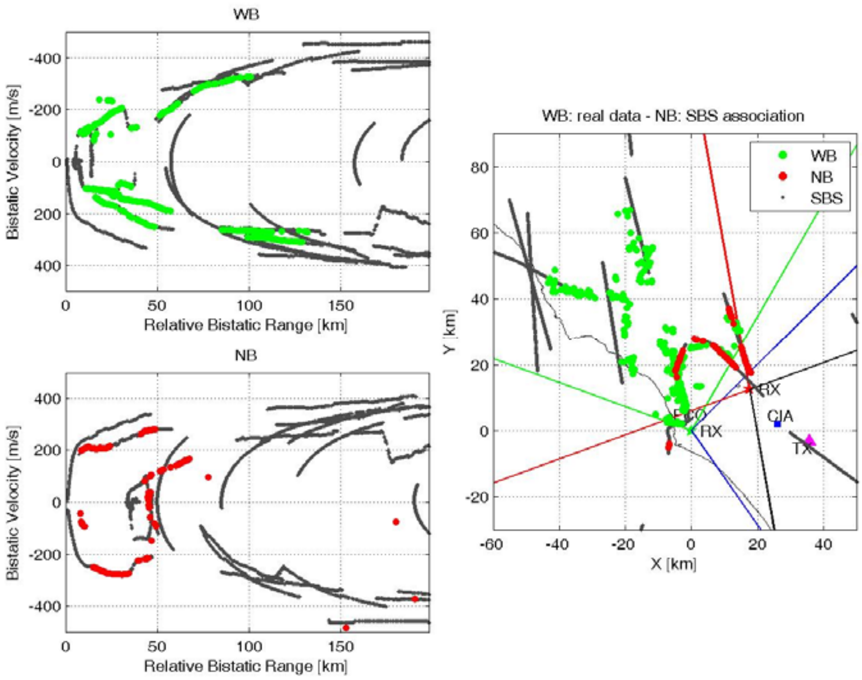

Figure 98 – Detection results, files 1-83

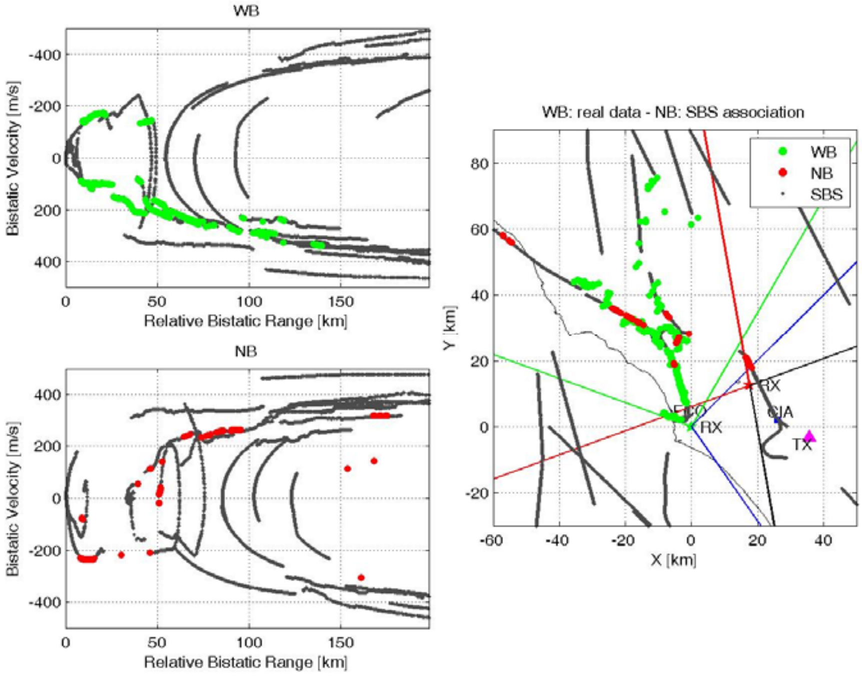

Figure 99 – Detection results, files 84-166

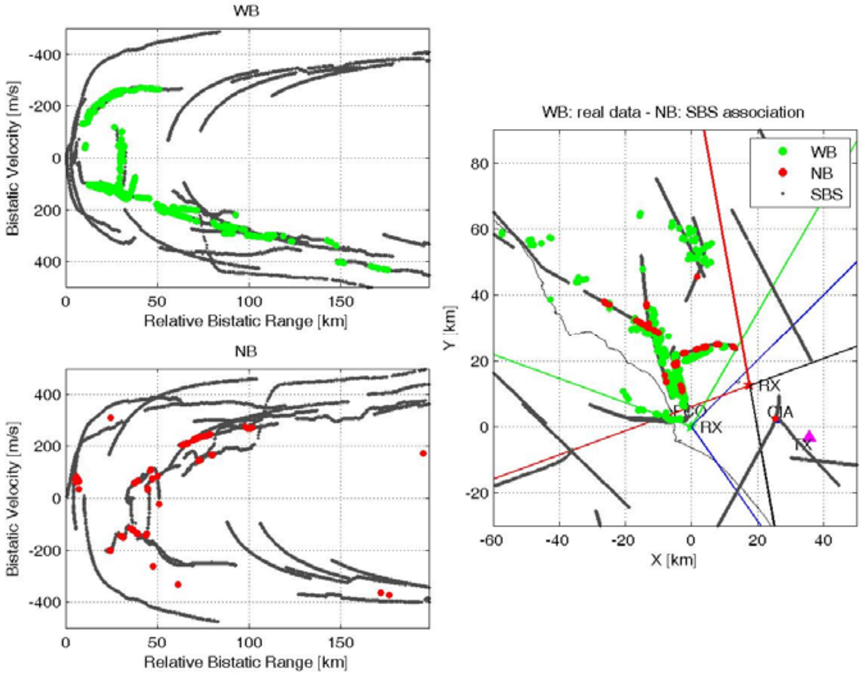

Figure 100 – Detection results, files 167-249

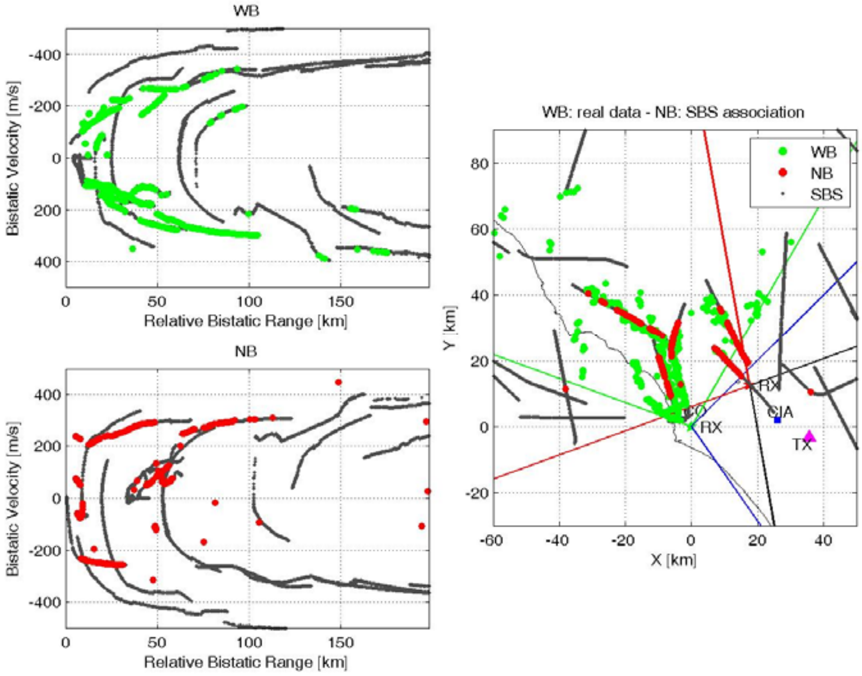

Figure 101 – Detection results, files 250-332

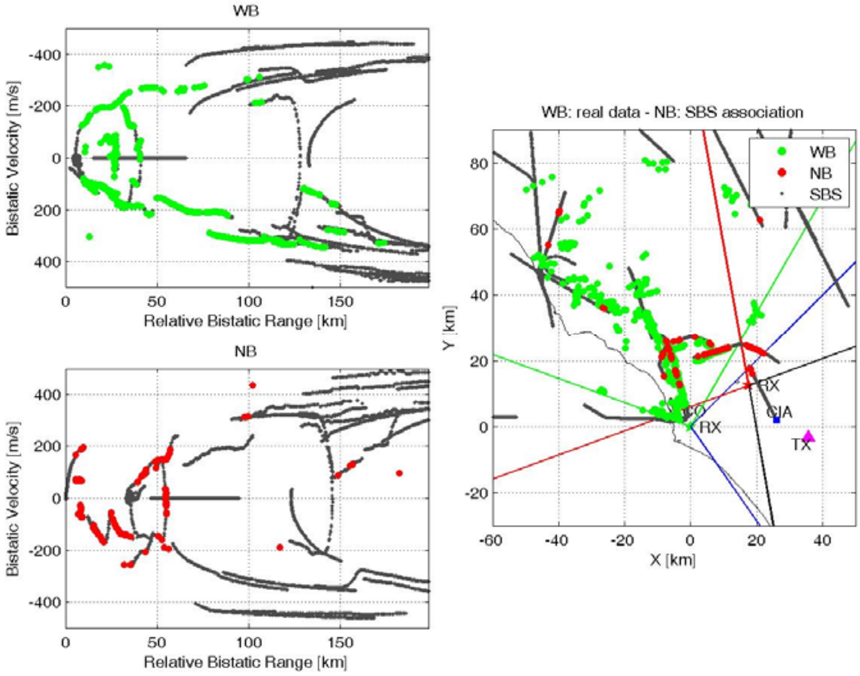

Figure 102 – Detection results, files 333-415

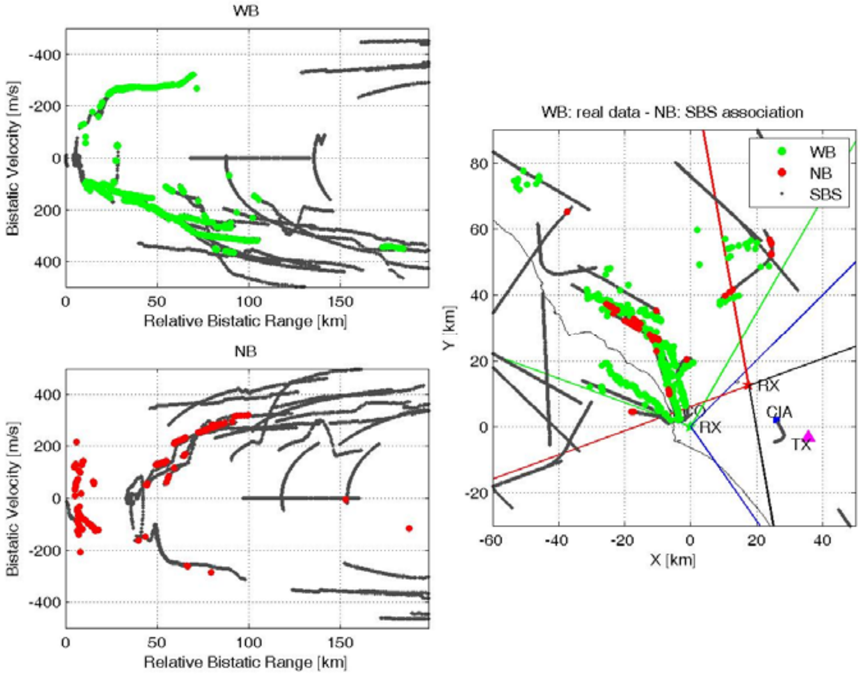

Figure 103 – Detection results, files 416-498

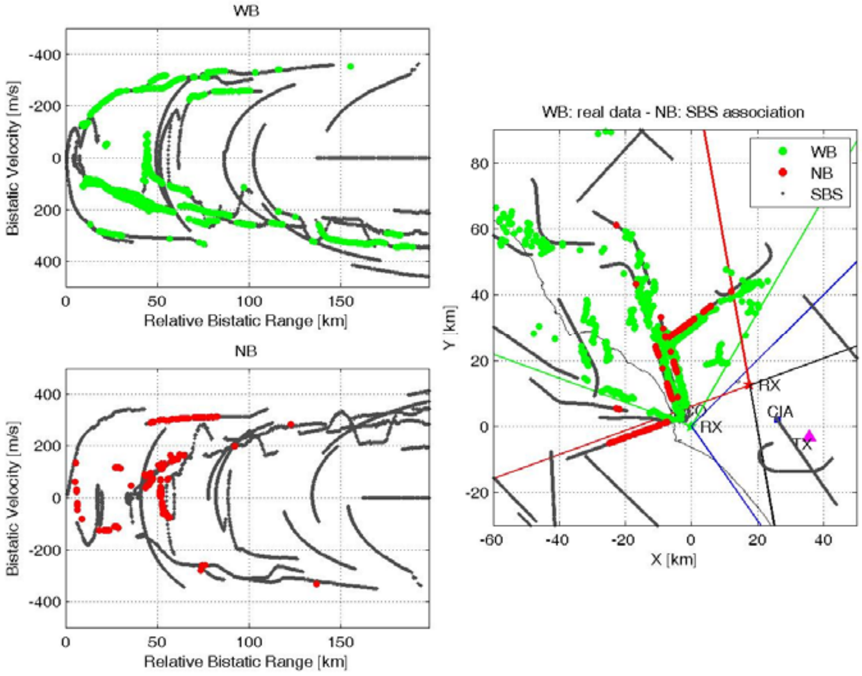

Figure 104 – Detection results, files 499-581

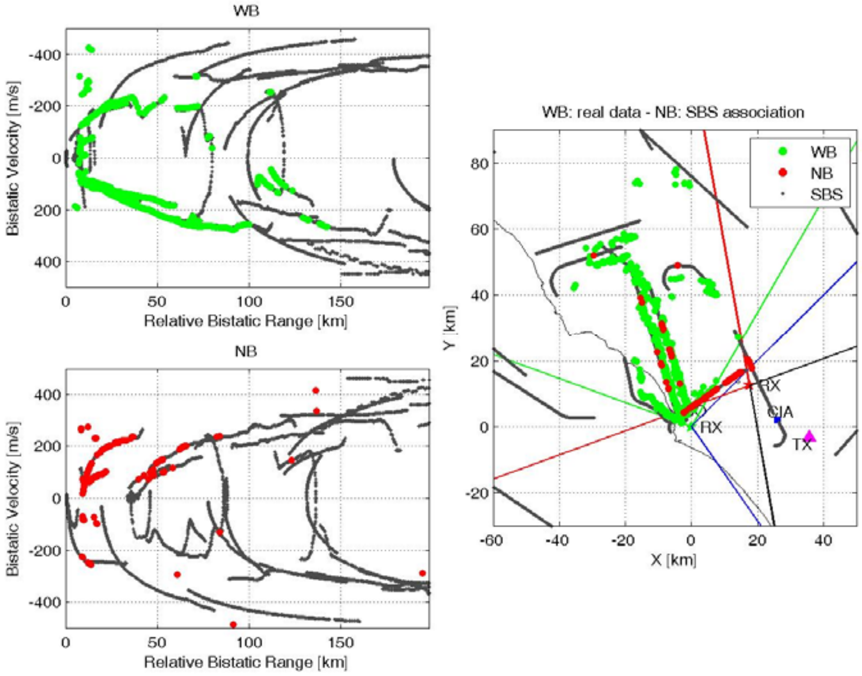

Figure 105 – Detection results, files 582-664

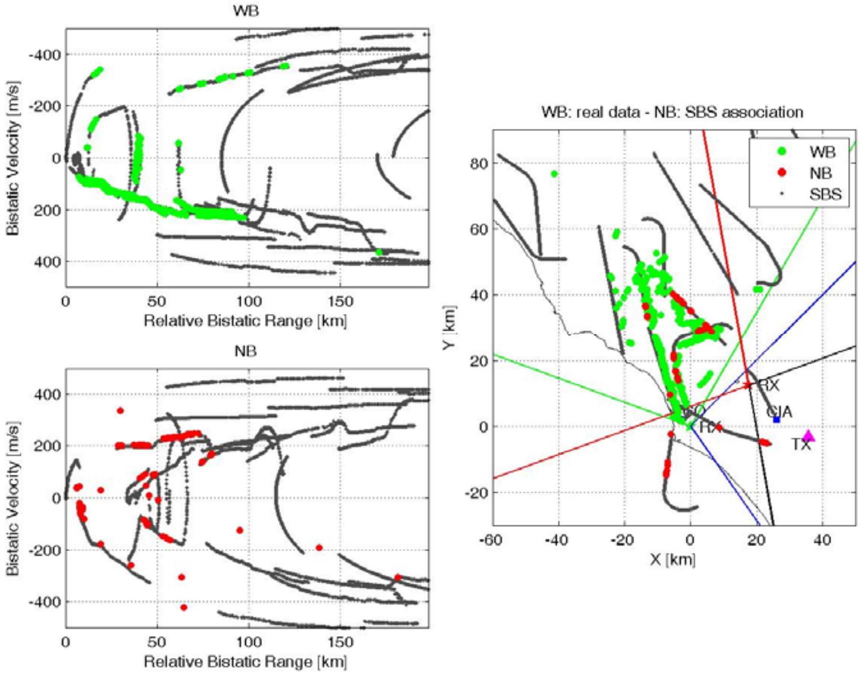

Figure 106 – Detection results, files 665-747

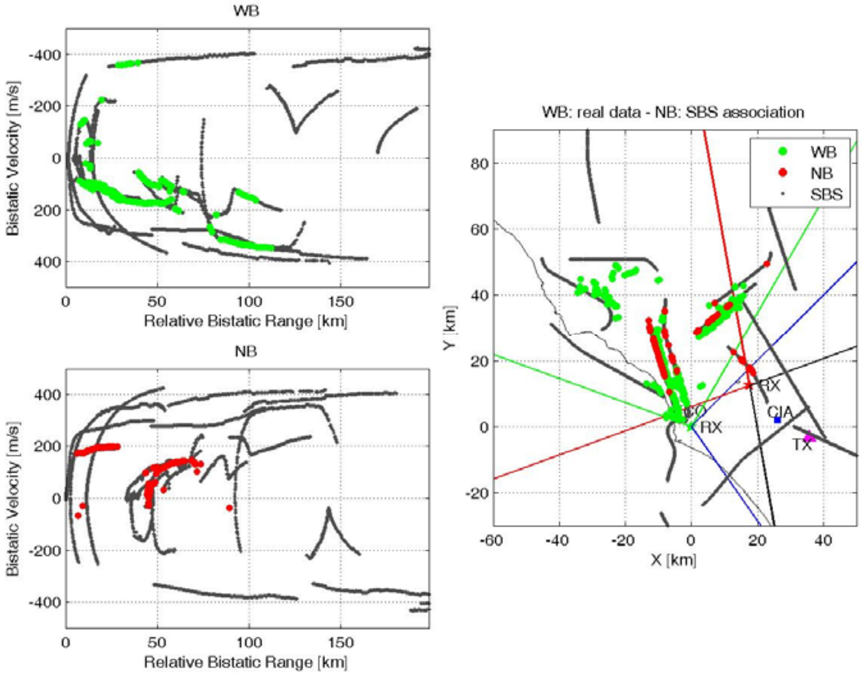

Figure 107 – Detection results, files 748-830

4.7.1.1.7. WB MF INTEGRATION VS NB SINGLE CHANNEL (92.7 MHZ) RESULTS

In this section are reported the detection results obtained with the Wide-Band receiver and Narrow-Band receiver proposed and tested in the Sections 4.4 and 4.5).

For each group of files, corresponding to a time interval of about 3.5 minutes, the left Figures report the detection results over the bistatic range-velocity plane. The green plots and the red plots indicate passive radar detection results obtained by WB and NB receivers respectively, while the live ATC registrations are reported in grey.

The right figure shows the results of target localization over the x-y plane. The grey traces refer to the true air traffic, the green colour is used to indicate the results obtained with the WB receiver passive radar, while the red plots indicate the live ATC registration corresponding to the detection obtained by the NB sensor; the triangle marker indicates the Tx of opportunity, the star represents the Rx position, while the blue markers indicate the Leonardo da Vinci FCO and Ciampino CIA airports).

Notice that the WB receiver is located in Site 3A (as mentioned in Section 4.6) and exploits a configuration with 2 surveillance antennas for angular localization (DoA estimation). For the NB receiver, a single surveillance antenna has been used: as a consequence, it is not possible to estimate the angular localization of the targets, then, the results reported in the x-y domain related to the NB system are purely indicative and correspond to the portions of live ATC registration associated to target detections (highlighted in red in the right figure).

Also, in the following Figures, the WB results refer to the MF integration with 90.3, 94.5 and 103.0 MHz FM radio channels, while the NB results refer to the single FM radio channel 92.7 MHz.

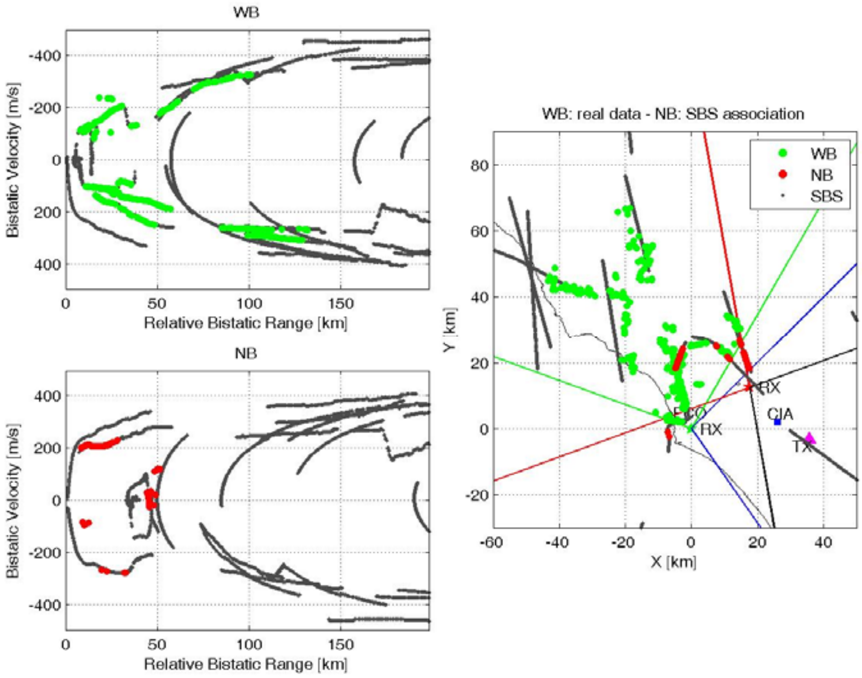

Figure 108 – Detection results, files 1-83

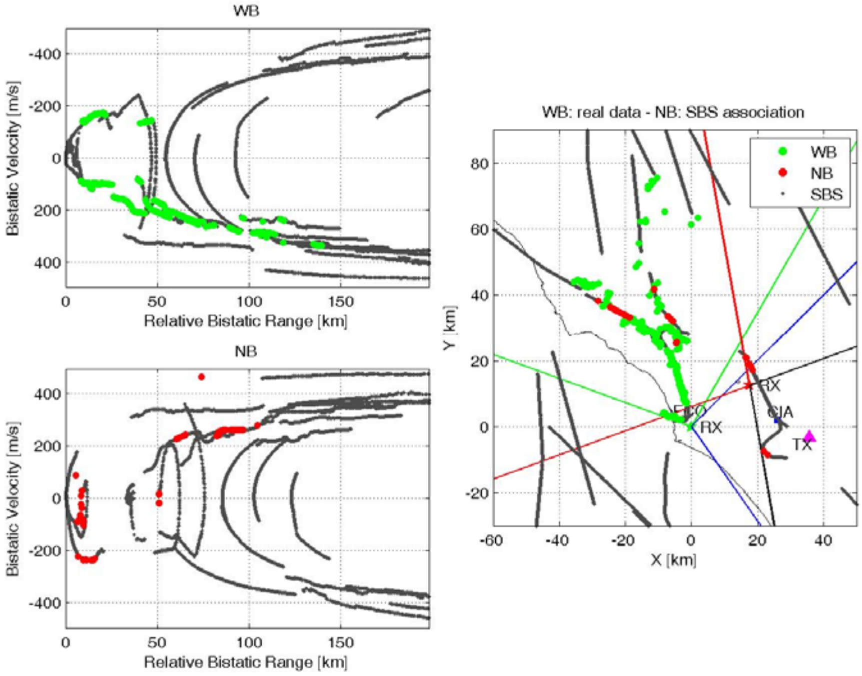

Figure 109 – Detection results, files 84-166

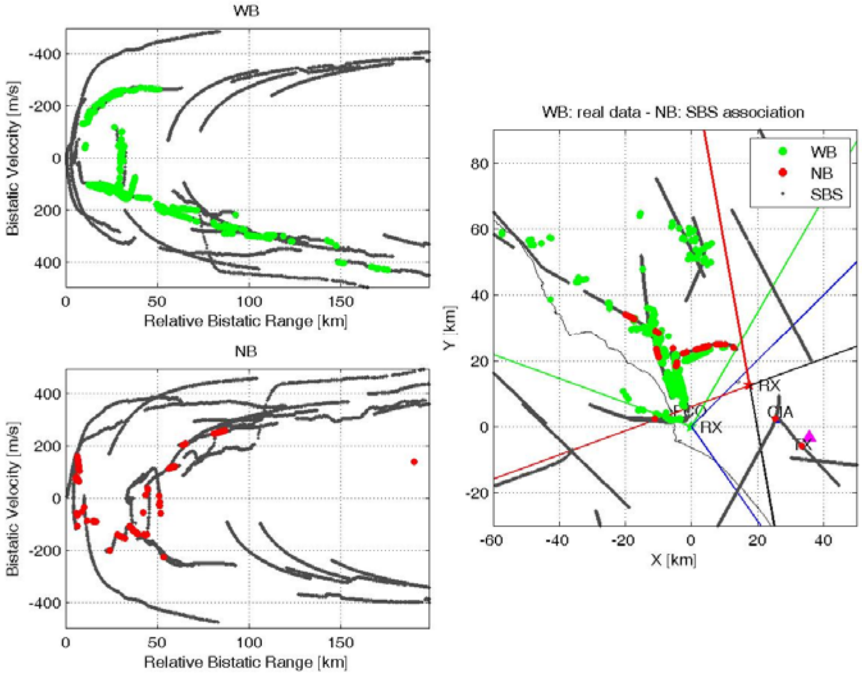

Figure 110 – Detection results, files 167-249

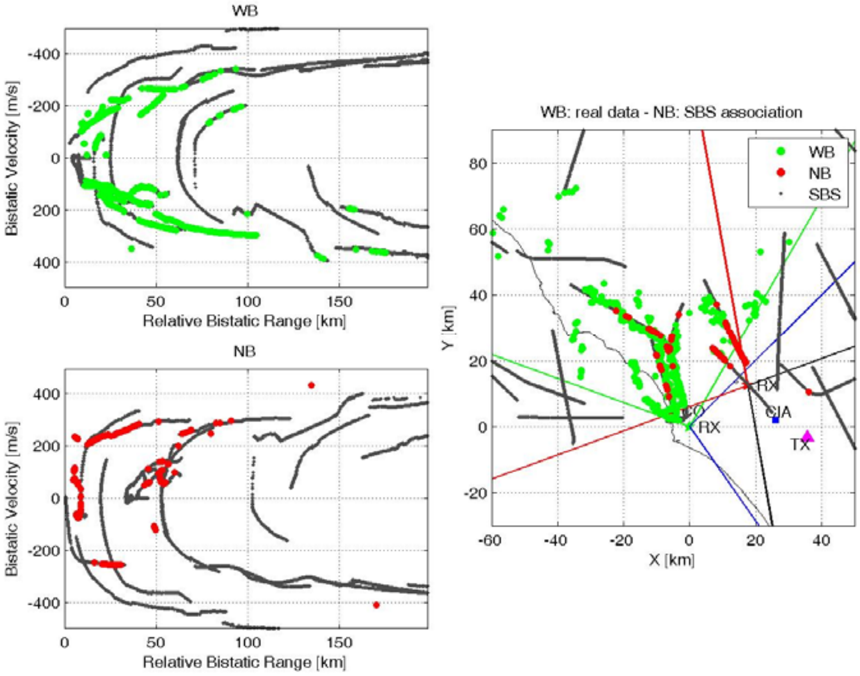

Figure 111 – Detection results, files 250-332

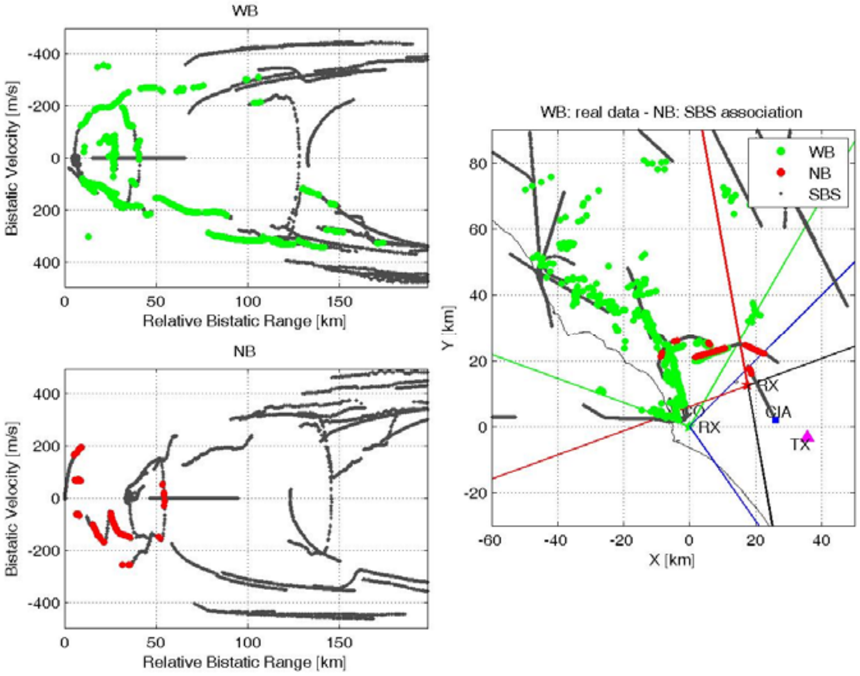

Figure 112 – Detection results, files 333-415

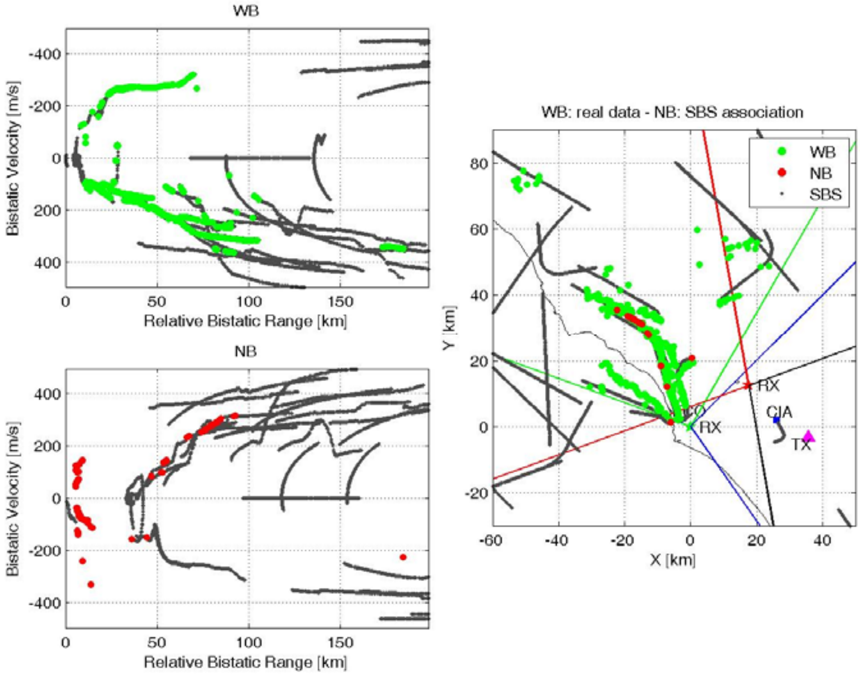

Figure 113 – Detection results, files 416-498

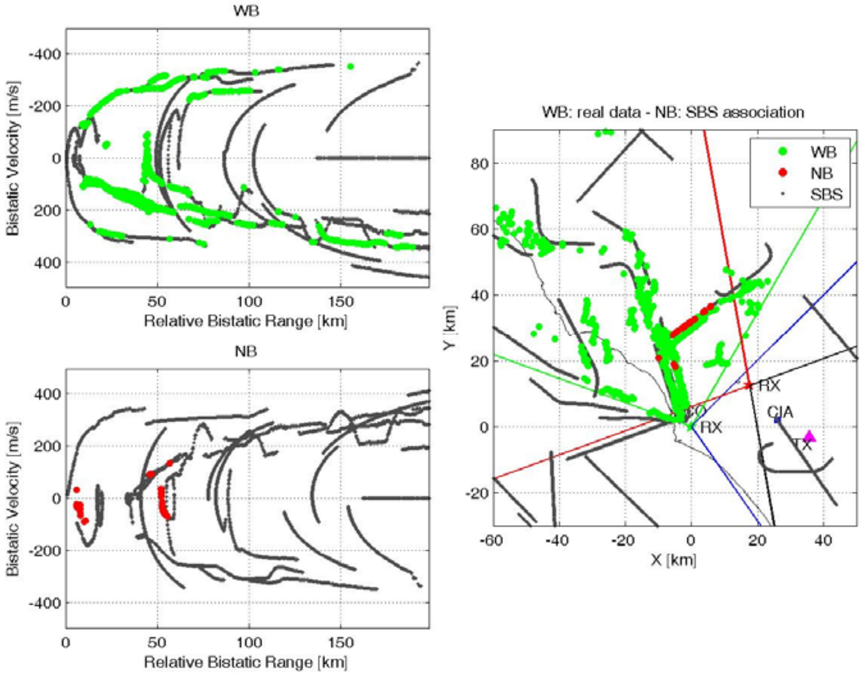

Figure 114 – Detection results, files 499-581

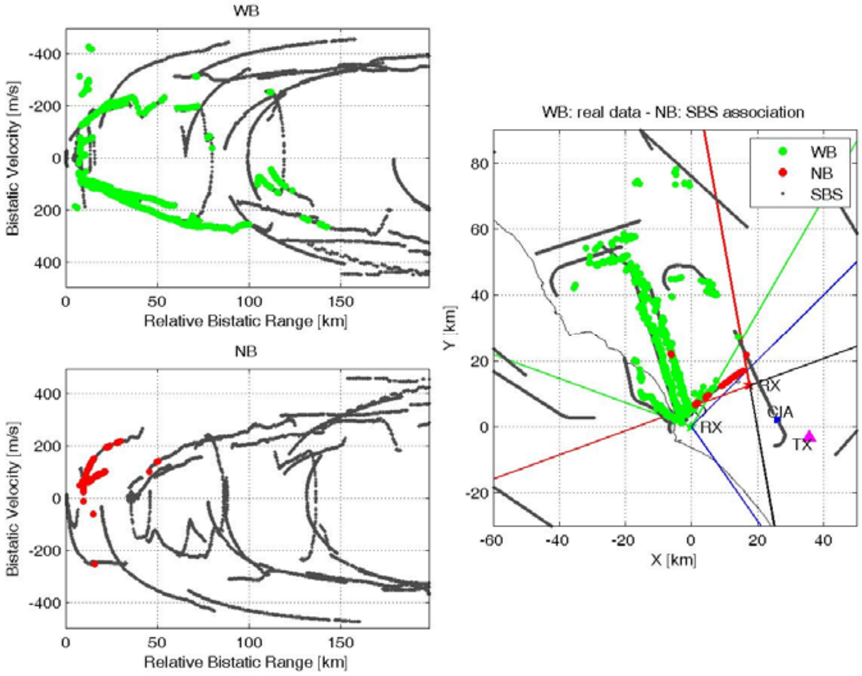

Figure 115 – Detection results, files 582-664

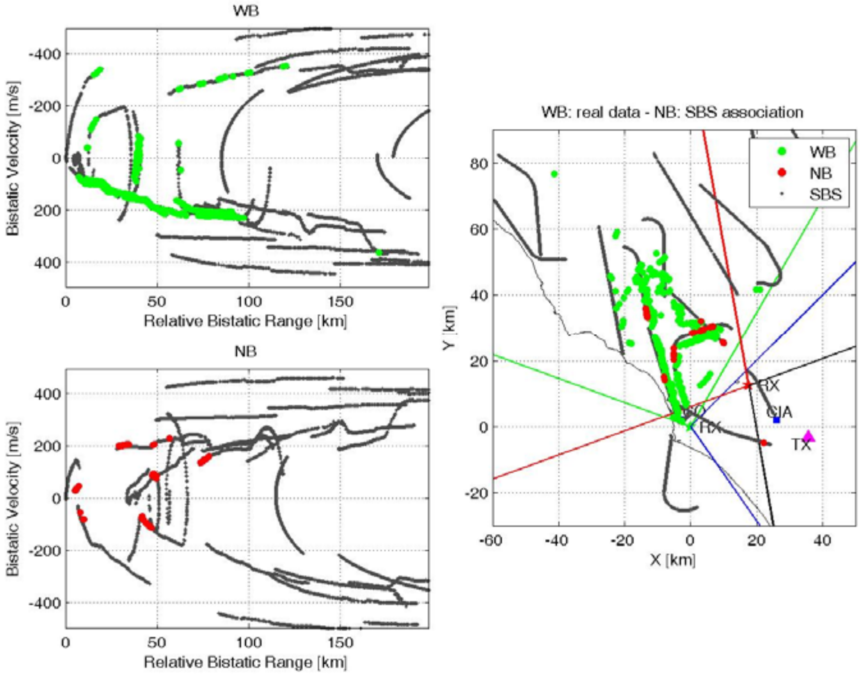

Figure 116 – Detection results, files 665-747

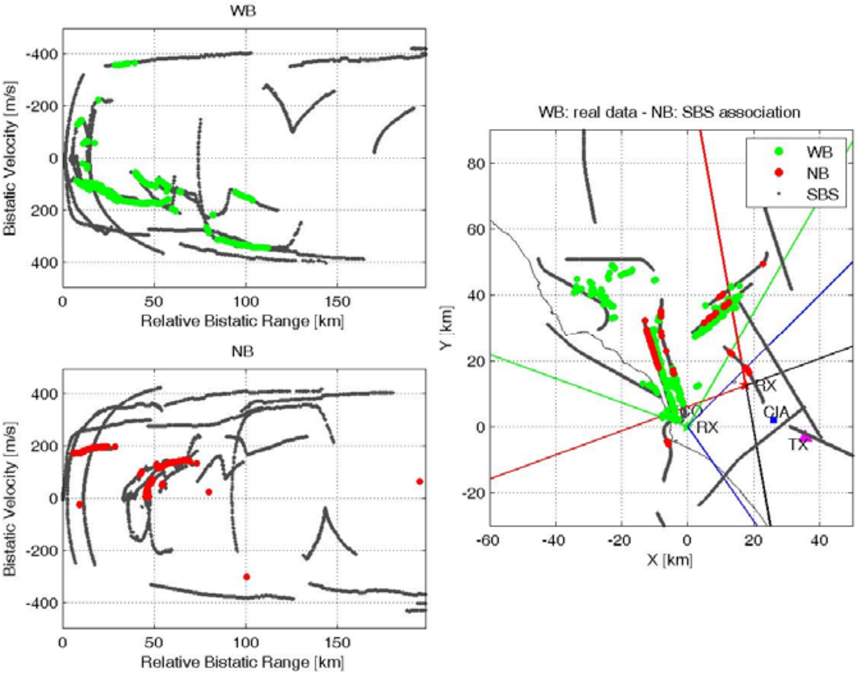

Figure 117 – Detection results, files 748-830

4.7.1.2. ACQUISITION OF DEDICATED FLIGHT TARGET

In this Section are reported the detection results obtained with the WB FM-based PBR during the acquisition campaign, performed on 12th December 2012 in cooperation with Selex-SI and ENAV, with a dedicated flight target. Multiple FM radio channels have been acquired by means of the WB prototype developed by DIET Department of University of Roma “La Sapienza”, described in Section 4.4 and 4.5.

Notice that the results obtained and reported in this Section represent the raw data provided by the passive sensor to the merging function of the ARGUS 3D system.

The aim of this analysis is to verify the effectiveness of the passive sensor for target detection and localization of a small target for the validation of the ARGUS 3D system. Specifically, we report the results obtained in the Site 3A (see Figure 50) on 12th December 2012 at 18.36.06 for an acquisition duration of 60 minutes (1400 files, acquisitions of 1.15 s each).

The target used in this acquisition campaign is a small aircraft (Piaggio P180) flying at low altitude in a medium range distance along the trajectory concerted with Selex-SI for the test bed validation of the ARGUS 3D project.

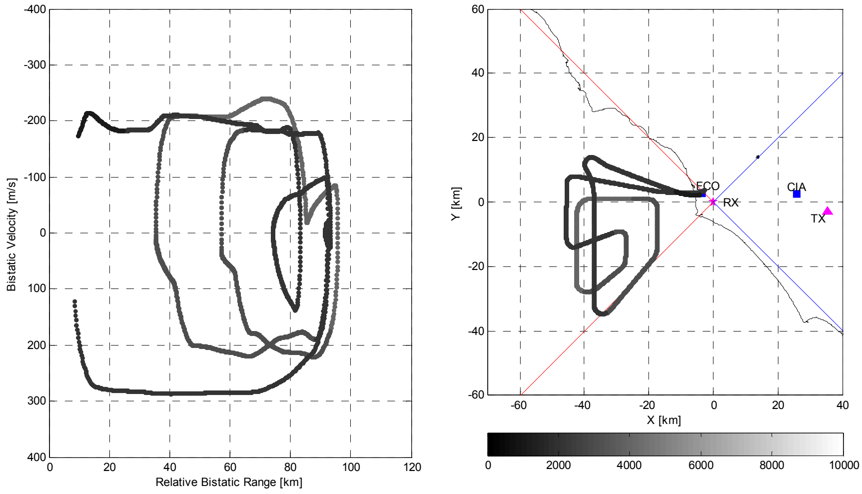

Figure 118 – Cooperative target flight trajectory (Bistatic Range/Bistatic Velocity and X/Y domains)

In Figure 118, the GPS trace of the cooperative flight trajectory is reported in grey scale related to the target quote (see right figure), while the corresponding bistatic-range bistatic-velocity track obtained from the conversion of the GPS data is reported on the left.

In the following sub-Sections, the left figure reports the detection results over the bistatic range-velocity plane (the coloured plots indicate passive radar detections while the live ATC registrations are reported in grey scale related to the targets quote); the right figure shows the results of target localization over the x-y plane (the grey scale traces refer to the true air traffic while different colours are used to indicate the results obtained with the passive radar; the triangle marker indicates the Tx of opportunity, the star represents the Rx position, while the blue markers indicate the Leonardo da Vinci - FCO - and Ciampino - CIA - airports).

By using single bistatic couples, target localization is performed by jointly exploiting the bistatic range and DoA measures provided by the single passive sensor (as described in Deliverable D4.1, Section 2.3). Notice that all (x,y) measures are affected by angle ambiguity due to the interferometric approach. Specifically, the angular measures, and its relative ambiguity, are dependent by the wavelength corresponding to the specific carrier frequency of the exploited FM radio channel (for example, for the FM radio channel 88.0 MHz, the ambiguity interval is about [-58.5°, 58.5°] while for 108.0 MHz the same interval is about [-44°, 44°]). So, each detected target, independently of its real angle with respect to the surveillance antenna pointing, will result in a measure located inside this ambiguity interval.

In the following Sub-Sections, for this acquisition campaign are reported the results obtained with each acquired single FM radio channel, and after the application of the MF integration algorithm. Notice that the reported results for this specific acquisition campaign refer only to the cooperative flight with the aircraft provided by ENAV for the system validation (the commercial air traffic in the same area has been removed).

In particular, the single FM radio channels are:

- 94.5 MHz (Section 4.7.1.2.1)
- 99.6 MHz (Section 4.7.1.2.2)
- 106.6 MHz (Section 4.7.1.2.3)
- 107.1 MHz (Section 4.7.1.2.4)

The MF elaboration has been performed by integrating the following group of FM radio channels:

- 94.5 – 106.6 – 107.1 MHz (Section 4.7.1.2.5)

4.7.1.2.1. SINGLE FM RADIO CHANNEL 94.5 MHZ

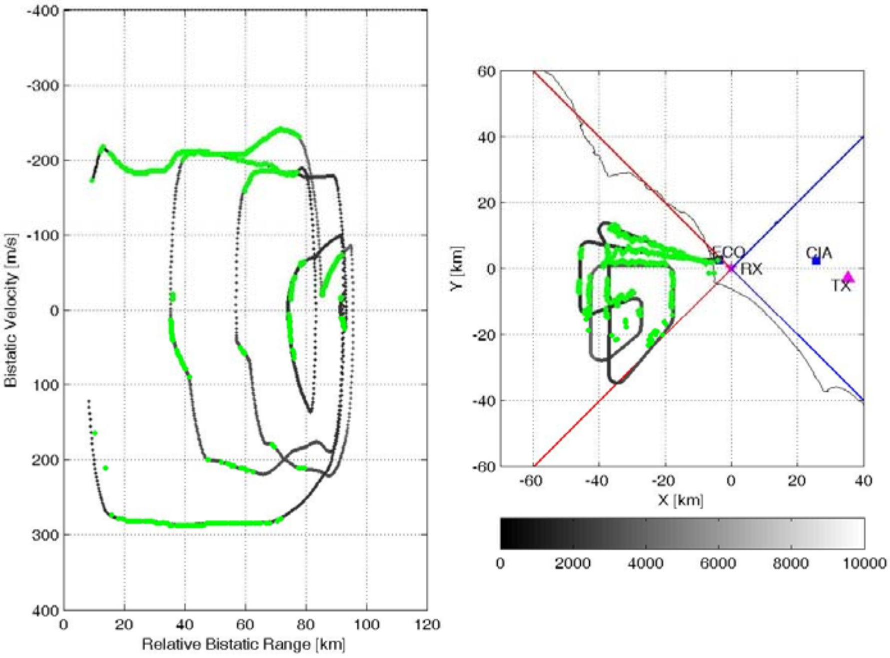

Figure 119 – Detection results, FM radio channel 94.5 MHz, files 1-1000

4.7.1.2.2. SINGLE FM RADIO CHANNEL 99.6 MHZ

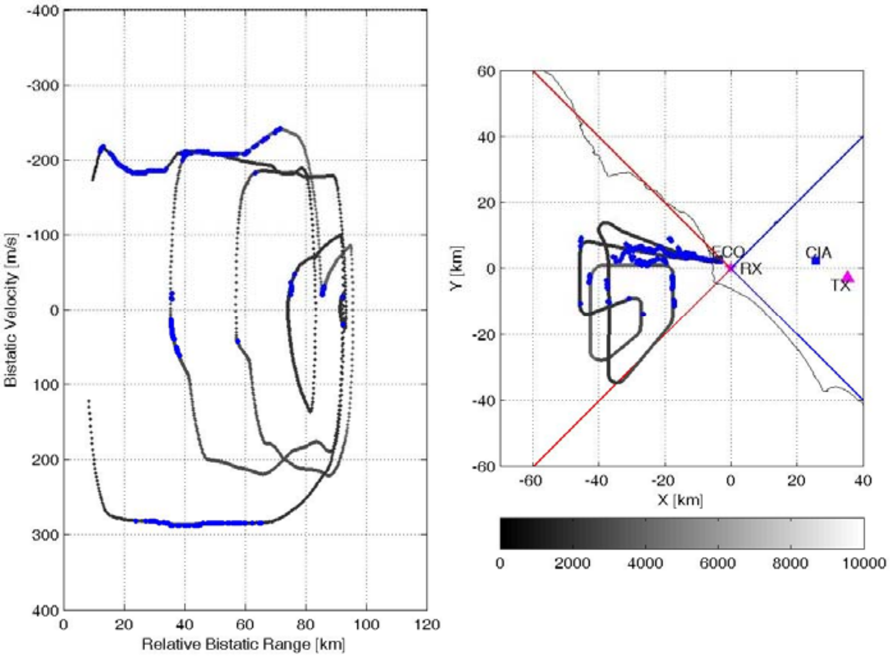

Figure 120 – Detection results, FM radio channel 99.6 MHz, files 1-1000

4.7.1.2.3. SINGLE FM RADIO CHANNEL 106.6 MHZ

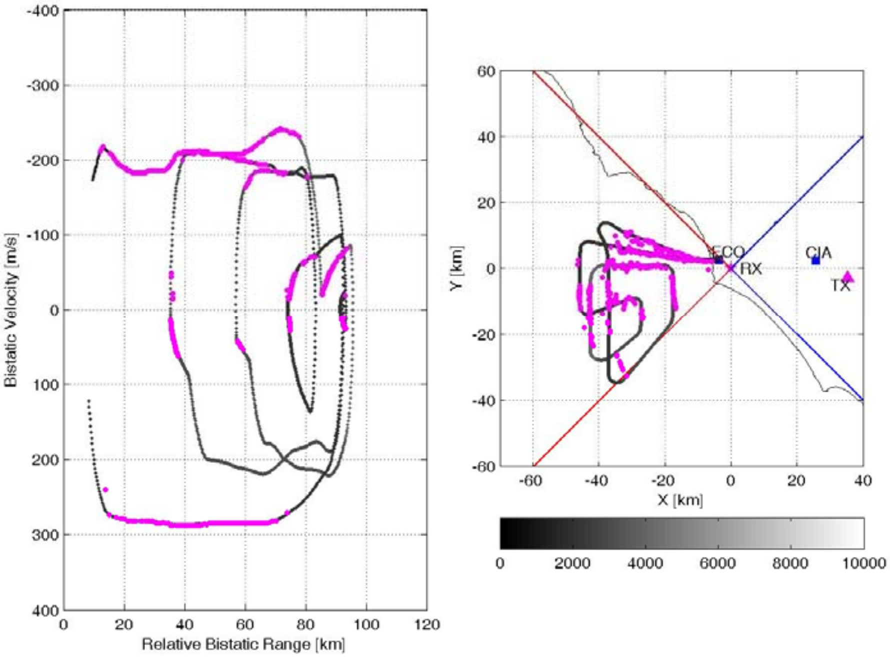

Figure 121 – Detection results, FM radio channel 106.6 MHz, files 1-1000

4.7.1.2.4. SINGLE FM RADIO CHANNEL 107.1 MHZ

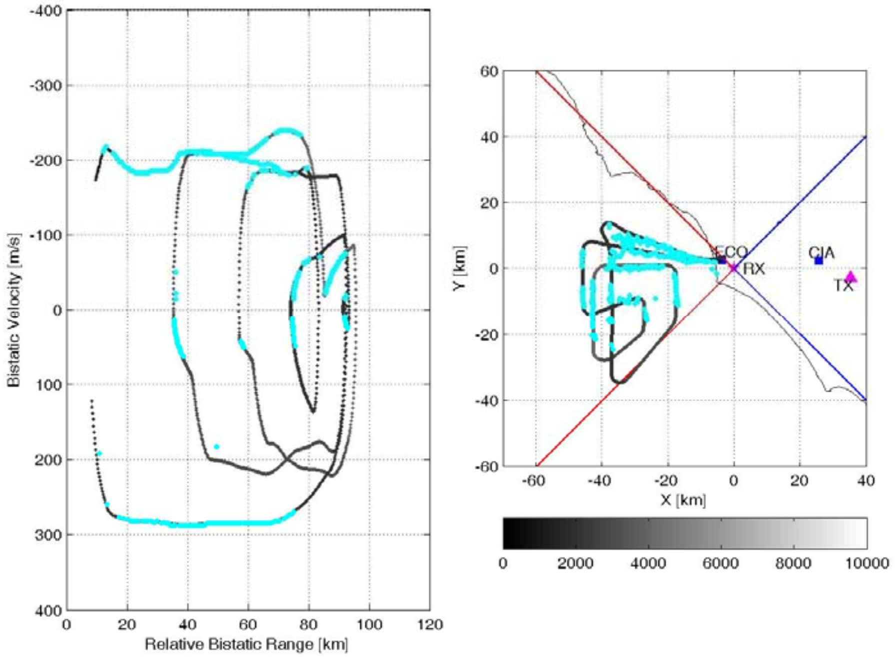

Figure 122 – Detection results, FM radio channel 107.1 MHz, files 1-1000

4.7.1.2.5. MULTI-FREQUENCY INTEGRATION FM RADIO CHANNELS 94.5 – 106.6 – 107.1 MHZ

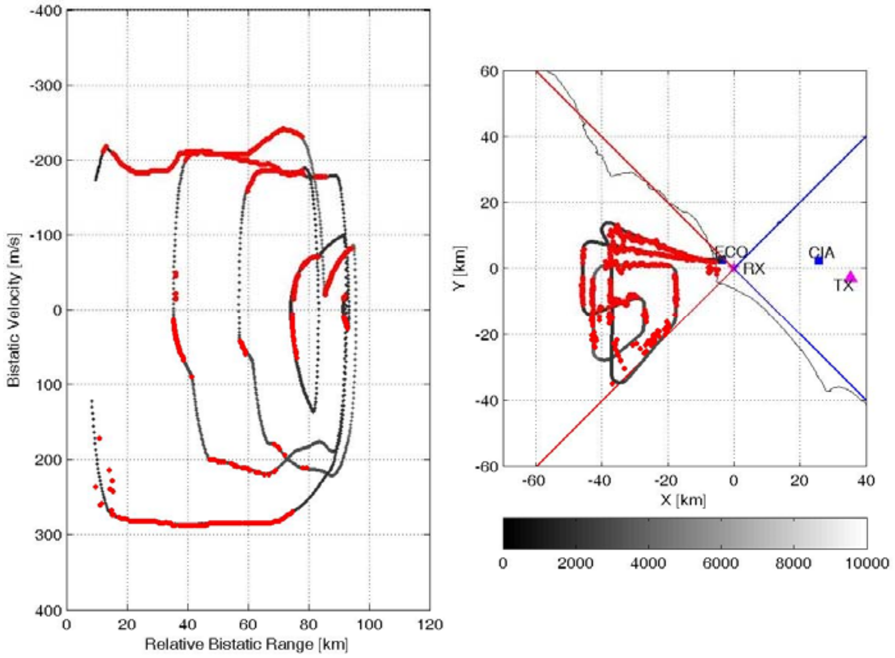

Figure 123 – Detection results, FM radio channels 94.5 – 106.6 – 107.1 MHz, files 1-1000

4.8. CONCLUTIONS

In Section 4.7 are reported the detection and localization results obtained with the FM-based PBR sensor.

Sensor concept, definition of the system characteristics and the processing techniques for the single Multi-Frequency passive radar system have been described in Section 2.

The test bed set-up for the FM-based PBR sensor validation, including the prototypes hardware description and tests, and the validation analysis plan, has been reported in Sections 4.4 and 4.5.

Raw data have been collected with the experimental passive radar sensor and have been off-line processed in order to extract the single detections in bistatic-range bistatic-velocity (Doppler) domain. Additionally, the angular target localization has been performed through DoA estimation and by means of the multiple channel receiver.

The effectiveness of the proposed solution has been assessed by evaluating the FM-based PBR detection capabilities in a short range against live ATC registrations and also against a cooperative target flying at low altitude.

The extensive analysis, of the data collected and processed, showed as expected that the detection performance of the passive sensor are largely dependent on the considered FM radio channel, the instantaneous transmitted waveform and the instantaneous characteristics of the propagation. A preliminary activity was the selection of some FM radio channels for each Site of interest based on the proper parameters described in Section 4.6 In the analysis of the results obtained with different single FM radio channels acquired simultaneously, is clearly visible that the detection performances change with the considered channel (see for example Figure 120, referring to FM radio channel 99.6 MHz, where it is easy to notice the lower number of cooperative flight detections with respect to the other FM radio channels, 94.5, 106.6 and 107.1 MHz - Figure 119, Figure 121 and Figure 122, respectively).

As a general result, and with reference to the civil air traffic, the FM radio channels 94.5 and 103.0 MHz result on the average the best performing radio channels, thus allowing to obtain the best detection performance in terms of number of plots and coverage area.

In order to increase the performance of the passive sensor, the MF integration stage has benn introduced in the processing scheme. This technique has required the use of the WB receiver prototype to acquire multiple radio channels simultaneously. For the acquisition campaigns (reported in Section 4.7.1.1.5) the MF integration has been performed with different groups of three FM radio channels. In each acquisition campaign, after the application of the MF approach, an increase of the performance has been obtained with respect to the use of the single FM radio channels, and this is clearly visible in all results showed in this document.

It is worth mentioning that the passive radar system performance could be further improved by optimizing the hardware section of the receiver. In fact, the hardware section of the developed sensors has been basically conceived in order to demonstrate the effectiveness of the passive radar concept, and resorting to low cost solutions (COTS components). On the contrary, great attention and effort has been putted into the development and optimization of innovative processing techniques in order to obtain a well performing FM-based PBR.

A performance comparison between the two receivers developed by DIET Department has been reported for the acquisition campaign carried on 11th June 2012 (see Sections 4.7.1.1.6 and 4.7.1.1.7). The data collected with the WB receiver have been processed with the MF integration approach while the results obtained with the NB receiver have been obtained with three different single FM radio channels. The NB system allowed to detect targets in a short range, despite its performance are slightly worst with respect to the WB receiver. Moreover, the NB prototype has not been used for other acquisition campaigns because the angular target localization is not available with this system yet.

Comparing the results obtained in each acquisition campaign by using single FM radio channels and with the MF integration approach, it is possible to assert that the MF integration guarantees a performance improvement keeping its characteristic of robustness respect to the strongly time-varying characteristics of the transmitted waveforms and of the channel propagation. As a consequence, the proposed MF approach is clearly able to provide the robustness and continuity of operation that are generally difficult to guarantee for FM-based passive bistatic radar, thus removing one of their major weaknesses and making them more attractive for reliable surveillance applications.

As mentioned, all detection results showed in this report are represented in bistatic-range bistatic-velocity (Doppler) domain and in x-y domain. The x-y localization has been performed by DoA estimation and the achievable performance in terms of DoA estimation accuracy highly depends on the use of a single or multiple FM radio channels. Specifically, advanced MF DoA estimation techniques have been introduced to enhance the MF system performance by making it less affected by the instantaneous behaviour of the integrated FM channels, thus resulting in an increased angular localization accuracy with respect to the single FM channel operation.

In conclusion, the presented analysis allowed us to assess the effectiveness of the conceived FM-based single MF passive radar sensor for surveillance purposes. Obviously the single passive sensor is intended to provide highly reliable performance at short ranges.

5. WIFI-BASED PBR

5.1. INTRODUCTION

In the latest years, the problem of air transport security has always been a priority for the EU aviation industry, since airports represent a natural target for terroristic acts. The airport can be considered a sensible target for any crimes for different reasons:

- the large amount of people simultaneously located in the airport areas with limited emergency exits;
- the potentially high level of damage for a high number of people with a limited effort;
- the impact of the terroristic action on the public opinion with repercussion on world economy, as a side-effect of the personal fears from potential passengers, can become extremely wide;
- the use of hijacked aircrafts (A/C) as lethal weapons against civil targets.

Moreover, the airport security problem is very complex. To provide an effective and reliable security level, a large number of issues have to be considered, including the following ones:

- the wide extent together with the highly non-homogeneous characteristics of the areas to be monitored;
- the wide range of possible and potential weapons to be considered: liquid or solid explosives, metallic and non-metallic objects, guns, etc.;
- the high concentration and the heterogeneous typology of people with continuously changing positions and densities.

The current methods to find hazardous materials brought inside the terminal by suspicious person are only by manual inspection, cameras, walk-through metal detector and x-rays. However, the manual inspection is very time consuming; the effectiveness of visual cameras largely depends on the human factor (capability to identify a suspicious person); the walk-through metal detector can detect only metallic objects and the x-rays are considered harmful to human health (so they are be used only for bags and luggage). After the recent events many airports are installing and requiring the control through the so-called body-scanners that are able to do a complete scan of the entire body of a person. However the system implies the transit of all passengers through the scanner for a period of a few tens of seconds each, which improves security but may have a significant impact on waiting times for passengers and on privacy related issues.

The above mentioned limitations have been addressed by the ATOM (Airport detection and Tracking Of dangerous Materials by passive and active sensors arrays) project, funded by the European Union, 7th framework program, theme #7 Transport (including Aeronautics), Grant agreement no.: 234014, [25]. ATOM is a 3 year project which started in July 2009. Its consortium is composed of 11 partners from 7 EU Member States (Italy, The Netherlands, Germany, Greece, Hungary, Spain, Romania), including industry, research organizations and final users. Specifically, DIET Department of University of Rome “La Sapienza” is responsible for the design of passive radar network for detection and localization of people carrying out dangerous tools.

An overview of the ATOM project is provided in the following Section. A prototype description of two passive receiver developed is reported in Section 5.3. In Sections 5.4 and 5.5 tests, controlled experiments and the acquisition campaigns are described. Finally, in Section 5.6 summarize the results obtained with the passive sensor.

5.2. ATOM EU PROJECT

The overall objective of ATOM project is to design and develop an innovative detection and surveillance system able to enhance the security level in the airport areas, by detecting hidden hazardous materials/tools (including explosives) and tracking people concealing these forbidden items, without interfering with the normal airport operations; while directly enhancing the airport security, ATOM system will also indirectly contribute to protect A/C from terrorist or other criminal acts.

The development of an innovative system based on a multi-sensor approach that integrates active and passive radar sensors, as well as its integration with currently used surveillance systems in order to obtain an integrated security system with enhanced capabilities of detection and tracking of dangerous tools and materials, is the core of the research activities foreseen in the ATOM project.

Following this approach, the ATOM system will improve the security level not only in the gate area, but at a preliminary stage, also in the terminal area of the airport. Specifically, the ATOM system foresees two levels of control, as illustrated in Figure 124:

- a first one at the airport entrance, where an automatic detection system controls all the people (passengers and others) and alerts the security operators when a suspicious person is detected. The tracking system allows the security operators to track suspicious people and analyze their behavior in order to preserve the security in the airport.
- The second control is placed at the gate entrance, where the detection system controls all the passengers. After this second control the suspicious people are subjected to the regular screening.

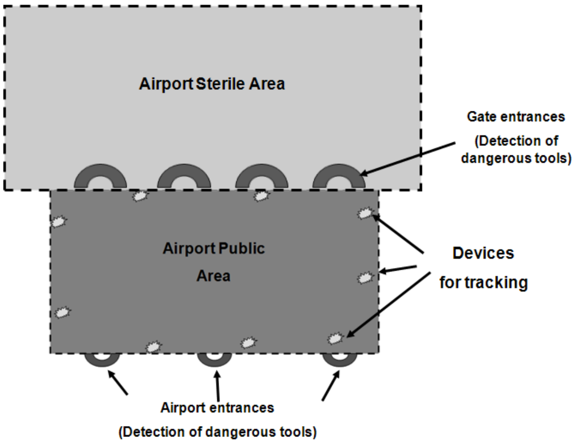

Figure 124 - Distribution of detection and tracking sensors of ATOM system in the airport area

5.2.1. SYSTEM ARCHITECTURE

In this section the ATOM system architecture is described. The overall architecture is divided in two main blocks (see Figure 124):

- Terminal area, where there are three different sub-systems: detection system I (airport entrance), tracking system and data management system;
- Gate area, where only detection system II is foreseen (no tracking system is required at gate entrance); in this area, suspicious people should be immediately stopped by the staff avoiding that they remain in the sterile area.

5.2.1.1. DETECTION SYSTEMS

The two detection systems (I and II, see Figure 125) are composed of 15÷35GHz Ultra Wide Band (UWB) radar and W-band active radar sensors which, after proper signal processing, send information to their respective data fusion block. The output of this block is the input for the Decision Support System (DSS). The DSS automatically detects the dangerous person or send the information to the security operator (that decides whether to alert the security staff or leave free access to the observed person). From the DSS threshold settings, the performance of the overall system can be determinate.

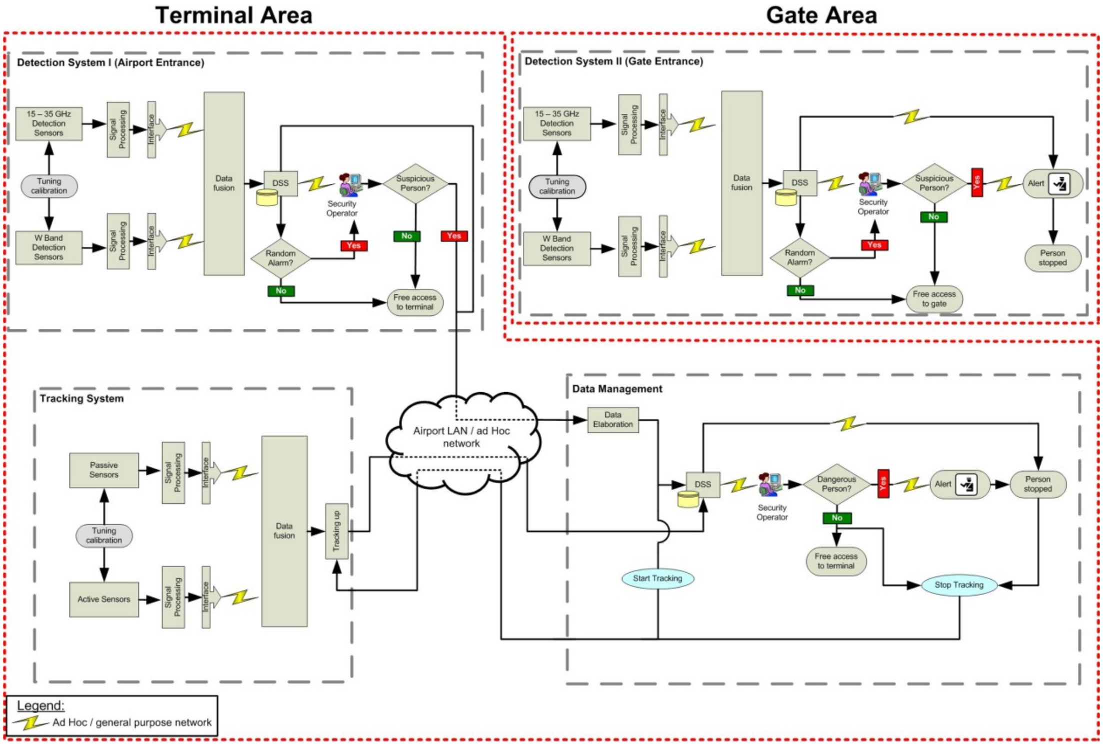

Figure 125 - ATOM architecture

Detection system I, located at airport entrance, is directly connected, by a dedicate communication network, to data management block which distributes information to both the tracking system and the security operator.

Detection system II, located in the gate area, is similar to the first one, but requires an higher security level. Any suspicious person in the gate area has to be stopped and identified as soon as possible. This requires a more severe threshold in the DSS. When the system detects (automatically or by the security operator) a suspicious person, the security staff is alerted immediately in order to stop the threat.

5.2.1.2. TRACKING SYSTEM

The tracking system (reported in Figure 125) is composed by passive and active radar sensors. A data fusion block is required to combine the data provided by different kinds of sensors and to perform the tracking of suspicious persons. The tracking system is enabled by the management block when the detection system I identifies a possible threat in the terminal area. The connection between different blocks is guaranteed by a dedicate communication network. The output of the tracking stage is processed by the management block. The idea is that tracking the suspicious people, after a detection has been declared, allows the security personnel to arrive to the appropriate entrance and search the correct person.

5.2.1.3. DATA MANAGEMENT

Data management block is the core of the whole system. It processes the data coming from the detection system I and from the tracking system by a proper DSS. Through the use of a proper database, the DSS is able to automatically detect threats and to immediately alert the security staff. When a suspicious object is detected, but it is not well classified by the DSS, a security operator can take the decision taking into account the information provided by the DSS itself and observing the scene through a monitor. The security operator decides whether to allow or not free access to airport sterile area to the observed person. In any case, when the security operator determines that there is not any threat or when the suspicious person is stopped, the tracking system is disabled.

5.2.2. ATOM SENSORS

As previously mentioned, different types of sensors are foreseen for the detection and tracking systems, respectively: imaging sensors, able to detect suspicious people concealing dangerous tools and active/passive radar, able to provide localization of people already marked as suspicious. A brief sensors overview is reported in the following.

5.2.2.1. IMAGING SENSORS

As already mentioned, two different imaging sensors able to detect suspicious people concealing dangerous tools are foreseen by ATOM: W-band detection sensors and UWB detection sensor.

5.2.2.1.1. W-BAND RADAR

High-complexity equipment in the W-band (75÷111GHz) has been studied and developed. In particular, while the sensor hardware is just one component that influences the overall performance, another important point is the number of sensors and their spatial arrangement which in turn impacts directly the measurement speed and thus the practical applicability.

Within the ATOM project, three netted sensors were developed and built at the Fraunhofer FHR. Moreover, three configurations of the sensors have been investigated aiming at combining the advantages of all proposed methods:

- Rotating W-Band radar above person
- Rotating W-Band radar in front of person
- 2D mechanical scan with W-Band radar

5.2.2.1.2. UWB RADAR

Laboratory experiments have been carried out at Technology University of Delft (TUD) in order to test the feasibility of less expensive medium-complexity approaches in the 15÷35GHz frequency range, where UWB transmission is exploited.

The operational band of 15-35 GHz has been selected in order to obtain high cross- and down-range resolution of centimeter order along with sufficient penetration capability of the radar signal, which allows to see through clothes and meanwhile to inspect the hand-held luggage of a passenger. The centimeter level of resolution suffices for shape reconstruction of weapons, e.g. a gun, and in the meantime it respects the ethical issues of inspecting a person without showing his detailed physical features.

The UWB sensor is expected to deliver a high resolution 3-D image of a passenger, i.e. it must employ a certain scanning procedure, either mechanical or electronically. The mechanical scanning means realization of synthetic aperture radar (SAR) when transmit-receive (Tx-Rx) antenna pair moves along given 2-D aperture and acquires a data with a fine spatial step. The electronically scanning requires implementation of an array with a specific configuration of Tx and Rx antennas.

The aperture of UWB sensor essentially defines the effective size of a focused radar image while the operational distance should not exceed that size in order to have a cross-range resolution comparable with the central wavelength of UWB signal. This means that a person under inspection should stay not farther away from the sensor than one meter.

The fusion of the imaging systems used for detection is one main part of the research activities conducted in the project. The two systems are expected to yield large benefits concerning the identification of different items, especially the 15÷35GHz system due to the 20GHz bandwidth. Furthermore, an higher detection rate is expected using different operating frequencies and setups in the two considered systems. Also, the different geometries foreseen for the two systems allow them to compensate each other, thus making the identification of suspicious persons more reliable. The use of high-frequency (and high-energy) active radars for the detection of concealed weapons and explosives represents a scientific innovation of the ATOM project.

5.2.2.2. ACTIVE/PASSIVE RADAR

As previously mentioned, tracking of suspicious people within the terminal area is foreseen by the ATOM project by exploiting both active and passive sensors.

5.2.2.2.1. ACTIVE RADAR

The active radar system consists of 5 small radar sensors capable of continuous-wave and frequency-modulated continuous-wave mode that operate around 24 GHz (K-band) with a bandwidth of around 450 MHz. The practical range of each sensor for an average human being is around 20 meters. Each sensor consists of a low cost COTS radar module and a backboard to control the module, and to perform AD and DA conversion as well as amplification. The backboard has been designed and made at Thales Netherland premises (Delft).

5.2.2.2.2. PASSIVE RADAR

By exploiting sources of illumination widely available in the airport environment (such as WiFi signals), an innovative tracking system based on Passive Radar networks may allow a wide space coverage. This shows also very desirable characteristics as covert operation, absence of emissions and therefore absence of ethical issues for public health.

The fusion of the two tracking sensors is also a portion of scientific innovation developed inside the ATOM project. Moreover, the use of FMCW active radars for the very short range people tracking can complement the passive radar to provide higher accuracy especially in small areas, as corridors.

5.3. PROTOTYPE DESCRIPTION

Two different architectures for the realization of a multi-channel WiFi-based PBR receiver have been developed and fielded with proper laboratory tests and acquisition campaigns. Specifically, the two considered solutions are:

- Super heterodyne receiver
- Homodyne receiver

The Super heterodyne solution, sketched in Figure 126, foresees a conversion stage to a desired Intermediate Frequency (IF), adequate filtering stages to select the single channel of interest, and the A/D conversion. The homodyne solution is based on an analog demodulation of the signals. The A/D conversion is performed at Base-Band (BB) at low sample rate with respect to the super heterodyne receiver.

5.3.1. WIFI SUPER HETERODYNE RECEIVER

The block diagram of the super heterodyne receiver is sketched in Figure 126.

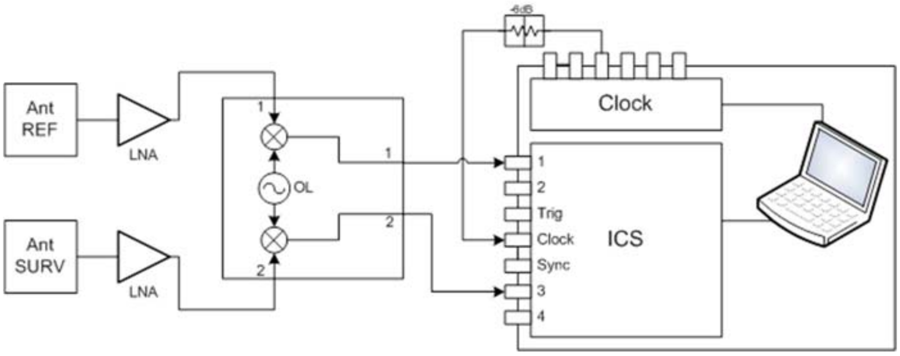

Figure 126 - WiFi super heterodyne receiver

The A/D conversion is performed by means of the ICS-554 PMC module (produced by GE Fanuc Embedded Systems). This module consists of four 14-bit ADCs sampling synchronously the properly amplified analogue signals from up to four input channels. A detailed description of this data capture module is reported in sub-section 4.4.3.

The analog components required for the RF Front-End realization and for data capture, have been selected through a market analysis. In most cases COTS components have been chosen. The principal selected devices and relative characteristics are:

- **WiFi access point** used as transmitter of opportunity is a DLINK DAP 1160.

Figure 127 – WiFi Access Point DLINK DAP 1160

The main features of this product are:

- selectable WiFi channel
- selectable output power
- selectable data-rate

- **Antennas DLINK ANT24-1200** used to perform the experiments.

Figure 128 – WiFi Antenna DLINK ANT24-1200

The main features of this product are:

- 2.4GHz Frequency Range
- 80 degrees beam-width over the horizontal plane
- 23 degrees of beam-width over the vertical plane
- 12 dBi of gain
- 15 dB of front-to-back ratio
- SMA-Female Connector, 3m Length Patch Cable with RP-SMA to RP-SMA supplied
- sizes 33×9.3×2.07 cm

- **RF3867 Low Noise Amplifier.** This component is a dual-channel low noise amplifier with high output IP3. The amplifier is self-biased from a single voltage supply with 50Ω input and output ports. The useful frequency range is from 700MHz to 3800MHz. A 0.8dB noise figure and 36dBm OIP3 performance is achieved with a 5V VDD, 180mA.

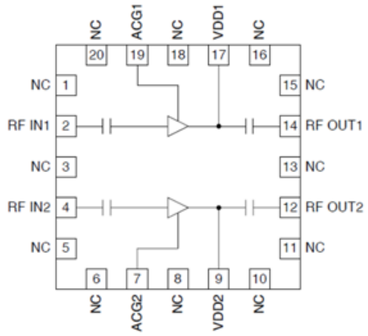

Figure 129 – RF 3867 Functional block diagram

The main features of this product are:

- Low Noise and High Intercept Point
- Adjustable Bias Current for Enhanced IP3
- Single 2.5V to 6.0V Power Supply
- 700MHz to 3800MHz Operation

- **RF2051 RF Mixers with integrated wideband RF PLL/VCO.** The RF2051 is a low power, high performance, wideband RF frequency conversion chip with integrated local oscillator (LO) generation and a pair of RF mixers. The RF synthesizer includes an integrated fractional-N phase locked loop with voltage controlled oscillators (VCOs) and dividers to produce a low-phase noise LO signal with a very fine frequency resolution. The LO generation blocks have been designed to continuously cover the frequency range from 300MHz to 2400MHz. The RF mixers are very broad band and operate from 30MHz to 2500MHz at the input and output, enabling both up and down conversion.

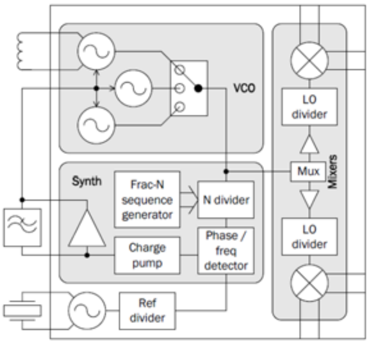

Figure 130 – RF 2051 Functional block diagram

The main features of this product are:

- 30MHz to 2.5GHz Frequency Range
- Fractional-N Synthesizer
- Very Fine Frequency Resolution 1.5Hz for 26MHz Reference
- Low Phase Noise VCO
- Two High-Linearity RF Mixers
- Mixer Input IP3 +18dBm

- **Data capture ICS-554B by GE Fanuc Embedded Systems**, widely described in sub-section 4.4.3.

5.3.2. WIFI HOMODYNE RECEIVER

The block diagram of the homodyne receiver is sketched in Figure 131.

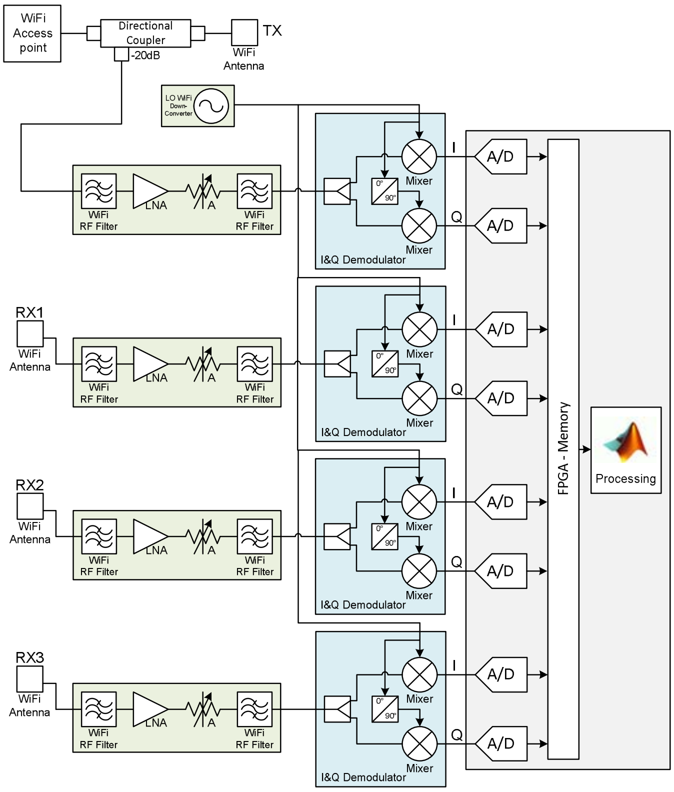

Figure 131. WiFi homodyne receiver

In this system, the down-conversion from RF to BB is performed by a I&Q quadrature demodulator that provides to the A/D converter the signal splitted into I and Q paths. The A/D conversion is performed by means of the X3-10M data-capture (by Innovative Integration). This is an XMC IO module featuring eight simultaneously sampled 16-bit, 25 MSPS A/D channels designed for high speed data acquisition applications. Data acquisition control, signal processing, buffering, and system interface functions are implemented in an on board Xilinx Spartan3A DSP FPGA.

A commercial WiFi access point was used as transmitter of opportunity. Its antenna output was connected to the transmitting antenna while a directional coupler was used to send a -20dB copy of the transmitted signal to the first receiving channel of a four-channel receiving system. This allowed to collect the reference signal. At the same time, three surveillance antennas were directly connected to three separate channels of the receiving system to collect the surveillance signals. The antennas used to perform the experiments are commercial WiFi antennas for indoor applications (by DLINK).

The analog components required for the RF Front-End realization and for data capture, have been selected through a market analysis. In most cases COTS components have been chosen. The principal selected devices and relative characteristics are:

- **WiFi access point**: see sub-section 5.3.1
- **Antennas DLINK ANT24-1200:** see sub-section 5.3.1
- **RF3867 Low Noise Amplifier:** see sub-section 5.3.1
- **ADL5382** is a broadband **quadrature I-Q demodulator** that covers an RF input frequency range from 700 MHz to 2.7 GHz. With a NF = 14 dB, IP1dB = 14.7 dBm, and IIP3 = 33.5 dBm at 900 MHz, the ADL5382 demodulator offers outstanding dynamic range suitable for the demanding infrastructure direct-conversion requirements. The differential RF inputs provide a well-behaved broadband input impedance of 50 Ω and are best driven from a 1:1 balun for optimum performance.

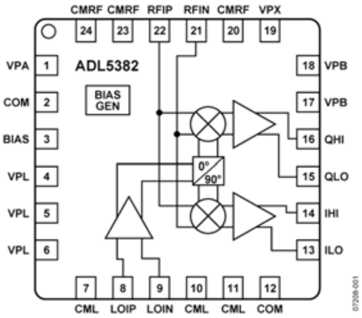

Figure 132 – ADL5382 Functional block diagram

The main features of this product are:

- 700 MHz to 2.7 GHz Quadrature Demodulator
- Input IP3 30.5 dBm @1900 MHz
- Input P1dB: 14.7 dBm @ 1900 MHz
- Noise figure (NF) 15.6 dB @ 1900 MHz
- LO drive 0 dBm
- Voltage conversion gain: ~4 dB
- Phase accuracy: ~0.2°
- Amplitude balance: ~0.05 dB
- Demodulation bandwidth: ~370 MHz
- Baseband I/Q drive: 2 V p-p into 200 Ω
  Single 5 V supply

- **ADL5380** is a broadband **quadrature I-Q demodulator** that covers an RF/IF input frequency range from 400 MHz to 6 GHz. With a NF = 10.9 dB, IP1dB = 11.6 dBm, and IIP3 = 29.7 dBm @ 900 MHz, the ADL5380 demodulator offers outstanding dynamic range suitable for the demanding infrastructure direct-conversion requirements. The differential RF inputs provide a well-behaved broadband input impedance of 50 Ω and are best driven from a 1:1 balun for optimum performance.

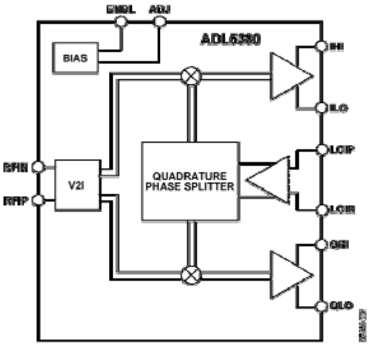

Figure 133 – ADL5380 Functional block diagram

The main features of this product are:

- 400 MHz to 6 GHz Quadrature Demodulator
- Input IP3 28 dBm @1900 MHz
- Input P1dB (IP1dB): 11 dBm @ 2700 MHz
- Noise figure (NF) : 12.3 dB @ 2700 MHz
- Voltage conversion gain: ~7 dB
- Quadrature demodulation accuracy @ 2700 MHz
- Phase accuracy: ~0.5°
- Amplitude balance: ~0.07 dB
- Demodulation bandwidth: ~390 MHz
- Baseband I/Q drive: 2 V p-p into 200 Ω
- Single 5 V supply

- **ADL8347** is a single chip, broadband **2.7GHz quadrature demodulator**. The part integrates 65dB linear-in-dB AGC, divided between RF input and at the baseband outputs following the mixers. The In-phase and Quadrature signals are brought out off chip for filtering prior to the final output amplifier stage. The final output amplifiers allow the user to adjust the DC common mode level to provide a direct interface into a dual channel I/Q ADC.

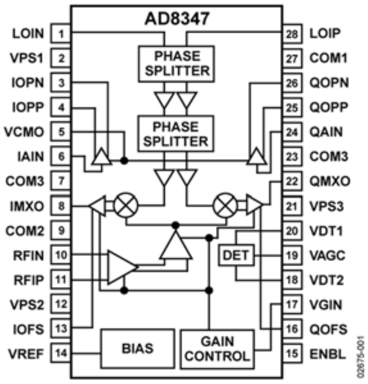

Figure 134 – AD8347 Functional block diagram

The main features of this product are:

- 0.8÷2.7 GHz Direct Conversion Quadrature Demodulator
- Integrated RF and baseband AGC amplifiers
- Quadrature phase accuracy 1° typ
- I/Q amplitude balance 0.3 dB typ
- Third-order intercept (IIP3) +11.5 dBm @ min gain
- Noise figure 11 dB @ max gain
- AGC range 69.5 dB
- Baseband level control circuit
- Low LO drive −8 dBm
- ADC-compatible I/Q outputs
- Single supply 2.7 V to 5.5 V

- **ADF4360-0** is a **fully integrated integer-N synthesizer** and voltage controlled oscillator (VCO). The ADF4360-0 is designed for a center frequency of 2600 MHz. In addition, a divide-by-2 option is available, whereby the user gets an RF output of between 1200 MHz and 1360 MHz. Control of all the on-chip registers is through a simple 3-wire interface. The device operates with a power supply ranging from 3.0 V to 3.6 V and can be powered down when not in use.

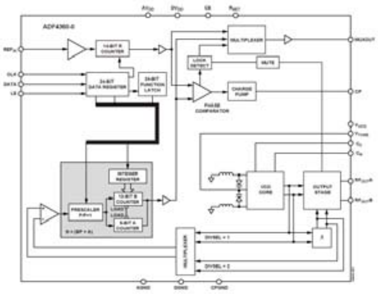

Figure 135 – ADF4360-0 Functional block diagram

The main features of this product are:

- Output frequency range: 2400 MHz to 2725 MHz
- Divide-by-2 output
- 3.0 V to 3.6 V power supply
- 1.8 V logic compatibility
- Integer-N synthesizer
- Programmable dual-modulus prescaler 8/9, 16/17, 32/33
- Programmable output power level
- 3-wire serial interface
- Analog and digital lock detect
- Hardware and software power-down mode

5.3.3. A/D CONVERTER – X3-10M

As previously mentioned, the A/D conversion is performed by means of the X3-10M XMC IO module (produced by Innovative integration). X3-10M (see

Figure 136) is a eight, 16-bit, 25 MSPS A/D channels module designed for high speed instrumentation and analysis. It has a nominal signal input impedance of 1 MOhms in differential standard.

Figure 136 – X3-10M

Flexible trigger methods include counted frames, software triggering and external triggering. The sample rate clock is either an external clock or on-board programmable PLL clock source.

Data acquisition control, signal processing, buffering, and system interface functions are implemented in a Xilinx Spartan3A DSP FPGA, 1.8M gate device. Two 512Kx32 memory devices are used for data buffering and FPGA computing memory.

The logic can be fully customized using VHDL and MATLAB using the Framework Logic toolset. The MATLAB BSP supports real-time hardware-in-the-loop development using the graphical, block diagram Simulink environment with Xilinx System Generator.

The PCI Express interface supports continuous data rates up to 180 MB/ s between the module and the host. A flexible data packet system implemented over the PCIe interface provides both high data rates to the host that is readily expandable for custom applications.

Figure 137 shows a simplified block diagram of the X3-10M board. The board uses eight 16-bit A/D Converters, Linear LTC2202.

The sampling clock and the trigger can be either internal or external. The internal AD clock is programmable up to 25 MHz.

The A/D can be operate in a number of different modes. In the continuous mode, data is continuously converted on all selected channels and supplied to the PCI Bus interface upon application of a trigger signal, until the acquisition is disabled. In capture mode, a fixed number of samples are acquired upon each application of the trigger. The number of samples acquired at each application of the trigger is programmable with a resolution of four samples per channel or less, up to the maximum capacity of the buffer.

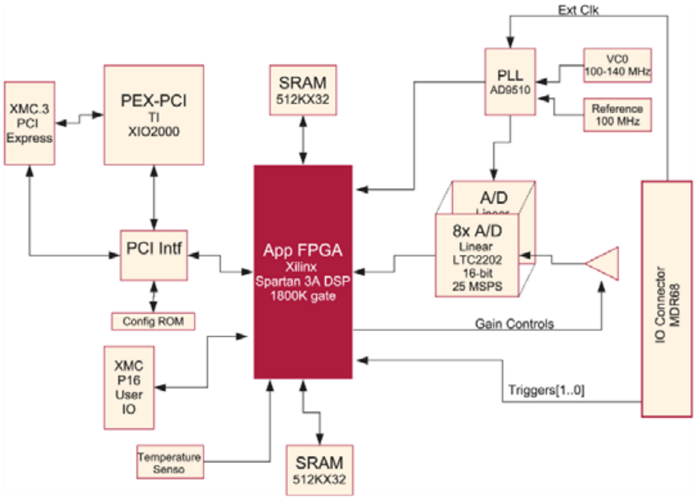

Figure 137 – X3-10M block diagram

X3-10M technical specifications are summarized in the following:

- 8 simultaneously sampling 16-bit, 25 MSPS A/Ds
- Programmable input: +/-2V, +/-1V, +/-0.4V, +/-0.1V
- High impedance, differential inputs
- Xilinx Spartan3A DSP, 1.8M gate FPGA
- 4MB SRAM
- Programmable Low Jitter PLL time-base
- Framed, software or external triggering
- Log acquisition timing and events
- 44 bits digital IO on P16
- Power Management features
- XMC Module (75x150 mm)
- PCI Express (VITA 42.3)

5.4. TESTS AND CONTROLLED EXPERIMENTS

Different tests have been performed in order to verify the performance of the conceived WiFi-based PBR receiver. The tests are based on the evaluation of the disturbance cancellation and detection capability of the system. Two channel test benches have been realized with different I&Q demodulator in order to select the best performing component for the system. In the following Sub-Sections are reported the test bench configuration, a Table that summarize the system parameter set and measured (SNR and cancellation values), and the Auto Correlation or the 2D correlation obtained.

Specifically, the tests regards:

- 2D Auto Correlation with ADL5382 I&Q Demodulator
- 2D Cross Correlation with ADL5382 I&Q Demodulator
- 2D Auto Correlation with ADL5380 I&Q Demodulator
- 2D Auto Correlation with AD8347 I&Q Demodulator

The component selected for the realization of the multiple channel receiver for WiFi signals is the ADL5380.

5.4.1. 2D AUTO CORRELATION – ADL5382

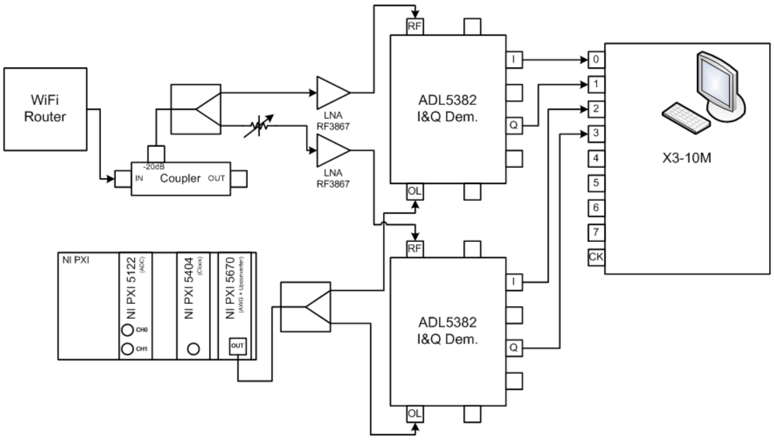

Figure 138. ADL5382 Auto Correlation test bench

Test	Power [dBm]	Att [dB]	P_ch1 [dBm]	P_ch2 [dBm]	SNR_ch1 [dB]	SNR_ch2 [dB]	Canc teo [dB]	Canc media [dB]	Diff Canc [dB]
1	7	20	-9,8	-9,9	54,1	54,3	51,2	39,1	12,1
2	7	29	-9,7	-19,6	54,1	44,5	44,0	35,8	8,3
3	7	38	-9,9	-28,3	54,0	35,9	35,8	33,7	2,1
4	7	47	-9,8	-39,5	54,0	24,6	24,6	24,4	0,1

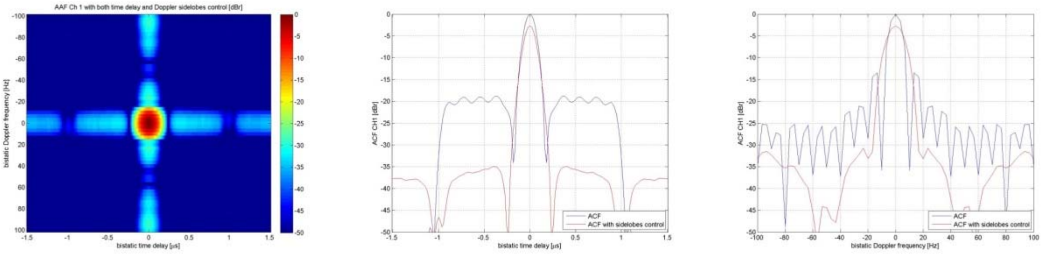

(a) (b) (c)

Figure 139 – Test 1: ACF (a), range cut (b), velocity cut (c)

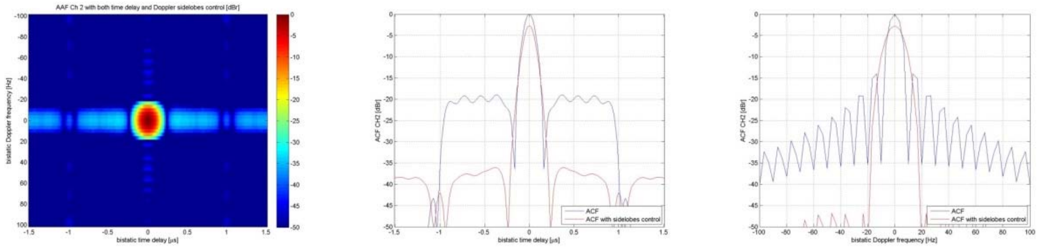

(a) (b) (c)

Figure 140 – Test 2: ACF (a), range cut (b), velocity cut (c)

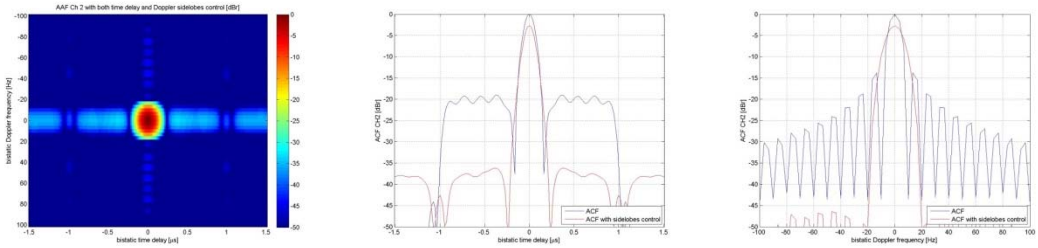

(a) (b) (c)

Figure 141 – Test 3: ACF (a), range cut (b), velocity cut (c)

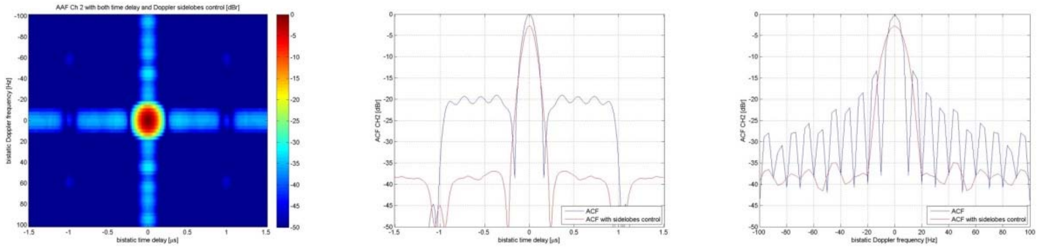

(a) (b) (c)

Figure 142 – Test 4: ACF (a), range cut (b), velocity cut (c)

5.4.2. 2D CROSS CORRELATION – ADL5382

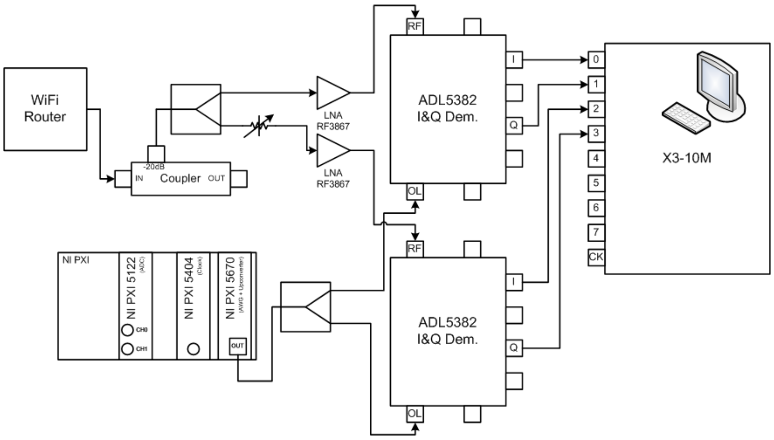

Figure 143. ADL5382 Cross Correlation test bench

Test	Power [dBm]	Att [dB]	P_ch1 [dBm]	P_ch2 [dBm]	SNR_ch1 [dB]	SNR_ch2 [dB]	Canc teo [dB]	Canc media [dB]	Diff Canc [dB]
5	7	20	-9,8	-9,9	54,1	54,3	51,2	39,1	12,1
6	7	29	-9,7	-19,6	54,1	44,5	44,0	35,8	8,3
7	7	38	-9,9	-28,3	54,0	35,9	35,8	33,7	2,1
8	7	47	-9,8	-39,5	54,0	24,6	24,6	24,4	0,1

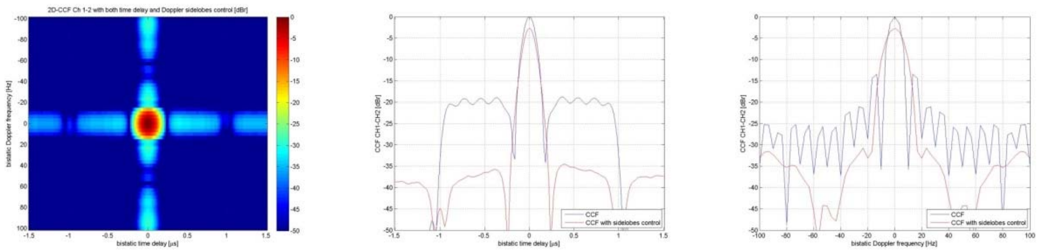

(a) (b) (c)

Figure 144 – Test 5: CCF (a), range cut (b), velocity cut (c)

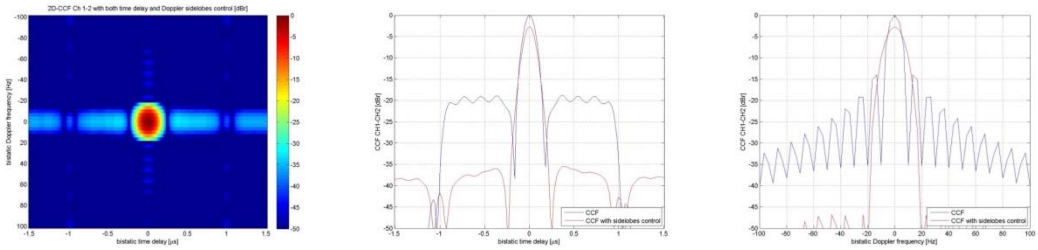

(a) (b) (c)

Figure 145 – Test 6: CCF (a), range cut (b), velocity cut (c)

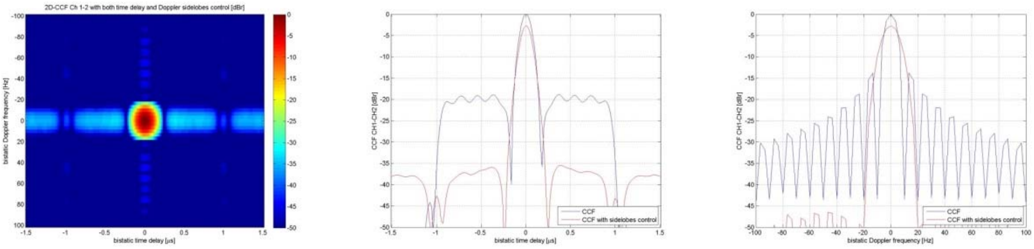

(a) (b) (c)

Figure 146 – Test 7: CCF (a), range cut (b), velocity cut (c)

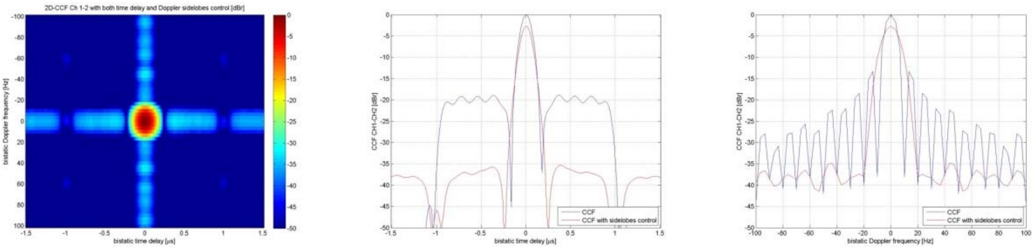

(a) (b) (c)

Figure 147 – Test 8: CCF (a), range cut (b), velocity cut (c)

5.4.3. 2D AUTO CORRELATION – ADL5380

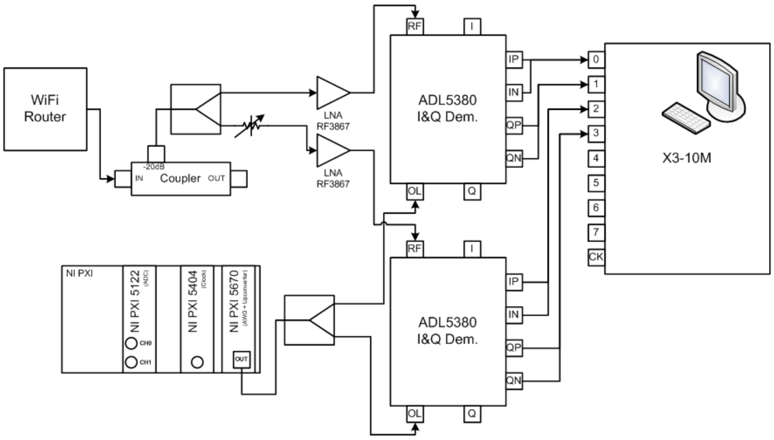

Figure 148. ADL5380 Auto Correlation test bench

	Power [dBm]	Att [dB]	P_ch1 [dBm]	P_ch2 [dBm]	SNR_ch1 [dB]	SNR_ch2 [dB]	Canc teo [dB]	Canc media [dB]	Diff Canc [dB]
9	7	20	5,3	5,9	59,0	59,9	56,4	25,7	30,7
10	7	29	5,6	-3,7	59,4	50,3	49,8	22,9	27,0
11	7	38	5,6	-13,9	59,3	40,2	40,1	23,6	16,5
12	7	47	5,6	-22,0	59,3	32,1	32,1	22,7	9,4

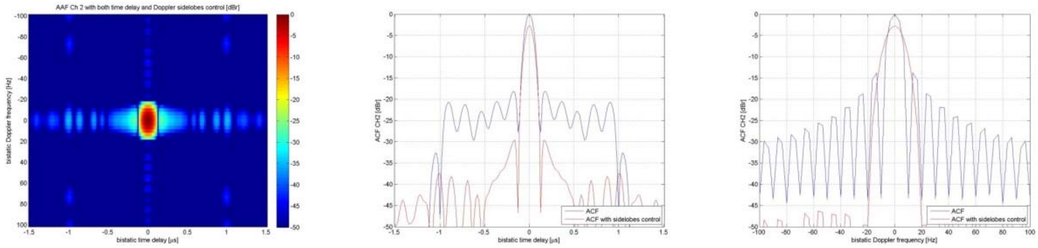

(a) (b) (c)

Figure 149 – Test 9: ACF (a), range cut (b), velocity cut (c)

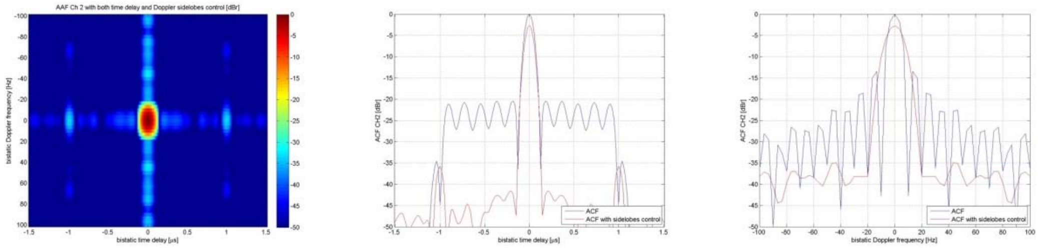

(a) (b) (c)

Figure 150 – Test 10: ACF (a), range cut (b), velocity cut (c)

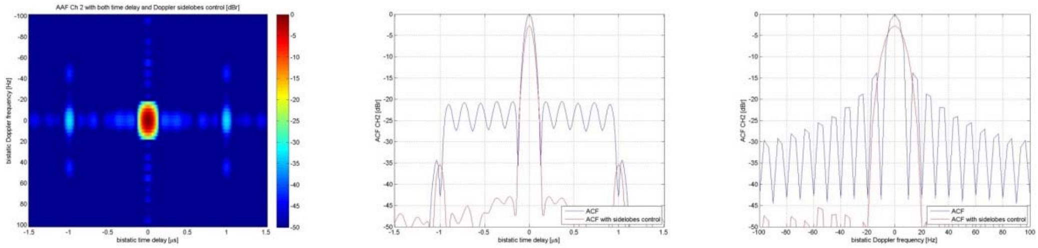

(a) (b) (c)

Figure 151 – Test 11: ACF (a), range cut (b), velocity cut (c)

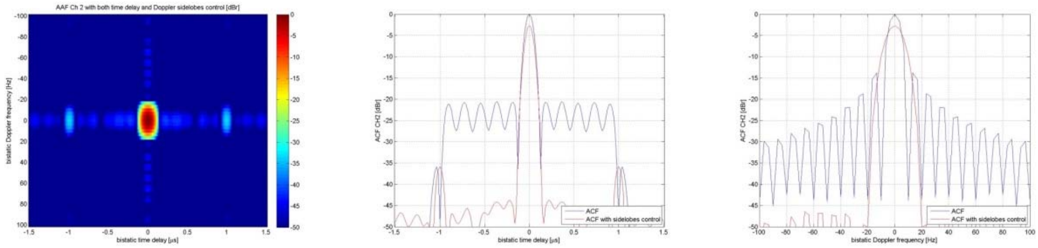

(a) (b) (c)

Figure 152 – Test 12: ACF (a), range cut (b), velocity cut (c)

5.4.4. 2D AUTO CORRELATION – AD8347

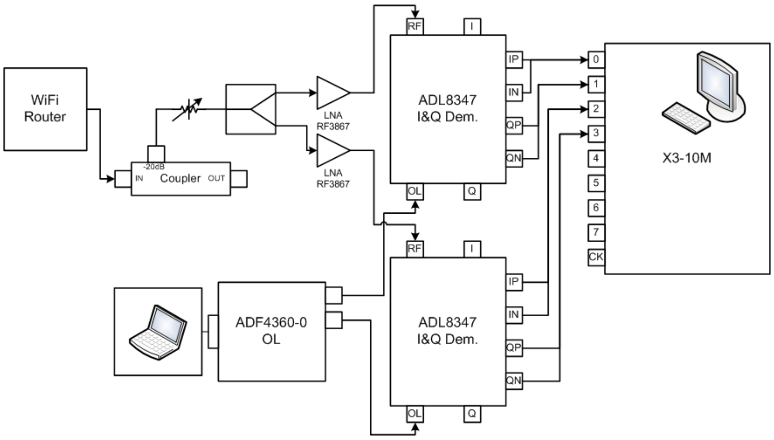

Figure 153. AD8347 Auto Correlation test bench

Test	Power [dBm]	Att [dB]	P_ch1 [dBm]	P_ch2 [dBm]	SNR_ch1 [dB]	SNR_ch2 [dB]	Canc teo [dB]	Canc media [dB]	Diff Canc [dB]
13	7	20	3,9	4,6	30,6	31,3	27,9	21,3	6,6
14	7	29	3,0	4,1	29,9	30,8	27,3	23,8	3,5
15	7	38	2,6	3,7	29,4	30,4	26,9	23,8	3,1
16	7	47	2,3	3,4	28,9	30,0	26,4	23,7	2,8

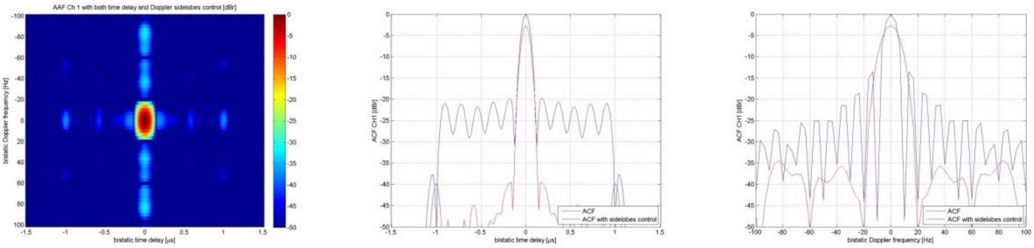

(a) (b) (c)

Figure 154 – Test 13: ACF (a), range cut (b), velocity cut (c)

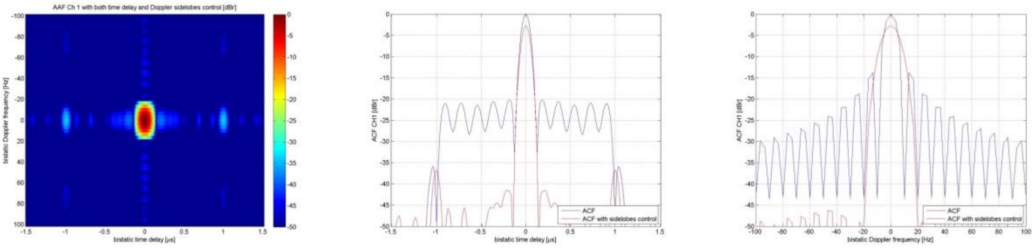

(a) (b) (c)

Figure 155 – Test 14: ACF (a), range cut (b), velocity cut (c)

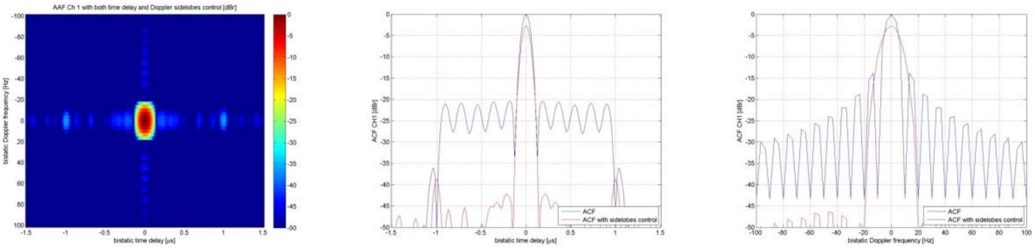

(a) (b) (c)

Figure 156 – Test 15: ACF (a), range cut (b), velocity cut (c)

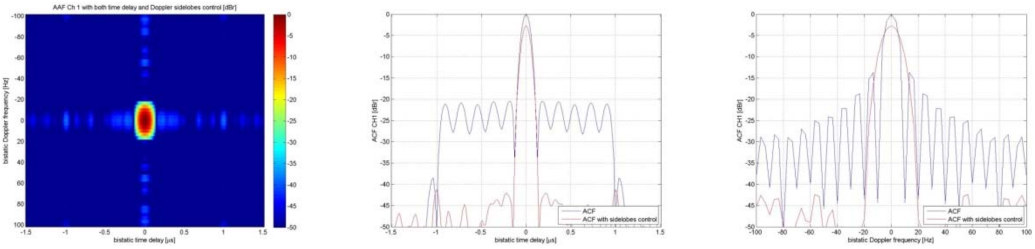

(a) (b) (c)

Figure 157 – Test 16: ACF (a), range cut (b), velocity cut (c)

5.5. ACQUISITION CAMPAIGNS

Different experimental tests have been performed in two different sets that are described in the following. The first scenario was an outdoor one while the latter was an indoor one.

5.5.1. INDOOR SCENARIO

The indoor scenario chosen for the demonstration of the WiFi-based passive radar sensor is shown in **Figure 164**. It consists of a wide exhibition hall of the "Nuova Fiera di Roma" (Rome). Particularly, the sizes of the exhibition hall are approximately 77 meters of width and 120 meters of length. It is assumed that the co-ordinates of the transmitter of opportunity location are (0,0) m.

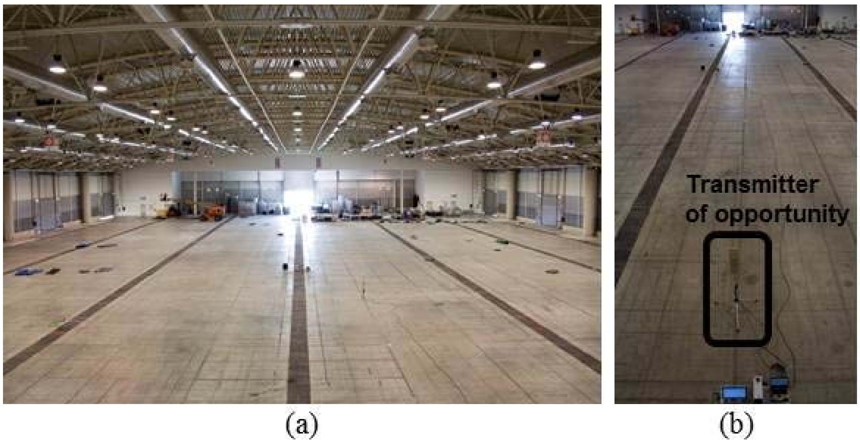

Figure 158. Indoor scenario for the passive radar demonstration

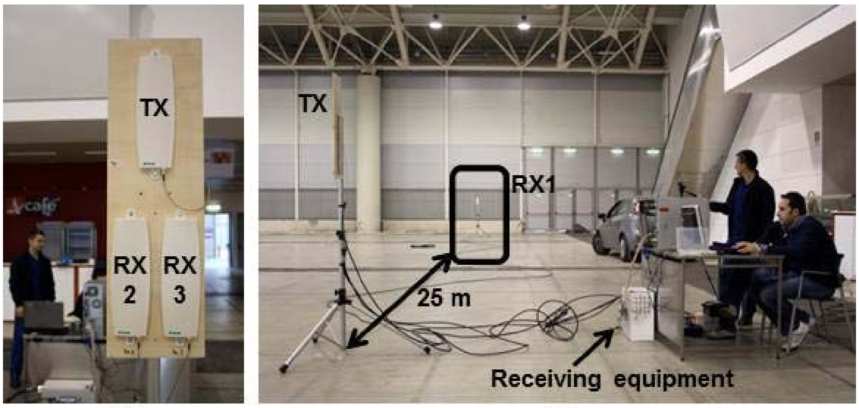

(a) (b)

Figure 159. Antennas configuration for the indoor passive radar demonstration

Three receiving antennas (RX) were used to perform the experiments. Two receiving antennas, RX 2 and RX 3, were placed a few tens of centimetres below the TX, both in a quasi mono-static configuration with the transmitter of opportunity (see Figure 159a). Moreover, the relative distance between RX 2 and RX 3 was set in order to enable target's DoA estimation by exploiting an interferometric approach. Finally, receiver RX 1 was located in a bi-static configuration with respect to TX (see Figure 159b). The baseline was set to 25 m so that RX1 is located at (25,0) m.

5.5.2. OUTDOOR SCENARIO

Different experimental tests have been performed in an outdoor scenario sketched in Figure 160. It consists of a wide parking area located in Cisterna di Latina (near Rome).

A single transmitter of opportunity (TX) and 3 receiving sensors (RX) were used to perform the experiments. In particular, the TX was located at the point represented with the coordinates (0,0) m while the first receiver (RX 1) was located in (25,0) m in a bi-static configuration with respect to TX. RX 2 and RX 3 were placed a few tens of centimeters below the TX, both in a quasi mono-static configuration with the transmitter of opportunity. In particular, their relative distance was set in order to enable target's Direction of Arrival (DoA) estimation by exploiting an interferometric approach.

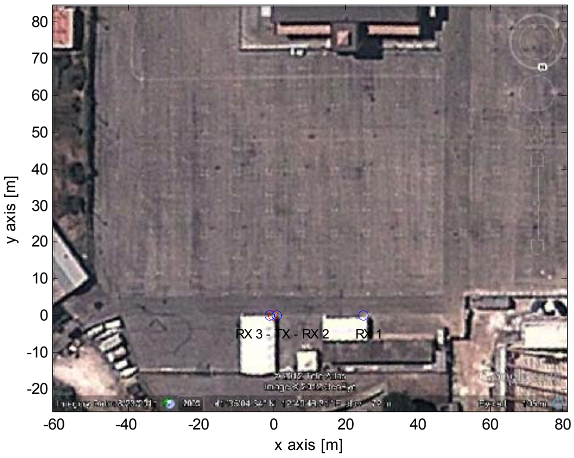

Figure 160 - Outdoor scenario for the passive radar demonstrations

Two experimental tests have been performed in the considered scenario:

in the first test, a single human target moved in front of the transmitter of opportunity toward the antennas location (see blue arrow in Figure 5);

in the second test, two human targets moved simultaneously in the parking area. As is depicted in Figure 5, both the target started moving at the same time from the same location (approximately the point (0,35) m). They moved very close each other for a while (approximately, since the point (0,15) m has been reached), then one of them (the red one in Figure 5) changed his walking direction toward point (10,5) m.

Figure 161a focuses on the displacement of TX, RX2 and RX3. As is apparent, RX 2 and RX 3 were placed very close each other. In particular, their relative distance was set in order to enable target's Direction of Arrival (DoA) estimation by exploiting an interferometric approach. Finally, Figure 161b shows the dislocation of the bi-static receiver RX1.

(a) (b)

Figure 161 – Antennas configuration for the outdoor passive radar demonstration

5.5.3. WIFI-BASED PBR PROCESSING SCHEME

The basic WiFi-based PBR processing scheme is depicted in Figure 162.

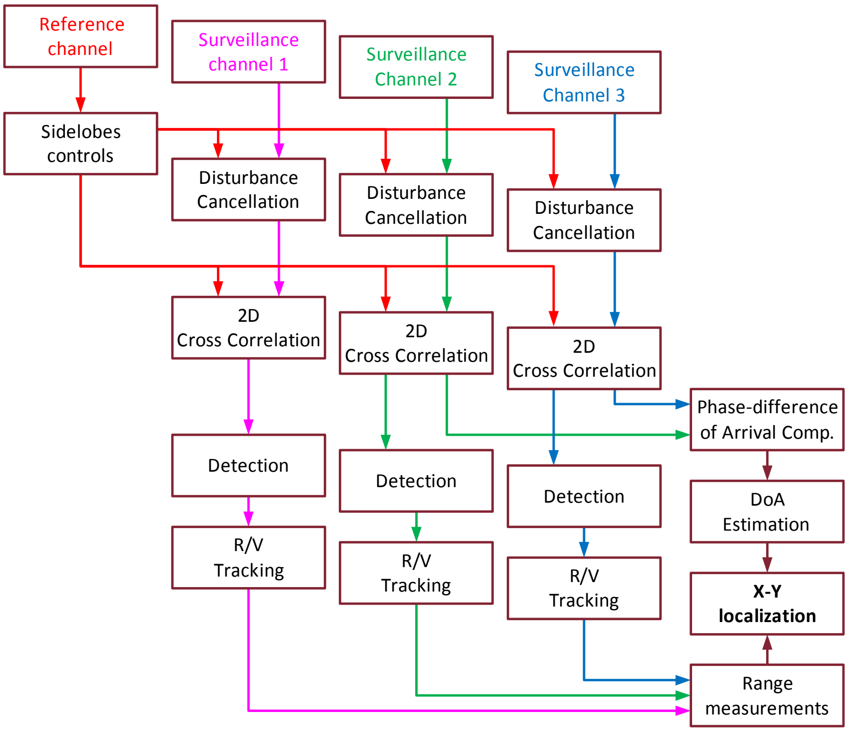

Figure 162. WiFi-based PBR processing scheme

The exploited waveform of opportunity is defined by IEEE 802.11 Standards, [25]. In Europe the WiFi transmission frequencies are located in the 2.4 GHz spectrum (between 2.412 and 2.472 GHz). Specifically, the Direct Sequence Spread Spectrum (DSSS) modulation is used with an instantaneous bandwidth of 11 MHz which results in a range resolution of about 15 m. Morover, a velocity resolution of 0.125 m/s can be obtained with a coherent integration time of 0.5 s. The surveillance signal contains undesired scaled and delayed replicas of the reference signal due to the reflections from the stationary background of the scene, which can mask the target echoes. The Extensive Cancellation Algorithm (ECA) presented in [7] is therefore applied to remove such contributions. After the cancellation stage, the range compression is performed on a pulse-by-pulse basis through a cross-correlation between the reference signal and the surveillance signal. The target detection process is based on the evaluation of the two-dimensional Cross-Correlation Function (2D-CCF), i.e. the range-Doppler map.

As discussed in [27], the WiFi signal Ambiguity Function shows high sidelobes structures which may strongly affect the target detection capabilities. To reduce such effects, the range sidelobes reduction techniques proposed in [28]-[29] are preliminarily applied to the signal collected at the reference channel.

Finally, X-Y target localization can be estimated, [30]. A simple and effective way to accomplish this result is based on the exploitation of target range measures only. In this case, at least two bistatic couples are needed to simultaneously collect two different range measures of the target in the scene. More generally, if N range measures are collected, the target positioning can be performed through an iterative algorithm based on solving the system of N equations and two unknowns. Alternatively, by exploiting a couple of properly displaced surveillance antennas, an interferometric approach can be used to effectively estimate the target echo Direction of Arrival (DoA) with the WiFi-based passive radar.

5.6. EXPERIMENTAL RESULTS

This sub-section reports the results for the WiFi-based passive radar. In particular, two experimental results are shown for the indoor scenario and two test have been performed in the outdoor one.

5.6.1. RESULTS FOR THE INDOOR SCENARIO

Different experimental tests have been performed in the considered scenarios.

In the first one, a man moves toward the transmitter of opportunity location with constant velocity and angle of arrival approximately equal to zero degrees (see Figure 163a).

After the application of the processing steps described in Sub-section 5.5.3 (see Figure 162), different kinds of detections have been obtained, reported in Figure 164:

- false alarms, which might be easily discarded by a tracking algorithm
- Doppler ambiguities, due to the WiFi pulses repetition period that is equivalent to radar pulse repetition time. Such detections might be easily discarded by a tracking algorithm
- target detections
- multipath effects, which might be caused by reflections of the target echo over surrounding buildings or obstacles (e.g. metallic fence, etc.).

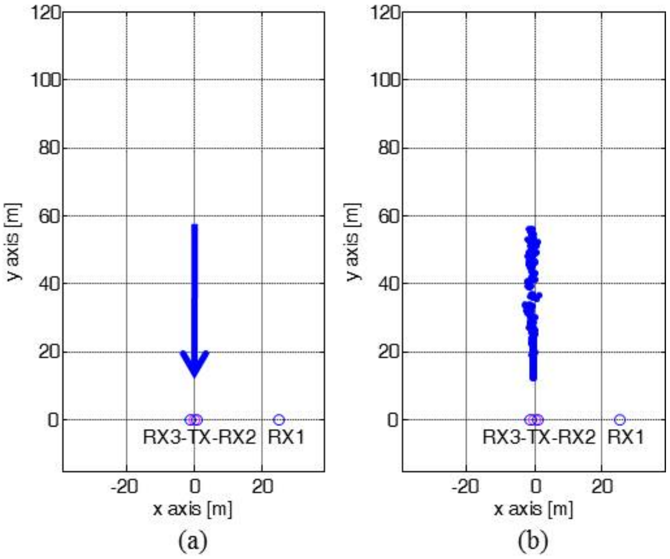

Figure 163. Test 1: (a) geometry, (b) localization results

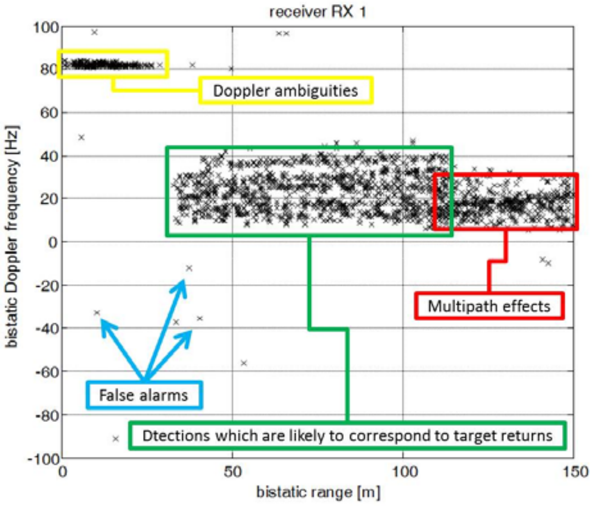

Figure 164. Detections over the range/Doppler frequency bi-static planes for a simple human target detection experiment

As is apparent, wide Doppler spectrum is experienced in the case of human targets detection experiments. In fact, different parts of the human body (above all, torso, head, arms, upper and lower legs and feet) move with different velocities which results in a row of Doppler side-peaks around the main target detection point. For the purpose of the analysis here reported (target detection and localization), the Doppler frequency side-peaks might prevent the correctness of the detection algorithm and thus reduce the localization accuracy. In order to prevent such effects, the Doppler side-peaks have to be automatically identified and discarded. To accomplish with this result, a simple linear filtering strategy (based on the Kalman’s algorithm) is considered as follows:

- the plots (range/Doppler/DoA measures) collected at the generic time-step are used to predict the subsequent system state
- at the next time-step, among all the available plots suitable for association, the closest one to the prediction is selected and the algorithm is reiterated.
- This should allow to discard the Doppler side-peaks which, being related to parts of human body whose velocity changes fast, are characterized by a fast-varying effect.

Figure 165 shows with the green circle markers the selected plots for the target detection experiment depicted in Figure 163a. As is apparent, the selected plots show a quite stable Doppler frequency state without strong interferences with the Doppler side-peaks.

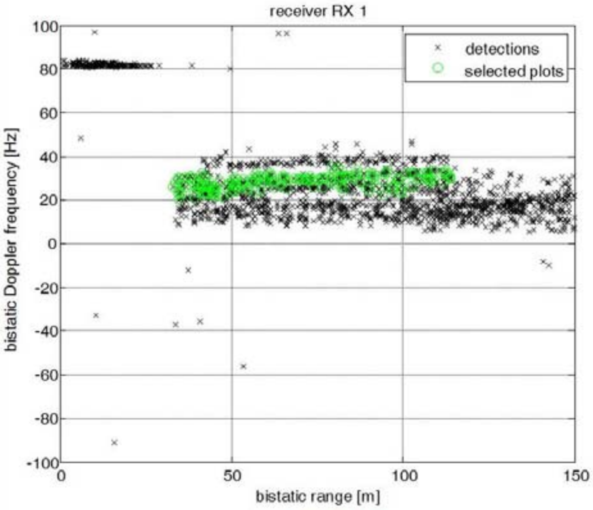

Figure 165. Selected plots over the range/Doppler frequency bi-static planes for a simple human target detection experiment

The selected plots provide the target bi-static range and Doppler frequency measurements reported, respectively, in Figure 166 and Figure 167 (blue curve for the bi-static receiver RX 1 and red curve for the quasi mono-static receiver RX 2). As is apparent, the collected measures are well in line with the test geometry (see Figure 163a). In fact, while the target moves, both the bi-static ranges decrease with the bi-static range of RX 2 decreasing faster. Similarly, when the target is far from the antennas location, the measured Doppler frequencies are almost the same. In contrast, when the target is going to approach the transmitter location, the Doppler frequency measured by RX 1 decreases faster.

Moreover, the phase-difference between RX 2 and RX 3 at the target detection point can be used to estimate the target's echo DoA. The result is shown in Figure 168.

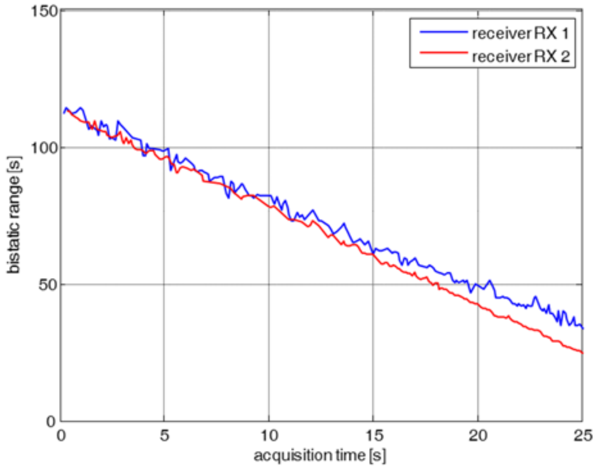

Figure 166. Bi-static range measurements for a simple human target detection experiment

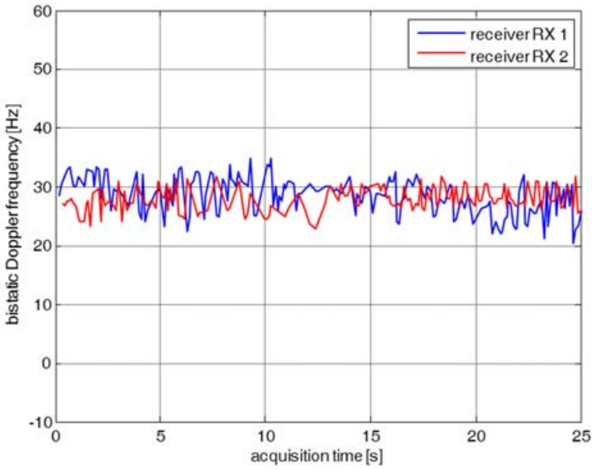

Figure 167. Doppler frequency measurements for a simple human target detection experiment

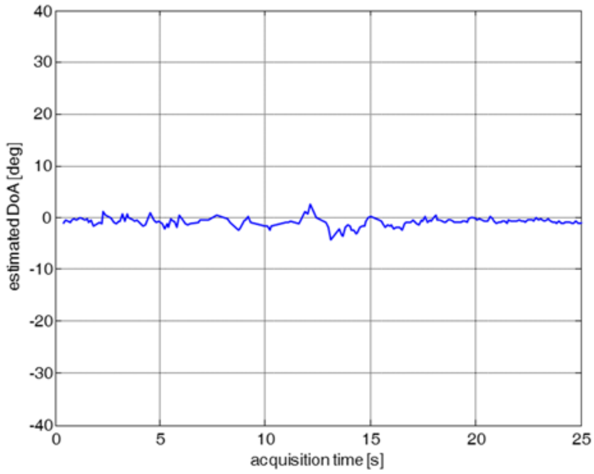

Figure 168. Estimated target's echo angle of arrival for a simple human target detection experiment

As is apparent, the estimated DoA is approximately equal to zero, well in line with the test geometry (see Figure 163a).

Once the range/Doppler frequency/DoA measures are collected, target localization might be performed and the obtained sequence of localizations, reported in Figure 163b, nicely match with the test geometry with only small deviations which are mainly due to the range/DoA estimation accuracies.

The second indoor experiment has been performed with two human targets. They start walking very close each other approximately from point (8,60) m. When they reach point (0,40) m, both of them change their walking direction. In particular, as depicted in Figure 169a, one of them moves toward the transmitter of opportunity, while the other moves along the opposite direction.

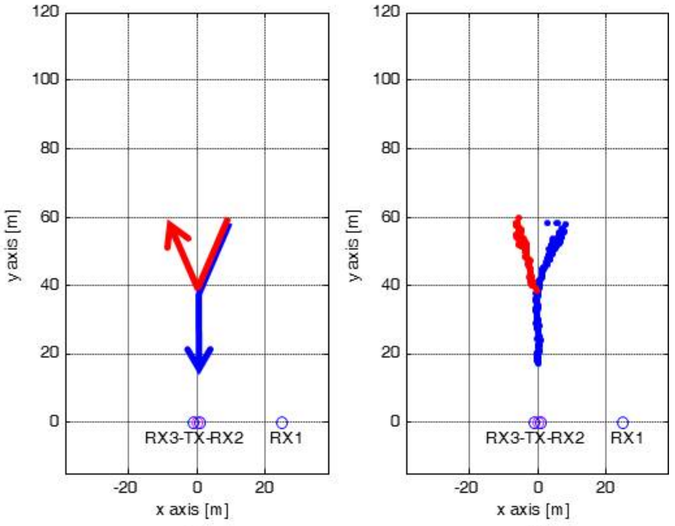

(a) (b)

Figure 169. Test 2: (a) geometry, (b) localization results

After the application of the processing steps described for the test 1, the sequence of localizations shown in Figure 169b is obtained. As is apparent, till the targets move very close each other, just a single target is detected and localized. In fact, in such case both the targets appear at the same range/Doppler frequency location, thus preventing the possibility of resolving them. When they move along different paths, their respective detections have different Doppler frequency values thus making it possible to resolve and localize both of them.

5.6.2. RESULTS FOR THE OUTDOOR SCENARIO

The first outdoor experimental test has been performed with a single human target. In particular, a man moved in front of the transmitter of opportunity toward the antennas location (see Figure 170 left). The sequence of the obtained localizations is reported in Figure 170 (right).

As is apparent, the obtained target's sequence of localizations nicely meets the test's ground truth. The small deviations arising from the measurement accuracies might be significantly smoothed by the sub-sequent tracking algorithm.

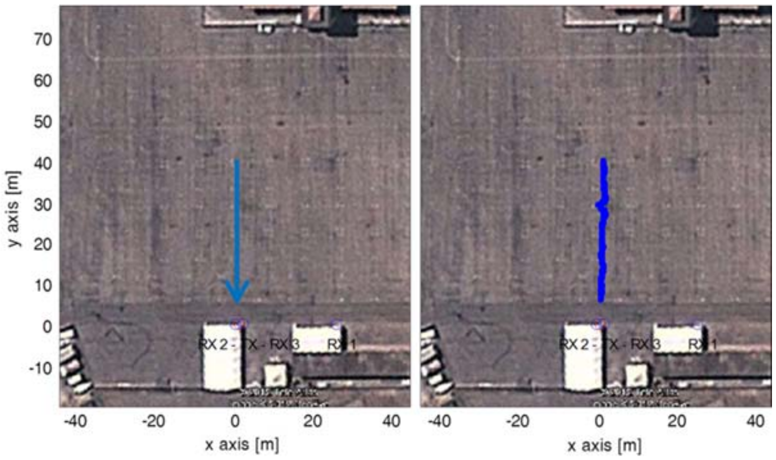

Figure 170. First outdoor demonstration. (a) ground truth, (b) sequence of localizations.

The second outdoor experiment has been performed with two human targets moving simultaneously in the parking area. As is depicted in Figure 171 (left), both the target started moving at the same time from the same location (approximately the point (0,35) m). They moved very close each other for a while (approximately, since the point (0,15) m has been reached) till one of them (the red one in Figure 171 left) changed his walking direction toward point (10,5) m.

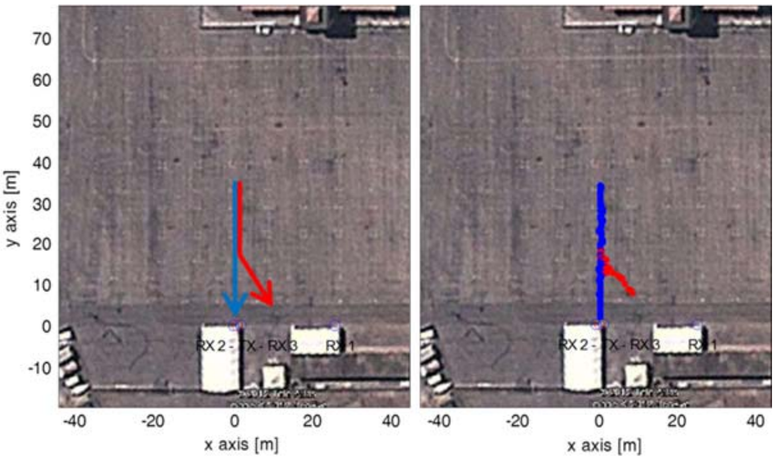

Figure 171. Second outdoor demonstration. (a) ground truth, (b) sequence of localizations.

The sequence of the obtained localizations for the second outdoor experiment is thus reported in Figure 171 (right). As is apparent, till the targets moved very close each other, just a single target has been detected and localized. In fact, in such case both the targets appear at the same range/Doppler frequency location thus preventing the possibility of resolving them. On the brightside, when the second target changes its walking direction, it appears at a different Doppler frequency location on both the bi-static range/Doppler frequency planes thus making it possible to resolve the targets and correctly localize both of them.

5.7. HIGH RESOLUTION CROSS-RANGE PROFILING VIA ISAR PROCESSING

Following the consideration that the resolution of the WiFi-based PBR is typically limited to tenths of meters in the range direction, due to the limited frequency bandwidth occupied by the available signals (e.g. 11÷18m for WiFi depending on the adopted modulation), it is of great interest the possibility to obtain high resolution images of the observed targets. In principle, for targets with a motion component in the cross-range direction, it is possible to achieve a higher (cross-range) resolution by applying Inverse Synthetic Aperture Radar (ISAR) processing schemes.

In this Section we introduce an appropriate processing scheme for the WiFi-based passive radar signals that allows us to achieve high resolution cross-range profiles of moving targets. The proposed approach is also demonstrated showing an experimental case study.

5.7.1. ISAR PROCESSING SCHEME

The ISAR processing scheme is depicted in Figure 172. As apparent, the ISAR processing exploited to provide the high cross-range resolution must follow the typical stages required to obtain an effective WiFi-based passive radar.

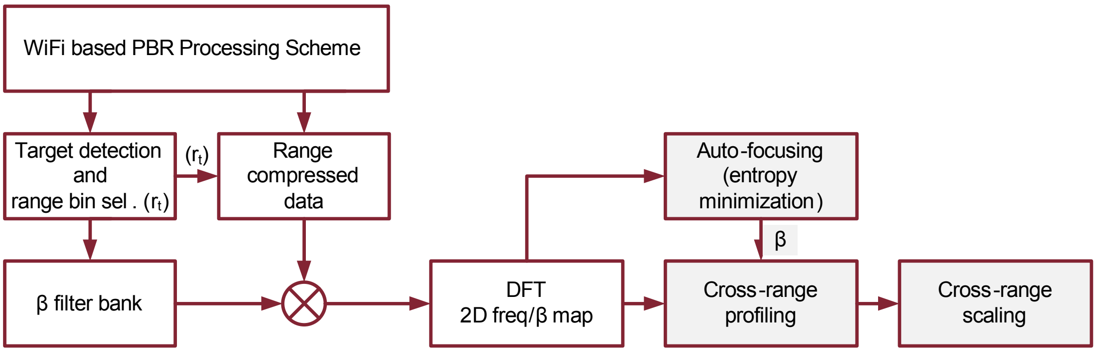

Figure 172. Sketch of the ISAR processing scheme

As it has been discussed in [31], the ISAR processing is applied against the compressed data at the selected range bin of the target. In particular, since the target motion parameters are unknown by the receiver, as in the typical ISAR case, a first autofocusing stage is needed. Such autofocus process can be obtained by applying a quadratic phase compensation to the received signal characterized by a parameter β spanning an appropriate range of possible physical values ([31]). The estimated value β_m is selected as the one providing the absolute minimum of the entropy cost function evaluated as in [32]. Based on the estimated version β_m, the reference chirp is available for cross-range matched filtering, which can be performed by convolution. Once the R_0 is known from the cross-range compressed target, and the estimate of β_m is known, also the velocity can be obtained as $v = (\beta_m R_0)^{1/2}$, which is directly used to scale the output of the convolution, mapping times into cross-range distances ([31]).

5.7.2. ACQUISITION SCENARIO

The experimental setup is depicted in Figure 173. Two identical cars move from point A to point B with a velocity of about 4.5 m/s and a fixed displacement. Each car has a length of about 4 m. A quasi-monostatic configuration was adopted for the two antennas which were mounted one on top of the other. The router was configured to transmit in channel 1 of the WiFi band (2,412 MHz).

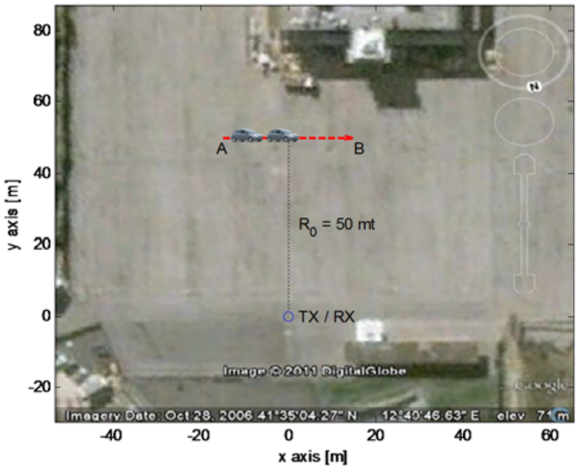

Figure 173. Cross-range profiling test.

5.7.3. DISTURBANCE REMOVAL AND EXPERIMENTAL RESULTS

The impact of the disturbance cancellation stage, both on the target motion parameter estimation and the target profiling stages, has been analyzed with reference to a simulated scenario ([33]) and to the experimental setup described in the previous Sub-section.

Figure 174 compares the Doppler spectrum of the collected data in absence (blue curve) or in presence (black curve) of the cancellation stage performed through the conventional ECA-B algorithm, [34]. Moreover, the spectrum obtained with a modified version of the ECA-B algorithm is shown in red.

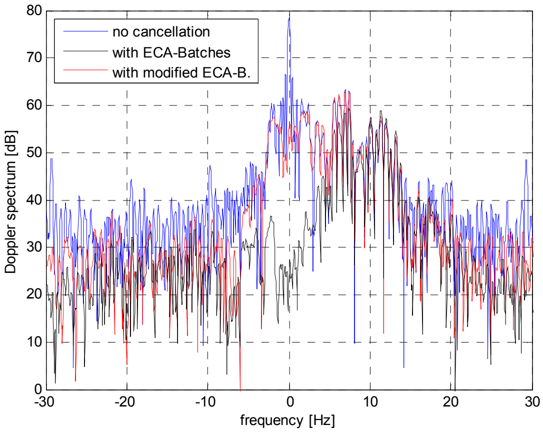

Figure 174. Cancelled signal Doppler spectrum

Without cancellation (see the blue curve) the obtained Doppler spectrum shows both a strong zero-Doppler contribution and an useful targets component (visible with the blue spread around the main peak). The presence of the strong stationary contribution prevents the correctness of the autofocus stage. After the application of the ECA-B algorithm, (see the black curve) the disturbance removal stage has effectively removed the strong stationary contribution with a clutter attenuation greater than 40 dB. However, the filter cancellation notch in the Doppler dimension has also reduced the target contributions at low Doppler frequencies. This might degrade the effectiveness of the ISAR processing which instead needs the entire Doppler frequency history of the target. The results obtained with the modified version of the ECA-B algorithm show the improvement of this solution which is able to preserve the signal contribution at low Doppler frequencies with respect to the ECA-B algorithm.

Figure 175 shows a cross-range profile of the two targets considered in the experiment.

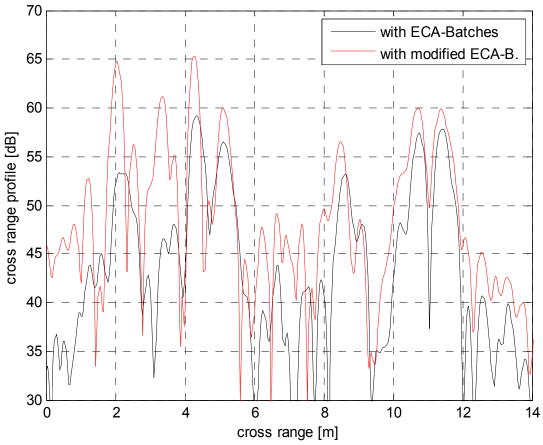

Figure 175. Cross-range profiles for the considered experiment

As is apparent, two similar patterns of scatters are clearly visible, that correspond to the main scattering centers of the two identical cars used for the considered experiment. A cross-range resolution of about 29 cm is obtained.

Moreover it is easy to notice that, for this particular experiment, the modified ECA-B cancellation approach proposed in [34] allows to significantly preserve the target SNR during the disturbance removal stage. Thus the proposed technique allowed us both to remove the undesired contributions from the surveillance signal and to correctly obtain a cross-range profile of the moving targets.

5.8. CONCLUSIONS

In this Section, an overview of the ATOM project has been presented. A passive radar system based on WiFi transmissions has been introduced. In order to clarify the role and the performance of this sensor, the WiFi-based PBR has been described in detail. Specifically, the sensor architecture, its processing scheme, and some examples of detection and localization results (in real indoor scenarios) have been illustrated. In particular, it has been verified that it is possible to correctly estimate the human targets' range, Doppler frequency and DoA as well as properly localize them in indoor and outdoor scenarios. Also, targets moving along the same path very close each other are not resolved by the passive radar, since they appear at the same range/Doppler frequency location while targets moving along different paths can be resolved and correctly localized even if they pass very close each other at a certain location.

Finally, an overview of the techniques introduced to increase the cross range resolution via ISAR processing has been proposed.

6. DVB-SH-BASED PBR

6.1. INTRODUCTION

In this section, a study of a receiver for DVB-SH signals is reported. The DVB-SH is introduced for television transmissions from satellite platforms to mobile devices. The potentialities of a passive radar based on geostationary satellite signals of opportunity are correlated to the wide coverage of the system and its availability. On the contrary, the main drawback is the low power level of the communication signal. In the following Sub-Sections, the dimensioning of the receiving system is reported, with specific reference to the DVB-SH test transmission provided by Eutelsat 10A platform.

6.2. DVB-SH-BASED PBR GENERAL REQUIREMENTS

In order to realize a passive radar based on a satellite illuminator of opportunity, an extensive analysis of the characteristics of existing satellite transmissions has been carried out: the Equivalent Isotropic Radiated Power (EIRP), the single communication channel bandwidth used and the available time for signal integration have been considered [35]. The satellite selected as illuminator of opportunity for the passive system design is EUTELSAT 10A (called Eutelsat W2A). The

EUTELSAT 10A is located at 10 degrees East, one of Eutelsat's long-standing orbital locations and a key position for data and professional video networks. The EUTELSAT 10A satellite features a major innovation by carrying an S-band payload enabling delivery, for the first time, of mobile multimedia broadcast services according to the standard DVB-SH (mobile TV, digital radio…) directly onto user mobile terminals and vehicles in Europe. The Ku-band payload on EUTELSAT 10A offers an enhanced Widebeam footprint serving Europe, North Africa and the Middle East. A second Ku-band beam serves southern Africa and Indian Ocean islands, and enables connectivity between Africa and Europe. The C-band payload provides pan-African coverage, extending to India and parts of Asia as well as Latin America, for broadband and telecommunications services.

The main characteristics of EUTELSAT 10A are summarized in Table 22.

Platform	Thales Alenia Space Spacebus 4000-C4
Quote	35840 Km
Latitude	0.01° N
Longitude	10.05 ° E
Coverage	lat:33.5°N - 48.1°N lon:5.3°E – 19.9°E
Launch date	2009, April 3rd
Power available	15400 W
EIRP	72 dBW
Uplink	n.a.
Downlink DVB-SH	Bandwidth: 2170-2200 MHz 6 channel of 5MHz Mode SH-A in OFDM mode SH-B in TDM
modulations	OFDM: Qpsk, 16Qam TDM: Qpsk, 8psk, 16Apsk

Table 22 – EUTELSAT 10A characteristics

6.2.1. RF FILTERS FOR EUTELSAT 10A RECEIVER

The downlink bandwidth of the EUTELSAT 10A satellite starts from 2170 MHz to 2200 MHz (bandwidth of 30 MHz) and in this band there are 6 communication channel (F1, F2, F3, F4, F5, and F6). Each channel has a bandwidth of 5 MHz and only one channel is transmitted from the satellite platform that is in test mode (other channels are used for the terrestrial service). The downlink channel used to cover the Italian area is selected by the service provider among F4 (2187.5 MHz), F5 (2192.5 MHz) and F6 (2197.5 MHz) carrier frequencies. Therefore, the bandwidth of interest for the passive system is 2185-2200 MHz.

In order to select this bandwidth of interest, different filtering stages are required:

- A first RF filter with low loss and slightly selective immediately downstream of the antenna
- A second RF filter more selective (according to the specifications shown below) downstream of an LNA with gain between 10 and 20 dB
- An IF filter more or less selective in function of the configurations shown below

In order to define the first RF filter characteristics, it is necessary to consider the transmissions out of the band used for the satellite transmissions. In urban areas, the bandwidth 2150-2170 MHz (very close to that of interest) is allocated for T-UMTS FDD (Frequency Division Duplexing – downlink) signals.

Two downlinks bandwidth have been considered for the filter specifications:

- 4.75 MHz (5 MHz nominal bandwidth of a single DVB-SH channel) in order to perform the channel selection at RF
- 15 MHz in order to perform the satellite downlink bandwidth selection at RF.

The selectivity desired is between 50 dB and 70 dB.

6.2.1.1. CHANNEL SELECTION AT RF

The block diagram of the filtering stages for the channel selection at RF is reported in Figure 176.

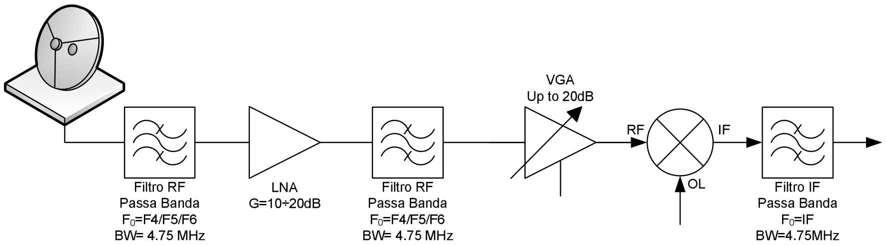

Figure 176 – Channel selection at RF - Filtering stages

The analysis of the characteristics of the filters have been carried out by means of the K&L Microwave Filter Wizard (http://www.klfilterwizard.com)

The simulation of the first RF filter has been realized for the channel F4 (2187.5MHz). The parameters introduced in the K&L Filter Wizard are reported in Figure 177.

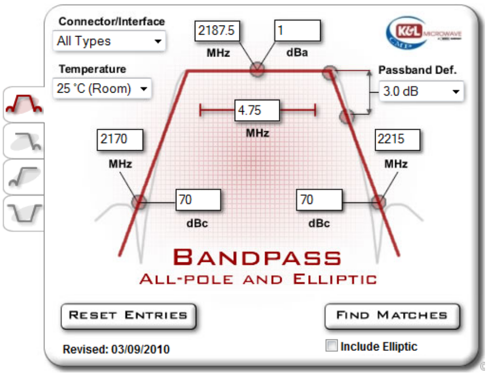

Connector/Interface: All Types
Temperature: 25 °C (Room)
Passband Def.: 3.0 dB
2187.5 MHz
1 dBa
4.75 MHz
2170 MHz
2215 MHz
70 dBc
70 dBc
☐ Include Elliptic
Revised: 03/09/2010

Figure 177 – Channel selection at RF – first filter at RF parameter

The filter response simulation obtained according to the parameter reported in Figure 177 is reported in Figure 178.

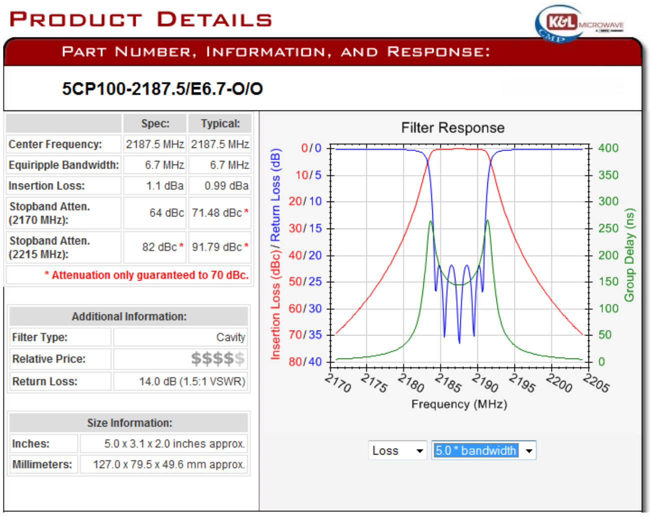

PRODUCT DETAILS

PART NUMBER, INFORMATION, AND RESPONSE:

5CP100-2187.5/E6.7-O/O

	Spec:	Typical:
Center Frequency:	2187.5 MHz	2187.5 MHz
Equiripple Bandwidth:	6.7 MHz	6.7 MHz
Insertion Loss:	1.1 dBa	0.99 dBa
Stopband Atten. (2170 MHz):	64 dBc	71.48 dBc *
Stopband Atten. (2215 MHz):	82 dBc *	91.79 dBc *

* Attenuation only guaranteed to 70 dBc.

Additional Information:	
Filter Type:	Cavity
Relative Price:	$$$$$
Return Loss:	14.0 dB (1.5:1 VSWR)

Size Information:	
Inches:	5.0 x 3.1 x 2.0 inches approx.
Millimeters:	127.0 x 79.5 x 49.6 mm approx.

Figure 178 – Channel selection at RF – first filter response simulation

As clearly visible in Figure 178, in order to obtain a selectivity of about 70 dB, a first RF filter with 5 poles and an equiripple bandwidth of 6.7 MHz can be used.

The second RF filter must be more selective (with a bandwidth of 4.75MHz, according to the DVB-SH standard). The simulation of this filter response is reported in Figure 179.

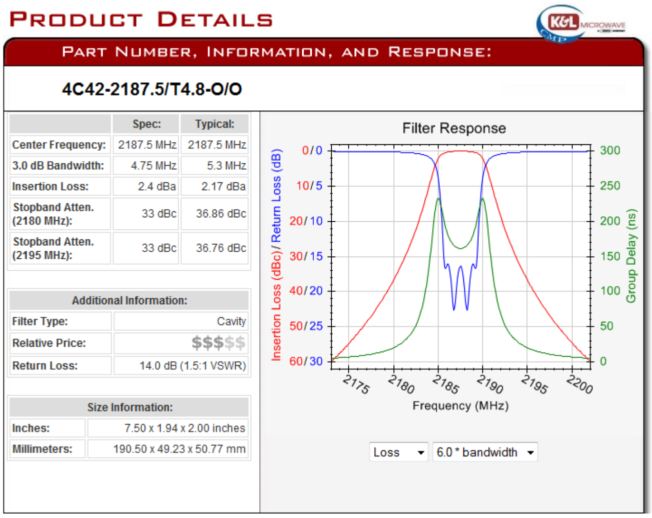

PRODUCT DETAILS

PART NUMBER, INFORMATION, AND RESPONSE:

4C42-2187.5/T4.8-O/O

	Spec:	Typical:
Center Frequency:	2187.5 MHz	2187.5 MHz
3.0 dB Bandwidth:	4.75 MHz	5.3 MHz
Insertion Loss:	2.4 dBa	2.17 dBa
Stopband Atten. (2180 MHz):	33 dBc	36.86 dBc
Stopband Atten. (2195 MHz):	33 dBc	36.76 dBc

Additional Information:	
Filter Type:	Cavity
Relative Price:	$$$$$
Return Loss:	14.0 dB (1.5:1 VSWR)

Size Information:	
Inches:	7.50 x 1.94 x 2.00 inches
Millimeters:	190.50 x 49.23 x 50.77 mm

Figure 179 – Channel selection at RF – second filter response simulation

Considerations about IF filters will be reported in following sections.

6.2.1.2. ALL SATELLITE BANDWIDTH SELECTION AT RF

In order to realize a flexible system able to acquire all possible DVB-SH channels transmitted by EUTELSAT 10A (F4, F5 e F6), the RF filters should have a bandwidth of 15 MHz (from 2185 MHz to 2200 MHz). The block diagram of the filtering stages for all satellite bandwidth selection at RF is reported in Figure 180.

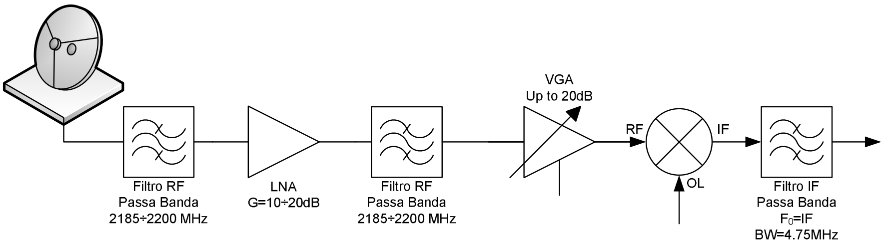

Figure 180 – All bandwidth selection at RF - Filtering stages

In this case, the IF filter can be identical to the one described in the previous Sub-Section.

The parameters used in order to simulate a first RF filter are reported in Figure 181.

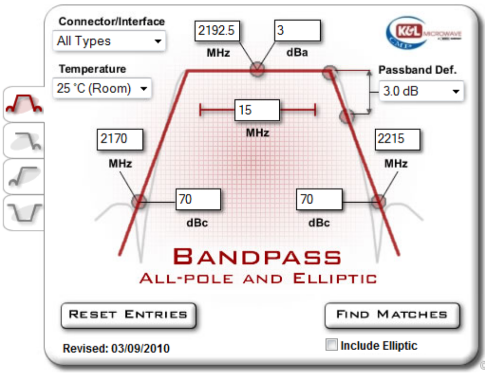
Connector/Interface: All Types

Temperature: 25 °C (Room)

Passband Def.: 3.0 dB

2192.5 MHz

3 dBa

15 MHz

2170 MHz

2215 MHz

70 dBc

70 dBc

Revised: 03/09/2010

☐ Include Elliptic

Figure 181 – All bandwidth selection at RF – first filter at RF parameter

The filter response simulations obtained According to the parameter reported in Figure 177 are reported in Figure 182 and Figure 183.

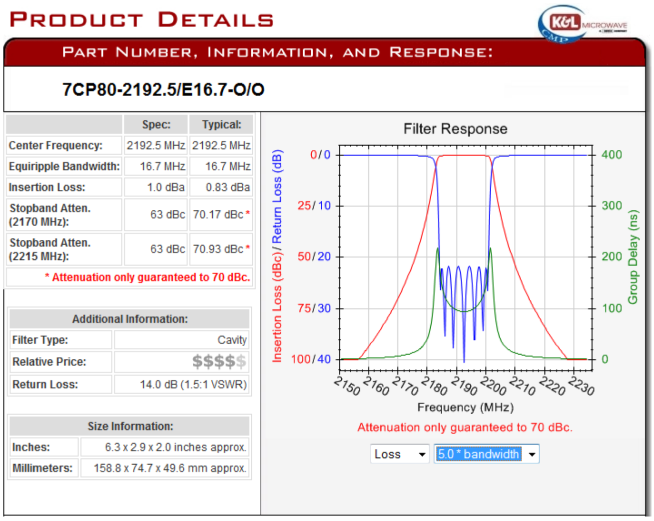
PRODUCT DETAILS

PART NUMBER, INFORMATION, AND RESPONSE:

7CP80-2192.5/E16.7-O/O

	Spec:	Typical:
Center Frequency:	2192.5 MHz	2192.5 MHz
Equiripple Bandwidth:	16.7 MHz	16.7 MHz
Insertion Loss:	1.0 dBa	0.83 dBa
Stopband Atten. (2170 MHz):	63 dBc	70.17 dBc *
Stopband Atten. (2215 MHz):	63 dBc	70.93 dBc *

* Attenuation only guaranteed to 70 dBc.

Additional Information:	
Filter Type:	Cavity
Relative Price:	$$$$$
Return Loss:	14.0 dB (1.5:1 VSWR)

Size Information:	
Inches:	6.3 x 2.9 x 2.0 inches approx.
Millimeters:	158.8 x 74.7 x 49.6 mm approx.

Figure 182 – All bandwidth selection at RF – first filter response simulation

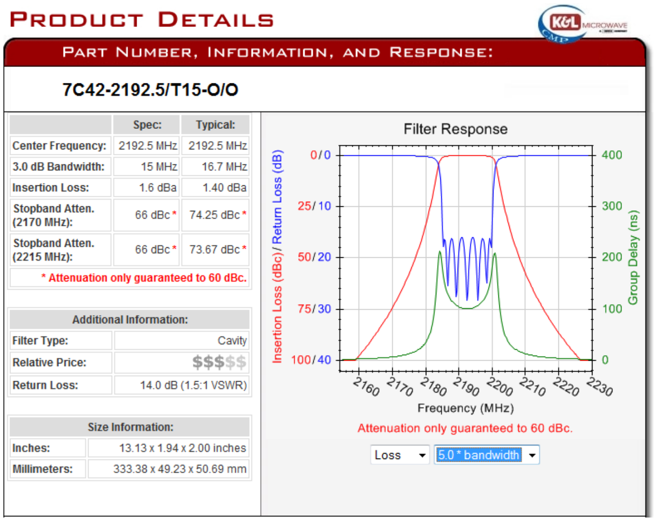

PRODUCT DETAILS

PART NUMBER, INFORMATION, AND RESPONSE:

7C42-2192.5/T15-O/O

	Spec:	Typical:
Center Frequency:	2192.5 MHz	2192.5 MHz
3.0 dB Bandwidth:	15 MHz	16.7 MHz
Insertion Loss:	1.6 dBa	1.40 dBa
Stopband Atten. (2170 MHz):	66 dBc *	74.25 dBc *
Stopband Atten. (2215 MHz):	66 dBc *	73.67 dBc *

* Attenuation only guaranteed to 60 dBc.

Additional Information:	
Filter Type:	Cavity
Relative Price:	$$$$$
Return Loss:	14.0 dB (1.5:1 VSWR)

Size Information:	
Inches:	13.13 x 1.94 x 2.00 inches
Millimeters:	333.38 x 49.23 x 50.69 mm

Attenuation only guaranteed to 60 dBc.

Figure 183 – All bandwidth selection at RF – second filter response simulation

In both cases, the filters have 7 poles with a little difference in terms of pass band. Both filters can be used in the RF section of the receiver.

6.2.2. SYSTEM ARCHITECTURES

Different system architectures can be considered in order to realize the passive system:

6.2.2.1. HOMODYNE ARCHITECTURE

I&Q demodulation of the signal from RF to BB

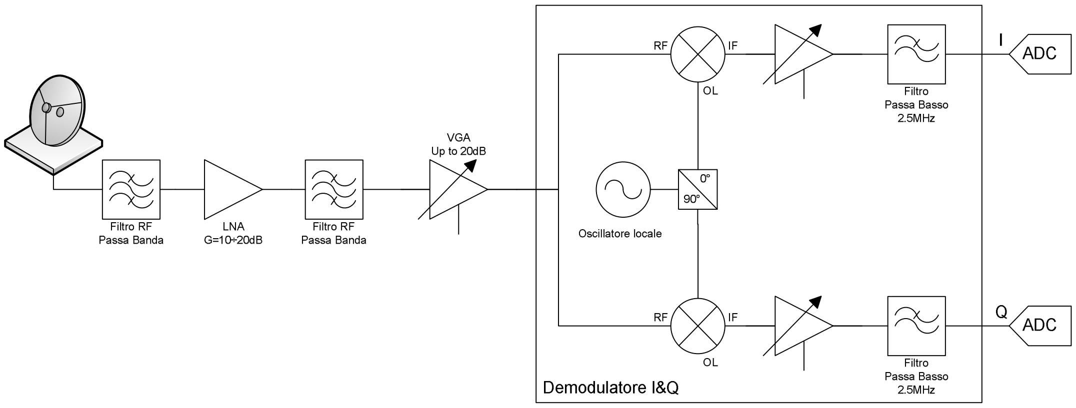

Figure 184 – EUTELSAT 10A homodyne architecture

6.2.2.2. SUPER HETERODYNE ARCHITECTURE

Single down-conversion from RF to an IF in the interval 20-70 MHz.

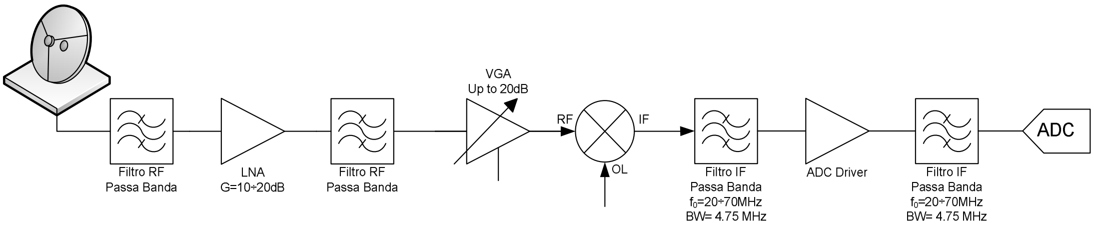

Figure 185 – EUTELSAT 10A Super heterodyne architecture

6.2.2.3. DOUBLE CONVERSION ARCHITECTURE

Double down-conversion from RF to IF1 (220-380 MHz) and from IF1 to IF2 (5-20 MHz).

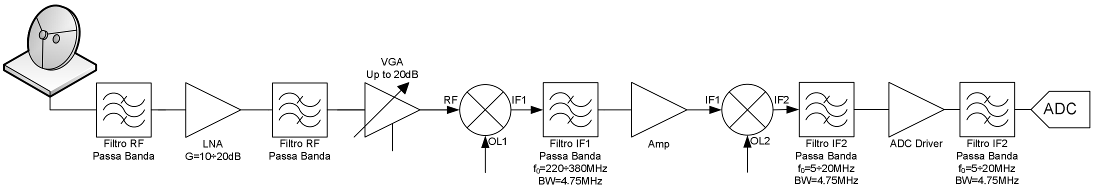

Figure 186 – EUTELSAT 10A Double Conversion architecture

The selection of the desired architecture has been performed after the study of the frequency plane reported in the following Sub-Section.

6.2.3. FREQUENCY PLANE

A preliminary analysis has been carried out in order to define a proper frequency plane for the satellite receiver.

The following analysis refers to the system architectures reported in the previous Sub-Section. The considered RF filter has been previously described in Sub-Section 6.2.1.2 and its able to select the bandwidth from 2185 MHz to 2200 MHz (DVB-SH channels F4, F5 and F6). Therefore, for the evaluation of the mixer intermodulation products, only these three DVB-SH channels have been considered.

All the mixer intermodulation products have been calculated by Matlab simulation:

$$IF_{m,n} = m * RF \pm n * OL \qquad m,n = 0,1,\ldots,10 \tag{91}$$

The desired signals are:

$$\begin{aligned} IF_{1,1} &= RF - OL \qquad && RF > OL \\ IF_{1,1} &= OL - RF \qquad && RF < OL \end{aligned} \tag{92}$$

In Figure 187, all the intermodulation products frequencies are reported in function of the Local Oscillator frequency. Notice that the RF is set at 2192.5 MHz

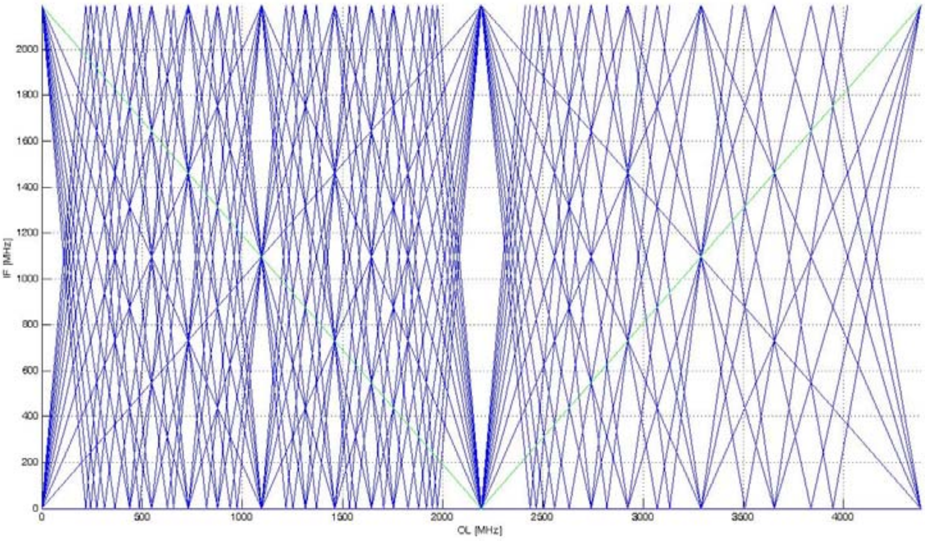

Figure 187 – EUTELSAT 10A mixer intermodulation products (RF 2192 MHz) – In green $IF_{1,1}$

From Figure 187 it is possible to identify an appropriate IF preventing the overlap of the undesired contribution on the desired converted channel (at IF).

Figure 188 shows the mixer intermodulation products with reference to the architecture reported in Sub-Section 6.2.2.2 (Super heterodyne receiver). The desired IF should be in the interval 20-70 MHz. The bandwidth of the considered RF filter is 15 MHz. The green lines represent the desired channel IF ($IF_{1,1}$), while the blue lines represent the undesired mixer intermodulation products.

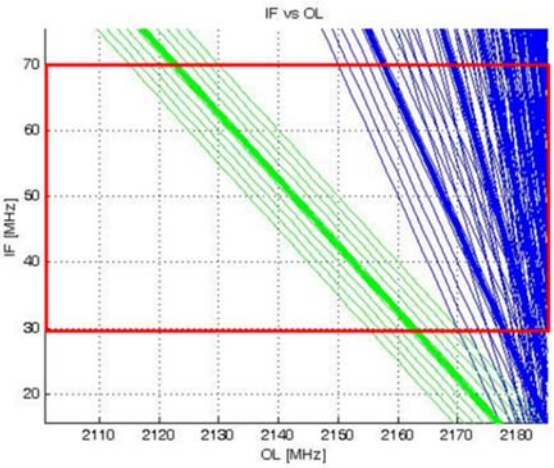

Figure 188 – EUTELSAT 10A mixer intermodulation products (RF 2192 MHz) – In green $IF_{1,1}$ – IF=15÷75 MHz

As clearly visible, an IF from 30 MHz to 70 MHz can be used in order to prevent the overlap of the desired and undesired intermodulation products. Therefore, for the super heterodyne architecture, an IF greater than 30 MHz has to be selected.

Regarding the architecture reported in Sub-Section 6.2.2.3 (Double Conversion receiver), the frequency plane analysis has been performed in order to select the two IF values of the system.

Also in this case, the bandwidth of the considered RF filter is 15 MHz and the green lines represent the desired channel IF ($IF_{1,1}$), while the blue lines represent the undesired mixer intermodulation products.

In the following analysis, the mixer intermodulation products represented are reported in Figure 189.

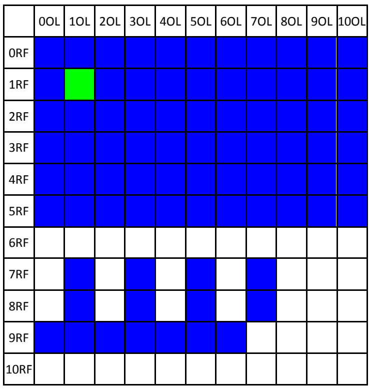

	0OL	1OL	2OL	3OL	4OL	5OL	6OL	7OL	8OL	9OL	10OL
0RF	🟦	🟦	🟦	🟦	🟦	🟦	🟦	🟦	🟦	🟦	🟦
1RF	🟦	🟩	🟦	🟦	🟦	🟦	🟦	🟦	🟦	🟦	🟦
2RF	🟦	🟦	🟦	🟦	🟦	🟦	🟦	🟦	🟦	🟦	🟦
3RF	🟦	🟦	🟦	🟦	🟦	🟦	🟦	🟦	🟦	🟦	🟦
4RF	🟦	🟦	🟦	🟦	🟦	🟦	🟦	🟦	🟦	🟦	🟦
5RF	🟦	🟦	🟦	🟦	🟦	🟦	🟦	🟦	🟦	🟦	🟦
6RF											
7RF		🟦		🟦		🟦		🟦			
8RF		🟦		🟦		🟦		🟦			
9RF	🟦	🟦	🟦	🟦	🟦	🟦	🟦				
10RF											

Figure 189 – EUTELSAT 10A mixer intermodulation products considered

Figure 189 shows the mixer intermodulation products (desired in green and undesired in blue) in the IF1 interval from 210 MHz to 390 MHz. The admissible values of IF are highlighted with red rectangles.

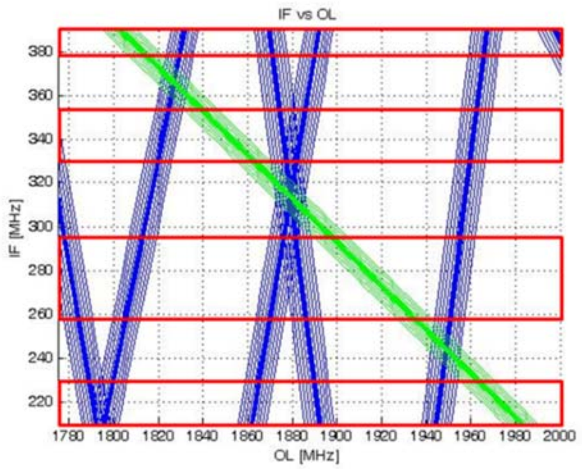

Figure 190 – EUTELSAT 10A mixer intermodulation products (RF 2192 MHz) – In green IF1 – IF=210÷390 MHz

For the second down conversion stage, the desired value for the IF2 is between 10 MHz and 20 MHz. the results for this case are reported in Figure 191 and Figure 192 for IF1=340 MHz and IF1=220 MHz, respectively.

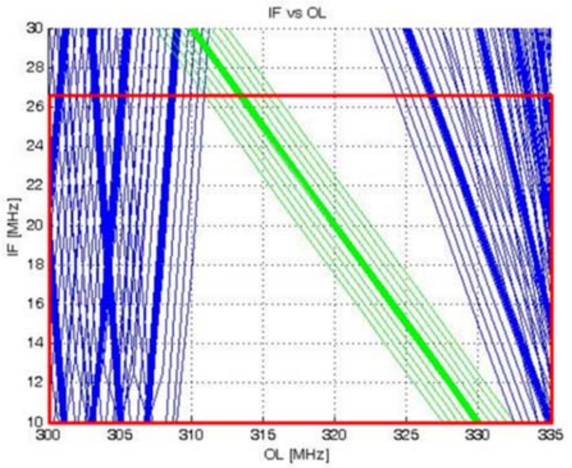

Figure 191 – EUTELSAT 10A mixer intermodulation products (RF 2192 MHz) – In green IF2 – IF1= 340MHz – IF=10÷30 MHz

If the value of IF1 is 340 MHz, the IF2 can be selected in the interval 10-26 MHz.

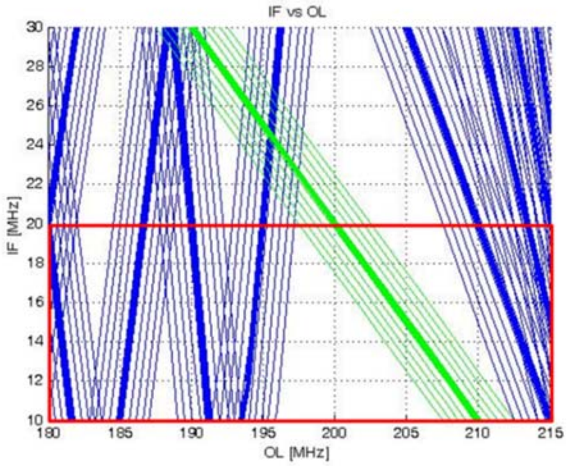

Figure 192 – EUTELSAT 10A mixer intermodulation products (RF 2192 MHz) – In green IF2 – IF1= 220MHz – IF=10÷30 MHz

If the value of IF1 is 220 MHz, the IF2 can be selected in the interval 10-20 MHz.

Concluding, for the Double Conversion architecture, the IF1 can be selected by means of the results obtained in Figure 192, while the IF2 can be set in the interval 10-20 MHz.

In order to complete the analysis of the system filters, following are reported three possible IF filter response simulations.

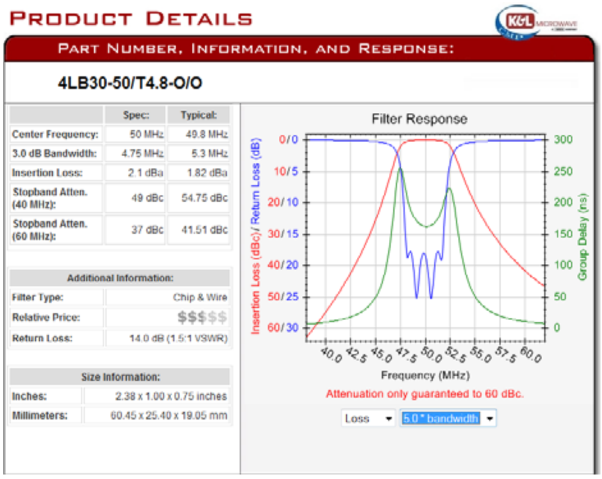

PRODUCT DETAILS

PART NUMBER, INFORMATION, AND RESPONSE:

4LB30-50/T4.8-O/O

	Spec:	Typical:
Center Frequency:	50 MHz	49.8 MHz
3.0 dB Bandwidth:	4.75 MHz	5.3 MHz
Insertion Loss:	2.1 dBa	1.82 dBa
Stopband Atten. (40 MHz):	49 dBc	54.75 dBc
Stopband Atten. (60 MHz):	37 dBc	41.51 dBc

Additional Information:	
Filter Type:	Chip & Wire
Relative Price:	$$$$$
Return Loss:	14.0 dB (1.5:1 VSWR)

Size Information:	
Inches:	2.38 x 1.00 x 0.75 inches
Millimeters:	60.45 x 25.40 x 19.05 mm

Attenuation only guaranteed to 60 dBc.

Figure 193 – EUTELSAT 10A IF filter simulation (IF 50 MHz) for super heterodyne architecture

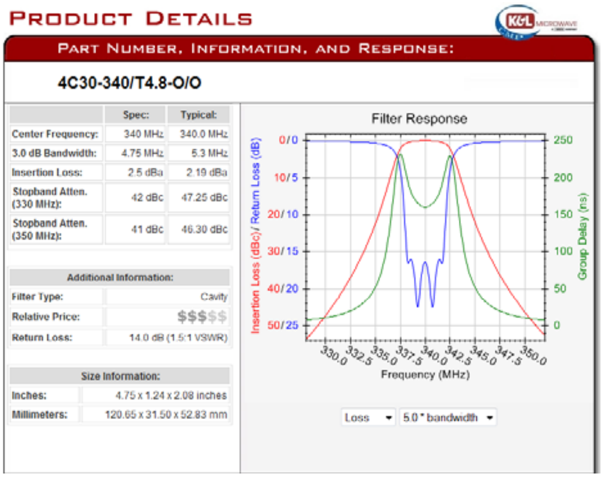

PRODUCT DETAILS

PART NUMBER, INFORMATION, AND RESPONSE:

4C30-340/T4.8-O/O

	Spec:	Typical:
Center Frequency:	340 MHz	340.0 MHz
3.0 dB Bandwidth:	4.75 MHz	5.3 MHz
Insertion Loss:	2.5 dBa	2.19 dBa
Stopband Atten. (330 MHz):	42 dBc	47.25 dBc
Stopband Atten. (350 MHz):	41 dBc	46.30 dBc

Additional Information:	
Filter Type:	Cavity
Relative Price:	$$$$$
Return Loss:	14.0 dB (1.5:1 VSWR)

Size Information:	
Inches:	4.75 x 1.24 x 2.08 inches
Millimeters:	120.65 x 31.50 x 52.83 mm

Figure 194 – EUTELSAT 10A IF1 filter simulation (IF1 340 MHz) for Double Conversion architecture

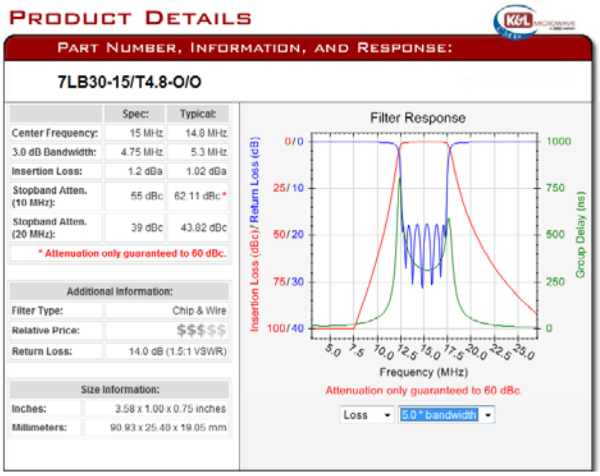

PRODUCT DETAILS

PART NUMBER, INFORMATION, AND RESPONSE:

7LB30-15/T4.8-O/O

	Spec:	Typical:
Center Frequency:	15 MHz	14.8 MHz
3.0 dB Bandwidth:	4.75 MHz	5.3 MHz
Insertion Loss:	1.2 dBa	1.02 dBa
Stopband Atten. (10 MHz):	55 dBc	62.11 dBc*
Stopband Atten. (20 MHz):	39 dBc	43.82 dBc

* Attenuation only guaranteed to 60 dBc.

Additional Information:	
Filter Type:	Chip & Wire
Relative Price:	$$$$$
Return Loss:	14.0 dB (1.5:1 VSWR)

Size Information:	
Inches:	3.58 x 1.00 x 0.75 inches
Millimeters:	90.93 x 25.40 x 19.05 mm

Attenuation only guaranteed to 60 dBc.

Figure 195 – EUTELSAT 10A IF2 filter simulation (IF2 15 MHz) for Double Conversion architecture

6.3. PROTOTYPE DESCRIPTION

The Super Heterodyne receiver architecture has been selected for the realization of the preliminary tests of the DVB-SH based PBR. A single receiving chain of the proposed solution is sketched in Figure 196.

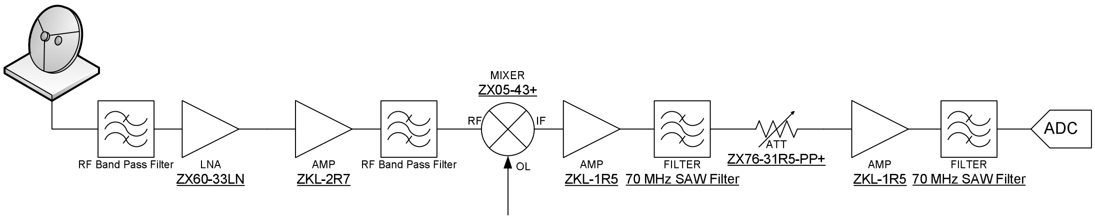

Figure 196 - Architecture of DVB-SH receiver

The RF Filters provide rejection of out-of-band interference and nonlinearity effects. Between the RF filters there are two RF amplifiers (ZX60-33LN by Mini-Circuits, Low Noise Amplifier - 50 to 3000 MHz and ZKL-2R7 by Mini-Circuits, Amplifier - Medium Power 10 to 2700 MHz). These amplifiers provide a low noise figure, to minimize the degradation of the overall radar noise figure due to subsequent components. After a down-conversion stage from RF to IF (about 70 MHz), two IF band-pass SAW filters provide the rejection of unwanted signals and the selection of the desired radio channel. At IF, two amplifiers (ZKL-1R5 by Mini-Circuits, Amplifier - Medium Power 10 to 1500 MHz) and a digital step attenuator (ZX76-31R5-PP+ by Mini-Circuits, Digital Step Attenuator - DC to 2400 MHz - 0,5 to 31,5 dB) provide proper amplification of the signal. The signal is digitized by A/D conversion for the off-line digital processing.

The A/D conversion is performed by means of the NI PXI 5122 data capture by National Instruments. This consists in a double channel, 14 bit A/D converter with variable Vertical Range (0.2V, 0.4V, 1V, 2V, 4V), analog input bandwidth of 100 MHz (about 80MHz with VR= 0.2V) and maximum sample rate of 100 MHz.

The reference signal is collected by means of a parabolic antenna that operate at 2200 MHz with a Gain of about 21dB. The diameter of the parabolic reflector is 1.2m and the beam width (at -3dB) is 12°. The feed used is a Short Back Fire Antenna (SBFA) as reported in Figure 197.

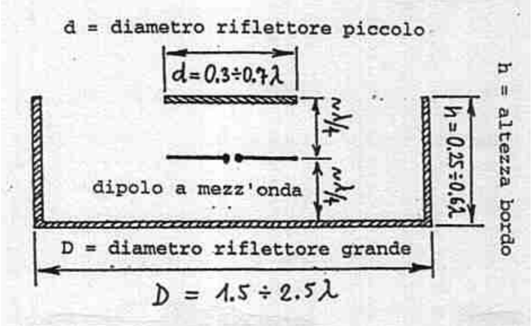

Figure 197 - SBFA

The Feed is composed by two reflectors:

- A little reflector that has a diameter of 0,3÷0,7λ
- A big reflector that has a diameter of 1,5÷2,5λ

An hybrid allows to receive the signals in circular polarization.

6.4. TESTS AND CONTROLLED EXPERIMENTS

Preliminary tests have been performed with the developed DVB-SH receiver. These tests are related to signal acquisition and demodulation, and to Auto-Ambiguity Function evaluation.

The acquisitions have been carried out in the center of Rome, on the roof of the DIET Dept. of University of Rome "La Sapienza".

Figure 198 shows the DVB-SH signal spectrum acquired during the preliminary test (2187.5 MHz). The signal has been acquired by means of the NI PXI 5122 data capture. The sampling frequency was 80 Mhz and the spectrum is reported after a resampling operation to the frequency 40/7 MHz (according to the DVB-SH standard). Figure 199 show the demodulated signal in the complex domain.

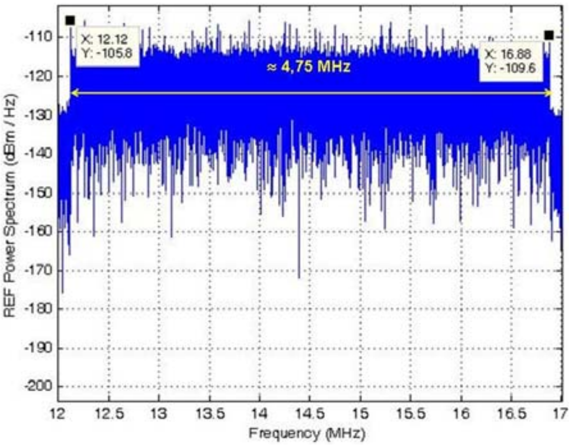

Figure 198 – DVB-SH Signal Spectrum

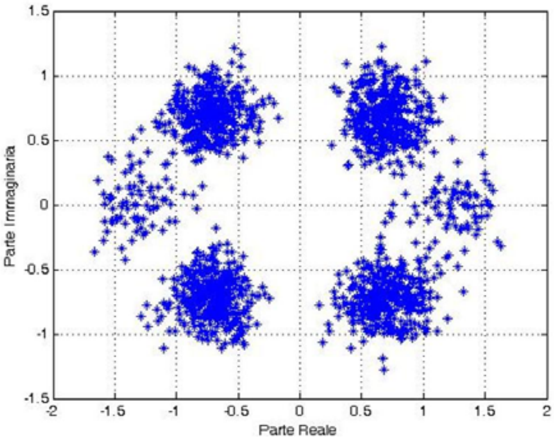

Figure 199 – DVB-SH Signal Demodulation

The signal acquired results transmitted in 2K-Mode.

6.5. CONCLUSIONS

In this section, a preliminary study regarding a passive radar based on DVB-SH signals of opportunity is reported. The general requirements and three possible architectures for DVB-SH receiver have been introduced. A simple demonstrator has been realized, developed and fielded during preliminary tests. The future work will concern the use of the proposed receiver in order to realize an effective DVB-SH based PBR, through the use of multiple receiving chains.

7. CON MULTI-SIGNAL PBR RECEIVING SCHEME

7.1. INTRODUCTION

The broadcast transmitters available in the environment represent some of the most attractive choices for surveillance purposes, in function of their different coverage. Specifically the most common signals for PBRs in use today are: Frequency Modulated (FM) radio broadcast, Digital Audio and Video Broadcast (DAB, DVB-T), WiMAX and WiFi, etc.. The use of waveforms of opportunity with different features allows to obtain very different PBR systems in particular with reference to the achievable coverage and range resolution. Moreover, depending on the type of target under observation, it is possible to integrate the results obtained with PBRs that exploit different waveforms of opportunity in order to improve the coverage performance with respect to the single PBR sensor.

In this Section, I present the receiver architecture for a Multi-Band PBR developed and tested. The proposed receiver provides a low cost and versatile platform in order to:

- obtain a re-configurable PBR system for short-, medium-, and long-range surveillance;
- evaluate the performance obtained with different signals of opportunity for passive radar;
- implement and test algorithms for target tracking, data fusion and multi-sensor fusion.

7.2. ARCHITECTURE DESCRIPTION

The block diagram of the proposed receiver architecture is reported in Figure 2 for a single receiving chain of the PBR multi-standard receiver. The entire prototype system, realized with Commercial Off-the-Shelf (COTS) components, is described in this Section. Different architectures are implemented for different signals of opportunity. In particular, the Double conversion scheme is adopted only for the FM Radio and DVB-T waveforms, while the homodyne receiver is used for the WiFi standard.

Notice that a scheme with additional flexibility can be obtained by allowing the possibility for the signals at the output of the RF–FE to avoid the upconversion stage and be input directly to the I&Q demodulator. This can be effectively exploited for the signals in the frequency band where the I&Q demodulator acts with the best performance.

Three different FEs are considered in input, to select and condition the different kinds of signals. The RF Filters provide rejection of out-of-band interference and non-linearity effects, including image rejection. Three kinds of RF filters are foreseen that allow to select the signal bandwidths of interest:

- FM RF Filter: 87.5-108.0 MHz
- DVB-T RF Filter: 470.0-870.0 MHz
- WiFi RF Filter: 2400-2500 MHz.

A LNA provides a low noise figure in order to minimize the degradation of the overall noise figure due to subsequent components. An adjustable RF attenuator provides increased dynamic range with respect to that provided by the mixer.

After the FE, with reference to FM and DVB-T sections, there is an up-conversion stage from the desired channel carrier frequency to a fixed IF. An IF band-pass filter provides the rejection of unwanted signals and the selection of a single channel (or a small group of adjacent channels). According to the communication standards, the IF filters are different:

- FM IF Filter: BW=200 kHz (single channel selection)
- DVB-T IF Filter: BW=8 MHz.

The three receiver sections are then connected, by means of a switch, to a common part of the system which performs the down-conversion from IF (for FM and DVB-T signals) or RF (for WiFi signals) to BB;

this operation is performed by a I&Q Quadrature demodulator that provides to the A/D converter the signal splitted into I and Q paths to facilitate the image rejection in the digital domain. The A/D conversion is performed by means of the X3-10M data-capture (by Innovative Integration). This is an XMC IO module featuring eight simultaneously sampled 16-bit, 25 MSPS A/D channels designed for high speed data acquisition applications. Data acquisition control, signal processing, buffering, and system interface functions are implemented in an on board Xilinx Spartan3A DSP FPGA.

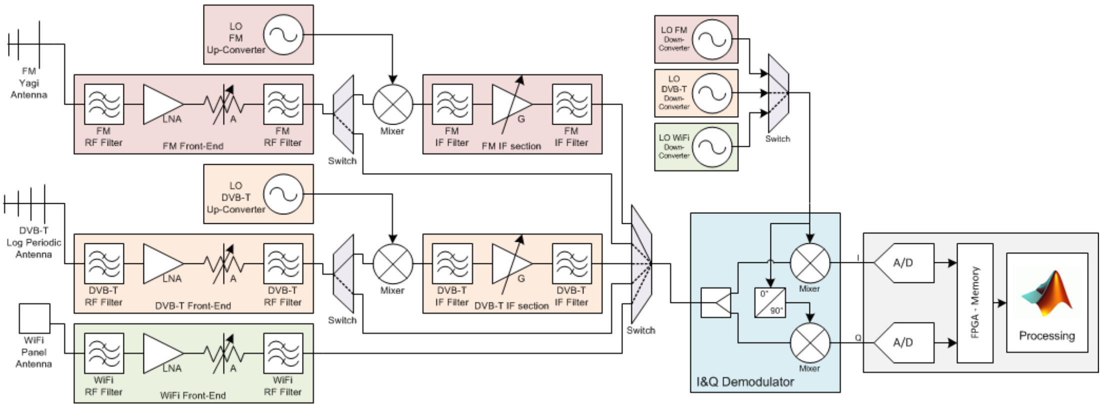

Figure 200 – Multi Signal PBR architecture

The working principle of the Double Conversion receiver in the frequency domain, with reference to the DVB-T signal, is described in Figure 201. The sequence shows the spectra of the DVB-T signal along the receiving chain. The Radio Frequency section, by means of the RF filters, allows to select the whole DVB-T band. After the band selection, this receiver system translates the center frequency of the desired TV channel from RF to an IF greater than the maximum carrier frequency for the selected channel band (up-conversion), using a mixer with a variable frequency LO. The advantage of this scheme is that the tracking filter can be eliminated because the up-conversion stage moves out of band the first mixer image frequency. A band-pass filter stage is used at IF to remove any undesired up-converted frequency components (including the image-band signal), allowing only desired channel to pass to the second mixer stage. The selected channel at IF is then frequency translated directly to baseband, or to a very low IF, using a fixed frequency synthesizer. Finally, the digitalization is performed by means of a couple of A/D converters after the digitalization.

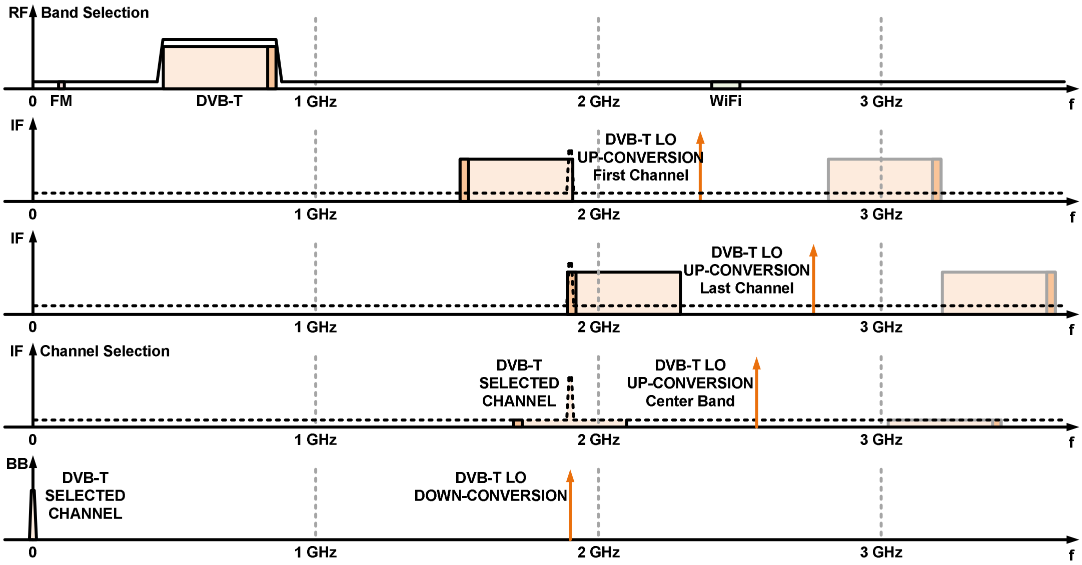

Figure 201 – Multi Signal PBR architecture – Working Principle

7.3. TESTS AND EXPERIMENTAL RESULTS

To show the performance of the flexible prototype, we refer to the case of Air Traffic Control (ATC) Surveillance by FM-based PBR, to medium range surveillance with DVB-T and to short range surveillance with WiFi signals.

7.3.1. AIR TRAFFIC CONTROL SURVEILLANCE BY FM-BASED PBR

The performance of the developed FM-based PBR receiver (in Up-conversion Superheterodyne configuration) is based on the evaluation of its disturbance cancellation and detection capability. The two channel receiver configuration scheme of the FM based PBR is reported in Figure 202 and the test bench realized in order to perform the preliminary tests is reported in Figure 203.

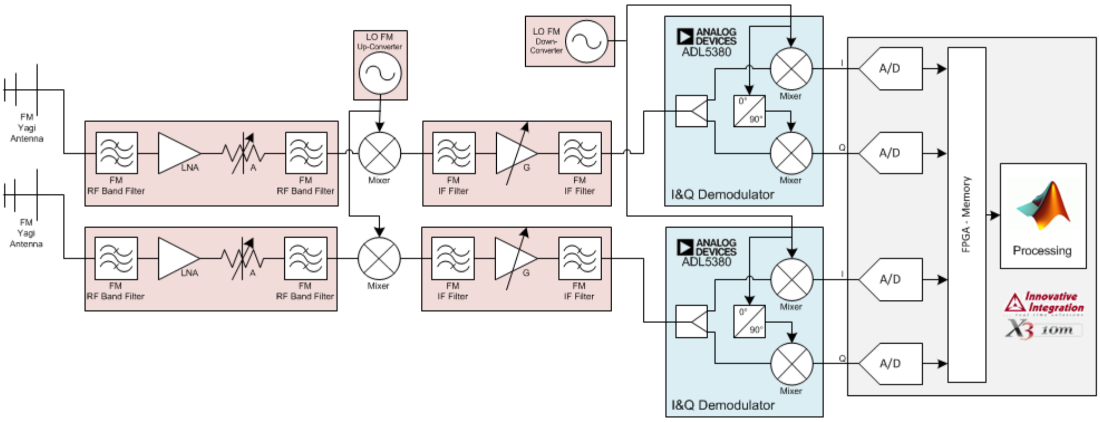

Figure 202 – Multi Signal PBR architecture – FM configuration

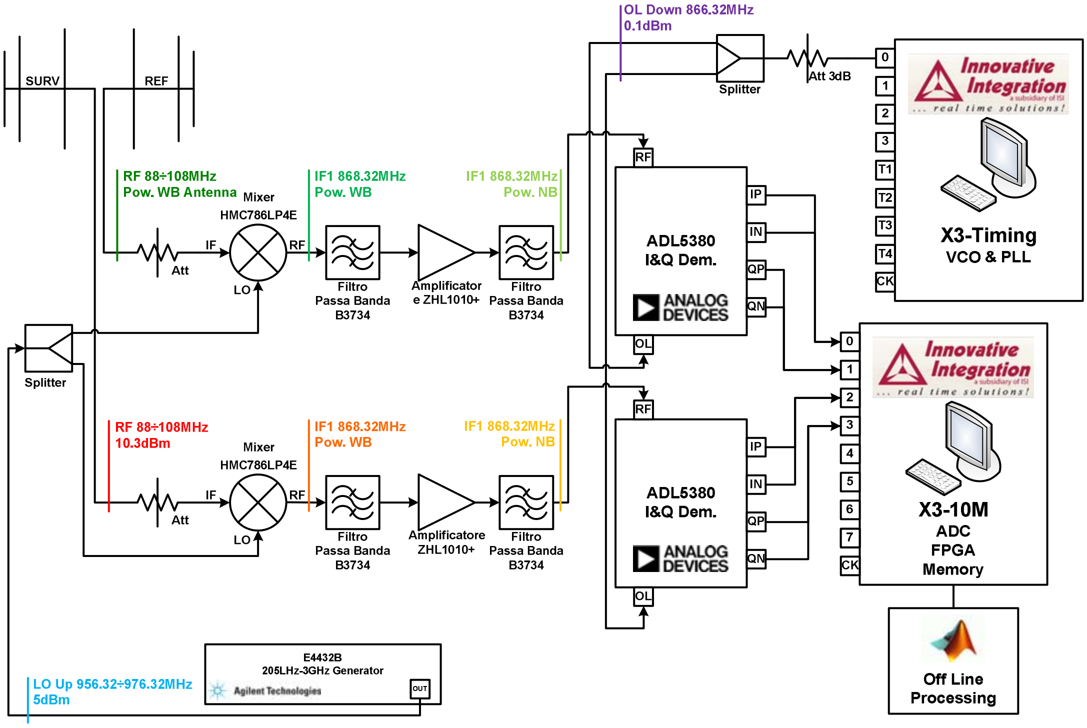

Figure 203 – Multi Signal PBR architecture – FM configuration – Test bench

Different tests have performed, in controlled situations, to evaluate the theoretical maximum cancellation level that can be obtained with the proposed receiver architecture. The acquired data sets were processed using the cancellation algorithms described in Section 2.3.1: specifically, the Extensive Cancellation Algorithm (ECA) was used, which exploits the Least Square (LS) approach to minimize the surveillance channel power at the output of the cancellation filter.

Table 23 summarizes the cancellation values obtained for the FM radio channels of interest. Each row contains the Direct-to-Noise Ratio (DNR) measured over the two receiving channels, the theoretical cancellation (function of DNR value), the measured cancellation (obtained as the ratio between the power levels measured, over a 200 kHz bandwidth, at the input and at the output of the cancellation filter), and the difference between theoretical and measured cancellation (CA Loss). As is apparent, this solution is able to achieve cancellation values comparable with the theoretical reference.

Ch Radio [MHz]	DNR REF [dB]	DNR SURV [dB]	CA TEO [dB]	CA MEAS [dB]	CA LOSS [dB]
90.7	61.0	60.2	57.6	54.7	2.8
91.2	56.6	55.7	53.1	51.8	1.3
92.4	65.8	64.8	62.2	55.9	6.3
103.0	60.0	60.4	57.2	55.1	2.0
105.3	58.5	59.3	55.9	52.2	3.7

Table 23 – Disturbance Cancellation value for FM-based PBR

Different acquisition campaigns have been carried out in Rome. Two directive Yagi antennas, with about 7dBi gain, 16dB of Front-to-Back (FtB) ratio and about 90° of azimuth main beam, were used. The Reference antenna was steered toward a transmitter located on Monte Cavo (about 25km South-East of Rome), while the Surveillance antenna was pointed at 180°. The Surveillance antenna pattern includes many of the standard arrival/departure routes of the Leonardo Da Vinci (Fiumicino) Airport.

Figure 204 – Multi Signal PBR architecture – FM configuration – Reference scenario

In terms of detection capability, most of the targets in the Surveillance antenna beam are correctly detected by our receiver. In the following figures the system detections (in red), are reported in the Bistatic Range/Bistatic Velocity domain, after a proper tracking operation. The ATC registrations (in gray) are also reported in order to verify the effectiveness of the detection capability. In particular, Figure 205 and Figure 206 shows the detections for the FM radio channel 92.4 MHz, evaluated over a time interval of about 7 minutes.

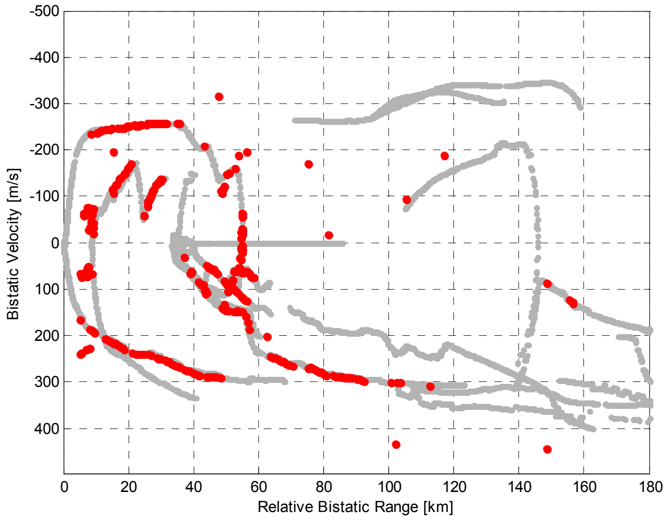

Figure 205 – Multi Signal PBR architecture – FM configuration – Detection results

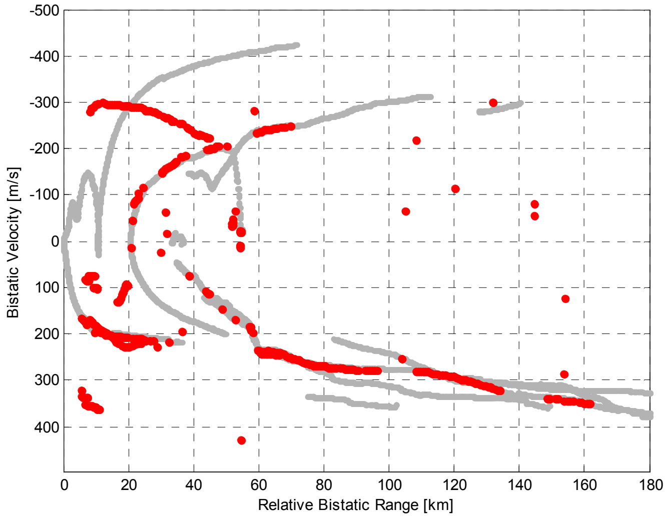

Figure 206 – Multi Signal PBR architecture – FM configuration – Detection results

7.3.2. SIGNAL PROCESSING PRELIMINARY TEST FOR DVB-T-BASED PBR

Preliminary tests have been performed with the developed DVB-T-based PBR receiver configuration (in Homodyne configuration). The tests concern the DVB-T signal acquisition and demodulation, the Auto-Ambiguity Function evaluation. The two channel receiver configuration scheme of the DVB-T-based PBR is reported in Figure 207 and the test bench realized in order to perform the preliminary tests is reported in Figure 208.

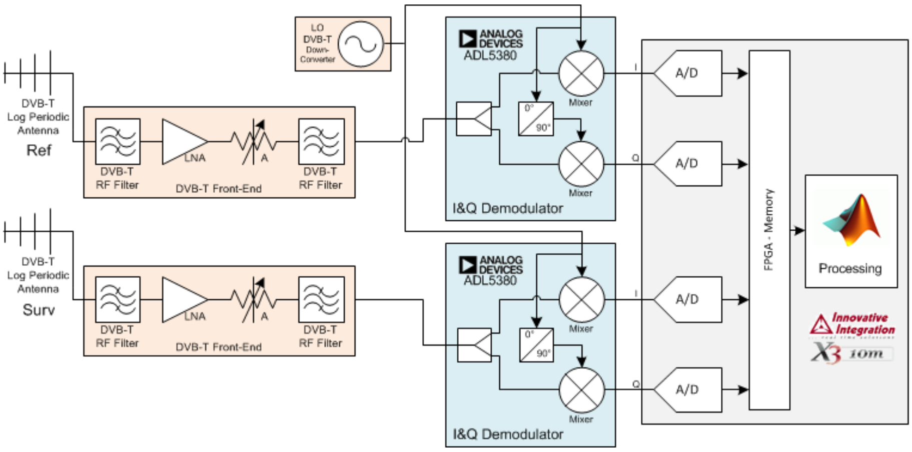

Figure 207 – Multi Signal PBR architecture – DVB-T configuration

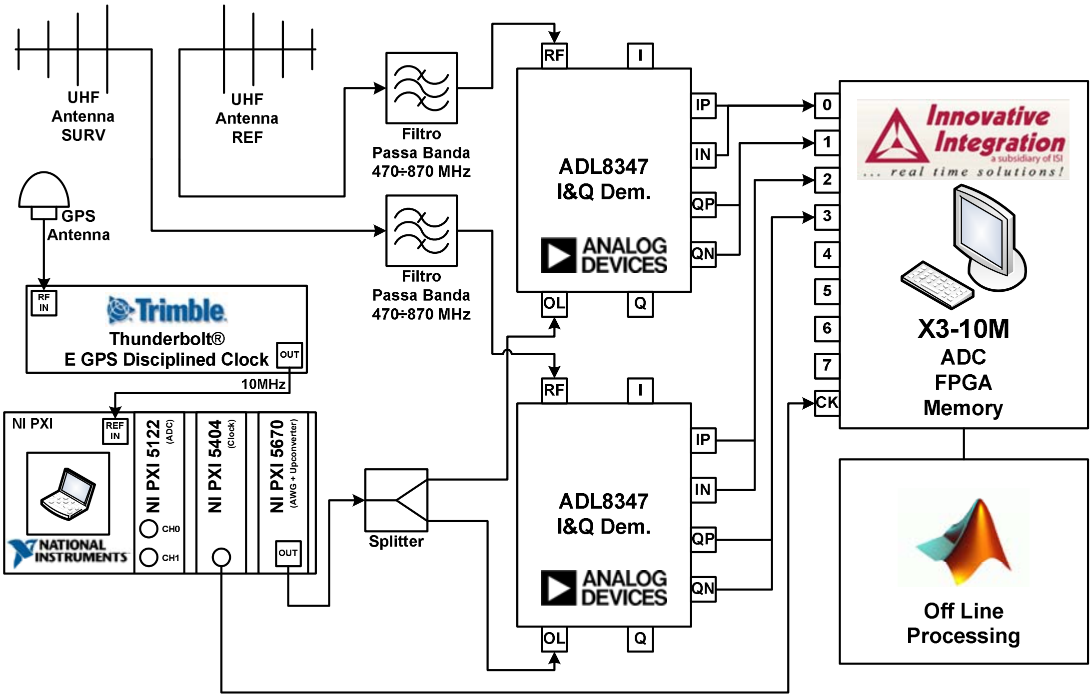

Figure 208 – Multi Signal PBR architecture – DVB-T configuration – Test bench

Table 24 summarizes the parameters of the DVB-T signal acquired for the preliminary tests. Each row contains the Tx Mode of the signal (according to the DVB standard), the use of GPS synchronization system (in this case the reference of the system is not locked with the GPS signal), the frame delay, the carrier frequency offset and the sampling offset. The last three values are necessary in order to use the Saini-Cherniakov algorithm for DVB-T synchronization and Ambiguity function evaluation [36]-[39].

Ch DVB-T [MHz]	Tx Mode	GPS	Frame delay [ms]	Carrier Frequency Offset [Hz]	Sampling Offset
634	8K-MODE, GI 1/32	No	1,052625	50,5814	4.7712e-8

Table 24 – Disturbance Cancellation value for FM-based PBR

Figure 209 shows the DVB-T signal spectrum acquired during the preliminary tests (634 MHz). The signal has been acquired after analog demodulation by means of the X3-10M data capture. The sampling frequency was 16 Mhz and the spectrum is reported after a resampling operation to the frequency 64/7 MHz (according to the DVB-T standard). Figure 210 show the demodulated signal in the complex domain. The modulation of the signal results 64-QPSK.

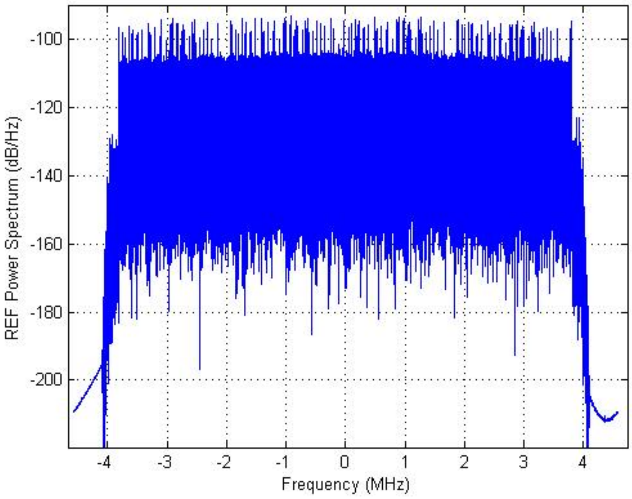

Figure 209 – Multi Signal PBR architecture – DVB-T configuration – Signal Spectrum

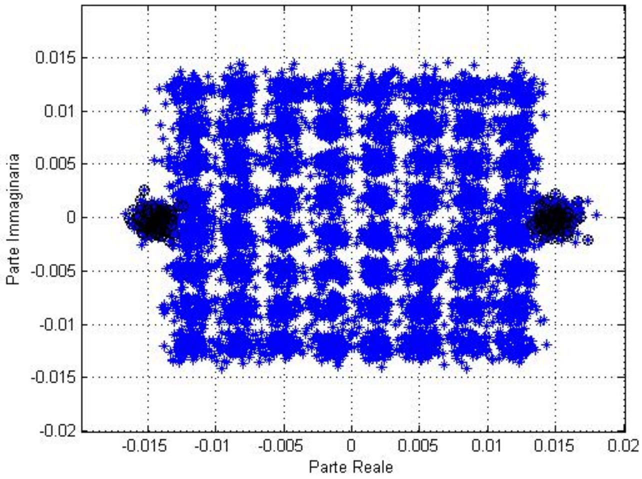

Figure 210 – Multi Signal PBR architecture – DVB-T configuration – Signal Demodulation

Figure 211 shows the Auto-ambiguity function obtained on a simulated DVB-T signal. The peaks due to the waveform of opportunity characteristics are highlighted by red and white markers corresponding to two different thresholds of Peak-to-Sidelobe Ratio (PSLR), up to 30dB and >30dB, respectively. The Auto-ambiguity function obtained on a real DVB-T signal, acquired by means of the proposed system, is reported in Figure 212. As clearly visible, the results with a real data set are the same obtained with a simulated signal.

Finally, in Figure 213, the Auto-ambiguity function is reported after the application of the Saini-Cherniakov algorithm which performs the synchronization and the pilot blanking.

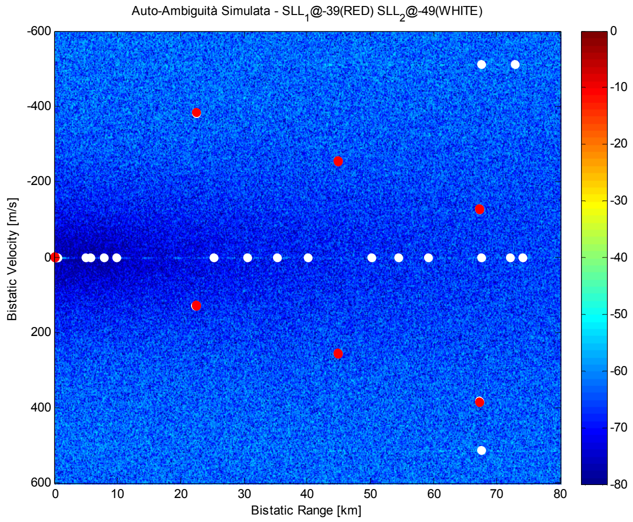

Figure 211 – Multi Signal PBR architecture – DVB-T configuration – Auto-Ambiguity Function Simulated Data

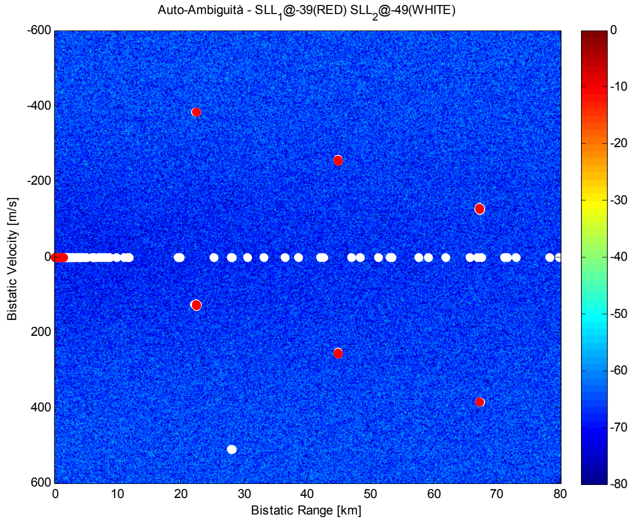

Figure 212 – Multi Signal PBR architecture – DVB-T configuration – Auto-Ambiguity Function Real Data

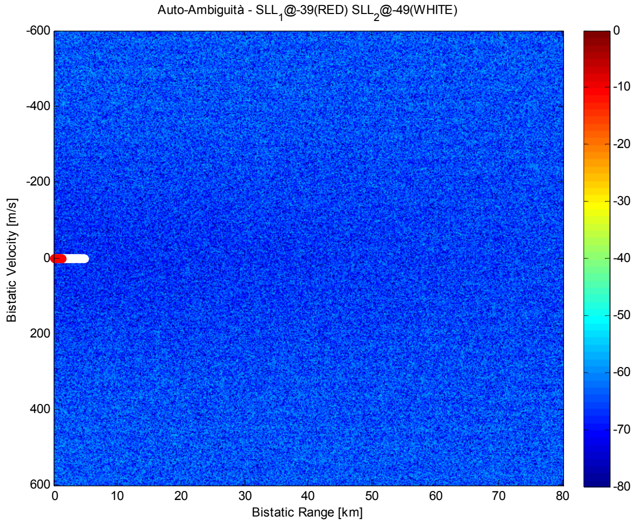

Figure 213 – Multi Signal PBR architecture – DVB-T configuration – Auto-Ambiguity Function Real Data and Synchronization processing

7.3.3. SHORT RANGE DETECTION AND LOCALIZATION OF MOVING TARGETS BY WIFI-BASED PBR

The results for short range detection and localization of moving targets by WiFi-based PBR are obtained with the receiver in homodyne configuration and its block diagram is reported in Figure 214. The waveform of opportunity following the IEEE 802.11 Standards, is located between 2.412 and 2.472 GHz.

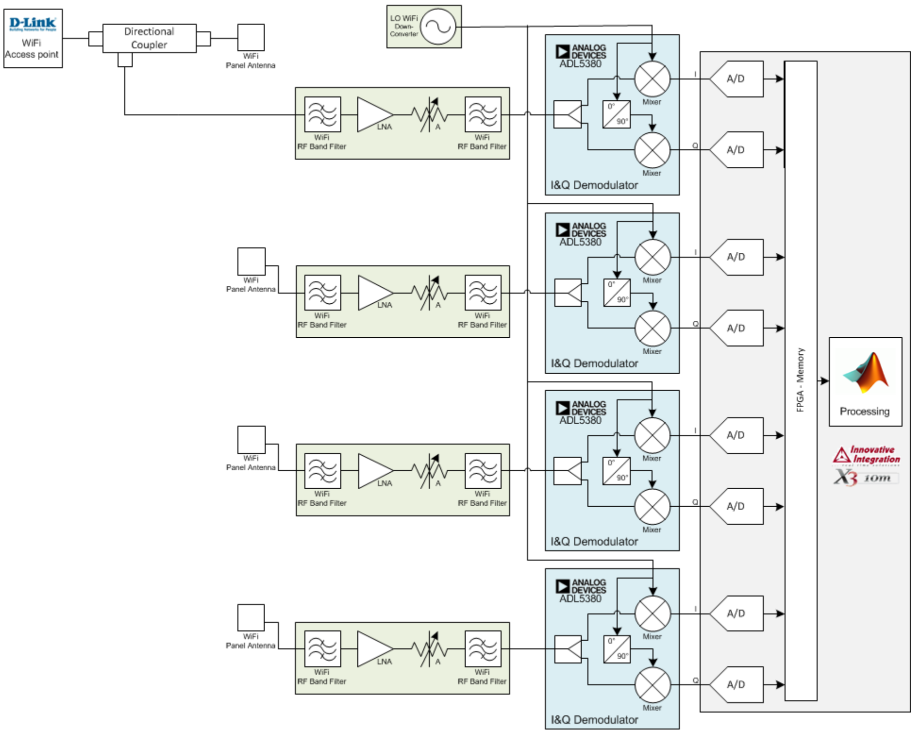

Figure 214 – Multi Signal PBR architecture – WiFi configuration

This system architecture, the acquisition campaigns and the results obtained by means of the developed receiver, have been widely described in Sections 5.3.2, 5.5 and 5.6.

7.4. CONCLUSIONS

In this section, a new architecture for a Multi-Band PBR receiver has been introduced, developed and fielded (during preliminary tests and acquisition campaigns). The effectiveness of the proposed solution has been assessed by using the receiver in different applications that allow to achieve an FM-based and a DVB-T-based PBR for long-, medium-range surveillance of air targets, and a WiFi-based PBR for short range localization of human targets. The future work will concern the use of the proposed receiver in order to realize an effective FM- and DVB-T-based PBR, through the use of multiple receiving chains with different FE configurations simultaneously.

8. CONCLUSIONS

In this thesis, different Passive Radar systems have been described. According to the specific application (e.g. Air Traffic Control Surveillance, detection and tracking of human targets) and waveform of opportunity (e.g. FM radio broadcast, DVB-SH, WiFi), different designs and implementations of PBR receivers have been reported.

In the first part of this thesis, Section 2, the working principles of PBR systems have been described. The specific processing techniques for PBR have been reported. In order to realize the PBR demonstrators described in Sections 4-7, proper Matlab algorithms have been implemented to obtain different passive systems (with off line processing). Also, a short overview of the waveforms of opportunity used in this work has been reported.

In Section 3, the most common architectures for telecommunication receivers that can be used to realize a passive radar system are shown. In particular, in Sections 4-7, different bock diagrams have been used as a function of the specific application and waveform of opportunity. The receiver scheme for each application has been selected by means of an extensive analysis performed to obtain the best performance (for PBR concept demonstration), and systems with the following features: ease of use, realization and low cost.

In Sections 4-7, three different passive radar systems, based on different waveforms of opportunity, have been presented. Each system is characterized by a waveform of opportunity and a specific surveillance application. In this work, the following waveforms of opportunity have been considered: FM radio broadcast, WiFi transmissions and DVB-SH.

In Section 4, the FM based PBR has been presented. Also, the general requirements of the system and two different architectures for a dedicated passive receiver have been described in detail. The core of the work about the FM system is represented by tests, controlled experiments and experimental results: laboratory tests have been carried out, and the two system have been used in different acquisition campaigns.

Specifically, in Section 4.7 have been reported the detection and localization results obtained with the FM-based PBR sensor. The test bed set-up for the FM-based PBR sensor validation, including the prototypes hardware description and tests, and the validation analysis plan, has been reported in Sections 4.4 and 4.5.

Raw data have been collected with the experimental passive radar sensor and have been off-line processed in order to extract the single detections in bistatic-range bistatic-velocity (Doppler) domain. Additionally, the angular target localization has been performed through DoA estimation and by means of the multiple channel receiver.

The effectiveness of the proposed solution has been assessed by evaluating the FM-based PBR detection capabilities in a short range against live ATC registrations and also against a cooperative target flying at low altitude.

The extensive analysis of the data collected and processed showed, as expected, that the detection performance of the passive sensor is largely dependent on the considered FM radio channel, the instantaneous transmitted waveform and the instantaneous characteristics of the propagation. A preliminary activity was the selection of some FM radio channels for each Site of interest based on the proper parameters described in Section 4.6. In the analysis of the results obtained with different single FM radio channels acquired simultaneously, is clearly visible that the detection performances change with the considered channel (see for example Figure 120, referring to FM radio channel 99.6 MHz, where it is easy to notice the lower number of cooperative flight detections with respect to the other FM radio channels, 94.5, 106.6 and 107.1 MHz - Figure 119, Figure 121 and Figure 122, respectively).

As a general result, and with reference to the civil air traffic, the FM radio channels 94.5 and 103.0 MHz result on the average the best performing radio channels, thus allowing to obtain the best detection performance in terms of number of plots and coverage area.

In order to increase the performance of the passive sensor, the MF integration stage has been introduced in the processing scheme. This technique has required the use of the WB receiver prototype to acquire multiple radio channels simultaneously. For the acquisition campaigns (reported in Section 4.7.1.1.5) the MF integration has been performed with different groups of three FM radio channels. In each acquisition campaign, after the application of the MF approach, an increase of the performance has been obtained with respect to the use of the single FM radio channels, and this is clearly visible in all results showed in this document.

It is worth mentioning that the passive radar system performance could be further improved by optimizing the hardware section of the receiver. In fact, the hardware section of the developed sensors has been basically conceived in order to demonstrate the effectiveness of the passive radar concept, and resorting to low cost solutions (COTS components). On the contrary, great attention and effort has been putted into the development and optimization of innovative processing techniques in order to obtain a well performing FM-based PBR.

A performance comparison between the two receivers developed by DIET Department has been reported for the acquisition campaign carried on 11th June 2012 (see Sections 4.7.1.1.6 and 4.7.1.1.7). Data collected with the WB receiver have been processed with the MF integration approach while the results obtained with the NB receiver have been obtained with three different single FM radio channels. The NB system allowed to detect targets in a short range, despite its performance are slightly worst with respect to the WB receiver. Moreover, the NB prototype has not been used for other acquisition campaigns because the angular target localization is not available with this system yet.

Comparing the results obtained in each acquisition campaign by using single FM radio channels and with the MF integration approach, it is possible to assert that the MF integration guarantees a performance improvement keeping its characteristic of robustness respect to the strongly time-varying characteristics of the transmitted waveforms and of the channel propagation. As a consequence, the proposed MF approach is clearly able to provide the robustness and continuity of operation that are generally difficult to guarantee for FM-based passive bistatic radar, thus removing one of their major weaknesses and making them more attractive for reliable surveillance applications.

As mentioned, all detection results showed in this report are represented in bistatic-range bistatic-velocity (Doppler) domain and in x-y domain. The x-y localization has been performed by DoA estimation and the achievable performance in terms of DoA estimation accuracy highly depends on the use of a single or multiple FM radio channels. Specifically, advanced MF DoA estimation techniques have been introduced to enhance the MF system performance by making it less affected by the instantaneous behaviour of the integrated FM channels, thus resulting in an increased angular localization accuracy with respect to the single FM channel operation.

In conclusion, the presented analysis allowed us to assess the effectiveness of the conceived FM-based MF passive radar sensor for surveillance purposes. Obviously the single passive sensor is intended to provide highly reliable performance at short ranges.

In Section 5, the concept of PBR has been applied to short range applications: detection and tracking of human targets and cars, in indoor and outdoor environments respectively. Specifically, an overview of the ATOM project has been presented (Airport detection and Tracking Of dangerous Materials by passive and active sensors arrays, funded by the European Union, 7th framework program, Theme #7 Transport including Aeronautics, Grant agreement no. 234014). In this Section, a passive radar system based on WiFi transmissions has been introduced and a description of two possible architectures for the low cost system realization has been reported. As for the FM-based system, in this case, the receiver has been realized with COTS components in order to test the processing techniques and obtain an effective WiFi-based PBR. The architecture of the sensor, its processing scheme, and different examples of detection and localization results have been illustrated.

Indoor and outdoor experiments have been performed with a single and a couple of human targets moving simultaneously in the environment. The localization results, for the both experiments, have been reported in Section 5.6.1 and 5.6.2. respectively. In the first (indoor and outdoor) experiment, the obtained sequence of target localizations nicely meets the test's ground truth. The small deviations arising from the measurement accuracies might be significantly smoothed by the subsequent tracking algorithm.

In the second (indoor and outdoor) experiment and in the second indoor experiment, the targets moved very close each other, so that only a single target has been detected and localized. In fact, in such case both the targets appear at the same range/Doppler frequency location thus preventing the possibility of resolving them. On the bright side, when the second target changes its walking direction, it appears at a different Doppler frequency location on both the bi-static range/Doppler frequency planes thus making it possible to resolve the targets and correctly localize both of them. In particular, it has been verified that it is possible to correctly estimate the human targets' range, Doppler frequency and DoA as well as properly localize them in indoor and outdoor scenarios. Also, targets moving along the same path very close each other are not resolved by the passive radar, since they appear at the same range/Doppler frequency location while targets moving along different paths can be resolved and correctly localized even if they pass very close each other at a certain location.

In Section 6, a preliminary study regarding a passive radar based on DVB-SH signals of opportunity has been reported. The work includes the definition of the general requirements and the selection of the best suited receiver architecture for DVB-SH signal. A two-channel simple demonstrator has been realized, developed and fielded during preliminary tests. The signal transmitted by the satellite has been correctly acquired and demodulated (according to the DVB-SH standard). The main limitation with this waveform of opportunity has been represented by the low power transmission provided by Eutelsat 10A platform. The dynamic of the system is strongly limited due to the power emission of the interesting signal because the transmission antenna has been damaged during the satellite launch.

The future work will concern the use of the proposed receiver in order to realize an effective DVB-SH based PBR, through the use of multiple receiving chains in order to perform experiments in different applications: short range air traffic control and short range surveillance of car targets. In future, with the availability of a new platform able to transmit a signal with an higher power level, the concept can be used to extend the ranges covered by this PBR system.

Finally, in Section 7, a flexible receiver architecture has been described for PBR applications. The presented system can exploit any of the many broadcast signals available in the frequency spectrum.

Specific front-ends receiver sections are foreseen for each selected waveform of opportunity, while a common part of the system performs the I&Q demodulation and the Analog-to-Digital (A/D) conversion. The proposed scheme can be used both for a direct I&Q conversion and for a double conversion (up-conversion stage from RF to IF and down-conversion from IF to BB) of the received signals for PBR applications. This allows to remove the image frequency even in the wide bandwidth occupied by the digital TV signals. A prototype of the proposed concept has been developed and fielded, with proper laboratory tests and real data acquisition campaigns.

The effectiveness of the proposed solution has been assessed by using the receiver in different applications that allow to achieve an FM-based and a DVB-T-based PBR for long-, medium-range surveillance of air targets, and a WiFi-based PBR for short range localization of human targets.

The future work will concern the use of the proposed receiver in order to realize an effective FM- and DVB-T-based PBR, through the use of multiple receiving chains with different FE configurations simultaneously.

REFERENCES

[1] "Special Issue on Passive Radar Systems," in *Radar, Sonar and Navigation*, June 2005.

[2] H. Griffiths and N. Long, "Television-based bistatic radar," Communication Radar Signal Processing, vol. 133, no. 7, pp. 649-657, December 1986.

[3] K.S. Kulpa and Z. Czekała, "Masking effect and its removal in PCL radar", IEE Proc. Radar Sonar Navig., Vol. 152, No. 3, June 2005, pp. 174-178.

[4] S. R.J. Axelsson, "Improved clutter suppression in random noise radar", URSI 2005 Commission F Symposium on Microwave Remote Sensing of the Earth, Oceans, Ice, and Atmosphere, April 2005.

[5] R. Cardinali, F. Colone, C. Ferretti, P. Lombardo, "Comparison of clutter and multipath cancellation techniques for passive radar", IEEE 2007 Radar Conference, Boston, (MA), USA, March 2007.

[6] F. Colone, R. Cardinali, P. Lombardo, "Cancellation of clutter and multipath in passive radar using a sequential approach", IEEE 2006 Radar Conference, Verona (NY), USA, April 24-27, 2006, pp. 393-399.

[7] F. Colone, D. W. O'Hagan, P. Lombardo, C. J. Baker "A multistage processing algorithm for disturbance removal and target detection in Passive Bistatic Radar", IEEE Transactions on Aerospace and Electronic Systems, Vol. 45, No. 2, April 2009, pp. 698-722.

[8] P. Falcone, F. Colone, P. Lombardo, T. Bucciarelli, "Range Sidelobes Reduction Filters for WiFi-Based Passive Bistatic Radar", EURAD 2009, Rome, Italy, 30 September-2 October 2009

[9] Baker, C.J.; Griffiths, H.D.; Papoutsis, I., "Passive coherent location radar systems. Part 2: waveform properties", IEE Proceedings on Radar, Sonar and Navigation, Vol. 152, Issue 3, June 2005, pp.160-168.

[10] P.E. Howland, D. Maksimiuk, G. Reitsma, "FM radio based bistatic radar" IEE Proceedings on Radar, Sonar and Navigation, Volume 152, Issue 3, 3 June 2005 Page(s):107-115.

[11] S. Haykin, "Adaptive filter theory", Prentice Hall, Upper Saddle River, NJ, USA, 2002, 4th edn.

[12] P. Lombardo, F. Colone, C. Bongioanni, A. Lauri, T. Bucciarelli, "PBR activity at INFOCOM: adaptive processing techniques and experimental results", 2008 IEEE Radar Conference, Rome, Italy, May 26-30, 2008.

[13] A.N. Morabito, M.G. Meyer, J.D. Sahr, "Improved computational performance for distributed passive radar processing through channelised data", IEE Proceedings on Radar, Sonar and Navigation, Vol. 152, Issue 3, June 2005, pp.179-184.

[14] D. Langellotti, F. Colone, C. Bongioanni, P. Lombardo, "Comparative study of ambiguity function evaluation algorithms for passive radar", International Radar Symposium 2009 – IRS 2009, Sept 9-11, 2009, Hamburg, Germany.

[15] M. Skolnik, "Radar Handbook", Mc Graw Hill , 3rd ed, 2008, ISBN: 978-0-07-148547-0.

[16] P. P. Gandhi and S. A. Kassam, "Analysis of CFAR processors in nonhomogeneous background", IEEE Transactions on Aerospace and Electronic Systems vol. 24, pp. 427-445, July 1988.

[17] E.K. Al-Hussaini, "Performance of the `smaller of' and `greater of' detectors integrating M pulses", Proceedings of the IEEE, Volume 76, Issue 6, June 1988, pp:731 – 733.

[18] H. Rohling, " Radar CFAR thresholding in clutter and multiple target situations", IEEE Transactions on Aerospace and Electronic Systems, vol. 19, pp. 608-621, July 1983.

[19] Li, X., and Bar-Shalom, Y.: 'Multitarget-multisensor tracking: principles and techniques' (YBS, 1995, 2nd edn.)

[20] Description of work of EU-project ARGUS3D, seventh framework programme, theme #10 security Grant agreement no.: 218041

[21] Griffiths, H.D.; Baker, C.J., “Passive coherent location radar systems. Part 1: performance prediction” IEE Proc. Radar, Sonar and Navigation, Volume 152, No. 3, June 2005, pp.153-159.

[22] A. Lauri, F. Colone, R. Cardinali, C. Bongioanni, P. Lombardo, “Analysis and emulation of FM radio signals for passive radar”, 2007 IEEE Aerospace Conference, Big Sky (MT), USA, 3-10 March 2007.

[23] N. J. Willis, Bistatic Radar, Artech House, 1991.

[24] IEEE Standard for Information technology: “Part 11: Wireless LAN Medium Access Control (MAC) and Physical Layer (PHY) specifications” (IEEE Std 802.11™-1999) – and following Supplements and Amendments (IEEE Stds 802.11a™-1999, 802.11b™-1999, 802.11b™-1999/Cor 1-2001, and 802.11g™-2003).

[25] R. Cardinali, R. Pigliacampo, E. Anniballi, M. Annunziata, "D2.1: ATOM system architecture", Deliverable of the European Collaborative Project ATOM, Contract 234014 FP7-AAT-2007-RTD-1, February 2010. (http://atom-project.eu)

[26] IEEE Standard for Information technology: “Part 11: Wireless LAN Medium Access Control (MAC) and Physical Layer (PHY) specifications” (IEEE Std 802.11™-1999) – and following Supplements and Amendments (IEEE Stds 802.11a™-1999, 802.11b™-1999, 802.11b™-1999/Cor 1-2001, and 802.11g™-2003).

[27] F. Colone, K. Woodbridge, H. Guo, D. Mason and C. J. Baker, “Ambiguity Function Analysis of Wireless LAN transmissions for passive radar", IEEE Trans. on Aerospace and Electronic Systems, January 2011 Issue.

[28] F. Colone, P. Falcone, C. Bongioanni, P. Lombardo, "WiFi-Based Passive Bistatic Radar: Data Processing Schemes and Experimental Results", Aerospace and Electronic Systems, IEEE Transactions on, vol.48, no.2, pp.1061-1079, April 2012.

[29] P. Falcone, F. Colone, P. Lombardo, T. Bucciarelli, “Range Sidelobes Reduction Filters for WiFi-Based Passive Bistatic Radar”, EURAD 2009, Rome, Italy, 30 September-2 October 2009.

[30] P. Falcone, F. Colone, A. Macera, P. Lombardo, "Localization and tracking of moving targets with WiFi-based passive radar", Radar Conference (RADAR), 2012 IEEE, pp.0705-0709, 7-11 May 2012.

[31] F. Colone, P. Falcone, A. Macera, P. Lombardo, "High resolution cross-range profiling with Passive Radar via ISAR processing", Proceedings of International Radar Symposium 2011, pp.301-306, 7-9 Sept. 2011.

[32] Li Xi, Liu Guosui, Jinlin Ni, "Autofocusing of ISAR images based on entropy minimization", Aerospace and Electronic Systems, IEEE Transactions on , vol.35, no.4, pp.1240-1252, Oct 1999.

[33] P. Falcone, F. Colone, P. Lombardo, D. Pastina, “WiFi-based passive ISAR for high resolution cross-range profiling of moving targets”, EUSAR 2012 – April 26, 2012 – Nürnberg, Germany.

[34] P. Falcone, F. Colone, A. Macera, D. Pastina, P. Lombardo, "Advances in ISAR processing for High Resolution Cross-Range Profiling with Passive Radar" International Radar Symposium, IRS 2012, Warszaw, Poland, May 23-25 2012.

[35] D. Cristallini, M. Caruso, P. Falcone, D. Langellotti, C. Bongioanni, F. Colone, S. Scafè, P. Lombardo, “Space-Based Passive Radar Enabled by the New Generation of Geostationary Broadcast Satellites”, 2010 IEEE Aerospace Conference, March 6-13, 2010, Big Sky, Montana (USA).

[36] R. Saini, M. Cherniakov, V. Lenive, “Direct path interference suppression in bistatic system: DTV based radar”, Proc. of the Int. Radar Conference 2003, pp. 309-314.

[37] R. Saini and M. Cherniakov, “DTV signal ambiguity function analysis for radar application”, IEE Proceedings on Radar, Sonar and Navigation, Vol. 152, Issue 3, June 2005, pp. 133-142.

[38] Z. Gao, R. Tao, Y. Ma, T. Shao, “DVB-T Signal Cross-Ambiguity Functions Improvement for Passive Radar”, Proc. of the 2006 CIE International Conference on Radar, Shanghai, China, October 16-19, 2006.

[39] C. Bongioanni, F. Colone, D. Langellotti, P. Lombardo, T. Bucciarelli, “A New Approach for DVB-T Cross-Ambiguity Function Evaluation”, Proceedings of European Radar Conference (EURAD 2009), Rome, Italy, 30 September-2 October 2009.

A. APPENDIX

A.1 RECEIVER POWER LEVELS EVALUATION IN FREE-SPACE PROPAGATION

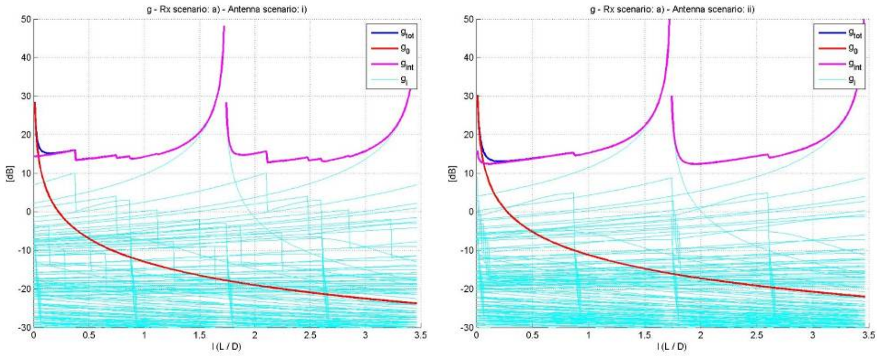

antenna i) antenna ii)

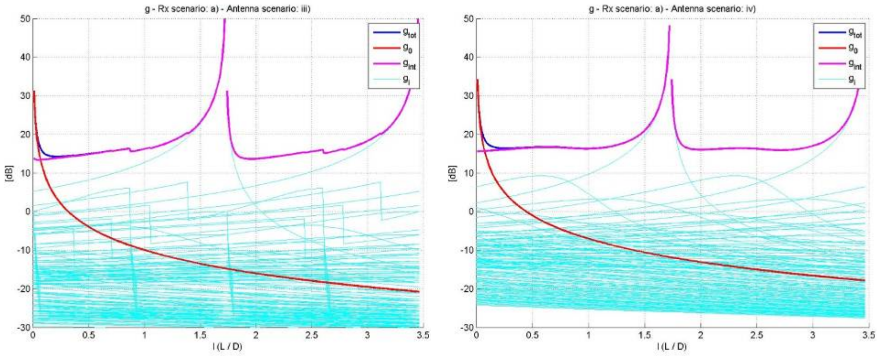

antenna iii) antenna iv)

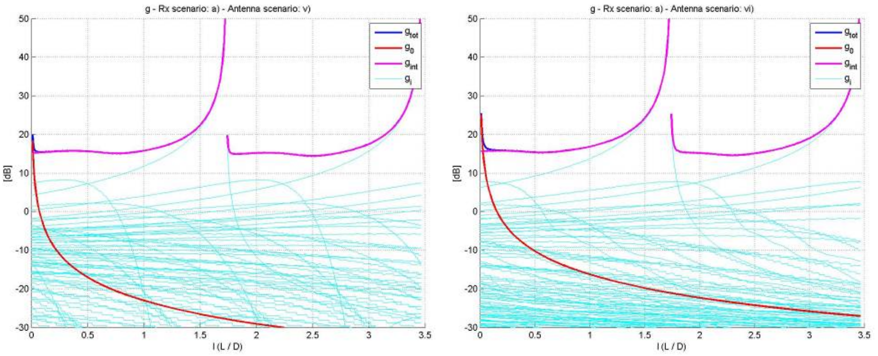

antenna v) antenna vi)

Figure 215 – Geometric terms for receiver case a) with different antennas

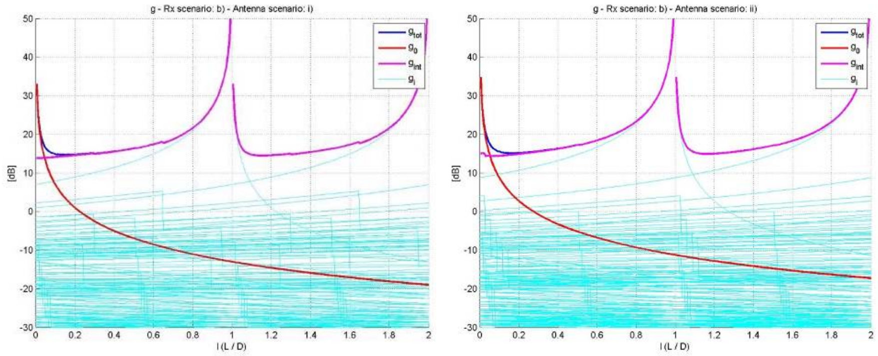

antenna i) antenna ii)

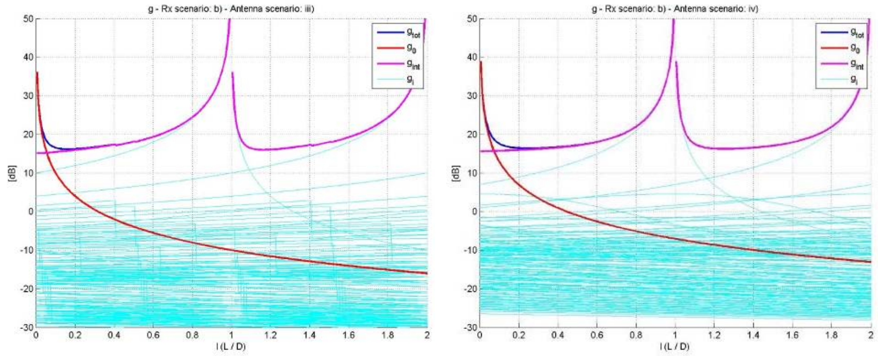

antenna iii) antenna iv)

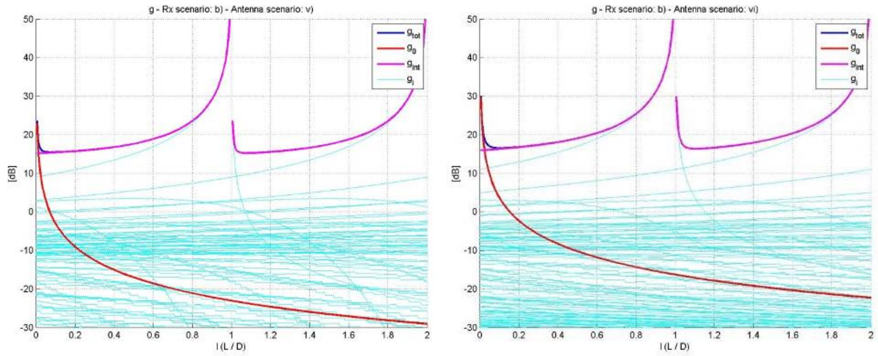

antenna v) antenna vi)

Figure 216 – Geometric terms for receiver case B) with different antennas

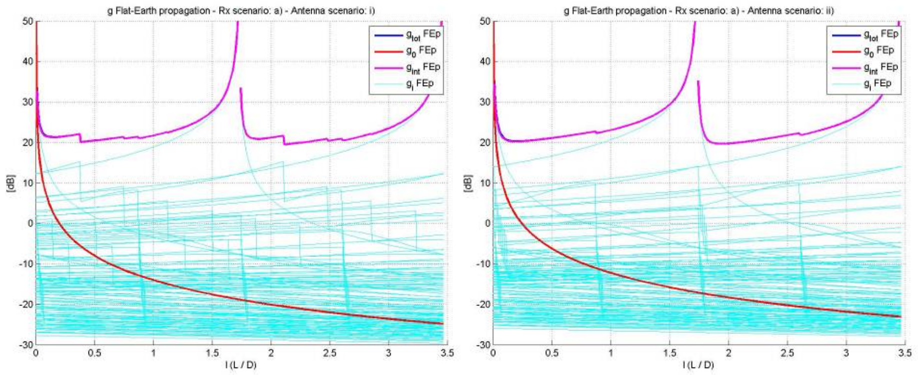

antenna i)

antenna ii)

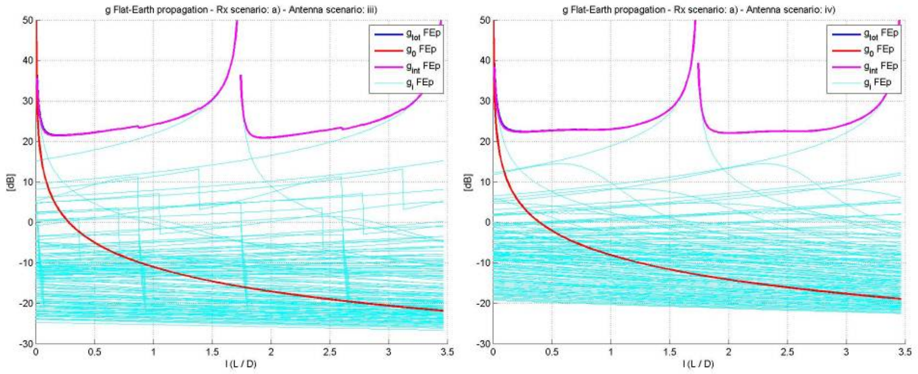

antenna iii)

antenna iv)

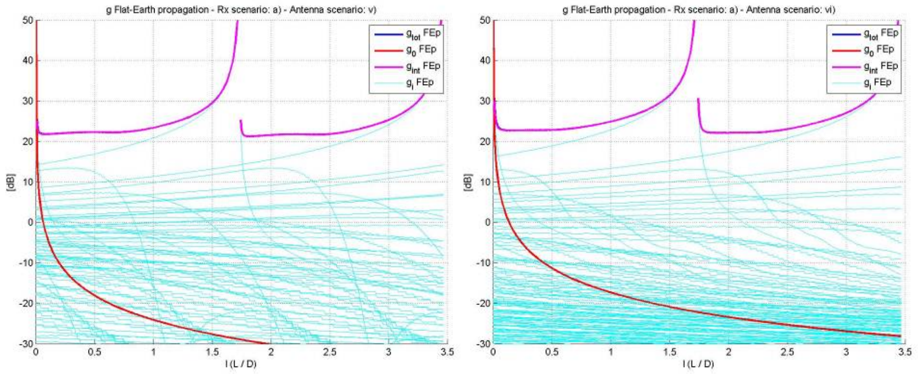

antenna v)

antenna vi)

Figure 217 – Geometric terms under flat-Earth propagation for receiver case a) with differ antenna patterns

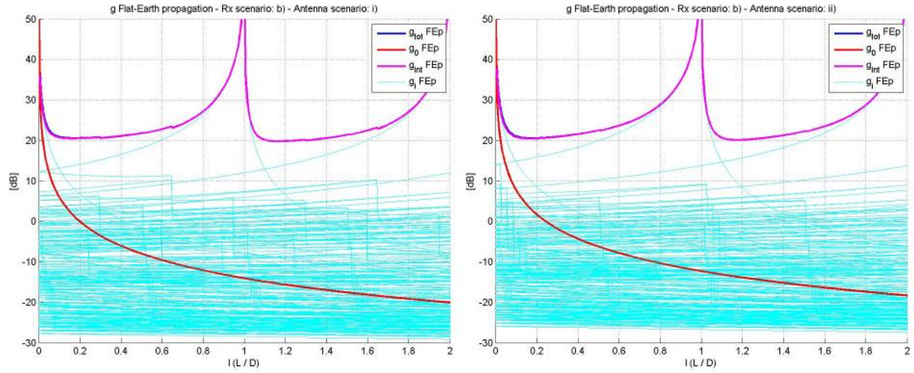

antenna i) antenna ii)

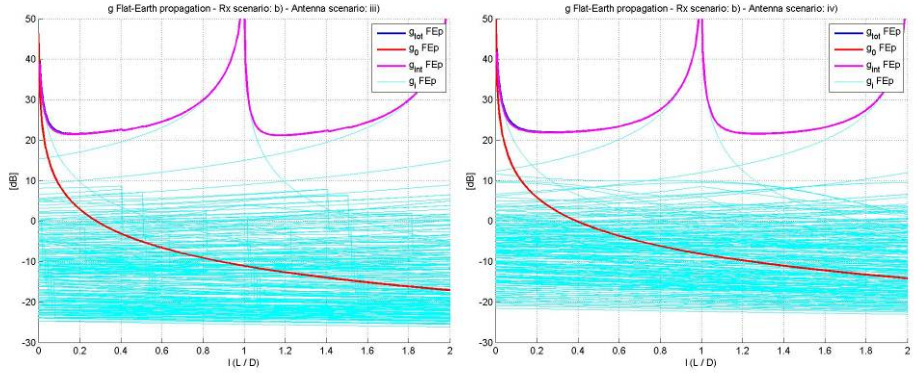

antenna iii) antenna iv)

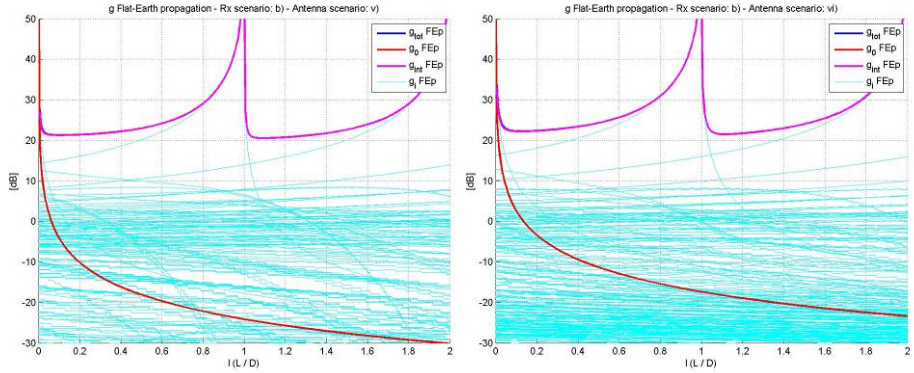

antenna v) antenna vi)

Figure 218 – Geometric terms under flat-Earth propagation for receiver case B) with differ antenna patterns

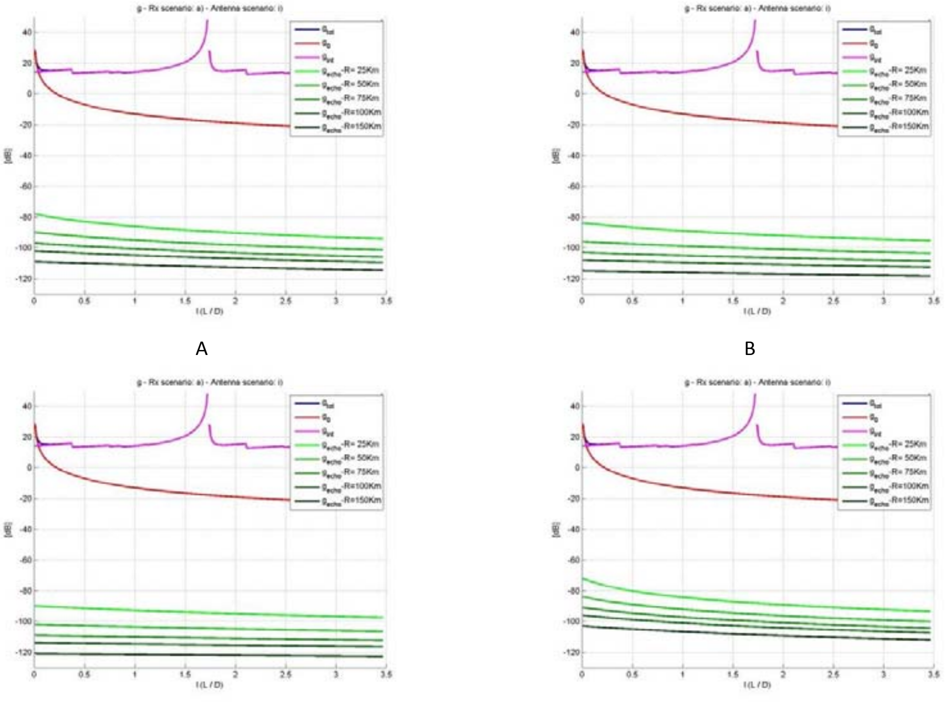

Figure 219 – Geometric terms for case a), antenna i). A: D=10km, B: D=20km, C: D=40km, D: D=80km

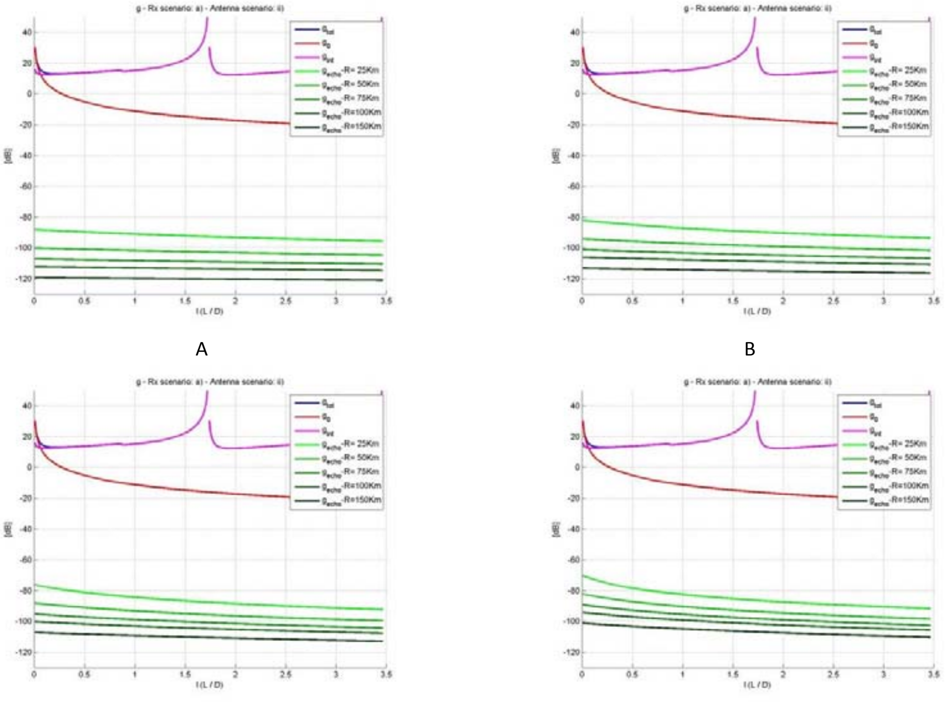

Figure 220 – Geometric terms for case a), antenna ii). A: D=10km, B: D=20km, C: D=40km, D: D=80km

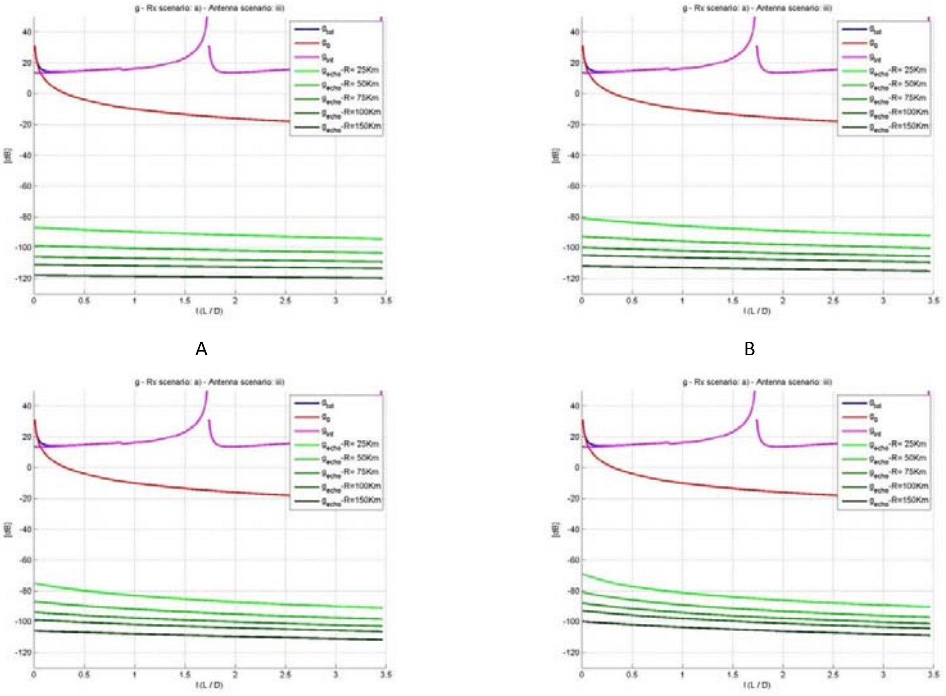

A B

C D

Figure 221 – Geometric terms for case a), antenna iii). A: D=10km, B: D=20km, C: D=40km, D: D=80km

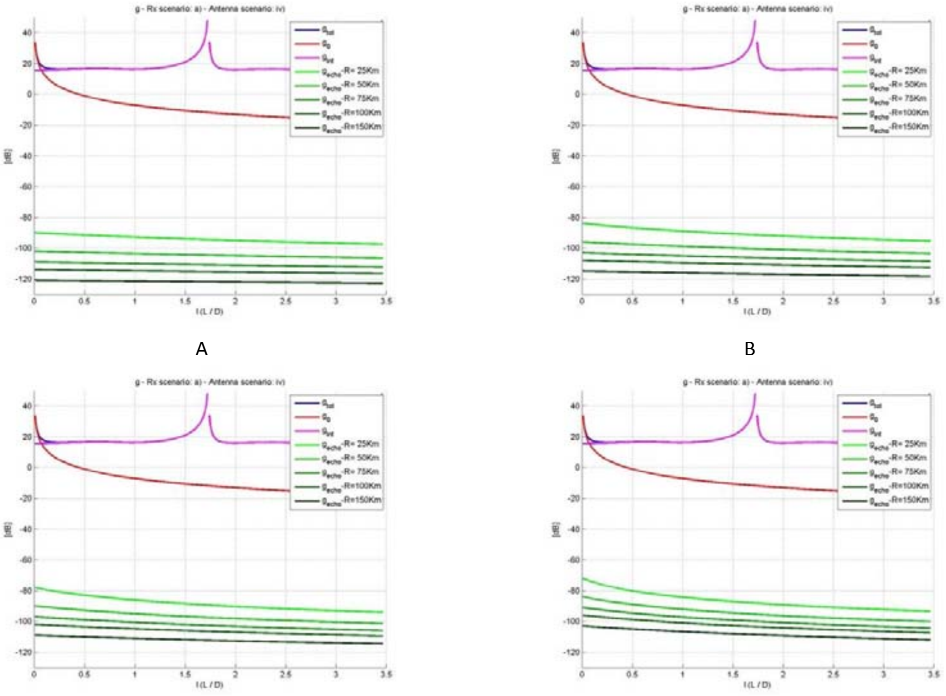

A B

C D

Figure 222 – Geometric terms for case a), antenna iv). A: D=10km, B: D=20km, C: D=40km, D: D=80km

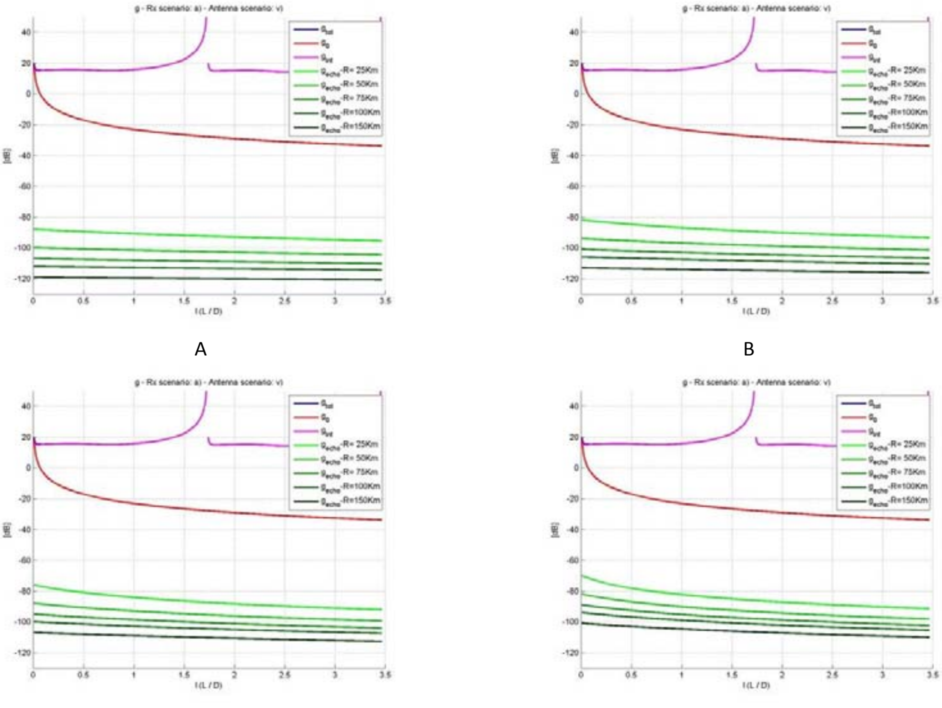

A B

C D

Figure 223 – Geometric terms for case a), antenna v). A: D=10km, B: D=20km, C: D=40km, D: D=80km

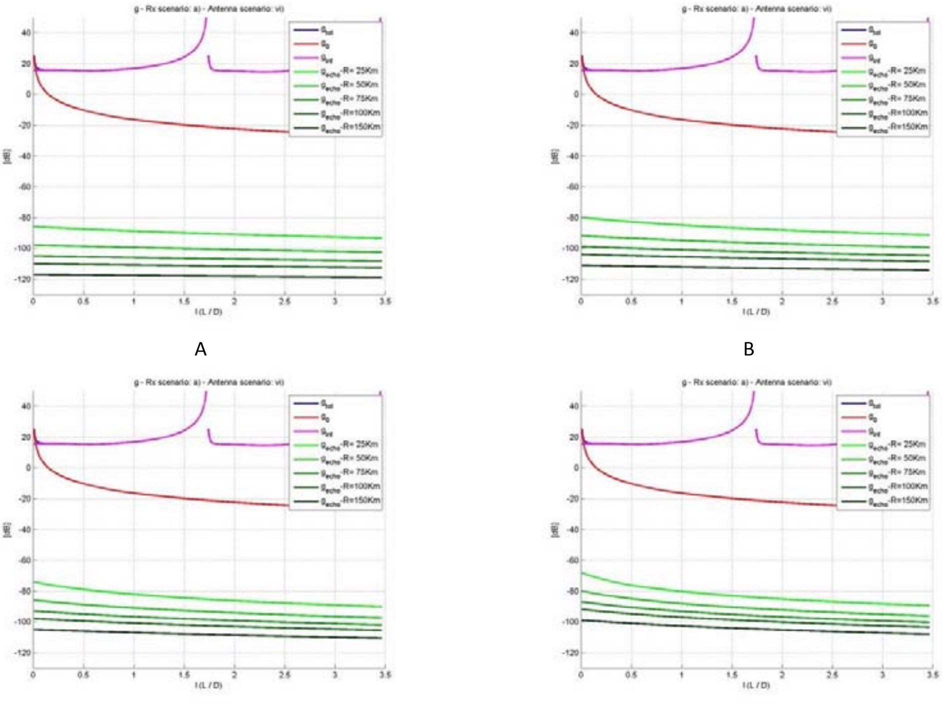

A B

C D

Figure 224 – Geometric terms for case a), antenna vi). A: D=10km, B: D=20km, C: D=40km, D: D=80km

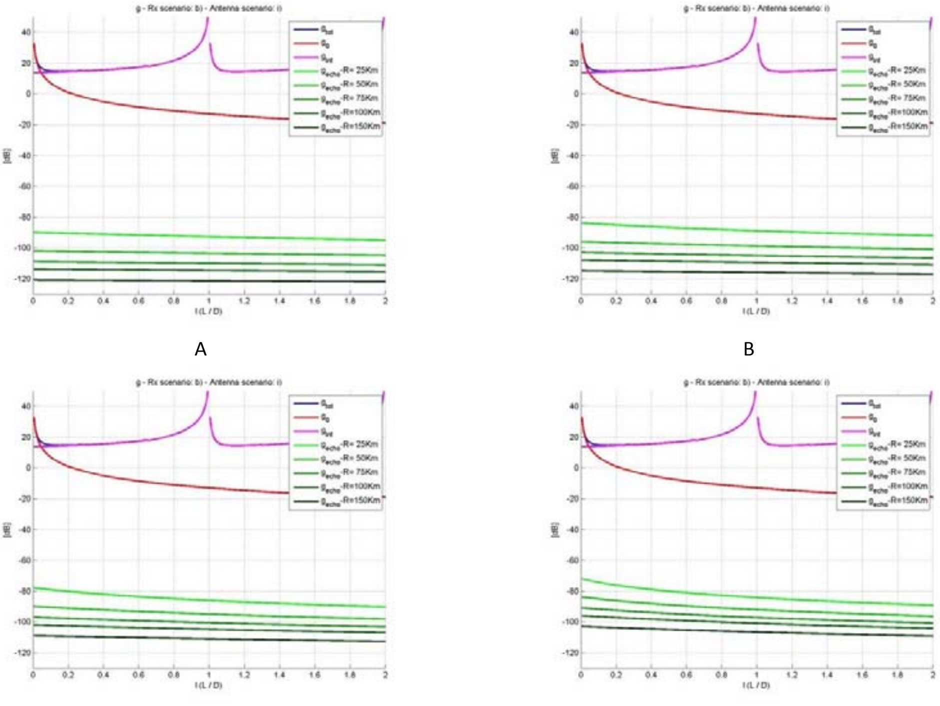

A

B

C

D

Figure 225 – Geometric terms for case b), antenna i). A: D=10km, B: D=20km, C: D=40km, D: D=80km

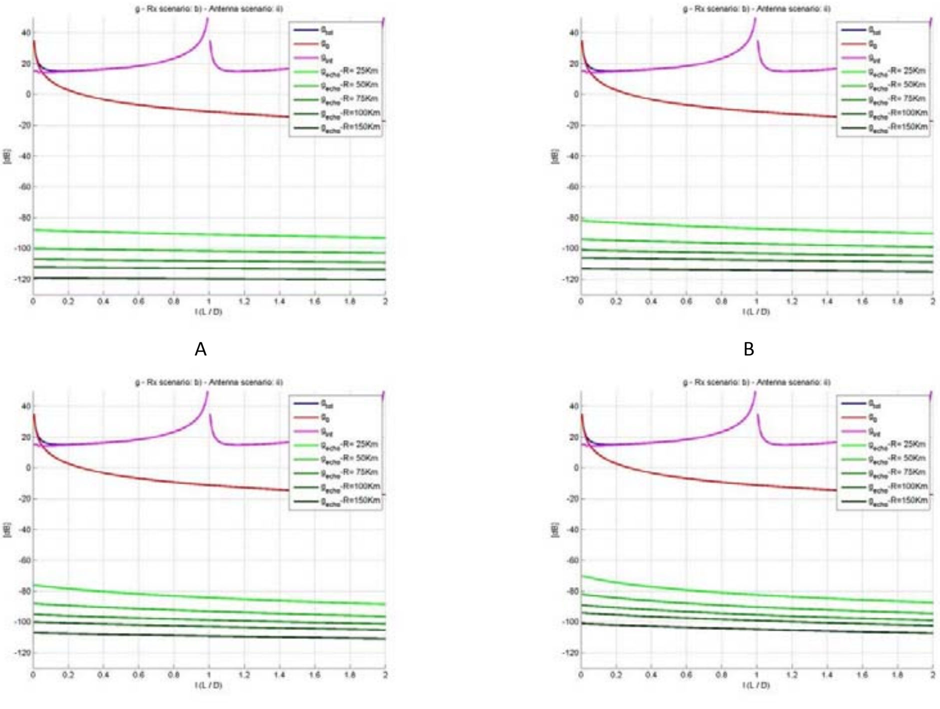

A

B

C

D

Figure 226 – Geometric terms for case b), antenna ii). A: D=10km, B: D=20km, C: D=40km, D: D=80km

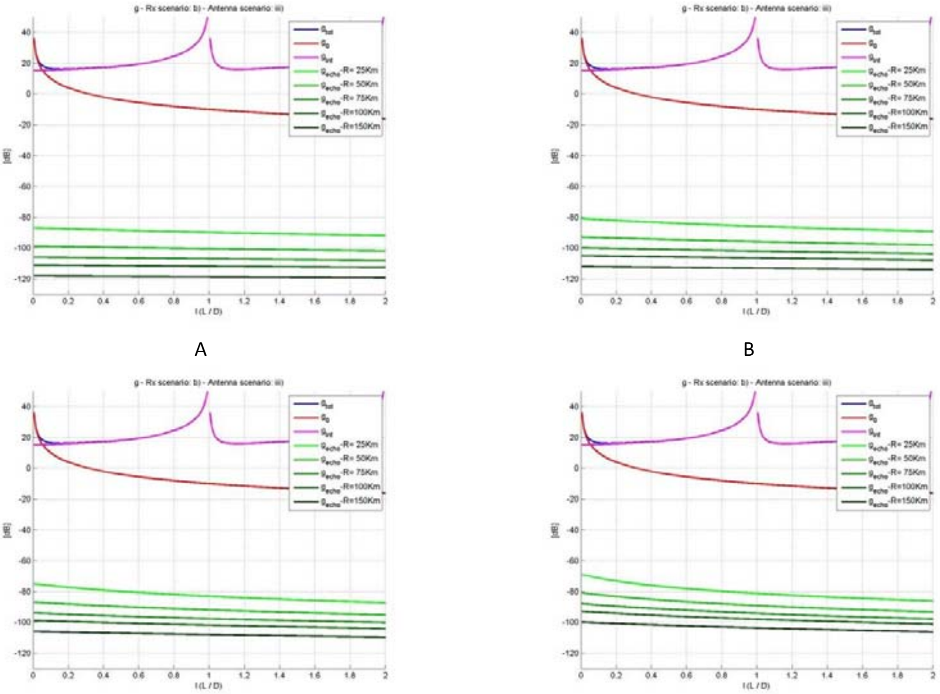

A

B

C

D

Figure 227 – Geometric terms for case b), antenna iii). A: D=10km, B: D=20km, C: D=40km, D: D=80km

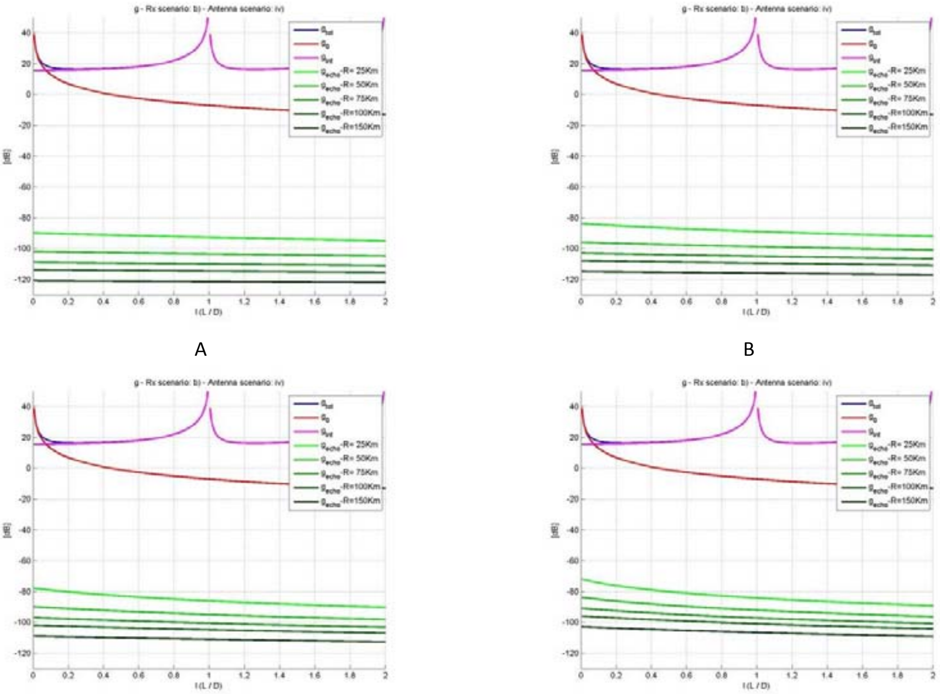

A

B

C

D

Figure 228 – Geometric terms for case b), antenna iv). A: D=10km, B: D=20km, C: D=40km, D: D=80km

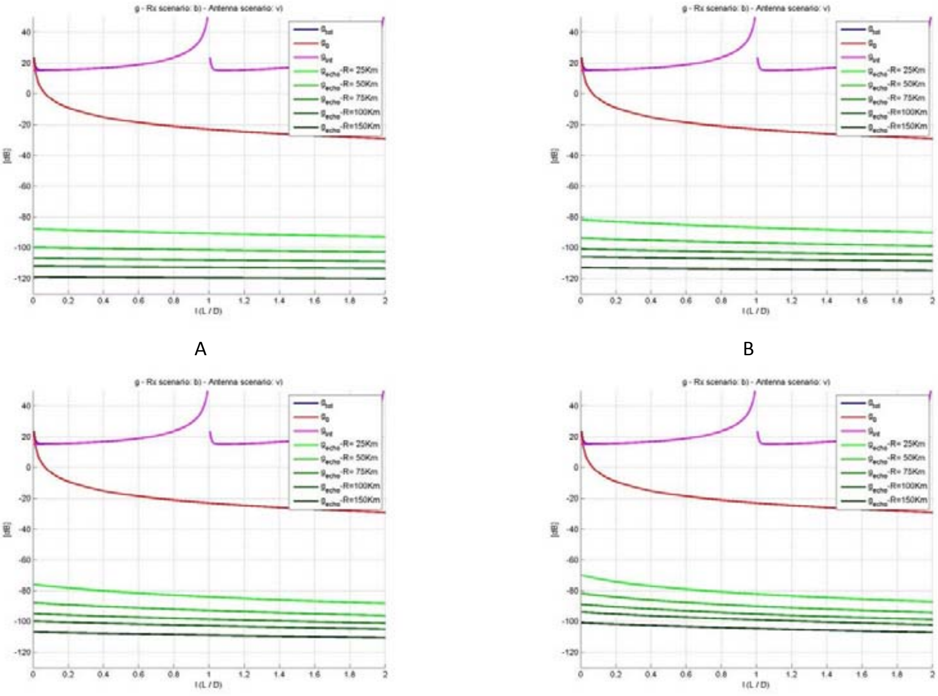

A

B

C

D

Figure 229 – Geometric terms for case b), antenna v). A: D=10km, B: D=20km, C: D=40km, D: D=80km

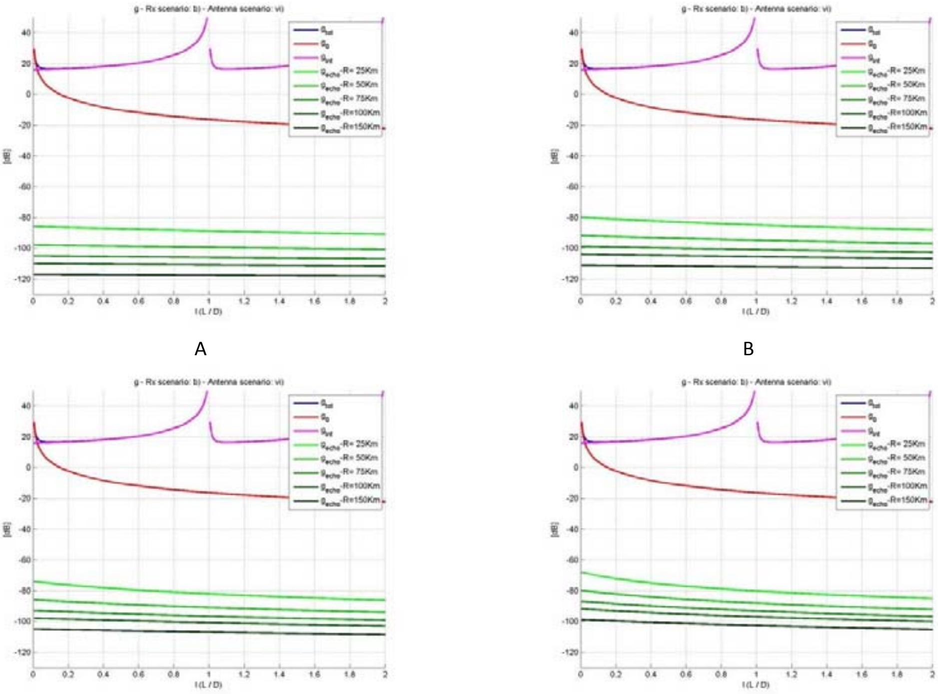

A

B

C

D

Figure 230 – Geometric terms for case b), antenna vi). A: D=10km, B: D=20km, C: D=40km, D: D=80km

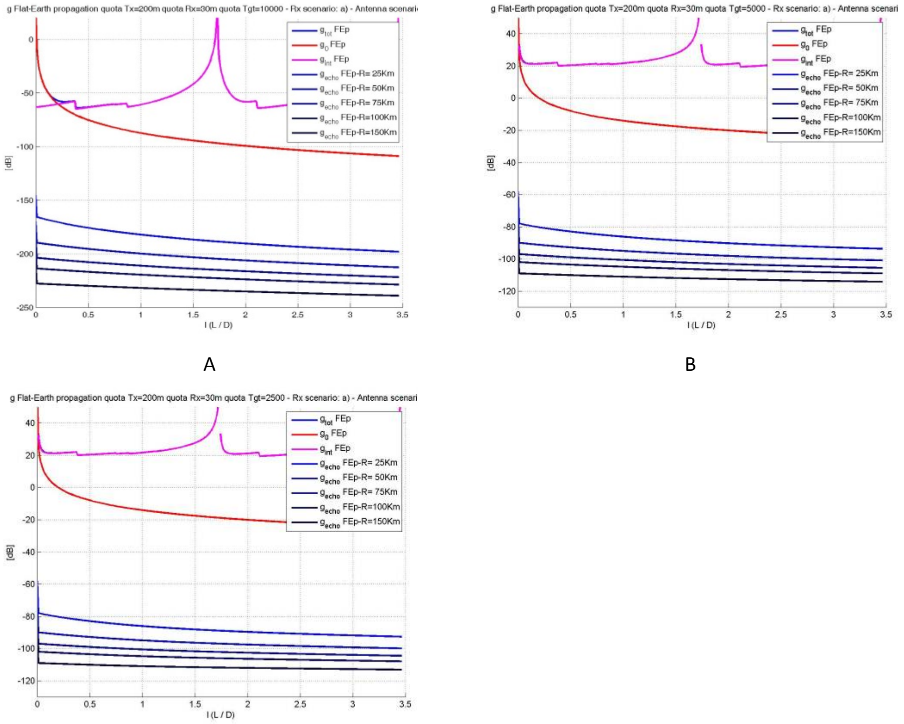

A

B

C

Figure 231 - Geometric terms for case a), antenna pattern i). A: hTgt=10km, B: hTgt=5km, C: hTgt=2.5km

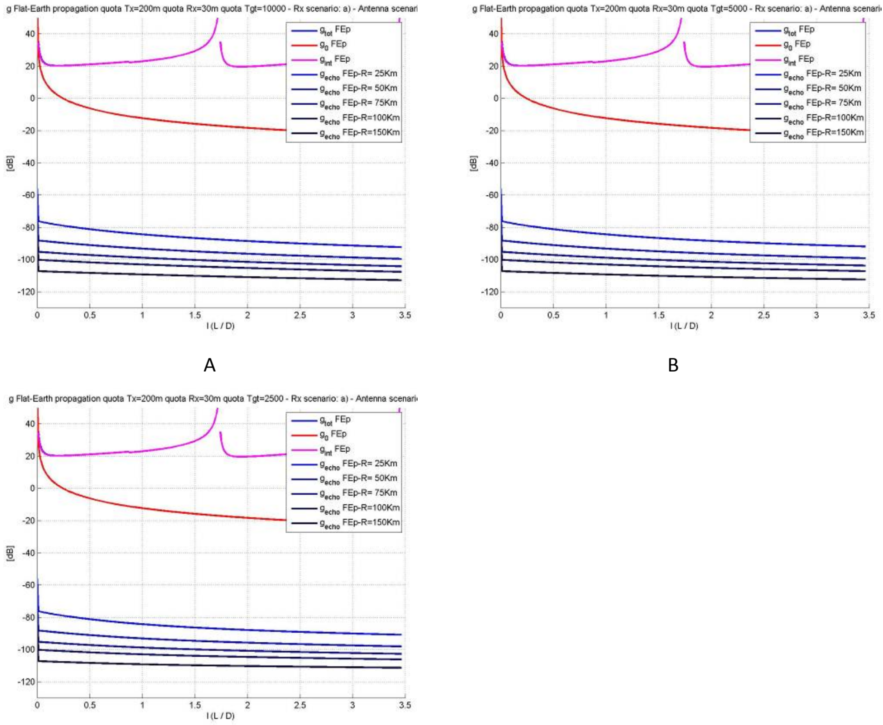

A

B

C

Figure 232 - Geometric terms for case a), antenna pattern ii). A: hTgt=10km, B: hTgt=5km, C: hTgt=2.5km

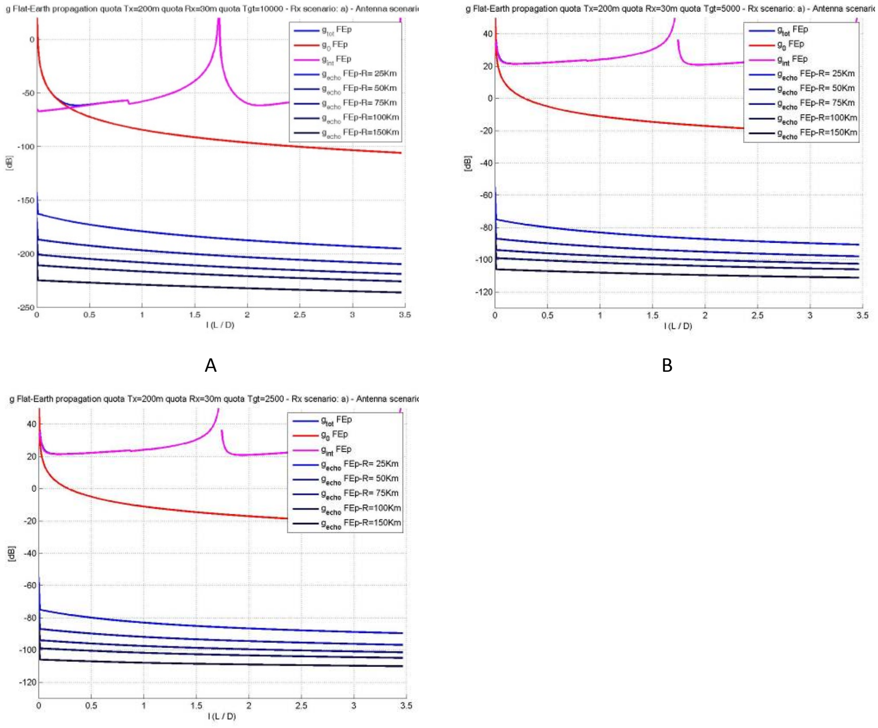

A

B

C

Figure 233 - Geometric terms for case a), antenna pattern iii). A: hTgt=10km, B: hTgt=5km, C: hTgt=2.5km

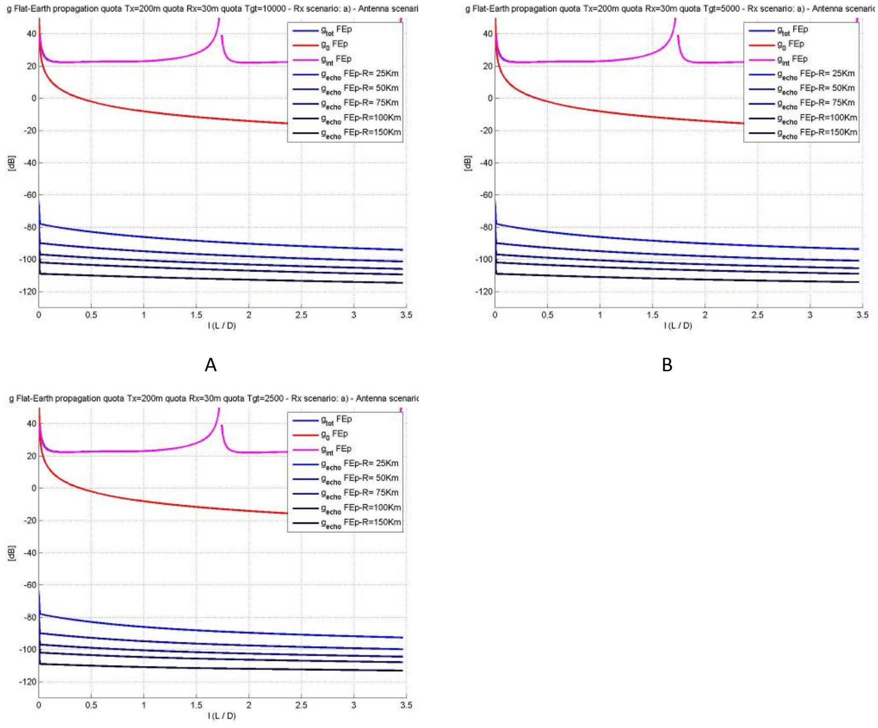

A

B

C

Figure 234 - Geometric terms for case a), antenna pattern iv). A: hTgt=10km, B: hTgt=5km, C: hTgt=2.5km

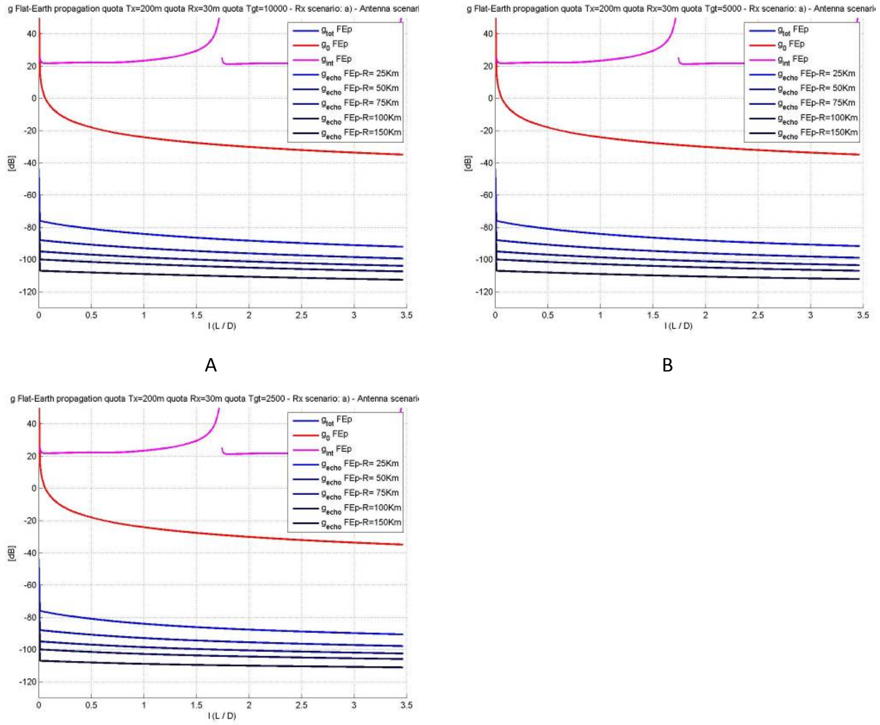

A B

C

Figure 235 - Geometric terms for case a), antenna pattern v). A: hTgt=10km, B: hTgt=5km, C: hTgt=2.5km

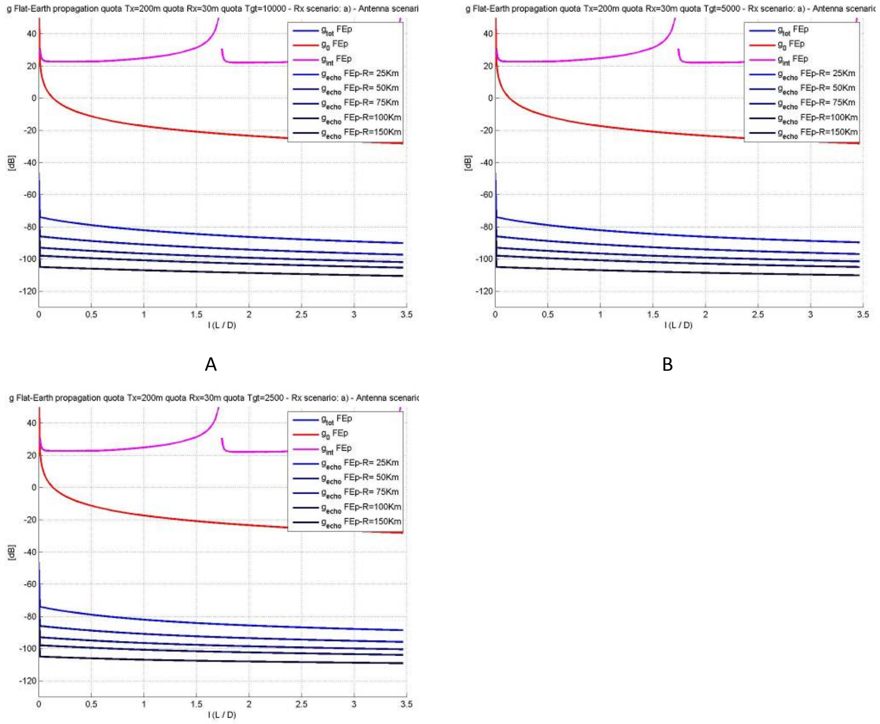

A B

C

Figure 236 - Geometric terms for case a), antenna pattern vi). A: hTgt=10km, B: hTgt=5km, C: hTgt=2.5km

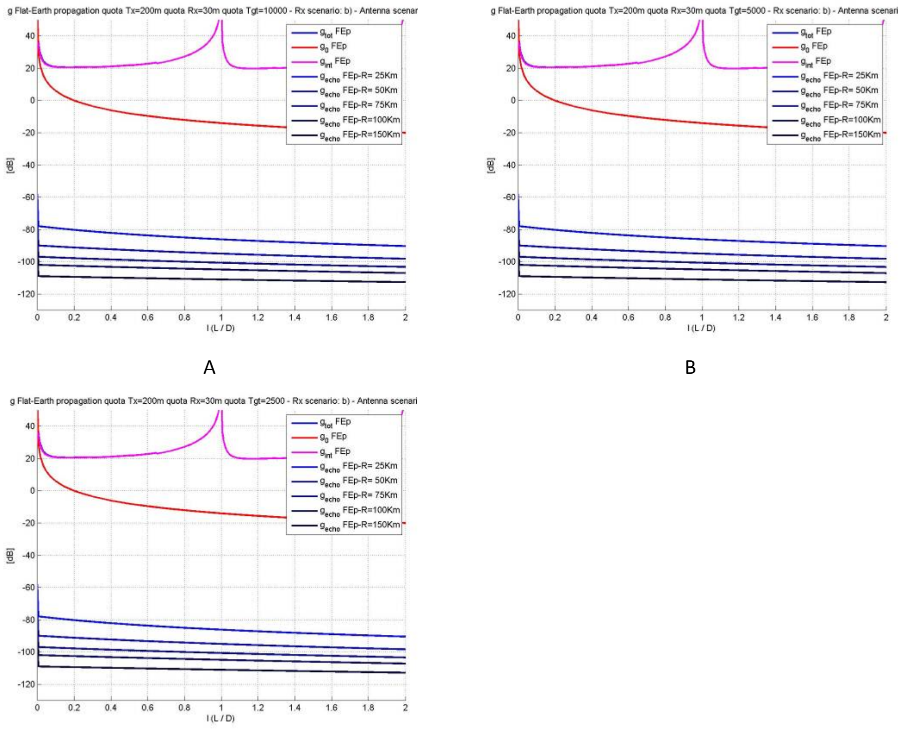

A B

C

Figure 237 - Geometric terms for case b), antenna pattern i). A: hTgt=10km, B: hTgt=5km, C: hTgt=2.5km

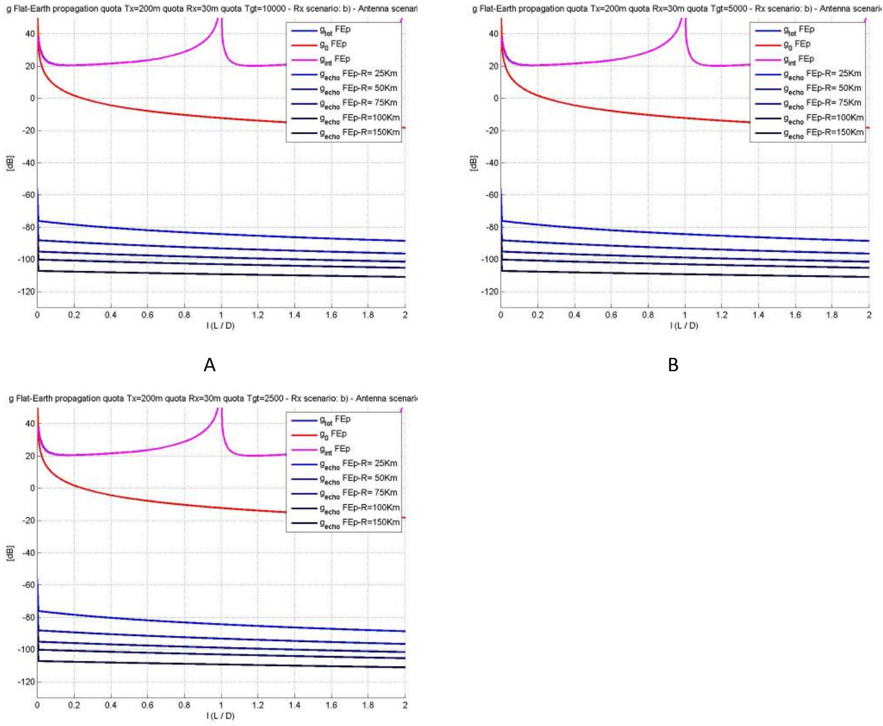

A B

C

Figure 238 - Geometric terms for case b), antenna pattern ii). A: hTgt=10km, B: hTgt=5km, C: hTgt=2.5km

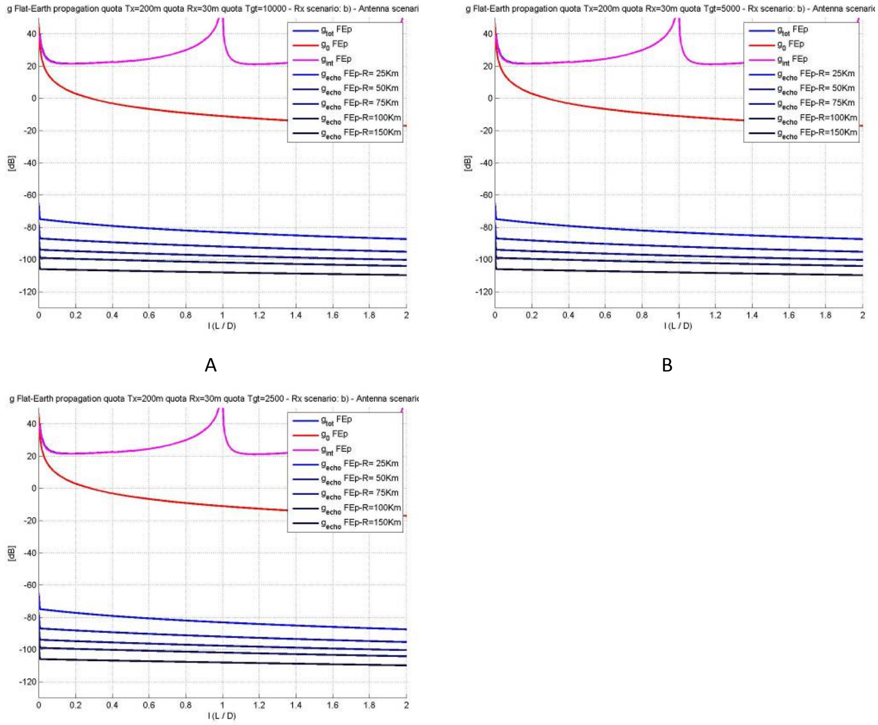

A

B

C

Figure 239 - Geometric terms for case b), antenna pattern iii). A: hTgt=10km, B: hTgt=5km, C: hTgt=2.5km

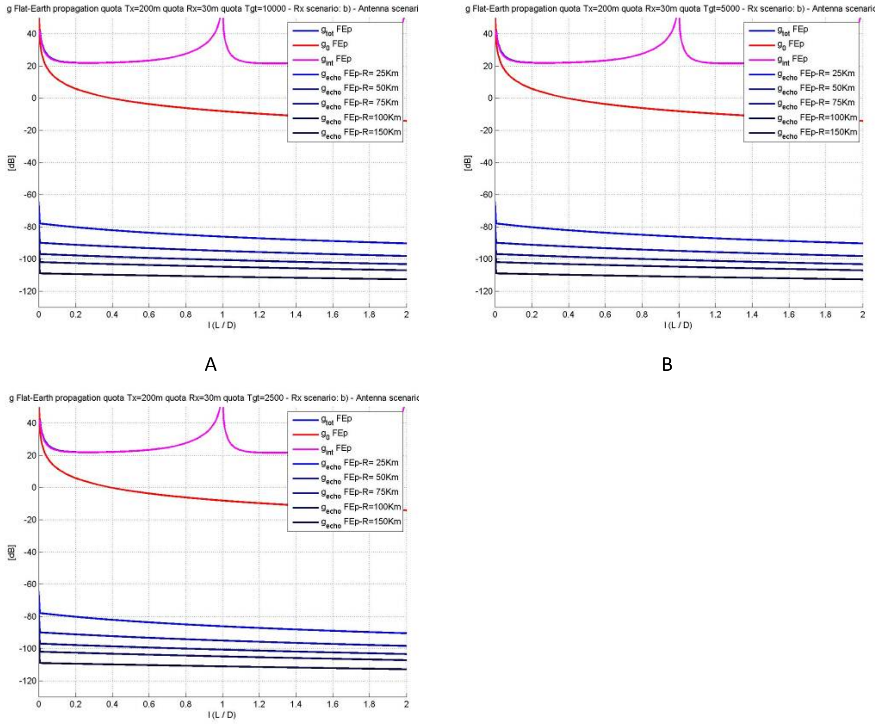

A

B

C

Figure 240 - Geometric terms for case b), antenna pattern iv). A: hTgt=10km, B: hTgt=5km, C: hTgt=2.5km

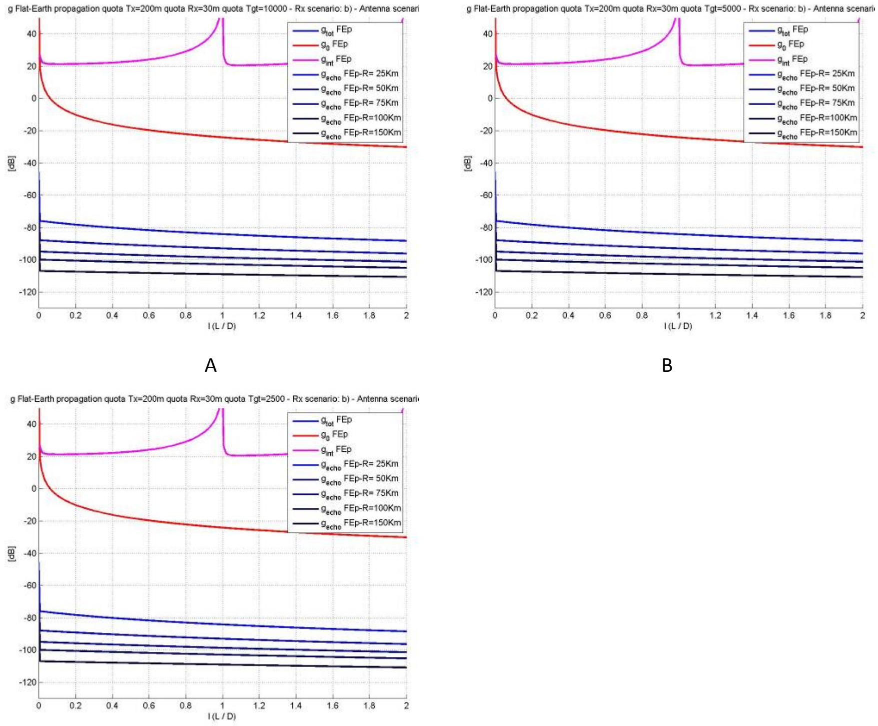

A

B

C

Figure 241 - Geometric terms for case b), antenna pattern v). A: hTgt=10km, B: hTgt=5km, C: hTgt=2.5km

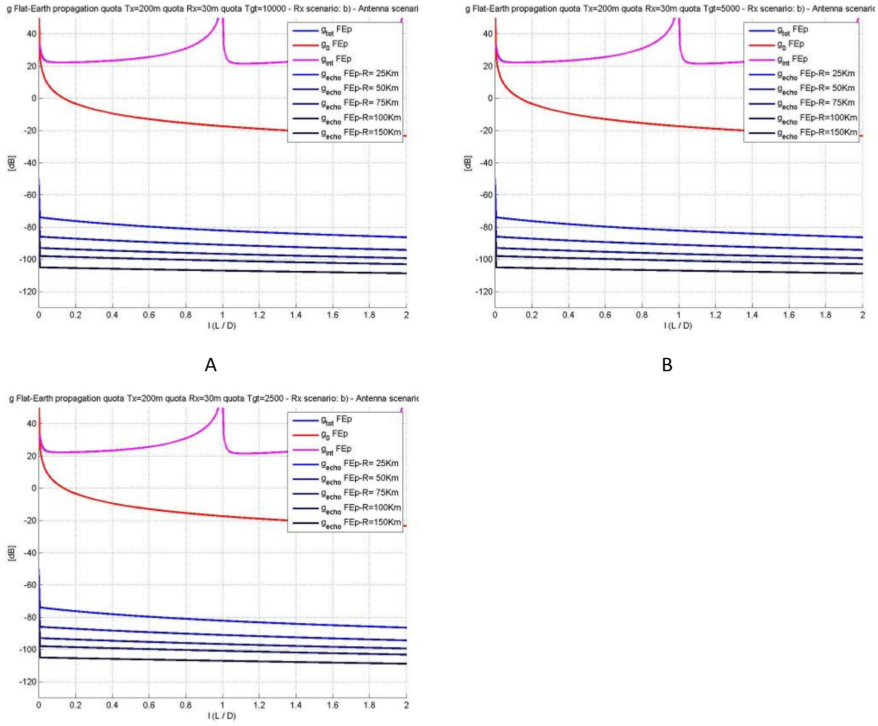

A

B

C

Figure 242 - Geometric terms for case b), antenna pattern vi). A: hTgt=10km, B: hTgt=5km, C: hTgt=2.5km